EXPANSION OF LOW- AND MID-VALENT ORGANOMETALLIC URANIUM CHEMISTRY

by

Caleb J. Tatebe

A Dissertation

Submitted to the Faculty of Purdue University

In Partial Fulfillment of the Requirements for the degree of

Doctor of Philosophy

Department of Chemistry

West Lafayette, Indiana

August 2019

THE PURDUE UNIVERSITY GRADUATE SCHOOL
STATEMENT OF COMMITTEE APPROVAL

Dr. Suzanne C. Bart, Chair
Department of Chemistry
Dr. Corey M. Thompson
Department of Chemistry
Dr. Christopher Uyeda
Department of Chemistry
Dr. David R. McMillin
Department of Chemistry

Approved by:
Dr. Christine A. Hrycyna
Head of the Graduate Program

Soli Deo Gloria

ACKNOWLEDGMENTS

I would be where am I today without the enduring support from my wife, Vanessa. From the willingness to move out to Indiana with me, to dealing with the late nights without me being home – there is nothing that Vanessa wouldn't do for me and I am grateful to spend my life with her.

If, for some reason, anyone is reading this, bear with me. There is a story to tell about how I made it through graduate school. I suppose it really began with the seeds sown by my high school chemistry teacher, Amy Hays. I was fortunate enough to attend Warren Gamaliel Harding High School when it still housed a full diploma for the International Baccalaureate (IB) program. For this program, I did *three* years of chemistry in high school; at the time, I just thought chemistry was much cooler than biology and I needed a higher-level science!

My first research experience was at Youngstown State University (YSU) while in Dr. Tim Wagner's 1516L course which exposed undergraduate students to real-life research as part of the course. For me, this meant preparing series of perovskites (AMX_3) with mixed ratios at the A or M site, as well as their analysis. I was hooked immediately, and with the guidance of Ashley Wolf, I was able to help future groups of students in this project, as well. Getting to help mentor students made me realize that I really loved helping others in the discovery process, which is where I first thought about teaching and mentoring more seriously. As I continued to mentor students over the next two and a half years, I began doing research in an organic synthetic group with Dr. Peter Norris. Working in the Norris lab gave me an immense appreciation for organic synthesis and methodology, but I knew that my heart was not in "traditional" organic synthesis as most groups were selling their chemistry in 2014. I would have never imagined that I would have been able to return to YSU and work in a professional capacity and as I write this, I am looking forward to this journey with great anticipation.

I would have never applied to Purdue's graduate program without the suggestion from my old labmate and lifetime friend Kyei Baffour. Kwaku convinced me that Purdue would be a good program for both of us and the rest is history. I wish Kyei all the best as he heads to Vanderbilt for his post-doc this summer!

There are many people within Purdue's chemistry department that are integral to my success as a graduate student. One thing that unifies all of these people is that they all put themselves aside to ensure that you can transition into the program, acclimate to a group, research efficiently, and ultimately succeed. It starts when you are accepted into the program and you get your first e-mail from Betty Hatfield. I'm not sure how many people really understand what a massive undertaking a symposium weekend can be, but I think that's because Betty does an outstanding job of organizing this large event. Once you arrive to campus, you would be wise to get acquainted with Rob Reason. On a daily basis, Rob will do whatever it takes to make sure that your time at Purdue is as stress-free as he can make it.

Jeanne Meyer is also of note on this list. I came to this department at a time when Kurt was on his way out [we overlapped for one year] and Jeanne was changing to his coordinator position. I enjoyed the better part of three years working closely with Jeanne when I was a head TA for 25X. Being new to our job titles at the same time always galvanized us and projected us to working to better the undergraduate teaching labs. In this vein, I want to acknowledge Stefan Paula. In addition to Jeanne and myself, Stefan was also in a new role at Purdue and we tackled supervising these lab sections together. I really appreciated how Stefan immediately had the perfect balance of being relaxed and professional in his approach to handling the lab sections. It is something that I hope to emulate in my further endeavors! [Congratulations and best wishes to Stefan at UC-Sacramento, by the way]

My time at Purdue was also made easier by the procurement and business offices within the department. It was overwhelming for me when I first learned of how vast the business office is for Purdue chemistry. It didn't take long for me to learn about how vital these persons were to my time as a graduate student. Specifically, Jane Johanning was my point-person for expense, group purchases, and payroll concerns. Jane was always able to make time to answer my questions whenever I had them. It wasn't much longer until I was ordering my own consumables and chemicals for myself or the group. As one might expect, this gets you acquainted with Darci Decamp and Suzy Gustafson – Darci and Suzy are two of the most helpful and honest people I met within the department and were no doubt crucial to my successes.

Some additional luxuries of being at a large department are the amenities in instrumentation and support staff. From the Amy Facility's Research Instrumentation Center (Pat Bishop), to PINMRF (John Harwood, Jerry Hirschinger), and to the X-ray laboratory (Phil Fanwick, Matt Zeller). Special mention to Matt Zeller, who came with me from YSU to Purdue to fill the role of crystallographer shortly after I started at Purdue.

I would like to also acknowledge all of my committee members for their support throughout the years. In addition to Professors David McMillin, Corey Thompson, and Chris Uyeda, I made a number of great friends and colleagues along the way. I would have to name those which have made significant contributions to my graduate school experience at Purdue; including, but not limited to Dr. John Kiernicki, Dr. Kwaku Kyei-Baffour, Dr. Ian Powers, Adharsh Raghavan, Dr. Talia Steiman, Jake Werth.

On a chemistry note, I am extremely grateful for the pioneering work that the late Jerry Trofimenko has contributed to my own career. Scorpionate ligands have richly enhanced the field of coordination chemistry and catalytic processes. A special mention to the fellow f-block chemists and for the ground work that they laid for f-element complexes which employ scorpionate ligands. The lion's share of this work was reported by Isabel Santos, Keith Bagnall, and Josef Takats – I could not imagine life without Tp^*_2UI!

I certainly could not achieve all of the chemistry and much more without the guidance and mentorship provided by Suzanne. Throughout my five years at Purdue, I was able to focus and harness the mental framework for how I would mentor students and function as a professional in the academic setting. A large part of this idea is certainly influenced by my interactions and experiences in the Scuzanne Catalina Bartolomucci Research Facility for the Enhancement of f-block Advancements.

Music is a large part of my way of keeping sane at work. For a special note, for all that they have done, I will share my eclectic mix of top played artists and bands: Switchfoot, NEEDTOBREATHE, kishibashi, Carly Rae Jepsen, insaneintherainmusic (Carlos Eiene), Amy Grant, Jars Of Clay, Kara Comparetto, and many more.

Finally, I would like to recognize all of the organizations which helped secure funding during my time at Purdue. Purdue University (teaching assistantships, Throckmorton Scholarship, SURF Graduate Mentor Award, Bilsland Fellowship), National Science Foundation (CHE-1149875, CAREER grant to Suzanne C Bart; CHE-1625543, MRI

program; 1665170, grant to SCB; CHE-1039689, Ill. St. Univ. funding for diffractometer), Department of Energy (Division of Chemical Sciences, Geosciences, and Biosciences, Office of Basic Energy Sciences Heavy Element Chemistry program through grants DE-SC0008479 to SCB).

TABLE OF CONTENTS

LIST OF TABLES

LIST OF FIGURES

ABSTRACT

Author: Tatebe, Caleb, J. PhD
Institution: Purdue University
Degree Received: August 2019
Title: Expansion of Low- and Mid-Valent Organometallic Uranium Chemistry
Committee Chair: Suzanne Bart

A series of uranium benzyl compounds supported by two hydrotris(3,5-dimethylpyrazolyl) borate (Tp*) ligands has been synthesized and characterized. In addition to the previously reported Tp*$_2$U(CH$_2$Ph) (**2-Bn**), examinations of both steric (*tert*-butyl, *iso*-propyl) and electronic (methoxy, picolyl) changes on the aromatic ring led to the formula Tp*$_2$U(CH$_2$Ar) (Ar = 4-*tert*-butylphenyl (**2-^{t}Bu**), 4-isopropyl (**2-^{i}Pr**), 2-picolyl (**2-pyr**), 3-methoxyphenyl (**2-OMe**). Treatment of the entire series of benzyl compounds with azidotrimethylsilane results in the formation of a neutral, monomeric U(III) compound, Tp*$_2$U(N$_3$) (**3-N$_3$**), and substituted benzyltrimethylsilane. While there was no observed change in reactivity among the benzyl compounds and Me$_3$SiN$_3$, treatment of these compounds with triphenylphosphine oxide saw unique carbon-carbon coupling occur for three of the substituted benzyl compounds. With a single equivalent of OPPh$_3$, the following products were isolated: Tp*$_2$U[OP(C$_6$H$_5$)(C$_6$H$_5$CH$_2$C$_6$H$_5$)] (**4-Ph**), Tp*$_2$U[OP(C$_6$H$_5$)(C$_6$H$_5$-*p*-*i*PrC$_6$H$_4$)] (**4-^{i}Pr**), Tp*$_2$U[OP(C$_6$H$_5$)(C$_6$H$_5$-*p*-*t*BuC$_6$H$_4$)] (**4-^{t}Bu**), Tp*$_2$U[OP(C$_6$H$_5$)(C$_6$H$_5$-*m*-OCH$_3$C$_6$H$_4$)] (**4-OMe**).

A family of uranium(IV) imido complexes of the form Tp*$_2$U(NR) (R = benzyl (**7-Bn**), *para*-tolyl (**7-Tol**), *para*-methoxyphenyl (**7-OMe**), 2,6-diethylphenyl (**7-detp**), 2,6-diisopropylphenyl (**7-dipp**)) have been generated by bibenzyl extrusion from **2-Bn**. When **7-Bn** and **7-Tol**, along with previously reported Tp*$_2$U(N-Ph) (**7-Ph**) and Tp*$_2$U(N-Ad) (**7-Ad**), are treated with isocyanates or isothiocyanates, they readily undergo [2π+2π]-cycloaddition to generate κ^2-ureato and κ^2-thioureato derivatives, respectively. Use of phenylisoselenocyanate with **7-Tol** and **7-Ph** generates a rare κ^2-selenoureato complex. Treating **7-Tol** and **7-OMe** with benzonitrile or 4-cyanopryidine results in unusual products of multiple bond metathesis, namely κ^1-amidinate U(IV) complexes.

A family of dinuclear bis(Tp*) (Tp* = hydrotris(3,5-dimethylpyrazolyl)borate) uranium compounds with conjugated organic linkers was synthesized to explore possible electronic communication between uranium ions. Trivalent diuranium phenyl alkynyl compounds, Tp*$_2$UCC(1,3-C$_6$H$_4$)CCUTp*$_2$ (**14-*meta***) or Tp*$_2$UCC(1,4-C$_6$H$_4$)CCUTp*$_2$ (**14-*para***), and tetravalent diuranium phenylimido compounds, Tp*$_2$U(N-1,3-C$_6$H$_4$-N)UTp*$_2$ (**15-*meta***) and Tp*$_2$U(N-1,4-C$_6$H$_4$-N)UTp*$_2$ (**15-*para***), were generated from trivalent Tp*$_2$UCH$_2$Ph. All compounds were fully characterized both spectroscopically and structurally. The electronic structures of all derivatives were interrogated using magnetic measurements, electrochemistry, and were the subject of computational analyses. All of this data combined established that little electronic communication exists between the uranium centers in these trivalent and tetravalent diuranium molecules.

Uranium mono(imido) species have been prepared via oxidation of Cp*U(^{Mes}PDI^{Me})(THF) (**16-Cp***) and [Cp^{P}U(^{Mes}PDI^{Me})]$_2$ (**16-Cp^P**) (Cp* = η^5-1,2,3,4,5-pentamethylcyclopentadienide; Cp^P = 1-(7,7-dimethylbenzyl)cyclopentadienide; ^{Mes}PDI^{Me} = 2,6-((Mes)N=CMe)$_2$C$_5$H$_3$N, Mes = 2,4,6-trimethylphenyl) with organoazides. Treating either with N$_3$DIPP formed uranium(IV) mono(imido) complexes, Cp^{P}U(NDIPP)(^{Mes}PDI^{Me}) (**17-Cp^P**) and Cp*U(NDIPP)(^{Mes}PDI^{Me}) (**17-Cp***), featuring reduced [^{Mes}PDI^{Me}]$^{1-}$. Addition of electron-donating 1-azidoadamantane (N$_3$Ad) to **16-Cp*** generated a dimeric product, [Cp*U(NAd)(^{Mes}HPDI^{Me})]$_2$ (**18**), from radical coupling at the *para*-pyridine position of the pyridine(diimine) ligand and H-atom abstraction, formed through a monomeric intermediate that was observed in solution but could not be isolated. To support this, Cp*U(^{t}Bu-^{Mes}PDI^{Me})(THF) (**16-^{t}Bu**), which has a *tert*-butyl group protecting the *para*-position, was also treated with N$_3$Ad, and the monomeric product, Cp*U(NAd)(^{t}Bu-^{Mes}PDI^{Me}) (**17-^{t}Bu**), was isolated. All isolated complexes were analyzed spectroscopically and structurally, and dynamic solution behavior was examined using electronic absorption spectroscopy.

CHAPTER 1. SYNTHESIS AND REACTIVITY OF URANIUM(III) BENZYL COMPOUNDS

1.1 Abstract

A series of uranium benzyl compounds supported by two hydrotris(3,5-dimethylpyrazolyl) borate (Tp*) ligands has been synthesized and characterized. In addition to the previously reported Tp*$_2$U(CH$_2$Ph) (**2-Bn**), examinations of both steric (*tert*-butyl, *iso*-propyl) and electronic (methoxy, picolyl) changes on the aromatic ring led to the formula Tp*$_2$U(CH$_2$Ar) (Ar = 4-*tert*-butylphenyl (**2-^{t}Bu**), 4-isopropyl (**2-^{i}Pr**), 2-picolyl (**2-pyr**), 3-methoxyphenyl (**2-OMe**). This family of compounds were prepared via salt metathesis between Tp*$_2$UI (**1-I**) and their respective substituted benzyl potassium compounds. Treatment of the entire series of benzyl compounds with azidotrimethylsilane results in the formation of a neutral, monomeric U(III) compound, Tp*$_2$U(N$_3$) (**3-N$_3$**), and substituted benzyltrimethylsilane. While there was no observed change in reactivity among the benzyl compounds and Me$_3$SiN$_3$, treatment of these compounds with triphenylphosphine oxide saw unique carbon-carbon coupling occur for three of the substituted benzyl compounds. With a single equivalent of OPPh$_3$, the following products were isolated: Tp*$_2$U[OP(C$_6$H$_5$)(C$_6$H$_5$CH$_2$C$_6$H$_5$)] (**4-Ph**), Tp*$_2$U[OP(C$_6$H$_5$)(C$_6$H$_5$-*p*-*i*PrC$_6$H$_4$)] (**4-^{i}Pr**), Tp*$_2$U[OP(C$_6$H$_5$)(C$_6$H$_5$-*p*-*t*BuC$_6$H$_4$)] (**4-^{t}Bu**), Tp*$_2$U[OP(C$_6$H$_5$)(C$_6$H$_5$-*m*-OCH$_3$C$_6$H$_4$)] (**4-OMe**). Using different phosphine oxide starting materials, namely tris(*p*-tolyl)phosphine oxide, affords a similar carbon-carbon coupled product, Tp*$_2$U[OP(*p*-tolyl)(C$_6$H$_4$(CH$_3$)CH$_2$C$_6$H$_5$)] (**4-tolyl**). All complexes have been characterized by ^{1}H, ^{11}B NMR, IR, and electronic absorption spectroscopies. Structural parameters for compounds were determined using X-ray crystallography.

1.2 Introduction

The field of organouranium chemistry has been of interest since the mid-twentieth century, when such compounds were predicted to be useful for isotope separation due to their presumed increased volatility.[1, 2] While uranium alkyls did not prove their versatility in this realm, these species have been of fundamental interest for comparison to their transition metal counterparts, with most of the strides being made for uranium(IV) derivatives.[3-7] More recently, new synthetic methodologies have allowed access to tri-, penta-, and hexavalent analogues.[8]

The actinides are suitable elements to activate inert molecules such as triphenylphosphine oxide, as they are highly reducing and oxophilic metals. Early actinides in particular regularly perform one electron chemistry, driven by their available redox couples. This is especially true for uranium, the most studied of all the actinides in organometallic chemistry,[9, 10] which has been shown to routinely reduce small, oxygenated organic molecules. Low-valent uranium species in particular have routinely been observed to generate and/or support organic radicals in solution.[11-14] For instance, Meyer and coworkers have demonstrated that treating [((^{Ad}ArO)$_3$tacn)U^{III}] ((^{Ad}ArO)$_3$tacn = 1,4,7-tris(3-adamantyl-2-hydroxy-5-*tert*-butylbenzyl)-1,4,7-triazacyclononane) with benzophenone generates a fleeting ketyl radical complex, [((^{Ad}ArO)$_3$tacn)U^{IV}(OC•Ph$_2$)], that head-to-tail *para*-couples, forming the Gomberg dimer derivative [((^{Ad}ArO)$_3$tacn)U^{IV}(OCPhPh−CPh$_2$O)U^{IV}((^{Ad}ArO)$_3$tacn)].[12] More recently, the Schelter group reported activation of N,N-dimethylbenzamide by U(N(SiMe$_3$)$_2$)$_3$, which forms tetravalent, charge separated U[OC•(Ph)(NMe$_2$)][N(SiMe$_3$)$_2$]$_3$, which features the first stabilized amide radical.[15]

Efforts in our group have focused on the synthesis, characterization and reactivity of organouranium species in the +3[16-18] and +4[19, 20] oxidation states. In regard to the former, we have demonstrated that utilizing sterically demanding hydrotris(3,5-dimethylpyrazolyl)borate (Tp*) ligands allows divergence from the bulky –CH(SiMe$_3$)$_2$ group,[4, 21-23] which is typically used for U(III), effectively supporting benzyl,[17, 24] neosilyl,[17] and methyl[17] substituents. In the latter case, we have shown that when uranium(IV) centers are benzylated, such species are stable in their homoleptic form, with no bulky ancillary ligands required due to the increased hapticity (η^4) of the benzyl group,

which saturates the coordination sphere.[19, 25, 26] These homoleptic compounds are even tolerant to ring substitution, facilitating isolation of the *p*-^{i}Pr, *p*-^{t}Bu, *m*-OMe, *o*-OMe, and *o*-picoline derivatives.[19] In this study, we sought to combine these systems to determine if the bis(Tp*) uranium(III) derivatives were also tolerant to the same ring substitution, given that uranium(III) is more electron rich and alkyl ligands are generally more reactive towards decomposition pathways. To this end, we employed substituted benzylpotassium salts, KCH_2Ph' (Ph' = *p*-^{i}PrPh, *p*-^{t}BuPh, *m*-OMePh, *o*-picolyl),[19] to generate this new family. These trivalent derivatives were stable and resulted in useful synthons, as treating these members with N_3SiMe_3 afforded $Tp^*_2UN_3$, which is the first monomeric, neutral, trivalent azide derivative for the actinides.

The Tp* ligand framework has been useful in isolating uranium(III) complexes featuring ligand radicals.[13] Treating trivalent $Tp^*_2U(CH_2Ph)$ (**2-Bn**), which serves as a source of $[Tp^*_2U]$, with an equivalent of benzophenone forms $Tp^*_2U(OC\bullet Ph_2)$,[27] which was characterized to contain a uranium(III) ion with one-electron reduced benzophenone. Formation of this species is attributed to the oxophilicity and reducing nature of uranium, which performs an electron transfer after initial benzophenone coordination creating a strong, anionic U-O bond.[27] The large bis(Tp*) framework prevents further coupling chemistry at the ligand radical, which is in contrast to the observation by Meyer. Based on this exciting result, we hypothesized that other oxygenated substrates could be activated in a one-electron process. We report the reactivity of a series of trivalent uranium benzyl species, both with and without *para*-substitution, with triphenylphosphine oxides. Rather than an isolable ligand radical, coupling of the benzyl group with the *para*-carbon of triphenylphosphine oxide was noted, contrasting our previous results with benzophenone in which the benzyl radical was extruded as bibenzyl. Full spectroscopic and structural characterization has been used to elucidate these interesting new structures from this unusual activation of $OPPh_3$.

1.3 Experimental

1.3.1 General Considerations

Air- and moisture-sensitive manipulations were carried out using standard Schlenk techniques or in an MBraun inert atmosphere drybox with an atmosphere of purified nitrogen. The MBraun drybox is equipped with a cold well designed for freezing samples as low as liquid nitrogen, as well as two -35 °C freezers for sample storage and crystallizations. Solvents (THF, pentane, toluene, diethyl ether) were dried and deoxygenated based on literature procedures using a Seca solvent purification system.[28] Benzene-d_6 was purchased from Cambridge Isotope Laboratories, dried with molecular sieves and sodium, and degassed by three freeze-pump-thaw cycles. Azidotrimethylsilane (Acros Organics), 1,4-cyclohexadiene (Sigma-Aldrich), 9,10-dihydroanthracene (Sigma-Aldrich), triphenylborane (Alfa Aesar), and triphenylphosphine oxide (Sigma-Aldrich) were purchased from commercial sources. Azidotrimethylsilane and 1,4-cyclohexadiene were degassed by three freeze-pump-thaw cycles and passed over an alumina plug before use. 9,10-dihydroanthracene was sublimed before use. Triphenylborane and triphenylphosphine oxide were dried before use. Benzylpotassium salts,[19] substituted tris(aryl)phosphine oxides,[29] $UI_3(THF)_4$,[30] Tp^*_2UI (**1-I**),[31] and Tp^*_2UBn (**2-Bn**)[24] were prepared using literature methods.

^1H, and ^{11}B NMR spectra were recorded on a Varian Inova 300 spectrometer operating at frequencies of 299.992 and 96.24 MHz, respectively. ^{31}P NMR spectra were recorded on a Mercury 300 spectrometer operating at a frequency of 121.43 MHz. All chemical shifts are reported relative to the peak for $SiMe_4$, using ^1H residual chemical shifts of C_6D_6 (7.16 ppm) as a secondary standard. ^{11}B chemical shifts are reported relative to the peak for $BF_3{\cdot}(Et_2O)$ (0.0 ppm). ^{31}P chemical shifts are reported relative to the peak for 85% H_3PO_4 in C_6D_6 (0.0 ppm). Spectra for paramagnetic molecules were obtained by using an acquisition time of 0.5 s, thus the peak widths reported have an error of ±2 Hz. For paramagnetic molecules, the ^1H NMR data are reported with the chemical shift, peak width at half-height (in Hz), integration value, and where possible, the peak assignment. Pulse-field gradient COSY spectra were obtained using a Bruker AV-III-HD spectrometer with a 5mm Z-gradient BBFO probe with an operating frequency at 400.17 MHz. Spectra were acquired using 20000 Hz sweep widths in both dimensions. In F2, 4 scans per increment

using 4096 data points and a relaxation delay of 1 second. In F1, 8 increments were acquired. The raw data were Fourier transformed into a final data matrix consisting of 4K points in F2 and 2K points in F1. Elemental analyses were performed by Midwest-Microlab, LLC (Indianapolis, Indiana). Solid-state infrared spectra were recorded using a Thermo Nicolet 6700 spectrophotometer with samples made by crushing the solids, mixing with dried KBr, and pressing into a pellet. Electronic absorption spectroscopic measurements were recorded at ambient temperature in dry solvent using sealed 1 cm quartz cuvettes with a Cary 6000i UV-Vis-NIR spectrophotometer.

Single crystals of **5-THF** suitable for X-ray diffraction were coated with poly(isobutylene) oil in a glovebox and quickly transferred to the goniometer head of a Rigaku Rapid II image plate diffractometer equipped with a MicroMax002+ high intensity copper X-ray source with confocal optics. Preliminary examination and data collection were performed with Cu Kα radiation (λ = 1.54184 Å). Single crystals of **2-^{i}Pr**, **2-^{t}Bu × 1-I**, and **2-pyr** were transferred to the goniometer head of a Bruker AXS D8 Quest diffractometer and analyzed at 100 K using monochromatic Mo Kα radiation (λ = 0.71073 Å) with the omega scan technique. Crystals of **2-OMe**, **3-N$_3$**, **4-OMe**, and **4-^{i}Pr** were transferred to the goniometer head of a Bruker AXS D8 Quest diffractometer and analyzed at 100 K using monochromatic Cu Kα radiation (λ = 1.54184 Å) with the omega scan technique. Crystals of **4-Ph** were transferred to the goniometer head of a Bruker AXS ApexII CCD diffractometer with a sealed tube fine focus X-ray tube and an Oxford Cryosystems low temperature device. Examination and data collection were performed with Mo Kα radiation (λ = 0.71073 Å). Data were collected, unit cells determined, and the data integrated and corrected for absorption and other systematic errors using the Apex2 or Apex3 suites of programs. The space groups were assigned and the structures were solved by direct methods using XPREP within the SHELXTL suite of programs and refined by full matrix least squares against F^2 with all reflections using Shelxl 2014 or Shelxl 2017[32] and the graphical interface Shelxle. Complete crystallographic data, in CIF format, have been deposited with the Cambridge Crystallographic Data Centre.

1.3.2 General synthesis for Tp*$_2$U(III) alkyl compounds.

A 20 mL scintillation vial was charged with Tp*$_2$UI (**1-I**) (0.500 g, 0.521 mmol) in 10 mL THF. To this stirring purple solution, an excess of substituted benzyl potassium salt (KCH_2-*p*-^{i}PrPh: 0.112 g, 0.652 mmol; KCH_2-*p*-^{t}BuPh: 0.121 g, 0.652 mmol; KCH_2-*m*-OMePh: 0.104 g, 0.652 mmol; KCH_2pyr: 0.085 g, 0.652 mmol) was added. The color of the solution became dark green after 2 h, the green solution was filtered over Celite, and volatiles were subsequently removed *in vacuo*. The resulting green powders were then washed with *n*-pentane (2 × 5 mL) and dried to afford dark green solids identified as **2-*p*-^{i}Pr** (0.458 g, 0.474 mmol, 91% yield), **2-*p*-^{t}Bu** (0.434 g, 0.443 mmol 85% yield), **2-*m*-OMe** (0.417 g, 0.438 mmol, 84% yield), or **2-*o*-Picolyl** (0.424 g, 0.459 mmol, 88% yield). Single crystals suitable for X-ray analysis were grown from a concentrated THF solution (**2-*p*-^{i}Pr**) or diffusion of a concentrated diethyl ether solution into toluene (**2-*p*-^{t}Bu** ,**2-*m*-OMe**, **2-*o*-Picolyl**) stored at -35 °C.

2-*p*-^{i}Pr: Elemental analysis of $C_{40}H_{57}B_2N_{12}U$, Calculated: C, 49.75; H, 5.95; N, 17.41. Found: C, 49.86; H, 5.93; N, 17.02. ^{1}H NMR (C_6D_6, 25 ºC): δ (ppm) = -11.19 (24, 18H, Tp*-C*H*$_3$), -2.77 (5, 18H, Tp*-C*H*$_3$), 0.30 (23, 2H, B-*H*), 5.70 (4, 6H, ^{i}Pr-C*H*$_3$), 7.25 (5, 6H, Tp*-C*H*), 9.93 (6, 1H, ^{i}Pr-C*H*), 17.82 (17, 2H, *meta*-C*H*), 24.42 (4, 2H, -C*H*$_2$), 26.59 (24, 2H, *ortho*-C*H*). ^{11}B NMR (C_6D_6, 25 ºC): δ (ppm) = -15.6. IR (KBr): $\nu_{B\text{-}H}$ = 2544, 2521 cm^{-1}.

2-*p*-^{t}Bu: Elemental analysis of $C_{41}H_{59}B_2N_{12}U$ was not performed due to co-crystallization of **1-I**. ^{1}H NMR (C_6D_6, 25 ºC): δ (ppm) = -11.29 (23, 18H, Tp*-C*H*$_3$), -2.88 (4, 18H, Tp*-C*H*$_3$), -0.03 (3, 2H, B-*H*), 5.69 (2, 9H, C(C*H*$_3$)$_3$), 7.13 (4, 6H, Tp*-C*H*), 17.89 (71, 2H, *o*-/*m*-C*H*), 24.72 (3, 2H, -C*H*$_2$), 26.48 (26, 1H, *m*-/*o*-C*H*). ^{11}B NMR (C_6D_6, 25 ºC): δ (ppm) = -15.4. IR (KBr): 2545, 2523 $\nu_{B\text{-}H}$ = cm^{-1}.

2-*m*-OMe: Elemental analysis of $C_{38}H_{53}B_2N_{12}OU$, Calculated: C, 47.86; H, 5.60; N, 17.63. Found: C, 47.37; H, 5.58; N, 17.42. ^{1}H NMR (C_6D_6, 25 ºC): δ (ppm) = -11.31 (23, 18H, Tp*-C*H*$_3$), -2.79 (14, 18H, Tp*-C*H*$_3$), -0.07 (3, 2H, B-*H*), 7.15 (6, 6H, Tp*-C*H*), 7.86 (4, 3H, -OC*H*$_3$), 10.49 (5, 1H, *o*-/*p*-C*H*), 17.37 (8, 1H, *o*-/*p*-C*H*), 20.98 (1, 2H, -C*H*$_2$), 24.90 (24, 1H, *m*-/*o*-C*H*), 27.29 (26, 1H, *m*-/*o*-C*H*). ^{11}B NMR (C_6D_6, 25 ºC): δ (ppm) = -14.0. IR (KBr): $\nu_{B\text{-}H}$ = 2556, 2522 cm^{-1}.

2-*o*-Picolyl: Elemental analysis of $C_{36}H_{50}B_2N_{13}U$, Calculated: C, 46.77; H, 5.45; N, 19.70. Found: C, 46.71; H, 5.42; N, 19.06. ^{1}H NMR (C_6D_6, 25 ºC): δ (ppm) = -27.65 (19, 3H, Tp*-C*H*$_3$), -23.68 (21, 3H, Tp*-C*H*$_3$), -11.78 (14, 3H, Tp*-C*H*$_3$), -11.33 (13, 3H, Tp*-C*H*$_3$), -5.56 (3, 2H, -C*H*$_2$pyr), -3.84 (7, 3H, Tp*-C*H*$_3$), -2.22 (22, 3H, Tp*-C*H*$_3$), -0.10 (7, 3H, Tp*-C*H*$_3$), 0.02 (7, 1H, Tp*-C*H*), 0.33 (7, 3H, Tp*-C*H*$_3$), 1.31 (7, 3H, Tp*-C*H*$_3$), 1.40 (16, 1H, Tp*-C*H*), 2.71 (7, 3H, Tp*-C*H*$_3$), 3.58 (15, 1H, *p*-C*H*), 3.87 (16, 3H, Tp*-C*H*$_3$), 4.37 (8, 1H, Tp*-C*H*), 7.45 (8, 1H, Tp*-C*H*), 8.58 (16, 1H, Tp*-C*H*), 10.86 (8, 1H, Tp*-C*H*), 10.98 (18, 3H, Tp*-C*H*$_3$), 11.47 (8, 1H, Tp*-C*H*), 15.53 (8, 1H, *m*-C*H*), 16.35 (8, 1H, *m*-C*H*), 17.43 (35, 1H, *o*-C*H*), 39.71 (26, 1H, Tp*-C*H*). ^{11}B NMR (C_6D_6, 25 ºC): δ (ppm) = -13.1, 2.9. IR (KBr): $\nu_{B\text{-}H}$ = 2555, 2519 cm^{-1}.

1.3.3 Synthesis of Tp*$_2$U(N$_3$) (**3-N$_3$**).

A 20 mL scintillation vial was charged with **2-CH$_2$Ph'** (**2-CH$_2$Ph**: 0.300 g, 0.325 mmol; **2-*p*-^{i}Pr**: 0.345 g, 0.357 mmol; **2-*p*-^{t}Bu**: 0.200 g, 0.204 mmol; **2-*m*-OMe**: 0.200 g, 0.210 mmol; **2-*o*-Picolyl**: 0.200 g, 0.216 mmol) in 8 mL THF. To this dark green solution, azidotrimethylsilane (**2-CH$_2$Ph**: 32.5 μL; **2-*p*-^{i}Pr**: 35.7 μL; **2-*p*-^{t}Bu**: 20.4 μL; **2-*m*-OMe**: 21.0 μL; **2-*o*-Picolyl**: 21.6 μL) was added *via* μsyringe and the solution immediately became blue-green. After 30 min, volatiles were removed *in vacuo*, affording a blue powder. This crude product was washed with *n*-pentane (4 × 5 mL) and dried again. This resulted in a blue powder (**2-CH$_2$Ph**: 0.236 g, 0.270 mmol, 83% yield; **2-*p*-^{i}Pr**: 0.242 g, 0.275 mmol, 77%; **2-*p*-^{t}Bu**: 0.112 g, 0.128 mmol, 63%; **2-*m*-OMe**: 0.166 g, 0.190 mmol, 91%; **2-*o*-Picolyl**: 0.152 g, 0.174 mmol, 80%) assigned as Tp*$_2$UN$_3$ (**3-N$_3$**).

Elemental analysis of $C_{59}H_{74}B_2N_{15}U$, Calculated: C, 57.25; H, 6.03; N, 13.58. Found C, 56.82; H, 5.93; N, 13.58. ^{1}H NMR (C_6D_6, 25 ºC): δ (ppm) = -15.00 (43, 18H, Tp*-C*H*$_3$), 1.28 (17, 18H, Tp*-C*H*$_3$), 7.67 (20, 6H, Tp*-C*H*), 10.12 (5, 2H, B-*H*). ^{11}B NMR (C_6D_6, 25 ºC): δ (ppm) = 10.6. IR (KBr): $\nu_{B\text{-}H}$ = 2558, 2523 cm^{-1}; ν_{N3} = 2073 cm^{-1}.

1.3.4 Synthesis of Tp*$_2$U[OP(C_6H_5)$_2$($C_6H_5CH_2$R)] (**4-R**).

A 20 mL scintillation vial was charged with Tp*$_2$U alkyl (**2-Bn**: 0.300 g, 0.325 mmol; **2-^{i}Pr**: 0.351 g, 0.363 mmol; **2-^{t}Bu**: 0.100 g, 0.102 mmol; **2-OMe**: 0.200 g, 0.208 mmol) in 7 mL THF. In a separate vial, one equivalent $OPPh_3$ (**2-Bn**: 0.090 g, 0.324 mmol; **2-^{i}Pr**: 0.101 g, 0.363 mmol; **2-^{t}Bu**: 0.028 g, 0.102 mmol; **2-OMe**: 0.058 g, 0.208 mmol) was dissolved in 3 mL THF. The $OPPh_3$ solution was added to the stirring alkyl solution. A color change from green to brown was observed (**2-Ph**: 5 min; **2-^{i}Pr**: 15 min; **2-^{t}Bu**: 30 min; **2-OMe**: 5 min). After additional stirring (**2-Ph**: 40 min; **2-^{i}Pr**: 35 min; **2-^{t}Bu**: 60 min; **2-OMe**: 35 min), volatiles were removed *in vacuo*, leaving a brown powder. Washing with *n*-pentane (3 × 5 mL) and drying afforded brown powders identified as Tp*$_2$U[OP(C_6H_5)$_2$($C_6H_5CH_2C_6H_5$)] (**4-Ph**) (0.368 g, 0.306 mmol, 94%), Tp*$_2$U[OP(C_6H_5)$_2$($C_6H_5CH_2$-*p*-^{i}PrC_6H_4)] (**4-^{i}Pr**) (0.397 g, 0.319 mmol, 87%), Tp*$_2$U[OP(C_6H_5)$_2$($C_6H_5CH_2$-*p*-^{t}BuC_6H_4)] (**4-^{t}Bu**) (0.102 g, 0.080 mmol, 80%) and Tp*$_2$U[OP(C_6H_5)$_2$($C_6H_5CH_2$-*m*-$OCH_3C_6H_4$)] (**4-OMe**) (0.249 g, 0.202 mmol, 96%). Single X-ray-quality crystals of **4-Ph** and **4-^{i}Pr** were obtained from a concentrated toluene solution layered with pentane stored at -35 ºC. Single X-ray quality crystals of **4-OMe** were obtained from the diffusion of hexamethyldisiloxane into a concentrated toluene solution.

4-Ph: Elemental analysis of $C_{55}H_{66}B_2N_{12}OPU$, Calculated: C, 54.97; H, 5.54; N, 13.99. Found: C, 54.59; H, 5.52; N, 13.89. ^{1}H NMR (C_6D_6, 25 ºC): δ (ppm) = -16.06 (58, 18H, Tp*-C*H*$_3$), 0.61 (6, 18H, Tp*-C*H*$_3$), 1.91 (6, d, 2H, benzyl-C*H*$_2$), 5.40 (16, 2H, cyclohexadiene-C*H)*, 6.16 (d, 2H, benzyl-*o/m*-C*H*, *J* =5.8 Hz), 6.37 (d, 2H, benzyl-*o/m*-C*H*, *J* = 6.4 Hz), 7.01 (19, 1H, *p*-phenyl-C*H*), 7.45 (10, 6H, Tp*-C*H*), 7.75 (33, 1H, cyclohexadiene-C*H*), 8.37 (840, 2H, Tp*-B*H*), 10.51 (t, 2H, *p*-phenyl-C*H*, *J* = 6.2 Hz), 10.78 (14, 4H, *o/m*-phenyl-C*H*), 15.15 (104, 2H, cyclohexadiene-C*H*), 21.72 (39, 4H, *o/m*-phenyl-C*H*). ^{11}B NMR (C_6D_6, 25 ºC): δ (ppm) = 7.2. ^{31}P NMR (C_6D_6, 25 ºC): δ (ppm) = 84.77. IR (KBr): ν_{B-H} = 2553, 2526 cm^{-1}.

4-^{i}Pr: Elemental analysis of $C_{58}H_{72}B_2N_{12}OPU$, Calculated: C, 56.00; H, 5.83; N, 13.51. Found: C, 55.52; H, 5.81; N, 13.89. ^{1}H NMR (C_6D_6, 25 ºC): δ (ppm) = -16.12 (63, 18H, Tp*-C*H*$_3$), 0.62 (6, 24H, Tp*-C*H*$_3$+*i*Pr-C*H*$_3$), 1.94 (8, d, 2H, benzyl C*H*$_2$, *J* = 5.6 Hz), 2.16 (m, 1H, ^{i}Pr-C*H*), 5.42 (16, 2H, cyclohexadiene-C*H)*, 6.12 (d, 2H, benzyl-*m*-C*H*,

J = 8.0 Hz), 6.24 (6, 2H, benzyl-*o*-C*H*, *J* = 8.1 Hz), 7.45 (12, 6H, Tp*-C*H*), 7.73 (23, 1H, cyclohexadiene-C*H*), 8.51 (130, 2H, Tp*-B*H*), 10.54 (t, 2H, *p*-phenyl-C*H*, *J* = 6.3 Hz), 10.81 (d, 4H, *o/m*-phenyl-C*H*, *J* = 6.0 Hz), 15.20 (99, 2H, cyclohexadiene-C*H*), 21.80 (53, 4H, *o/m*-phenyl-C*H*). ^{11}B NMR (C_6D_6, 25 ºC): δ (ppm) = 7.1. ^{31}P NMR (C_6D_6, 25 ºC): δ (ppm) = 83.78. IR (KBr): ν_{B-H} =2552, 2524 cm^{-1}.

4-^{t}Bu: Due to the presence of small amounts Tp*$_2$UI in this compound, reliable elemental analysis was not possible. This species does not affect the overall outcome of the reaction. ^{1}H NMR (C_6D_6, 25 ºC): δ (ppm) = -16.06 (65, 18H, Tp*-CH_3), 0.62 (7, 18H, Tp*-CH_3), 0.72 (s, 9H, *t*Bu-CH_3), 1.98 (d, 2H, benzyl-CH_2, J = 6.4 Hz), 5.41 (12, 2H, cyclohexadiene-C*H*), 6.18 (12, 2H, benzyl-o/m-C*H*, J = 8.2 Hz), 6.42 (d, 2H, benzyl-o/m-C*H*, J = 8.2 Hz), 7.44 (44, 6H, Tp*-C*H*), 8.42 (5, Tp*-B*H*), 10.53 (17, 2H, *p*-phenyl-C*H*, J = 6.3 Hz), 10.80 (d, 4H, *o*/*m*-phenyl-C*H*, J = 6.0 Hz), 15.18 (60, 2H, cyclohexadiene-C*H*), 21.75 (184, 4H, *o*/*m*-phenyl-C*H*). ^{11}B NMR (C_6D_6, 25 ºC): δ (ppm) = 6.8. ^{31}P NMR (C_6D_6, 25 ºC): δ (ppm) = 83.28. IR (KBr): ν_{B-H} = 2550, 2519 cm^{-1}.

4-OMe: Elemental analysis of $C_{56}H_{68}B_2N_{12}OPU$, Calculated: C, 55.32; H, 5.64, N, 13.82. Found: C, 53.9; H, 5.77; N, 13.31. Reliable elemental analysis of this compounds was not possible, likely a result of incomplete combustion.. ^{1}H NMR (C_6D_6, 25 ºC): δ (ppm) = -16.04 (548, 18H, Tp*-CH_3), 0.61 (6, 18H, Tp*-CH_3) 1.99 (12, d, 2H, benzyl-CH_2), 2.64 (2, 3H, benzyl-*m*-OCH_3), 5.44 (399, 2H, cyclohexadiene-C*H*), 5.84 (6, 2H, benzyl-*m*-C*H)*, 6.08 (6, 2H, benzyl-*o*-C*H* + benzyl-*o*/*p*-C*H*), 6.17 (15, 1H, cyclohexadiene-C*H*), 6.30 (t, 1H, benzyl-*m*-C*H*, *J* = 8.1 Hz) 7.44 (10, 6H, Tp*-C*H*), 8.43 (1306, 2H, Tp*-B*H*), 10.50 (t, 2H, *p*-phenyl-C*H*, *J* = 6.3 Hz), 10.76 (d, 4H, *o/m*-phenyl-C*H*, *J* = 6.0 Hz), 15.16 (49, 2H, cyclohexadiene-C*H*), 21.68 (39, 4H, *o/m*-phenyl-C*H*). ^{11}B NMR (C_6D_6, 25 ºC): δ (ppm) = 7.4. ^{31}P NMR (C_6D_6, 25 ºC): δ (ppm) = 84.71. IR (KBr): ν_{B-H} =2552, 2524 cm^{-1}.

1.3.5 Synthesis of of Tp*$_2$U[OP(*p*-tolyl)$_2$(C_6H_4(CH_3)$CH_2C_6H_5$)] (**4-tolyl**).

To a 20 mL scintillation vial, **2-Bn** (0.300 g, 0.325 mmol) was dissolved in 7 mL THF. In a separate vial, OP(*p*-tolyl)$_3$ (0.104 g, 0.325 mmol) was dissolved in 3 mL THF. The phosphine oxide was added to the stirring green benzyl solution and a color change was seen within 25 minutes to brown. After an additional 60 minutes, volatiles were

removed *in vacuo*, affording a brown powder. The crude product was washed with *n*-pentane (3 × 2 mL) and dried yielding brown powder (0.387 g, 0.314 mmol, 97%) assigned as Tp*$_2$U[OP(*p*-tolyl)$_2$(C$_6$H$_4$(CH$_3$)CH$_2$C$_6$H$_5$)] (**4-tolyl**).

^{1}H NMR (C$_6$D$_6$, 25 ºC): δ (ppm) = -16.19 (89, 18H, Tp*-C*H*$_3$), 0.76 (7, 18H, Tp*-C*H*$_3$), 0.79 (d, 6H, tolyl-C*H*$_3$, *J* = 7.6 Hz), 1.94 (2, 2H, benzyl C*H*$_2$), 4.26 (d, 6H, tolyl-C*H*3), 5.33 (d, 2H, cyclohexadiene-C*H*, *J* = 6.8 Hz*)*, 6.50 (m, 3H, benzyl-*o/m*-C*H* & benzyl-*p*-C*H*), 6.70 (d, 2H, benzyl-*o/m*-C*H*, *J* = 5.9 Hz), 7.45 (12, 6H, Tp*-C*H*), 8.77 (2, Tp*-B*H*), 10.70 (8, 2H, *p*-phenyl-C*H*), 10.71 (14, 4H, *o/m*-phenyl-C*H*), 15.27 (21, 2H, cyclohexadiene-C*H*), 21.56 (42, 4H, *o/m*-phenyl-C*H*). ^{11}B NMR (C$_6$D$_6$, 25 ºC): δ (ppm) = 7.76. 31P NMR (C$_6$D$_6$, 25 ºC): δ (ppm) = 86.52. Elemental analysis of C$_{58}$H$_{72}$B$_2$N$_{12}$OUP, Calculated: C 56.00; H 5.83; N 13.51. Found: 54.97; H 5.67; N 12.37. Reliable elemental analysis of this compounds was not possible, likely a result of incomplete combustion.

1.3.6 Synthesis of Tp*$_2$U[THF][BnBPh$_3$] (**5-THF**).

A 20 mL scintillation vial was charged with **2-Bn** (0.200 g, 0.217 mmol) in 4 mL THF. To this dark green solution, triphenylborane (0.026 g, 0.217 mmol) was added by difference and the solution immediately became translucent blue. After 30 min, volatiles were removed in vacuo, affording a blue oil. This oil was washed with *n*-pentane (5 × 5 mL) and dried again. This resulted in a blue powder (0.241 g, 0.195 mmol, 90% yield) assigned as Tp*$_2$U(THF)(BnBPh$_3$) (**5-THF**).

Elemental analysis of C$_{59}$H$_{73}$B$_3$N$_{12}$OU, Calculated: C 57.00; H 5.95; N 13.59. Found: 56.82; H 5.93; N 13.58. ^{1}H NMR (C$_6$D$_6$, 25 ºC): δ (ppm) = -11.95 (36, 18H, Tp*-C*H*$_3$), 0.32 (10, 18H, Tp*-C*H*$_3$), 1.42 (4, 4H, THF-C*H*$_2$), 3.58 (9, 4H, THF-C*H*$_2$), 7.42 (8, 6H, Tp*-C*H*). IR (KBr): ν_{B-H} =2552, 2520 cm^{-1}.

1.4 Results and Discussion

1.4.1 Synthesis of U(III) Benzyl Complexes

In an effort to better understand the limits of uncommon U(III) alkyl compounds, the use of substituted benzyl potassium salts from our group's previous report was targeted.[19] Using an adapted approach from the synthesis of Tp*$_2$UBn (**2-Bn**), an excess (1.2 equiv) of substituted benzyl potassium salts, KCH$_2$Ar (Ar = *p*-^{i}PrPh, *p*-^{t}BuPh, *m*-

OMePh, *o*-picolyl), were added to a THF solution of Tp*$_2$UI (**1-I**). For each instance, a color change from dark purple to dark green was observed within minutes of KCH_2Ar addition (Figure 1.1).

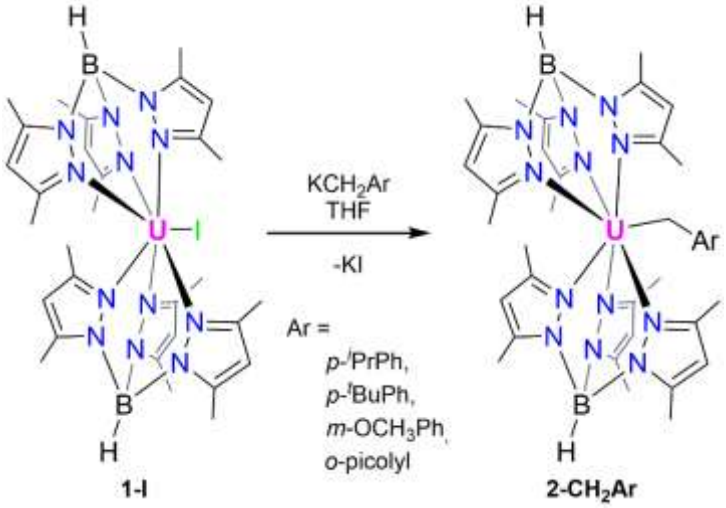

Figure 1.1. Synthesis of **2-CH$_2$Ar** from **1-I**.

The reaction mixture was worked up after two hours of stirring and green powders were isolated and assigned as Tp*$_2$U(CH$_2$Ar) (Ar = 4-^{i}PrPh (**2-^{i}Pr**), 4-^{t}BuPh (**2-^{t}Bu**), 3-OMePh (**2-OMe**), 2-picolyl (**2-pyr**)) by ^{1}H NMR spectroscopy. Interestingly, **2-^{i}Pr**, **2-^{t}Bu**, and **2-OMe** all have a paramagnetically broadened spectrum, with the appropriate number of resonances and their corresponding integration values for C_{2v} symmetry. Using the reported ^{1}H NMR spectrum as a guide, the diagnostic peak for the newly-prepared benzyl compounds is the methylene resonances, as they are the closest protons to the metal center (**2-^{i}Pr**: 24.42 ppm; **2-^{t}Bu**: 24.72 ppm; **2-OMe**: 20.98 ppm). Assessment by ^{11}B NMR spectroscopy displays a single chemical shift (**2-^{i}Pr** = -15.6 ppm; **2-^{t}Bu** = -15.4 ppm; **2-OMe** = -14.0 ppm) which is consistent with the previously reported shift for **2-Bn** (-15.4 ppm).[33] The ^{1}H NMR spectrum of **2-pyr** was a more complicated, C_1 symmetric spectrum, unlike the others in the family. This difference can be attributed to the coordination of the nitrogen atom of the picoline ring, which is similar bonding to the U(IV) homoleptic complex. Each of the 12 methyl groups of Tp* are inequivalent and therefore appear as 12 singlets (3H each). In addition, the C-H pyrazole shifts also are unique environments

represented by six (1H each) resonances. Continued analysis of this spectrum led to the assignment of four singlets between 3.58-17.43 ppm to be the four protons of the picolyl ring. A broad singlet at -5.56 ppm (2H) is assigned as the methylene protons for **2-pyr**. Interestingly, two distinct shifts (-13.1, 2.9 ppm) are seen in the ^{11}B NMR spectrum of **2-pyr**, likely due to the nitrogen-coordination to uranium. In addition to the multinuclear NMR spectra, the series of U(III) benzyl compounds were evaluated by IR spectroscopy (KBr pellet, room temp), which revealed two $\nu_{B\text{-}H}$ stretches (**2-^{i}Pr =** 2544, 2521 cm^{-1}; **2-^{t}Bu** = 2545, 2523 cm^{-1}; **2-OMe** = 2556, 2522 cm^{-1}; **2-pyr** = 2555, 2519 cm^{-1}), which is reported with other bis(Tp*)U complexes.

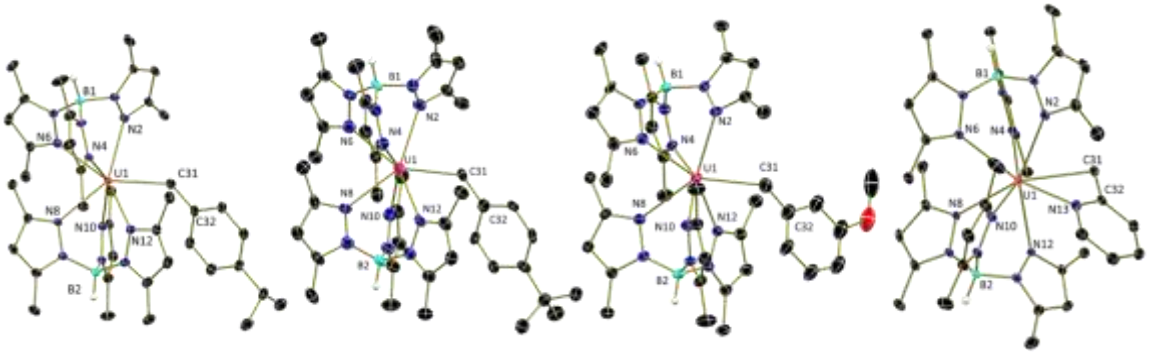

Figure 1.2. Molecular structures of **2-^{i}Pr**, **2-^{t}Bu × 1-I**, **2-OMe**, and **2-pyr** shown as 30% probability ellipsoids. Co-crystallized solvent molecules, selected hydrogen atoms, and disorder have been omitted for clarity.

To evaluate the structural properties of these compounds, single crystals of all compounds were grown for analysis by X-ray diffraction (Figure 1.2). Unfortunately, suitable crystals of pure **2-^{t}Bu** were not obtainable; analysis revealed that it was in fact a 0.95:0.05 co-crystal of **2-^{t}Bu** and **1-I.** In each case, refinement of the data showed the expected Tp*$_2$U(III) benzyl complex with two κ^3-Tp* ligands per uranium center (**2-^{i}Pr** – U-N$_{pyrazolyl}$: 2.528(3)-2.690(3) Å; **2-^{t}Bu** – U-N$_{pyrazole}$: 2.517(2)-2.703(2) Å; **2-OMe** – U-N$_{pyrazolyl}$: 2.524(5)-2.706(5) Å); **2-pyr** – U-N$_{pyrazolyl}$: 2.580(3)-2.736(3) Å) (Table 1.1). The U-C bonds for the series (**2-^{i}Pr** = 2.629(4) Å; **2-^{t}Bu** = 2.632(4) Å; **2-OMe** = 2.675(15) Å; **2-pyr** = 2.747(4) Å) are within the range of other reported uranium(III) alkyl bond distances, including **2-Bn** (2.57(2) Å),[24] Tp*$_2$U(CH$_2$SiMe$_3$) (2.601(9) Å),[34] Tp*U(CH$_2$Ph)$_2$ (2.615(7), 2.604(9) Å),[17] U(CH(SiMe$_3$)$_2$)$_3$ (2.48(2) Å),[21] and TpTp*U(CH$_2$Ph) (Tp =

hydrotris(pyrazolyl)borate) (2.56(2) Å).[18] Consistent with the solution ^{1}H NMR spectrum, the solid state molecular structure of **2-pyr** shows pyridine coordination taking on the aza-allyl coordination mode observed for U(CH_2*o*-Picolyl)$_4$.[19]

Table 1.1. Selected bond lengths of **2-^{i}Pr**, **2-^{t}Bu × Tp*$_2$UI**, **2-OMe**, **2-pyr**, and **3-N_3**.

	2-*i*Pr	**2-*t*Bu**	**2-OMe**	**2-pyr**	**3-N_3**
U1-N2	2.540(3) Å	2.675(2) Å	2.673(4) Å	2.736(3) Å	2.673(3) Å
U1-N4	2.528(3) Å	2.589(2) Å	2.524(5) Å	2.580(3) Å	2.530(3) Å
U1-N6	2.690(3) Å	2.585(2) Å	2.560(5) Å	2.709(3) Å	2.632(3) Å
U1-N8	2.652(3) Å	2.703(2) Å	2.612(5) Å	2.593(3) Å	2.655(3) Å
U1-N10	2.590(3) Å	2.517(2) Å	2.592(5) Å	2.621(3) Å	2.648(3) Å
U1-N12	2.589(3) Å	2.544(2) Å	2.706(5) Å	2.703(3) Å	2.558(3) Å
U1-N13	-	-	-	2.491(3) Å	2.321(4) Å
U1-C31	2.629(4) Å	2.632(4) Å	2.675(15) Å	2.747(4) Å	-

Further characterization by electronic absorption spectroscopy was performed on the family of uranium benzyl derivatives to confirm the +3 oxidation state of its members. All compounds have similar features in the near-infrared (NIR) region, characterized by a relatively intense absorption near 1250 nm (ca. 150 $M^{-1}cm^{-1}$) with additional broad features up through 1650 nm, consistent for U(III) ions (Figure 1.3).[35, 36] Across repeated measurements, **2-OMe** gave absorbances with lower molar absorptivities than the other benzyl complexes, possibly due to the electron donating effects from the methoxy substituent. The UV-visible region displays characteristic spectra similar to **2-Bn**'s previously reported spectra.[24]

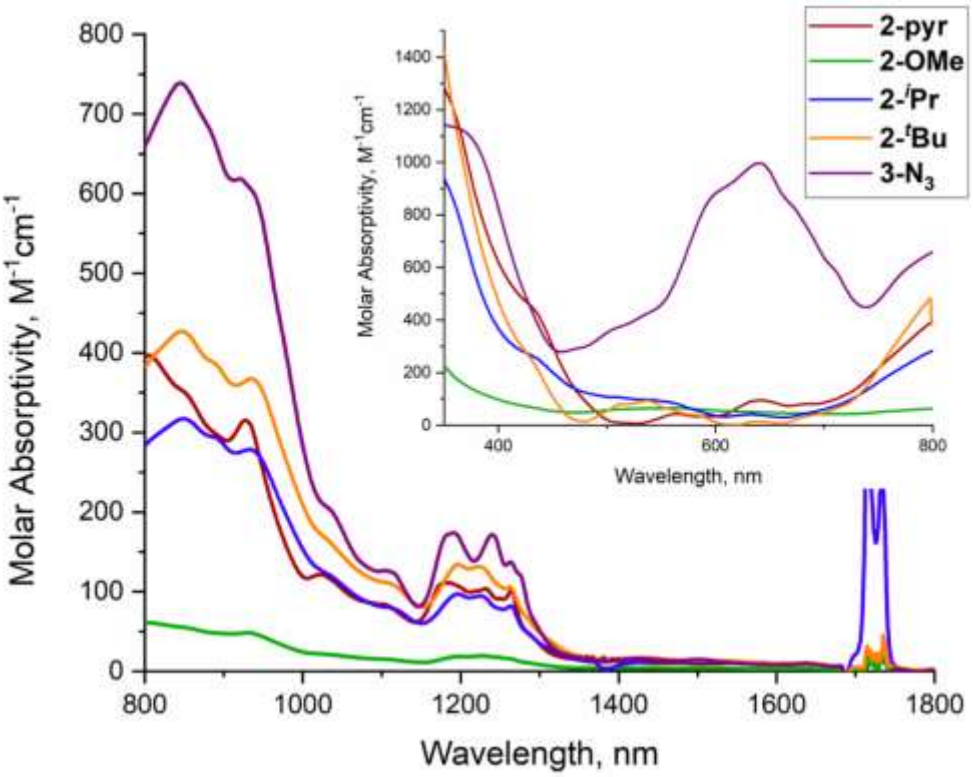

Figure 1.3. Electronic absorption spectra of **1-*o*-Picolyl** (red), **1-*m*-OMe** (green), **1-*p*-^{t}Bu** (orange), and **1-*p*-^{i}Pr** (blue) recorded from 300 to 1650 nm in THF at ambient temperature.

1.4.2 Reactivity With Azide

As expected based on our previous work, this new family of benzyl derivatives, **2-CH_2Ar**, are useful synthons to develop new uranium(III) derivatives. One target was a monomeric, neutral trivalent uranium azide, as previous examples have oxidation states ranging from +4 to +6 or are trivalent anions stabilized by a counteraction ([Na(18-crown-6)][Cp'$_3UN_3$] (Cp' = $C_5H_4SiMe_3$)).[37] Treating dark green THF solutions of **2-CH_2Ar** with one equivalent of azidotrimethylsilane ($SiMe_3N_3$) caused an immediate change to blue-green. After 30 min, volatiles were removed, and the resulting oil was washed with *n*-pentane to remove Me_3SiCH_2Ar,[38-40] affording a blue-green powder assigned as Tp*$_2UN_3$ (**3-N_3**) (Fig 1.4). Analysis by ^{1}H NMR spectroscopy revealed four resonances, consistent with C_{2v} symmetry. Two signals (18H) corresponding to the *endo*-(-15.00 ppm) and *exo*-methyl (1.28 ppm) groups were also observed for Tp*, with a singlet (6H) at 7.67 ppm for

the Tp*-C*H*. In this case, a very broad singlet (10.12 ppm) was also found for the Tp*-B-*H*. A single boron resonance is observable in the ^{11}B NMR spectrum (10.6 ppm), which is expected for the proposed symmetry. This is shifted from the uranium alkyl starting materials[33] and is consistent with other trivalent uranium complexes.[18, 35, 41] Two B-H stretches are visible by IR spectroscopy (KBr pellet) (2558, 2523 cm^{-1}), as noted for the **2-CH$_2$Ar** family. An asymmetric stretch for the terminal azide (2073 cm^{-1}) is consistent with other uranium-bound azide complexes (2055-2086 cm^{-1}).[30–32] As for the bis(Tp*)U alkyl compounds, the electronic absorption spectrum of **3-N$_3$** has an absorption at 1250 nm (ca. 200 M^{-1}cm^{-1}) and broad U(III)-like features in the NIR region. In the UV-visible region, there is a strong color-producing band at λ_{max} = 641 nm (996.8 M^{-1}cm^{-1}) (Figure 1.3).

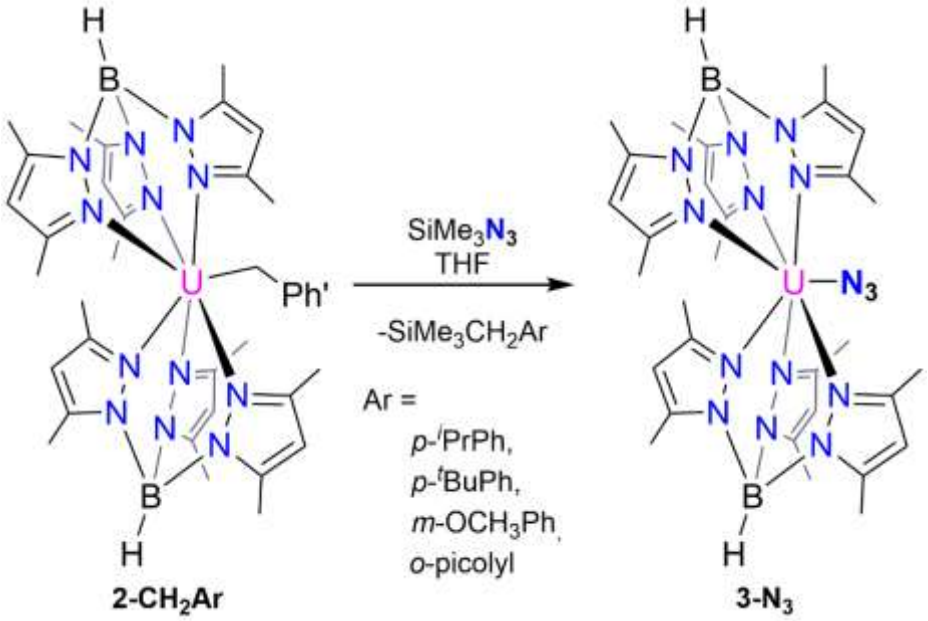

Figure 1.4. Reaction to prepare **3-N$_3$**.

Single, X-ray quality crystals of **3-N$_3$** were obtainable by cooling a concentrated toluene solution to -35 °C. Analysis revealed two κ^3-Tp* ligands on the seven-coordinate uranium center (Figure 1.5), with U-N$_{pyrazole}$ bond distances (2.530(6)-2.673(3) Å) (Table 1) consistent with other bis(Tp*) uranium compounds.[13, 42] The U-N$_{azide}$ bond length of 2.321(4) Å is significantly shorter than the U-N$_{pyrazole}$ distances, which is expected for a monodentate, monoanionic ligand. There have been U(IV),[43-56] U(V),[57] and U(VI)[58-61]

terminal azide complexes reported and bridging U(III) azide complexes,[37, 62] but to our knowledge, **3-N_3** is the first report of a monomeric, terminal U(III) azide complex. The U1-N13-N14 bond angle (166.0(3)°) is slightly bent, likely due to the crowded bis(Tp*) ligand framework. This U-N_{azide} angle is similar to those observed in other U-N_3 complexes ($Cp^*_2U(N(SiMe_3)_2)(N_3)$ = 163.5(17)°;[49] $((^{Ad}ArO)_3tacn)UN_3$ = 177.2(5)°, ((^{Ad}ArOH)$_3$tacn=1,4,7-tris(3-adamantyl-5-*tert*-butyl-2-hydroxybenzyl)1,4,7-triazacyclonone);[45] $U(N_3)(Tren^{TIPS})$ = 176.0(3)°, ($Tren^{TIPS}$ = tris(triisopropylsilylamidomethyl)amine)).[53] The linearity of the azide fragment (N13-N14-N15, 178.1(5)°) is expected and consistent with previously reported uranium azide complexes ($Cp^*_2U[N(Ph)(SiMe_3)](N_3)$ = 177.9(10)°;[51] $U(N(SiMe_3)_2)_3(N_3)_2$ = 179.5(4)°).[57] The intraligand bond distances (N13-N14 = 1.201(6) Å; N14-N15 = 1.154(6) Å) are similar to those in other reported azide complexes ($Cp^*_2U(O\text{-}2,6\text{-}iPr_2C_6H_3)(N_3)$ – N-N = 1.197(10), 1.172(11) Å)[50] and suggest that any charge is delocalized across all the nitrogen atoms within the azide fragment.

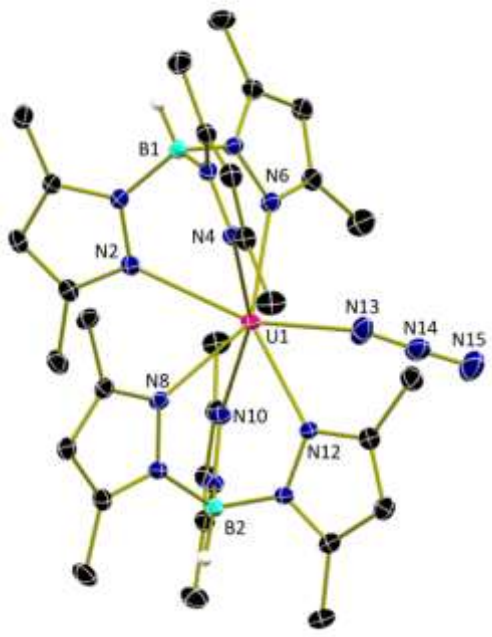

Figure 1.5. Molecular structure of **3-N_3** shown as 30% probability ellipsoids. Selected hydrogen atoms and co-crystallized solvent molecules omitted for clarity.

After isolation and characterization of **3-N_3**, attempts were made to induce dinitrogen loss to form the corresponding uranium(V) nitrido species. Photolysis using both UV or compact fluorescent lamps produced intractable mixtures of products, with the same result observed after prolonged heating as well. Addition of BPh_3 to **3-N_3** also appeared to result in immediate decomposition, giving a complicated NMR spectrum. In each case, there was not an obvious sign of effervescence which would indicate N_2 loss. Compound **3-N_3** is the latest entry into an established family of bis(Tp*) uranium(III) compounds bearing monoanionic ligands, including Tp*$_2$UX, where X = CH_3, F, Cl, I. Examining crystallographic data for these species affords an opportunity for a direct comparison of sterics, which can be modeled in a quantitative way using the Solid-G program.[63] This analysis uses "numerically calculated ligand steric parameters" from experimentally determined molecular structures to calculate the extent of the uranium coordination sphere that is blocked by its ligands (Table 1.2). The reported G(complex) value represents the sum of all ligands minus any overlap to give an absolute value for shielding. The percentage of the coordination sphere blocked by the Tp* and X ligands is also given. Based on the G(complex) for this system, we can see an expected trend for the halide series (F, Cl, I), in that the larger the halide substituent, the more of the coordination sphere that is blocked. Furthermore, the respective G(complex) values of 85.64% and 85.57% for **3-N_3** and Tp*$_2$UCH_3 show these derivatives are very similar in their degrees of coordinative saturation, and that this is on par with what is observed for **1-I**. Individually, however, the steric influence of the azide substituent on the uranium(III) ion is the same as for a fluoride substituent due to the affinity of the electropositive uranium for this electron withdrawing ligand.

Table 1.2. Solid angle parameters obtained from crystallographic data using Solid-G.

	3-N_3	**Tp*$_2$UCH_3[34]**	**Tp*$_2$UF[41]**	**Tp*$_2$UCl[64]**	1-I[65]
G(Tp*), %	38.61	37.60	37.73	37.51	38.42
	38.06	39.40	38.37	37.99	38.64
G(X), %	12.24	10.24	12.25	9.74	10.30
G(complex), %	85.64	85.57	84.72	85.20	85.78

1.4.3 Reactivity With Phosphine Oxides

To begin our studies, a solution of **2-Bn** was charged with an equivalent of $OPPh_3$, causing an immediate color change from green to brown to ensue. After 45 min, workup and analysis of the dark brown powder by ^1H NMR spectroscopy (25 °C, C_6D_6) revealed a complex, paramagnetically shifted spectrum, with no resonances for either starting material, indicating complete conversion to a new compound.

Due to the complexity of this ^1H NMR spectrum, structural assignment of this brown compound by X-ray diffraction was sought. Analysis of crystals obtained by slow diffusion of *n*-pentane into a concentrated toluene solution at -35 °C revealed the product as $Tp^*_2U[OP(C_6H_5)_2(C_6H_5CH_2C_6H_5)]$ (**4-Ph**) (Figure 1.6, left; Figure 1.7; Figure 1.9), which features a carbon-carbon bond between the benzyl group and the carbon at the *para*-position of one of the phenyl rings of $OPPh_3$. In addition to the new C-C bond, an elongation of the P=O bond and a new U-O bond are observed. The $U\text{-}N_{pyrazole}$ bond lengths for the pair of κ^3-Tp* ligands range from 2.529(3)-2.744(3) Å, which is consistent with other $U\text{-}N_{pyrazole}$ bond lengths for bis(Tp*)U(III) compounds.[31, 64, 66] The U-O bond distance (2.358(2) Å) is significantly longer than other anionic U(III)-O bond lengths (2.144-2.271 Å, Table 1.3) and is closer to that of dative U-O bond distances (2.350-2.584 Å, Table 1.3). We postulate this is an anionic bonding interaction but extreme steric hindrance at the uranium center creates the observed elongation.

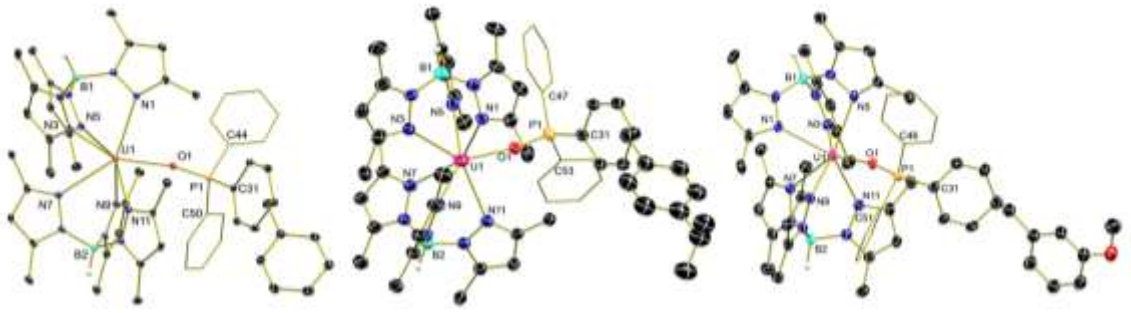

Figure 1.6. Molecular structures of **4-Ph**, **4-^{i}Pr**, and **4-OMe** (left to right) shown as 30% probability ellipsoids. Selected hydrogen atoms, disorder, and co-crystallized solvent molecules omitted for clarity.

To investigate this hypothesis, we sought to synthesize a similarly crowded uranium center with a dative U-O bond. Treating a THF solution of **2-Bn** with BPh_3 affords a blue powder assigned as $[Tp^*_2U(THF)][BnBPh_3]$ (**5-THF**). The molecular structure of **5-THF** as determined by X-ray diffraction of single crystals revealed a bis(Tp*)U cation with a datively-bound THF molecule, as well as a $BnBPh_3$ counteranion (Figure 1.8). The U-O bond distance of 2.609(3) Å is significantly longer than that for **4-Ph**, confirming assignment of the latter as an anionic U-O interaction.

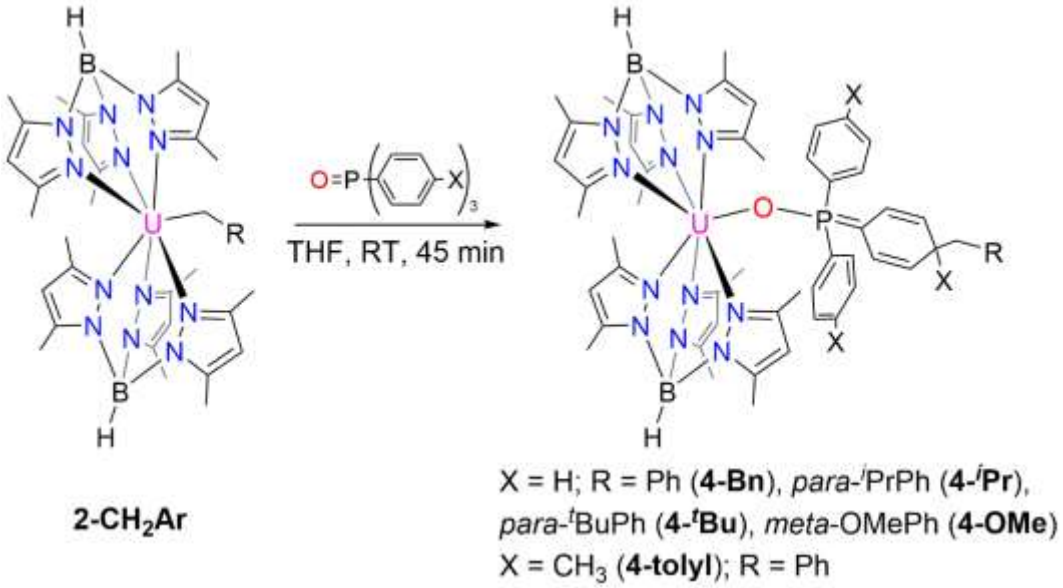

Figure 1.7. Reactions of **2-CH_2Ar** with phosphine oxides.

Further analysis of the structural parameters of **4-Ph** (Figure 1.9) highlight distortions in the triphenylphosphine oxide ligand. Comparison of the O-P bond length (1.548(2) Å) in **4-Ph** to those of datively coordinated phosphine oxide ligands in low-valent uranium complexes shows clear P=O bond reduction, ($Tp^*UCl_3(OP(OC_2H_5)_3)$ = 1.44(1) Å;[67] $Cp'_3U(OPPh_3)$ = 1.492(6) Å).[68] Examination of the P-C bond lengths shows two distinct bonding modes. For the phenyl ring that has undergone *para*-carbon coupling, the distance is shortened (P1-C31 = 1.718(4) Å) compared to the other two (P1-C44 = 1.816(3), P1-C50 = 1.813(4) Å). The latter distances are similar to that observed for $Cp'_3U(OPPh_3)$ (1.794(6)-1.799(8) Å)[68], which has a neutral $OPPh_3$ datively coordinated to a trivalent

uranium center. This shortened P-C bond distance results from reduction of the adjacent O-P bond and has not been previously observed for uranium compounds.

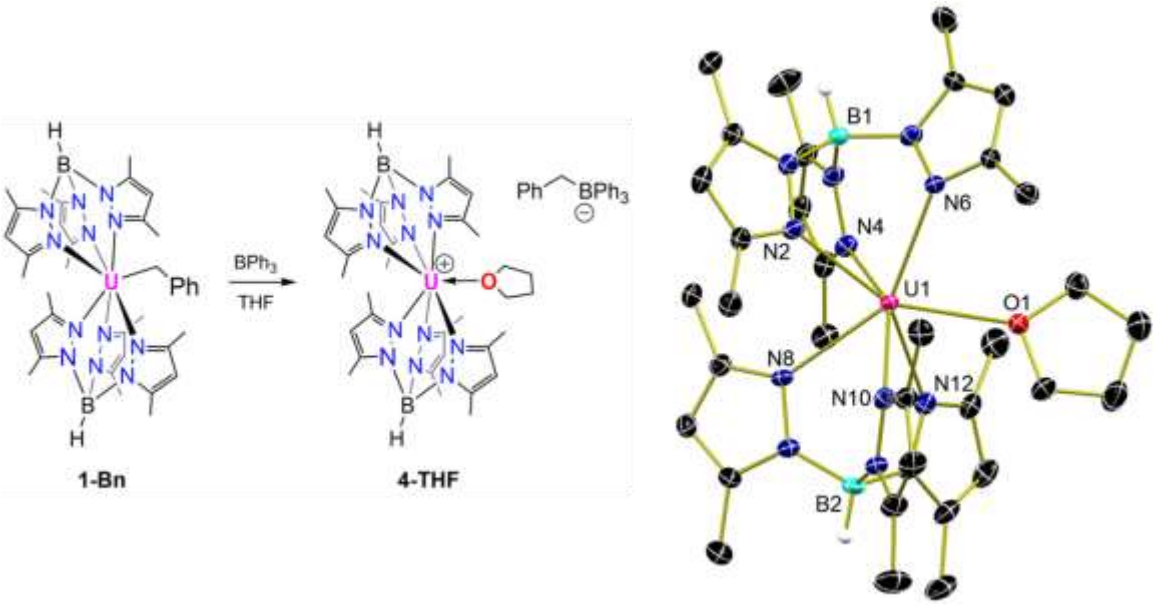

Figure 1.8. Reaction scheme for the synthesis of **5-THF** (left). Molecular structure of **5-THF** displayed at 30% probability ellipsoids with select hydrogen atoms, co-crystallized solvent molecules, and counter ions omitted for clarity (right).

Table 1.3. U-O bond comparison for U(III) complexes.

Compound (red = anionic; blue = dative)	**Bond Length (Å)**
4-Ph	2.358(2)
U(ODtbp)$_3$ **(ODtbp = OC$_6$H$_3$-Bu$^t_2$-2,6)**	2.151(3)-2.164(3)[69]
U(OAr^{Ad,Ad,Me})$_3$ **(OAr^{Ad,Ad,Me} = O-C$_6$H$_2$-2,6-Ad-4-Me**	2.151(3)-2.177(3)[70]
[Cp*[2,6-(Me$_3$C)$_2$-4-Me-C$_6$H$_2$O]U]$_2$(C$_6$H$_6$)	2.144(8)[71]
((ArO$_3$)tacn)U(NCCH$_3$) **(ArO$_3$(tacn) = 1,4,7-tris(3,5-di-*tert*- butyl-2-hydroxybenzyl)-1,4,7-triazacyclononane)**	2.258(5)-2.271(5)[46]
Tp*$_2$U[OC(CH$_3$)CH$_2$]	2.198(9)[16]
Tp^{Ph}UI(OPh)(THF)$_2$ **(Tp^{Ph} = hydrotris(3-phenylpyrazolyl) borate)**	2.184(2)[35]
Tp*$_2$U(O-C$_6$H$_3$-2,4,6-Me)	2.159(10)[64]
Tp^{iPr2}UI$_2$(OPPh$_3$) **(Tp^{iPr2} = hydrotris(3,5-di-*iso*-propyl-pyrazolyl)borate)**	2.350(11)[72]
Tp*UCl$_3$[OP(OC$_2$H$_5$)$_3$]	2.373(7)[67]
Cp'$_3$U(OPPh$_3$) (Cp' = MeC$_5$H$_4$)	2.389(6)[68]
UI$_2$[H(μ-H)B(3-^{t}Bu,5-Me-pz)$_2$](OPPh$_3$)$_2$	2.584(12)[73]
5-THF	2.609(3)

With these distortions noted in the O-P-C bonds for **4-Ph**, similarly the adjacent phenyl ring also displays unusual parameters; most notably, the ring has undergone a loss of aromaticity. The C-C bond distances display a pattern indicative of a cyclohexadienyl fragment (Figure 1.9) rather than an aromatic system. A recent report by Schelter *et al* shows this same loss of aromaticity from dimeric coupling of a uranium tris(amide) complex featuring a benzophenone radical to afford [N(SiMe$_3$)$_2$]$_3$U(OCPhPh-CPh-CPh$_2$O)U[N(SiMe$_3$)$_2$]$_3$.[15] Keay reports loss of aromaticity in a phenyl ring of a

triphenylphosphine oxide derivative can be facilitated by LDA (LDA = lithium diisopropylamide), forming a bicyclic triene.[74]

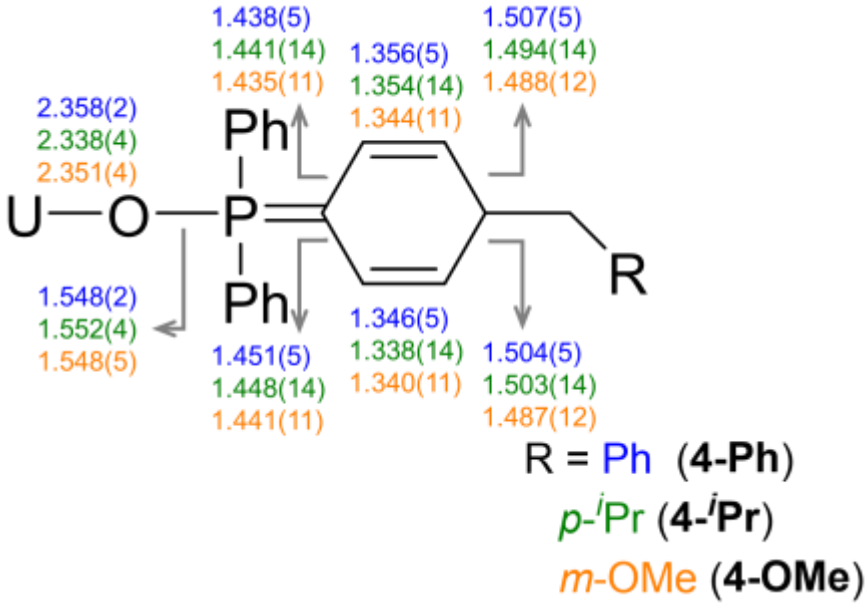

Figure 1.9. Selected bond metrics for **4-Ph**, **4-^{i}Pr**, and **4-OMe**.

The structural assignment of **4-Ph** provided insight into the complex solution ^{1}H NMR spectrum (Table 1.3). Thirteen resonances were observed ranging from -16 to 22 ppm, consistent with a C_s symmetric spectrum. Three resonances were observed for Tp* ligands, assignable to the *endo*- and *exo*-methyl groups and the pyrazole CH consistent with this symmetry assignment. The unmodified phenyl rings on the triphenylphosphine ligand show three resonances for the *para*, *meta*, and *ortho* protons (10.51, 21.72, 10.78 ppm, respectively). For the modified phenyl ring, two singlets (2H each) are assigned as the cyclohexadienyl resonances, and this was additionally confirmed by 2D ^{1}H correlation spectroscopy (COSY) (Appendix). The protons for the benzyl substituent for **4-Ph** are not paramagnetically shifted, likely due to their distance from the uranium. A broad singlet appearing at 8.37 ppm is assigned as the B-H of Tp*. There is a corresponding resonance at 7.2 ppm in the ^{11}B NMR spectrum, which is within the range of other bis(Tp*) U(III) complexes.[18, 41] A single resonance appears in the ^{31}P NMR spectrum at 84.77 ppm, which is significantly shifted from $OPPh_3$ (25.74 ppm, Appendix). The coordination of two κ^3-

Tp* ligands was also confirmed by IR spectroscopy (KBr pellet) with two B-H stretches (2553, 2526 cm^{-1}), common for bis(Tp*)U complexes.[16, 27, 75]

Electronic absorption spectroscopy was utilized to further characterize the oxidation state and color of **4-Ph** (Figure 1.10). The near infrared (NIR) region shows features characteristic of trivalent uranium at 1200 nm (200 $M^{-1}cm^{-1}$) (Figure 1.10), which are also observed for **2-Bn**.[24] An absorbance in the UV-visible region with λ_{max} at 565 nm (905 $M^{-1}cm^{-1}$) is responsible for the brown color observed for **4-Ph**.

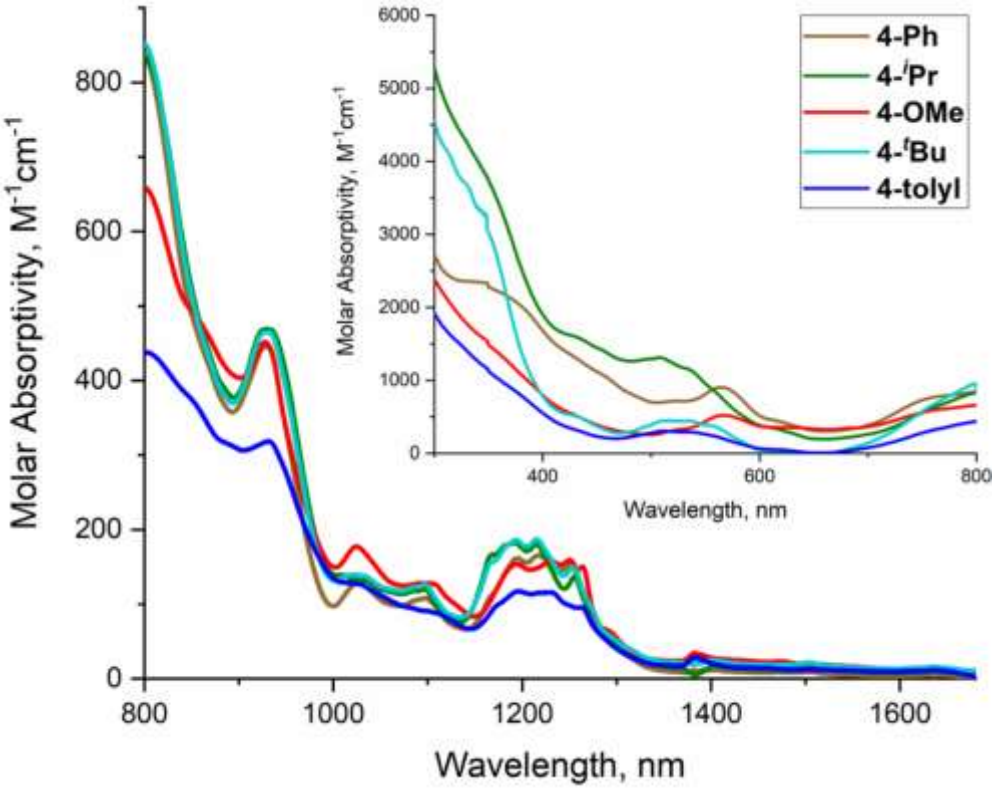

Figure 1.10. Electronic absorption spectra of **4-Ph**, **4-^{i}Pr**, **4-OMe**, **4-^{t}Bu**, and **4-tolyl** recorded from 350-1800 nm in THF at ambient temperature.

With full characterization of **4-Ph**, we sought to understand how steric and electronic variation of the benzyl substituents influenced the observed coupling chemistry. To this end, we employed previously discussed **2-CH_2Ar** family. Following the same procedure to make **4-Ph**, treating a stirring solution of either **2-^{i}Pr**, **2-^{t}Bu**, or **2-OMe** with $OPPh_3$ forms $Tp^*_2U[OP(C_6H_5)_2(C_6H_5CH_2$-*p*-$CH(CH_3)_2Ph)]$ (**4-^{i}Pr**), $Tp^*_2U[OP(C_6H_5)_2(C_6H_5CH_2$-*p*-$C(CH_3)_3Ph)]$ (**4-^{t}Bu**), and $Tp^*_2U[OP(C_6H_5)_2(C_6H_5CH_2$-*m*-

OCH_3Ph)] (**4-OMe**) (Figure 1.7), respectively, as brown powders. Overall, *para*-substitution slows the reaction rate, but does not prevent the C-C coupling.

All three of these compounds show ^{1}H NMR spectra that are analogous to **4-Ph**. Diagnostic peaks corresponding to the Tp* ligands and phenyl rings appear in the range from -16.06 to 21.80 ppm (Table 1.4). The cyclohexadienyl peaks were confirmed by COSY and the chemical shifts are akin to those observed for **4-Ph** (Appendix). Similar to **4-Ph**, the protons for the coupled phenyl ring all appear in the diamagnetic region of the ^{1}H NMR spectrum as expected. For **4-^{i}Pr** and **4-^{t}Bu**, two resonances (2H each) for the *meta* and *ortho* protons of the coupled benzyl fragment are seen (**4-^{i}Pr**: 6.12, 6.24 ppm; **4-^{t}Bu**: 6.18, 6.42 ppm), whereas four are observed for **4-OMe** (5.84, 6.08, 6.17, 6.30 ppm; 1H each). The substituted functional groups of **4-^{i}Pr** ($CH(CH_3)_2$ = 0.62 ppm; $CH(CH_3)_2$ = 2.16 ppm), **4-^{t}Bu** ($C(CH_3)_3$ = 0.72 ppm), and **4-OMe** (OCH_3 = 2.64 ppm) show little shift as compared to their diamagnetic reference value in their respective ^{1}H NMR spectra, likely due to their distance from the paramagnetic uranium center. Continued analysis by heteroatom NMR spectroscopy and infrared spectroscopy of this series is consistent with what was observed for **4-Ph** (Table 1.4). Two B-H stretches are observed by IR spectroscopy (KBr pellet), which is also seen with **4-Ph** (Table 1.4).

Table 1.4. Selected spectroscopic data for **4-Ph**, **4-^{i}Pr**, **4-^{t}Bu**, and **4-OMe**.

	4-Ph	**4-^{i}Pr**	**4-^{t}Bu**	**4-OMe**
Tp*-CH_3 (endo) (ppm)	-16.06	-16.12	-16.06	-16.04
Tp*-CH_3 (exo) (ppm)	0.61	0.62	0.62	0.61
Tp*-CH (ppm)	7.45	7.45	7.44	7.44
Cyclohexadienyl-CH (ppm)	5.40, 15.15	5.42, 15.20	5.41, 15.48	5.44, 15.16
Coupled-CH_2 (ppm)	1.91	1.94	1.98	1.99
^{11}B (ppm)	7.2	7.1	6.8	7.4
^{31}P (ppm)	84.77	83.78	83.28	84.71
IR: ν_{BH} (cm^{-1})	2553, 2526	2552, 2524	2550, 2519	2552, 2524

Further characterization of **4-^{i}Pr**, **4-^{t}Bu**, or **4-OMe** by electronic absorption spectroscopy (Figure 1.10) showed weak absorbances near 1200 nm (ca 200 $M^{-1}cm^{-1}$), as with the spectrum of **4-Ph**. The UV-visible region for the substituted family of products displays a broad absorbance in the region 475-600 nm.

To examine the unique coupled products further, a structural comparison of **4-^{i}Pr** and **4-OMe** was made using single crystal X-ray crystallography (Figure 1.6, Figure 1.9). Similar to **4-Ph**, these compounds show 7-coordinate uranium centers with pentagonal bipyramidal geometries. Both display U-$N_{pyrazole}$ distances in the same range as **4-Ph** (**2-^{i}Pr**: 2.541(5)-2.699(5) Å; **4-OMe**: 2.531(6)-2.728(6) Å). The U-O bond lengths (**4-^{i}Pr**: 2.338(4) Å; **4-OMe**: 2.351 (4) Å) are on the order of those of **4-Ph,** influenced by the steric pressure of the Tp* ligands. The P-O distance (**4-^{i}Pr** = 1.552(4) Å; **4-OMe**: 1.548(5) Å) is within error of that in **4-Ph**. A similar trend in bonding is seen for the P-C bonds in these two compounds, where the P-$C_{cyclohexadienyl}$ bond lengths (**4-^{i}Pr** = 1.748(11) Å; **4-OMe**: 1.711(8) Å) are shorter than the P-C_{Ph} bond lengths (**4-^{i}Pr** = 1.801(7), 1.823(6) Å; **4-OMe**: 1.808(8), 1.817(8) Å). The distances in the cyclohexadienyl fragment in **4-^{i}Pr** and **4-OMe** are similar to those in **4-Ph**, with alternating long-short bond distances (Figure 1.8).

Attempts to extend the chemistry beyond benzyl groups were unsuccessful. Treating **2-pyr**, with $OPPh_3$ did not result in the desired coupling chemistry. This is likely due to the aza-allyl coordination mode that does not facilitate benzyl radical formation and dissociation. Similarly, subjecting $Tp^*_2U(CH_2SiMe_3)$[34] to the same reaction conditions that generated **4-Ph** yielded no coupled product, but rather decomposition due to the lack of radical stabilization from the neosilyl group.

Next, the reactivity of $OPPh_3$ was explored for bis(Tp*)U compounds that are established to contain ligand radicals. Surprisingly, no coupled products were observed when treating either $Tp^*_2U(2,2'\text{-bpy})$[13] or $Tp^*_2U(OC\bullet Ph_2)$[27] with $OPPh_3$. In either case, no reaction was observed.

To study the effects of altering the electronics of the phosphine oxide, compound **2-Bn** was treated with a family of tris(aryl)phosphine oxides. Using tris(*p*-tolyl)phosphine oxide under the same experimental conditions afforded a brown powder with a paramagnetically-shifted ^{1}H NMR spectrum similar to **4-Ph**. This compound was isolated, characterized, and assigned as $Tp^*_2U[OP(p\text{-}CH_3C_6H_4)_2p\text{-}CH_3C_6H_4CH_2C_6H_5]$ (**4-tolyl**).

Multinuclear NMR and IR spectroscopies were also consistent with **4-Ph**. The electronic absorption spectrum of **4-tolyl** trends well with the previously discussed compounds in both the NIR and UV-visible regions (Figure 1.10). This reaction was markedly slower than the initial benzyl reaction to give **4-Ph**; a color change was not seen until 25 minutes of stirring with a total reaction time of 85 minutes.

Variation of the *para*-substituent on the triphenylphosphine oxide with heteroatom containing groups, including $–CF_3$ and –OMe, led to mixtures of products resulting from C-F[41] and C-O activation, respectively, pointing to the fluoro- and oxophilicity of low-valent uranium. Likewise using DMSO, Ph_2SO, or $OAsPh_3$ in lieu of triphenylphosphine oxides causes instantaneous conversion to previously reported Tp^*_2UO.[42] The sulfur analogue of $OPPh_3$, $SPPh_3$, does not react with **2-Bn** at all. These reactions highlight that the oxophilicities of both phosphorus and uranium are driving forces for the coupling reaction.[76] When tris(*p*-$N(Me)_2C_6H_4$)phosphine oxide is stirred with **2-Bn**, a complicated mixture of paramagnetic products is seen by ^{1}H NMR spectroscopy, with no evidence for the characteristic coupling product. No reaction between HMPA (HMPA = Hexamethylphosphoramide) and **2-Bn** occurs, which may be due to the difference in reduction potentials or the lack of a location to stabilize a ligand radical to promote coupling.

Experiments were performed to gain insight into the potential mechanism of the observed coupling chemistry. Using an excess of the hydrogen atom donors cyclohexadiene or dihydroanthracene in the synthesis of **4-Ph** produced no alteration in the ^{1}H NMR spectra, indicating no H-atom radical abstraction had occurred in either case. Next, the synthesis of **4-Ph** was performed at low temperature (-35 °C), which suspended its formation; production of **4-Ph** is seen upon warming to room temperature. Importantly, during the synthesis of **4-Ph** under any conditions, neither toluene nor bibenzyl was observed by ^{1}H NMR spectroscopy. This supports that benzyl radical coupling to the *para*-carbon of triphenylphosphine oxide is faster than respective H-atom abstraction or homocoupling.

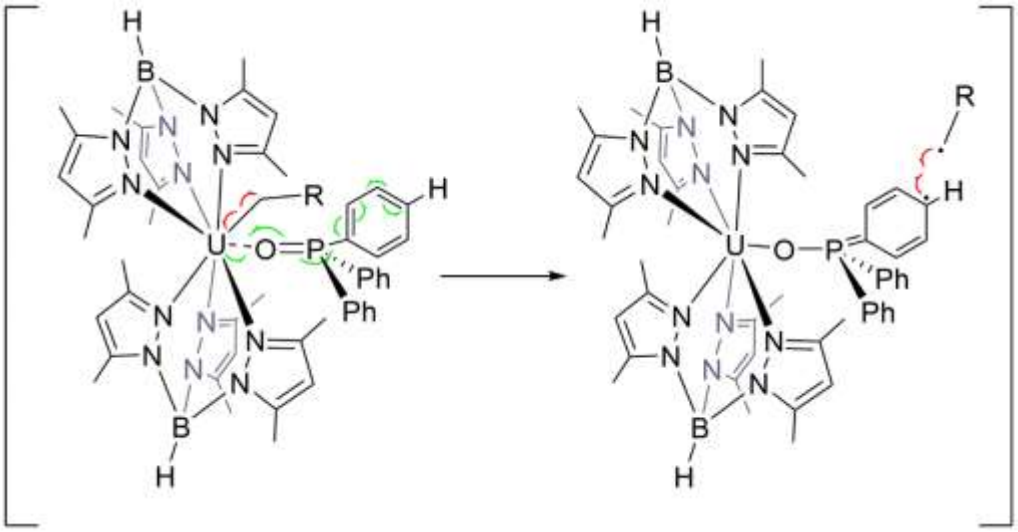

Figure 1.11. Proposed mechanism for carbon-carbon coupling.

With these experimental outcomes, a hypothesis for the mechanism of this reaction is presented in Figure 1.11. We propose that upon addition of $OPPh_3$ to a solution of **2-Bn**, $OPPh_3$ association with the uranium(III) center aides benzyl radical loss due to steric congestion. In concert, a putative [Tp^*_2U] fragment reduces $OPPh_3$ by one electron, which resonates around the phenyl ring to the *para*-position, where it reacts with the extruded benzyl radical, forming the coupled product. Reduction of the P=O bond converts the U-O bond from dative to anionic, allowing for the formation of the thermodynamically favored U-O bond. If benzyl radical loss happened prior to phosphine oxide coordination, it would be expected to observe decomposition of **2-Bn** in the presence of no substrate, which is not substantiated in a control experiment. The lack of bibenzyl or toluene formation from the reactions support that the benzyl radical is closely associated to the uranium species at all times, not leaving the coordination sphere during the course of the reaction.

An alternative reaction pathway (not pictured) is that homolytic scission of U-C takes place *after* the U-O anionic bond formation with incoming $OPPh_3$. This step would give rise to a transient U(IV) intermediate, $Tp^*_2U(CH_2Ph)OPPh_3$, which would get reduced back to U(III) after U-C homolytic scission. The reaction proceeds quickly enough that any benzyl radical could not exit the coordination sphere. While this cannot be eliminated as a possibility, there are currently no examples of Tp^*_2U(IV) complexes being reduced to Tp^*_2U(III) in the absence of strong alkali metal reductant known. Furthermore, previously

reported Tp*U(NMes)(CH_2Ph)(THF), which features a uranium(IV)-benzyl bond, is stable and fully characterized, showing no proclivity for a homolytic U-C scission and reduction back to uranium(III).[17]

1.4.4 Reactions with other reagents

In an effort to prepare uranium-element bonds which are less commonly reported, such as U-Si and U-P, the U(III) benzyl family was targeted for protonolysis reactivity. Reactions with various primary and secondary silanes resulted in the generation of desired substituted toluene, by ^{1}H NMR spectroscopy, but the paramagnetic products of these experiments were intractable mixtures. Stirring **2-OMe** with phenylphosphine led to decomposition of any paramagnetic complex, however when trimethylsilyldiphenylphosphine was used, conversion of **2-OMe** was seen by ^{1}H NMR spectroscopy, as well as a slight shift in the shade of green after 1 hr stirring (Figure 1.12). After this time, volatiles were removed *in vacuo* and a green powder was isolated. Analysis by ^{1}H NMR spectroscopy revealed the presence of the trimethylsilylated-benzyl species in the diamagnetic region with a single, paramagnetically-shifted species. Work-up using *n*-pentane allows for the isolation of the paramagnetic compound from any of the organic by-product, indicating conversion of **2-OMe** to the methoxy-substituted trimethylsilylbenzyl compound.

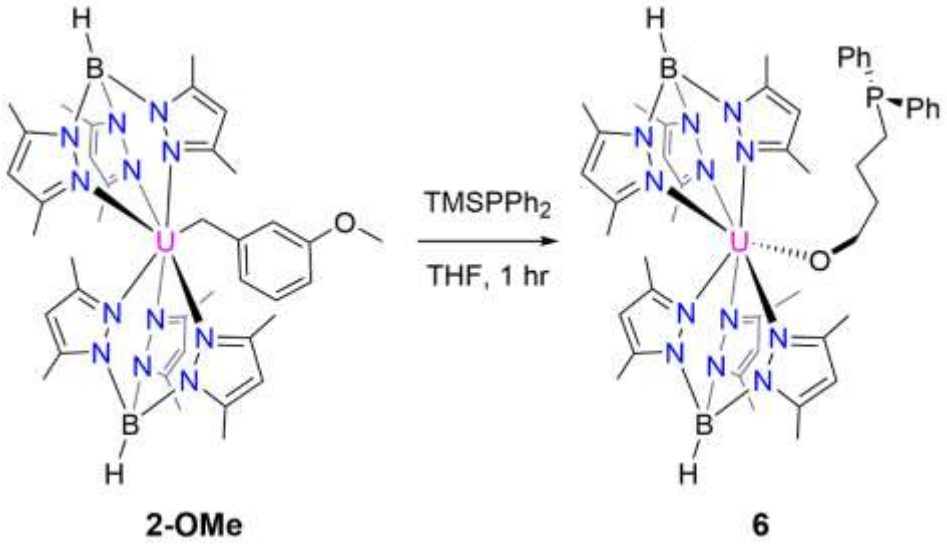

Figure 1.12. Preparation of **6** from **2-OMe**.

In order to better evaluate the isolated powder, crystals were grown from a solution of concentrated diethyl ether and analyzed using X-ray crystallography. The molecular structure revealed a seven-coordinate uranium center, but instead of a U-P bond, a new U-O bond (2.145(3) Å) is present (Figure 1.13); with this structure, the powder is assigned as $Tp^*_2U(O(CH_2)_4P(Ph))$ (**6**). Along with two κ^3-Tp* ligands, it appears that a THF molecule has been gone through ring-opening during the reaction, with a new C-P bond formed at the opposite end of the U-O bond. The observed $U\text{-}N_{pyrazolyl}$ bond lengths (2.569(3)-2.736(4) Å) are in a range consistent with the other reported complexes in this chapter.

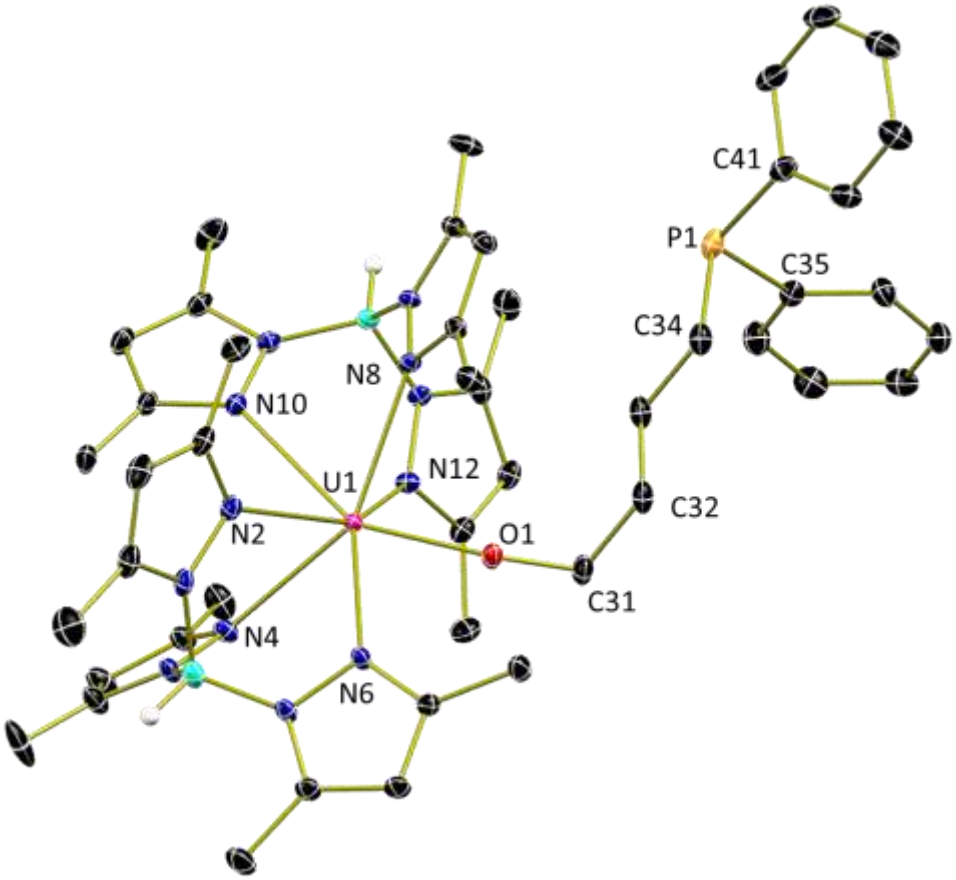

Figure 1.13. Molecular structure of **6** shown as 30% probability ellipsoids. Co-crystallized solvent molecules and selected hydrogen atoms omitted for clarity.

1.5 Conclusion

Overall, we have demonstrated that U(III) alkyl compounds, which are traditionally difficult to prepare, can be stabilized with the aid of the Tp^*_2U framework. The use of substituted benzyl potassium salts in preparation of $Tp^*_2UCH_2Ar$ compounds shows that U(III) can tolerate bulky substitution (*t*Bu, ^{i}Pr), different electronic functional groups (methoxy), and heteroatom coordination (pyridyl). This family of compounds has provided a novel route to the preparation of the first monomeric, neutral U(III) azide.

Further radical chemistry with the U(III) benzyl compounds is seen in the reactions featuring triphenylphosphine oxide, which results in rare carbon-carbon coupling at the 4-position of one of the aryl rings. Through steric and electronic variation of the benzyl compounds, this coupling reaction was not affected. This coupling reaction persists with alterations made at the *para*-position of the triphenylphosphine rings, albeit with a slower rate.

Even with the surprising carbon-carbon coupling reaction, the idealized mechanism is comprised of fundamental steps which are typically observed for bis(Tp*) U framework. Beginning with single electron transfer, formation of a strong U-O bond, and extrusion of benzyl radicals. In this set of reactions, specifically, the benzyl radical has an accessible place to couple [with the reduced triphenyl phosphine], rather than its more common homocoupling. The reactivity of triphenylphosphine oxide is noteworthy, as a result of this being seen as an inert ligand in coordination chemistry. Additionally, a coupling reaction of this nature has not be observed for any metals, emphasizing the unparalleled reactivity of actinides in organometallic chemistry.

CHAPTER 2. SYNTHESIS AND REACTIVITY OF U(IV) IMIDO COMPOUNDS

Reprinted (adapted) with permission from Tatebe, C.J., Zeller, M., Bart, S.C., *Inorganic Chemistry*, **2017**, *56*, 1956-1965. Copyright 2017, American Chemical Society. Reprinted (adapted) with permission from Tatebe, C.J., Collins, T.S., Barnett, G.R., Zeller, M., Bart, S.C., *Polyhedron*, **2019**, *158*, 1-7. Copyright 2019, Elsevier.

2.1 Abstract

A family of uranium(IV) imido complexes of the form Tp*$_2$U(NR) (R = benzyl (**7-Bn**), *para*-tolyl (**7-Tol**), *para*-methoxyphenyl (**7-OMe**), 2,6-diethylphenyl (**7-detp**), 2,6-diisopropylphenyl (**7-dipp**)) have been generated by bibenzyl extrusion from **2-Bn**. When **7-Bn** and **7-Tol**, along with previously reported Tp*$_2$U(N-Ph) (**7-Ph**) and Tp*$_2$U(N-Ad) (**7-Ad**), are treated with isocyanates or isothiocyanates, they readily undergo [2π+2π]-cycloaddition to generate κ^2-ureato and κ^2-thioureato derivatives, respectively. Use of phenylisoselenocyanate with **7-Tol** and **7-Ph** generates a rare κ^2-selenoureato complex. Treating **7-Tol** and **7-OMe** with benzonitrile or 4-cyanopryidine results in unusual products of multiple bond metathesis, namely κ^1-amidinate U(IV) complexes. All compounds were characterized using ^{1}H and ^{11}B NMR, infrared, and electronic absorption spectroscopies, and where possible, X-ray crystallography. The steric demands of the ligands were quantitatively assessed using computation modeling.

2.2 Introduction

Small molecule activation has been extensively studied within the actinide community due to the highly reducing nature of these elements.[10, 77, 78] Making use of actinide-element multiple bonds is a strategy with diverse reaction pathways dictated by the steric environment.[79, 80] Like early transition metal counterparts, actinide-element multiple bonds can undergo [2π+2π]-cycloaddition chemistry, facilitating a direct comparison of d- vs. f-block reactivity. Cycloaddition to transition metal-nitrogen multiple bonds is a key transformation that has broad applications across organic synthesis,[81] dinitrogen activation,[82] polymerization,[83, 84] and small molecule formation.[85] This process can be

more specifically applied to the synthesis of urea derivatives, which are fairly common based on the variety of κ^2-ureato complexes of niobium,[86] rhenium,[87] ruthenium,[88] titanium,[89, 90] tungsten,[91] and zirconium[92] synthesized *via* [2+2] cycloadditions of isocyanates.[87, 90, 91, 93-99]

Urea derivatives of uranium complexes fashioned from cycloaddition are much less common. In 2008, Boncella invoked formation of a uranium(VI) κ^2-ureato derivative from cycloaddition as an intermediate in imido exchange chemistry.[100] Computational comparison of the *N*,*N*- and *N*,*O*-bound isomers indicated that the former is actually lower in energy, a surprising result given the oxophilicity of uranium. This finding was corroborated by Meyer later that year with the report of the first solid state characterization of a κ^2-ureato ligand on uranium(V) in (($^{t\text{Bu}}$ArO)$_3$tacn)U(κ^2-*N*,*N*'-diphenylureato) (($^{t\text{Bu}}$ArOH)$_3$tacn = 1,4,7-tris(3,5-*tert*-butyl-2- hydroxybenzylate)-1,4,7-diazacyclononane), which is symmetrically coordinated through both nitrogen atoms after proposed isomerization from the *N*,*O*-bound isomer.[101] In subsequent studies in 2014, Boncella and co-workers reported the tetravalent κ^2-ureato complex, (κ^2-*N*,*N*'-1-Mes-3-dipp-ureato)U(Cl)$_2$(OPPh$_3$)$_2$ (Mes = 2,4,6-trimethylphenyl), which was formed from cycloaddition of dipp isocyanate (dipp = 2,6-diisopropylphenyl) to U(Ndipp)Cl$_2$(OPPh$_3$)$_3$.[102]

Nitrile reactivity has been studied for the early actinides – an important example of actinide (uranium, thorium) cycloaddition was reported by Eisen and co-workers[103, 104], who proposed this as an intermediate step during catalytic alkyne hydroamination. The κ^2-enamine ligands were later isolated by Andersen (U)[105] and Zi *et al* (Th)[106, 107], as the product of alkyne addition to An(IV) imido compounds, respectively. Boncella[102] and Meyer[101] have shown [2π+2π]-cycloaddition of uranium imidos with aryl isocyanates results in κ^2-ureato ligands for both U(IV) and U(V) compounds. Similar examples of κ^2-bound ligands have been isolated for Th imidos when treated with azides,[108] carbodiimides,[109] and nitriles.[110]

In recent studies, we have demonstrated [2π+2π] cycloaddition chemistry by a family of uranium(IV) imido species supported by the bulky bis-Tp* (Tp* = hydrotris(3,5-dimethylpyrazolyl)borate) ligand framework, including tetravalent imido derivatives, Tp*$_2$U(NR) (R = Ph, Mes, Ad) (Ad = 1-adamantyl),[111] as well as the fleeting uranium(IV)

hydrazido intermediate, Tp*$_2$U[η^1-(*N*)=N-N=CHSiMe$_3$].[112] These compounds all feature reactive uranium-nitrogen multiple bonds that are sterically accessible to react with a variety of substrates.[112] For instance, Tp*$_2$U[η^1-(*N*)=N-N=CHSiMe$_3$] is trapped as the uranium(IV) metallacycle, Tp*$_2$UN(N=CHSiMe$_3$)CH=CPh, by cycloaddition with the alkyne in phenylacetylene, rather than protonation chemistry from the terminal C-H bond in this substrate. Using Tp*$_2$U(N-R) (Tp* = hydrotris(3,5-dimethylpyrazolyl) borate; R = Ph, Mes, Ad), the corresponding U(IV) oxo, Tp*$_2$UO, can be prepared via treatment with *p*-tolualdehyde with simultaneous release of the substituted imine.[111] This exciting result let us to hypothesize that [2π+2π] cycloaddition chemistry could be expanded to a variety of substrates, including isocyanate and nitriles derivatives.

2.3 Experimental

2.3.1 General Considerations

Air- and moisture-sensitive manipulations were carried out using standard Schlenk techniques or in an MBraun inert atmosphere drybox with an atmosphere of purified nitrogen. The MBraun drybox is equipped with a cold well designed for freezing samples as low as liquid nitrogen, as well as two -35 °C freezers for sample storage and crystallizations. Solvents (THF, pentane, toluene, diethyl ether) were dried and deoxygenated based on literature procedures using a Seca solvent purification system.[28] Benzene-d_6 was purchased from Cambridge Isotope Laboratories, dried with molecular sieves and sodium, and degassed by three freeze-pump-thaw cycles. 2,6-Diisopropylphenylisocyanate (Alfa Aesar), phenylisocyanate (Sigma-Aldrich), and phenylisothiocyanate (Sigma-Aldrich) were purchased from commercial sources and distilled from CaH_2 before use. 1-Azidoadamantane (Sigma-Aldrich), 4-cyanopyridine (Acros Organics), and terephthalonitrile (Acros Organics) were purchased from commercial sources and used as received. Tp*$_2$UBn (**2-Bn**),[24] Tp*$_2$UI (**1-I**),[31] Tp*$_2$U(N-Ph) (**7-Ph**),[111] Tp*$_2$UNAd (**7-Ad**),[111] phenylisoselenocyanate,[113] *para*-tolylazide,[114] and benzyl azide[115] were made using previously reported methods. Other azides (azidobenzene, 2,6-diethylphenylazide, 2,6-diisopropylphenylazide, 4-methoxyphenylazide) were prepared using a modified literature procedure.[116]

^{1}H, and ^{11}B NMR spectra were recorded on a Varian Inova 300 spectrometer operating at frequencies of 299.992 and 96.24 MHz, respectively. ^{31}P NMR spectra were recorded on a Mercury 300 spectrometer operating at a frequency of 121.43 MHz. All chemical shifts are reported relative to the peak for $SiMe_4$, using ^{1}H residual chemical shifts of C_6D_6 (7.16 ppm) as a secondary standard. 11B chemical shifts are reported relative to the peak for $BF_3{\cdot}(Et_2O)$ (0.0 ppm). Spectra for paramagnetic molecules were obtained by using an acquisition time of 0.5 s, thus the peak widths reported have an error of ±2 Hz. For paramagnetic molecules, the ^{1}H NMR data are reported with the chemical shift, peak width at half-height (in Hz), integration value, and where possible, the peak assignment. Elemental analyses were performed by Midwest-Microlab, LLC (Indianapolis, Indiana). Solid-state infrared spectra were recorded using a Thermo Nicolet 6700 spectrophotometer with samples made by crushing the solids, mixing with dried KBr, and pressing into a pellet. Electronic absorption spectroscopic measurements were recorded at ambient temperature in dry solvent using sealed 1 cm quartz cuvettes with a Cary 6000i UV-Vis-NIR spectrophotometer.

Single crystals of **7-detp**, **7-*p*Tol**, **8-Ph**, **9-Ph**, and **10-Ph** suitable for X-ray diffraction were coated with poly(isobutylene) oil in a glovebox and quickly transferred to the goniometer head of a Rigaku Rapid II image plate diffractometer equipped with a MicroMax002+ high intensity copper X-ray source with confocal optics. Preliminary examination and data collection were performed with Cu Kα radiation (λ = 1.54184 Å). Crystals of **7-Bn** and **7-dipp** were transferred to the goniometer head of a Nonius KappaCCD diffractometer equipped with a graphite crystal and incident beam monochromator and examined with Mo Kα radiation (λ = 0.71073 Å). Single crystals of **11-Ph**, **11-pyr**, **12-pyr**, and **13-Tol** were transferred to the goniometer head of a Bruker AXS D8 Quest diffractometer and analyzed at 100 K using monochromatic Mo Kα radiation (λ = 0.71073 Å) with the omega scan technique. Crystals of **13-OMe** were transferred to the goniometer head of a Bruker AXS D8 Quest diffractometer and analyzed at 100 K using monochromatic Cu Kα radiation (λ = 1.54184 Å) with the omega scan technique. Data were collected, unit cells determined, and the data integrated and corrected for absorption and other systematic errors using the Apex2 or Apex3 suites of programs. The space groups were assigned and the structures were solved by direct methods using

XPREP within the SHELXTL suite of programs and refined by full matrix least squares against F^2 with all reflections using Shelxl 2014 or Shelxl 2017[32] and the graphical interface Shelxle. Complete crystallographic data, in CIF format, have been deposited with the Cambridge Crystallographic Data Centre.

2.3.2 General synthesis for Tp*$_2$U(IV) imido compounds (**7**):

A 20 mL scintillation vial was charged with **2-Bn** (0.100 g, 0.108 mmol) and 5 mL toluene. To this green solution, one equivalent RN_3 (R = Bn, *p*OMePh, detp, dipp, *p*Tol) (0.108 mmol; Bn = 0.014 g; OMe = 0.16 g; detp = 0.019 g; dipp = 0.022 g; *p*Tol = 0.017 g) was added, followed by an immediate evolution of nitrogen gas and color change from deep green to red-violet. Volatiles were removed *in vacuo*. The product mixtures were washed with pentane (2 × 5 mL) and dried to afford powders assigned as imido products Tp*$_2$U(N-Bn) (**7-Bn**), Tp*$_2$U(N-*p*OMePh) (**7-OMe**), Tp*$_2$U(N-detp) (**7-detp**), Tp*$_2$U(N-dipp) (**7-dipp**), and Tp*$_2$U(N-*p*Tol) (**x-*p*Tol**) (**x-Bn** = purple, 0.077 g, 0.082 mmol, 76% yield; **7-OMe** = red, 0.099 g, 0.102 mmol, 94% yield; **7-detp** = purple, 0.079 g, 0.080 mmol, 74% yield; **7-dipp** = deep purple, 0.088 g, 0.088 mmol, 81% yield; **7-*p*Tol** = red-purple, 0.066 g, 0.070 mmol, 65% yield). Single crystals of **7-Bn**, **7-*p*Tol** and **7-detp** were obtained by outward diffusion of a concentrated diethyl ether solution into a toluene solution at -35 ºC, and crystals of **7-dipp** were obtained from a concentrated solution of diethyl ether at -35 ºC.

7-Bn: Elemental analysis of $C_{37}H_{51}B_2N_{13}U$, Calculated: C, 47.40; H, 5.48; N, 19.42. Found: C, 46.87; H, 5.33; N, 18.95. ^{1}H NMR (C_6D_6, 25 °C): δ (ppm) = -20.58 (11, B-*H*), -6.79 (11, 18H, Tp*-C*H*$_3$), 1.50 (72, 18H, Tp*-C*H*$_3$), 5.28 (4, 6H, Tp*-C*H*), 16.91 (t, 1H, *p*-C*H*, *J* = 6.71 Hz), 19.87 (14, 2H, *m*/*o*-C*H*), 59.95 (84, 2H, *m*/*o*-C*H*).^{11}B NMR (C_6D_6, 25 °C): δ (ppm) = -64.75. IR (KBr) $\nu_{B\text{-}H}$ = 2560, 2515 cm^{-1}.

7-OMe: Elemental analysis of $C_{37}H_{51}B_2N_{13}OU$: Calculated: C, 46.61; H, 5.39; N, 19.10. Experimental: C, 46.00; H, 5.42; N, 17.88. ^{1}H NMR (C_6D_6, 25 °C): δ (ppm) =-20.98 (3, 2H, Tp* B-H), -6.80 (4, 18H, Tp*-CH_3), 2.85 (30, 18H, Tp*-CH_3), 5.48 (8, 6H, Tp*-CH), 21.18 (2, 3H, -OCH_3), 52.80 (21, 2H, Ar-H), 77.82 (21, 2H, Ar-H). ^{11}B NMR (C_6D_6, 25 °C): δ (ppm) = -66. IR (KBr pellet): $\nu_{B\text{-}H}$ = 2556, 2525 cm^{-1}.

7-detp: Reliable elemental analysis could not be obtained due to incomplete combustion: Elemental analysis of $C_{40}H_{57}B_2N_{13}U$, Calculated: C, 49.04; H, 5.87; N, 18.59. Found: C, 46.43; H, 5.63; N, 17.44. ^{1}H NMR (C_6D_6, 25 °C): δ (ppm) = -81.03 (11, 6H, Tp*-C*H*$_3$), -25.44 (7, B-*H*), -20.03 (2, 2H, Tp*-C*H*), -18.24 (5, 6H, Tp*-C*H*$_3$), -13.40 (4, 6H, Tp*-C*H*$_3$), -7.42 (5, 2H, Tp*-C*H*), 7.03 (4, 6H, -PhCH$_2$C*H*$_3$), 11.12 (21, 6H, Tp*-C*H*$_3$) 20.84 (24, 6H, Tp*-C*H*$_3$), 27.95 (13, 1H, *p*-C*H*), 41.88 (3, 2H, Tp*-C*H*), 53.87 (248, 2H, -PhC*H*$_2$CH$_3$) 54.83 (176, 2H, -PhC*H*$_2$CH$_3$), 55.90 (3, 2H, *m*/*o*-C*H*), 68.76 (15, 6H, Tp*-C*H*$_3$). ^{11}B NMR (C_6D_6, 25 °C): δ (ppm) = -76.92. IR (KBr) $\nu_{B\text{-}H}$ = 2550, 2521 cm^{-1}.

7-dipp: Elemental analysis of $C_{42}H_{61}B_2N_{13}U$, Calculated: C, 49.76; H, 6.66; N, 17.69. Found: C, 49.98; H, 6.02; N, 17.89. ^{1}H NMR (C_6D_6, 25 °C): δ (ppm) = -82.00 (10, 6H, Tp*-C*H*$_3$), -25.24 (4.75, B-*H*), -21.19 (10, 2H, Tp*-C*H*), -18.03 (7, 6H, Tp*-C*H*$_3$), -14.53 (4, 6H, Tp*-C*H*$_3$), -9.12, (4, 2H, Tp*-C*H*), 8.08 (90, 6H, Tp*-C*H*$_3$), 11.61 (7, 6H, C*H*$_3$), 12.42 (7, 6H, C*H*$_3$), 21.39 (583, 6H, Tp*-C*H*$_3$), 28.02 (3, 1H, *p*-C*H*), 43.25 (3, 2H, Tp*-C*H*), 55.69 (4, 2H, *m*/*o*-C*H*), 65.87 (61, 1H, *i*Pr-C*H*), 67.64 (41, 6H, Tp*-C*H*$_3$). ^{11}B NMR (C_6D_6, 25 °C): δ (ppm) = -75.35. IR (KBr) $\nu_{B\text{-}H}$ = 2553, 2521 cm^{-1}.

7-*p*Tol: Elemental analysis of $C_{37}H_{51}B_2N_{13}U$, Calculated: C, 47.40; H, 5.48; N, 19.42. Found: C, 47.02; H, 5.25; N, 18.68. ^{1}H NMR (C_6D_6, 25 °C): δ -21.21, (0.25, B-*H*), -6.89 (4, 18H, Tp*-C*H*$_3$), 2.81 (22, 18H, Tp*-C*H*$_3$), 5.48 (7, 6H, Tp*-C*H*), 38.50 (5, 3H, C*H*$_3$), 53.82 (8, 2H, *m*-C*H*), 78.69 (16, 2H, *o*-C*H*). ^{11}B NMR (C_6D_6, 25 °C): δ (ppm) = -66.60. IR (KBr) $\nu_{B\text{-}H}$ = 2553, 2528 cm^{-1}.

2.3.3 Alternate preparation of Tp*$_2$U(IV) imido compounds:

A 20 mL scintillation vial was charged with **1-I** (0.060 g, 0.063 mmol) and 5 mL THF. To this deep blue solution, one equivalent (0.063 mmol) of corresponding azide (Bn = 0.008 g; *p*OMePh = 0.009 g; detp = 0.011 g; dipp = 0.013 g; *p*Tol = 0.009 g) was added. An excess of potassium graphite (0.011 g, 0.079 mmol) was introduced and the reaction was allowed to stir for 1.5 h. After stirring, the resulting graphite and KI were removed *via* filtration. The filtrate was concentrated under reduced pressure. Crude products were washed with pentane (2 × 10 mL) to give **7-Bn** (0.049 g, 0.052 mmol, 82% yield), **7-OMe** (0.050 g, 0.052 mmol, 83% yield), **7-detp** (0.051g, 0.053 mmol, 84% yield), **7-dipp** (0.054 g, 0.053 mmol, 85% yield) or **7-*p*Tol** (0.051 g, 0.054 mmol, 87% yield).

2.3.4 Synthesis of κ^2-ureato compounds (**8**):

In a 20 mL scintillation vial, Tp*$_2$UNR (R = Ad: 0.060 g, 0.061 mmol; Bn: 0.060 g, 0.064 mmol; Ph: 0.052 g, 0.056 mmol; *p*Tol: 0.057 g, 0.061 mmol) was dissolved in 10 mL THF. To the deep red solution, one equivalent phenyl isocyanate (R = Ad: 0.007 mL, 0.061 mmol; Bn: 0.008 mL, 0.064 mmol; Ph: 0.006 mL, 0.056 mmol; *p*Tol: 0.007 mL, 0.061 mmol) was injected *via* microsyringe, and the reaction mixture was allowed to stir for 15 minutes, creating a red-orange solution. Volatiles were removed *in vacuo*. The crude products were washed with pentane (2 × 10 mL) to afford orange powders, assigned as Tp*$_2$U[κ^2-*N*,*N*'-1-phenyl-3-adamantylurea] (**8-Ad**), Tp*$_2$U[κ^2-(*N*,*N*'-1-phenyl-3-benzylureato)] (**8-Bn**), Tp*$_2$U[κ^2-(*N*,*N*'-diphenylureato)] (**8-Ph**), or Tp*$_2$U[κ^2-(*N*,*N*'-1-phenyl-3-*p*-tolylureato)] (**8-*p*Tol**) (**8-Ad**: 0.049 g, 0.045 mmol 73% yield; **8-Bn**: 0.061 g, 0.058 mmol, 90% yield; **8-Ph**: 0.048 g, 0.046 mmol, 82% yield; **8-*p*Tol**: 0.102 g, 0.097 mmol, 89% yield).

8-Ad: Reliable elemental analysis could not be obtained due to incomplete combustion: Elemental analysis of $C_{47}H_{64}B_2N_{14}OU$, Calculated, C, 51.28; H, 5.86; N, 17.81. Found, C 47.39; H, 4.90; N, 16.16 ^{1}H NMR (C_6D_6, 25 ºC): δ = -37.26 (33, 3H, Tp*-C*H*$_3$), -30.25 (25, 3H, Tp*-C*H*$_3$), -16.81 (9, 3H, Tp*-C*H*$_3$), -12.96 (137, H, B-*H*), -8.90 (3, 3H, Tp*-C*H*$_3$), -7.78 (2, 3H, Tp*-C*H*$_3$), -5.29 (5, 1H, Tp*-C*H*), -3.45 (12, 3H, Tp*-C*H*$_3$), -2.17 (3, 1H, Tp*-C*H*), -1.93 (4, 3H, Tp*-C*H*$_3$), -0.55 (5, 1H, Tp*-C*H*), -0.02 (22, 3H, Ad-C*H*), 0.30 (5, 3H, Ad-C*H*), 1.04 (d, 3H, Ad-C*H*, *J* = 10.64 Hz), 1.60 (d, 3H, Ad-C*H*, *J* = 11.41 Hz), 2.01 (9, 3H, Tp*-C*H*$_3$), 2.88 (12, 3H, Tp*-C*H*$_3$), 3.67 (11, 3H, Ad-C*H*), 4.18 (3, 3H, Tp*-C*H*$_3$), 7.95 (3, 1H, Tp*-C*H*), 9.98 (t, 1H, Ph: *p*-C*H*, *J* = 7.48 Hz), 14.01 (13, 5H, Tp*-C*H*$_3$/Ph: *o*/*m*-C*H*), 17.68 (2, 1H, Tp*-C*H*), 18.47 (2, 1H, Tp*-C*H*), 21.21 (17, 2H, Ph: *o*/*m*-C*H*), 42.89 (17, 3H, Tp*-C*H*$_3$). ^{11}B NMR (C_6D_6, 25 °C): δ (ppm) = -51.48, -19.31. IR (KBr): $\nu_{B\text{-}H}$ = 2559, 2515 cm^{-1}; $\nu_{C=O}$ = 1696 cm^{-1}

8-Bn: Reliable elemental analysis could not be obtained due to incomplete combustion: Elemental analysis of $C_{44}H_{56}B_2N_{14}OU$, Calculated, C, 50.01; H, 5.34; N, 18.56. Found, C 48.69; H, 5.34; N, 17.82 ^{1}H NMR (C_6D_6, 25 °C): δ = -38.94 (6, 3H, Tp*-C*H*$_3$), -24.69 (9, 3H, Tp*-C*H*$_3$), -18.84 (182, B-*H*), -17.18 (131, 3H, Tp*-C*H*$_3$), -11.02 (10, 3H, Tp*-C*H*$_3$), -8.92 (4, 3H, Tp*-C*H*$_3$), -8.83 (2, 3H, Tp*-C*H*$_3$), -6.30 (3 3H, Tp*-C*H*$_3$), -3.81 (4, 3H, Tp*-C*H*$_3$), -3.76 (4, 1H, Tp*-C*H*), -3.58 (5, 1H, Tp*-C*H*), -1.41 (12, 1H, Tp*-C*H*), 2.23 (5, 2H,

Bn: *m*/*o*-C*H*), 2.51 (7, 3H, Tp*-CH_3), 4.19 (26, 2H, -CH_2Ph), 4.59 (6, 3H, Tp*-CH_3), 8.77 (32, 1H, Bn: *p*-C*H*), 10.23 (t, 1H, Ph: *p*-C*H*, *J* = 7.32 Hz), 12.22 (t, 2H, Ph: *m*-C*H*, *J* = 7.70 Hz), 12.24 (21, 2H, Ph: *o*-C*H*), 17.11 (8, 1H, Tp*-C*H*), 20.55 (8, 1H, Tp*-C*H*), 27.32 (32, 2H, Bn: *m*/*o*-C*H*), 55.96 (13, 3H, Tp*-CH_3), 75.66 (4, 1H, Tp*-C*H*). ^{11}B NMR (C_6D_6, 25 °C): δ (ppm) = -28.68. IR (KBr): ν_{B-H} = 2556, 2512 cm^{-1}; $\nu_{C=O}$ = 1698 cm^{-1}.

8-Ph: Elemental analysis of $C_{43}H_{54}B_2N_{14}OU$, Calculated, C, 49.53; H, 5.22; N, 18.81. Found, C 48.67; H, 5.13; N, 17.37. ^{1}H NMR (C_6D_6, 25 °C): δ = -32.97 (49, 6H, Tp*-CH_3), -11.32 (153, B-*H*), -9.67 (17, 6H, Tp*-CH_3), -3.12 (5, 6H, Tp*-CH_3), -2.25 (8, 6H, Tp*-CH_3), -1.10 (13, 2H, Tp*-C*H*), 0.27 (3, 6H, Tp*-CH_3), 0.54 (7, 2H, Tp*-C*H*), 6.94 (t, 2H, *p*-C*H*, *J* = 6.88 Hz), 9.51 (17, 4H, *m*-C*H*), 10.53 (173, 4H, *o*-C*H*), 19.51 (16, 2H, Tp*-C*H*), 32.05 (20, 6H, Tp*-CH_3). ^{11}B NMR (C_6D_6, 25 °C): δ (ppm) = -49.62. IR (KBr): ν_{B-H} = 2557, 2521 cm^{-1}; $\nu_{C=O}$ = 1707 cm^{-1}.

8-*p*Tol: Elemental analysis of $C_{44}H_{56}B_2N_{14}OU$, Calculated, C, 50.01; H, 5.34; N, 18.56. Found, C 49.23; H, 5.00; N, 18.86 ^{1}H NMR (C_6D_6, 25 °C): δ = -33.88 (8, 3H, Tp*-CH_3), -32.52 (46, 3H, Tp*-CH_3), -11.13 (23, B-*H*), -10.73 (21, B-*H*), -9.57 (75, 3H, Tp*-CH_3), -9.35 (28, 3H, Tp*-CH_3), -3.05 (53, 3H, Tp*-CH_3), -2.88 (7, 3H, Tp*-CH_3), -2.45 (9, 3H, Tp*-CH_3), -1.34 (5, 1H, Tp*-C*H*), -1.12 (152, 3H, Tp*-CH_3), 0.09 (4, 3H, Tp*-CH_3), 0.41 (6, 1H, Tp*-C*H*), 0.78 (6, 3H, Tp*-CH_3), 1.87 (3, 1H, Tp*-C*H*), 2.74 (3, 1H, Tp*-C*H*), 4.78 (6, 3H, -CH_3), 6.57 (t, 1H, Ph: *p*-C*H*, *J* = 7.07 Hz), 8.83 (d, 2H, Ph: *m*-C*H*, *J* = 6.23 Hz), 9.03 (d, 2H, Ph: *o*-C*H*, *J* = 7.29 Hz), 10.13 (d, 2H, *p*Tol: *m*-C*H*, *J* = 6.30 Hz), 11.90 (d, 2H, *p*Tol: *o*-C*H*, *J* = 7.20 Hz), 19.26 (15, 1H, Tp*-C*H*), 19.44 (38, 1H, Tp*-C*H*), 29.34 (72, 3H, Tp*-CH_3), 33.34 (1552, 3H, Tp*-CH_3). ^{11}B NMR (C_6D_6, 25 °C): δ (ppm) = -48.41. IR (KBr): ν_{B-H} = 2561, 2507 cm^{-1}; $\nu_{C=O}$ = 1711 cm^{-1}.

2.3.5 Synthesis of κ^2-thioureato compounds (**9**):

A 20 mL scintillation vial was charged with Tp*$_2$UNR (R = Bn: 0.060 g, 0.064 mmol; Ph: 0.067 g, 0.073 mmol; *p*Tol: 0.100 g, 0.107 mmol) and 10 mL THF. To the deep red solution, one equivalent of phenylisothiocyanate (R = Bn: 0.011 mL, 0.064 mmol; Ph: 0.010 mL, 0.073 mmol; *p*Tol: 0.013 mL, 0.11 mmol) was added *via* microsyringe, and the reaction mixture was stirred for 15 minutes, creating a red-orange solution. Volatiles were removed *in vacuo*. The crude mixtures were washed with pentane (2 × 10 mL) to afford

orange powders assigned as Tp*$_2$U[κ^2-(*N*,*N*'-1-phenyl-3-benzylthioureato)] (**9-Bn**), Tp*$_2$U[κ^2-(*N*,*N*'-diphenylthioureato)] (**9-Ph**), or Tp*$_2$U[κ^2-(*N*,*N*'-1-phenyl-3-*para*-tolylthioureato)] (**9-*p*Tol**) (**9-Bn**: 0.062 g, 0.058 mmol, 90% yield; **9-Ph**: 0.073 g, 0.069 mmol, 96% yield; **9-*p*Tol**: 0.102 g, 0.095 mmol, 89% yield). Red single crystals of **9-Ph**, which were suitable for X-ray diffraction, were grown from a concentrated benzene solution at room temperature.

9-Bn: Reliable elemental analysis could not be obtained due to incomplete combustion: Elemental analysis of $C_{44}H_{56}N_{14}B_2SU$, Calculated C, 49.26; H, 5.26; N, 18. 28, Found, C, 45.41; H, 5.18; N, 16.96. ^{1}H NMR (C_6D_6, 25 °C): δ = -37.47 (19, 3H, Tp*-C*H*$_3$), -29.04 (19, 3H, Tp*-C*H*$_3$), -16.47 (204, B-*H*), -10.71 (16, 3H, Tp*-C*H*$_3$), -10.26 (15, 3H, Tp*-C*H*$_3$), -9.46 (77, 3H, Tp*-C*H*$_3$), -5.25 (15, 3H, Tp*-C*H*$_3$), -3.77 (26, 3H, Tp*-C*H*$_3$), -3.51 (17, 1H, Tp*-C*H*), -3.42 (77, 1H, Tp*-C*H*), -2.08 (15, 1H, Tp*-C*H*), -1.65 (16, 3H, Tp*-C*H*$_3$), -1.25 (15, 3H, Tp*-C*H*$_3$), 3.86 (29, 2H, -C*H*$_2$Ph), 4.69 (18, 2H, Bn: *m*/*o*-C*H*), 6.70 (28, 1H, Ph: *p*-C*H*), 7.42 (19, 3H, Tp*-C*H*$_3$), 7.78 (27, 2H, Ph: *m*/*o*-C*H*), 9.21 (25, 2H, Ph: *m*/*o*-C*H*), 15.27 (18, 3H, Tp*-C*H*$_3$), 18.71 (14, 1H, Tp*-C*H*), 22.05 (66, 1H, Bn: *p*-C*H*), 22.21 (24, 2H, Bn: *m*/*o*-C*H*), 49.66 (20, 3H, Tp*-C*H*$_3$),) 61.95 (35, 1H, Tp*-C*H*), 77.78 (36, 1H, Tp*-C*H*). ^{11}B NMR (C_6D_6, 25 °C): δ = -49.47. IR (KBr): ν_{B-H} = 2561, 2525 cm^{-1}, $\nu_{C=S}$ = 1542 cm^{-1}.

9-Ph: Elemental analysis of $C_{43}H_{54}N_{14}B_2SU$, Calculated C, 48.78; H, 5.14; N, 18.52, Found, C, 47.48; H, 4.97; N, 17.42. ^{1}H NMR (C_6D_6, 25 °C): δ = -34.67 (6, 6H, Tp*-C*H*$_3$), -12.30 (133, B-*H*), -10.32 (9, 6H, Tp*-C*H*$_3$), -3.76 (3, 6H, Tp*-C*H*$_3$), -2.61 (6, 6H, Tp*-C*H*$_3$), -2.57 (4, 2H, Tp*-C*H*), 0.10 (1, 2H, Tp*-C*H*), 0.31 (3, 6H, Tp*-C*H*$_3$), 6.66 (t, 2H, *p*-C*H*, *J* = 7.27 Hz), 8.90 (t, 4H, *m*-C*H*, *J* = 7.07 Hz), 11.09 (d, 4H, *o*-C*H*, *J* = 7.12 Hz), 20.45 (3, 2H, Tp*-C*H*), 34.34 (17, 6H, Tp*-C*H*$_3$). ^{11}B NMR (C_6D_6, 25 °C): δ = -48.31. IR (KBr) = ν_{B-H} 2565, 2519 cm^{-1}; $\nu_{C=S}$ 1542 cm^{-1}.

9-*p*Tol: Elemental analysis of $C_{44}H_{56}N_{14}B_2SU$, Calculated C, 49.26; H, 5.26; N, 18. 28, Found, C, 48.45; H, 5.39; N, 17.64. ^{1}H NMR (C_6D_6, 25 °C): δ = -35.25 (6, 3H, Tp*-C*H*$_3$), -34.05 (14, 3H, Tp*-C*H*$_3$), -12.73 (152, B-*H*), -11.87 (138, B-*H*), -10.37 (5, 3H, Tp*-C*H*$_3$), -10.25 (9, 3H, Tp*-C*H*$_3$), -3.95 (4, 3H, Tp*-C*H*$_3$), -3.48 (3, 3H, Tp*-C*H*$_3$), -3.44 (10, 3H, Tp*-C*H*$_3$), -2.62 (8, 2H, Tp*-C*H*), -1.83 (5, 3H, Tp*-C*H*$_3$), 0.07 (2, 1H, Tp*-C*H*), 0.13 (3, 3H, Tp*-C*H*$_3$), 0.60 (3, 3H, Tp*-C*H*$_3$), 0.77 (2, 1H, Tp*-C*H*), 4.16 (3, 3H, -C*H*$_3$), 6.40 (t,

1H, Ph: *p*-C*H*, *J* = 7.45 Hz), 8.60 (t, 2H, Ph: *m*-C*H*, *J* = 7.48 Hz), 9.13 (d, 2H, Ph: *o*-C*H*, *J* = 7.44 Hz), 10.05 (d, 2H, *p*Tol: *m*-C*H*, *J* = 7.58 Hz), 11.83 (2H, *p*Tol: *o*-C*H*, *J* = 7.76 Hz), 20.34 (3, 1H, Tp*-C*H*), 20.49 (3, 1H, Tp*-C*H*), 32.84 (11, 3H, Tp*-CH_3), 35.73 (14, 3H, Tp*-CH_3). ^{11}B NMR (C_6D_6, 25 °C): δ = -51.34. IR (KBr) $\nu_{B\text{-}H}$ = 2563, 2517 cm^{-1}; $\nu_{C=S}$ 1542 cm^{-1}.

2.3.6 Synthesis of κ^2-selenoureato compounds (**10**):

A 20 mL scintillation vial was charged with Tp*$_2$UNR (R = Ph: 0.080 g, 0.087 mmol; *p*Tol: 0.07 g, 0.075 mmol) and 10 mL THF. To the deep red solution, one equivalent of phenyl isoselenocyanate (R = Ph: 0.016 g, 0.087 mmol; 0.014 g *p*Tol, 0.075 mmol) was added *via* microsyringe, and the reaction mixture was allowed to stir for 8 hours, creating a red-orange solution. Volatiles were removed *in vacuo*, and crude products were washed with pentane (4 × 10 mL) to yield orange powders, assigned as Tp*$_2$U[κ^2-(*N*,*N*'-diphenylselenoureato)] (**10-Ph**) or Tp*$_2$U[κ^2-(*N*,*N*'-1-phenyl-3-*para*-tolylselenoureato)] (**10-*p*Tol**) (**10-Ph**: 0.077 g, 0.070 mmol, 80% yield; **10-*p*Tol**: 0.062 g, 0.055 mmol, 74% yield). Single crystals of **10-Ph**, suitable for X-ray diffraction were obtained from a concentrated benzene solution at room temperature.

10-Ph: Reliable elemental analysis could not be obtained due to the instability of compound **x-Ph**. ^{1}H NMR (C_6D_6, 25 °C): δ -34.93 (5, 6H, Tp*-CH_3), -12.70 (137, B-*H*), -10.52 (2, 6H, Tp*-CH_3), -3.75 (4, 6H, Tp*-CH_3), -2.91 (2, 2H, Tp*-C*H*), -2.83 (47, 6H, Tp*-CH_3), 0.31 (2, 6H, Tp*-CH_3), 0.46 (2, 2H, Tp*-C*H*), 6.68 (t, 2H, *p*-C*H*, *J* = 7.49 Hz), 8.87 (t, 4H, *m*-C*H*, *J* = 7.54 Hz), 11.46 (d, 4H, *o*-C*H*, *J* = 7.63 Hz), 20.63 (52, 2H, Tp*-C*H*), 34.94 (19, 6H, Tp*-CH_3). ^{11}B NMR (C_6D_6, 25 °C): δ = -51.62. IR (KBr): $\nu_{B\text{-}H}$ = 2566, 2508 cm^{-1}; $\nu_{C=Se}$ = 1542 cm^{-1}.

10-*p*Tol: Reliable elemental analysis could not be obtained due to the instability of compound **x-*p*Tol**. ^{1}H NMR (C_6D_6, 25 °C): δ -35.44 (17, 3H, Tp*-CH_3), -34.42 (8, 3H, Tp*-CH_3), -14.10 (19, B-*H*), -10.58 (2, 3H, Tp*-CH_3), -10.48 (18, 3H, Tp*-CH_3), -4.00 (2, 3H, Tp*-CH_3), -3.58 (2, 3H, Tp*-CH_3), -3.48 (3, 3H, Tp*-CH_3), -2.97 (2, 1H, Tp*-C*H*), -2.96 (3, 1H, Tp*-C*H*), -2.15 (3, 3H, Tp*-CH_3), 0.10 (2, 3H, Tp*-CH_3), 0.17 (2, 1H, Tp*-C*H*), 0.50 (2, 3H, Tp*-CH_3), 0.76 (2, 1H, Tp*-C*H*), 4.07 (2, 3H, -CH_3), 6.46 (t, 1H, Ph: *p*-C*H*, *J* = 7.47 Hz), 8.59 (t, 2H, Ph: *m*-C*H*, *J* = 7.59 Hz), 9.00 (d, 2H, Ph: *o*-C*H*, *J* = 7.55

Hz), 10.58 (d, 2H, *p*Tol: *m*-C*H*, *J* = 7.84 Hz), 12.07 (d, 2H, *p*Tol: *o*-C*H*, *J* = 7.56 Hz), 20.53 (2, 1H, Tp*-C*H*), 20.66 (28, 1H, Tp*-C*H*), 33.66 (7, 3H, Tp*-C*H*$_3$), 36.17 (9, 3H, Tp*-C*H*$_3$). ^{11}B NMR (C_6D_6, 25 ºC): δ = -52.78. IR(KBr) ν_{B-H} = 2564, 2522 cm^{-1}; $\nu_{C=Se}$ =1542 cm^{-1}.

2.3.7 Synthesis of Tp*$_2$U[κ^2-(*N*,*N*'-1-phenyl-3-dippureato)] (**8-dipp**):

A 20 mL scintillation vial was charged with **7-Ph** (0.085 g, 0.092 mmol) and 10 mL THF. To the deep red solution, one equivalent of dipp isocyanate (0.020 mL, 0.092 mmol) was added *via* microsyringe, and the reaction mixture was allowed to stir for 10 minutes, creating a red-orange solution. Volatiles were removed *in vacuo*, and the crude products were washed with pentane (4 × 10 mL) to yield an orange powder, assigned as Tp*$_2$U[κ^2-(*N*,*N*'-1-phenyl-3-dippureato)] (**8-dipp**) (0.084 g, 0.075 mmol, 81% yield).

Reliable elemental analysis could not be obtained due to the instability of compound **8-dipp**. ^{1}H NMR (C_6D_6, 25 °C): δ = -43.81 (6, 3H, Tp*-C*H*$_3$), -28.72 (9, 3H, Tp*-C*H*$_3$), -24.80 (160, B-*H*), -17.21 (4, 3H, Tp*-C*H*$_3$), -15.71 (6, 3H, Tp*-C*H*$_3$), -14.60 (3, 1H, dipp: *i*-PrC*H*), -13.63 (4, 3H, Tp*-C*H*$_3$), -10.82 (3, 3H, Tp*-C*H*$_3$), -9.89 (d, 2H, dipp: *m*-C*H*, *J* = 8 Hz), -7.84 (3, 1H, Tp*-C*H*), -7.59 (3, 3H, Tp*-C*H*$_3$), -7.52 (3, 1H, Tp*-C*H*), -2.33 (4, 1H, Tp*-C*H*), -1.56 (4, 3H, dipp-C*H*$_3$), -1.11 (3, 3H, dipp-C*H*$_3$), 1.98 (3, 3H, Tp*-C*H*$_3$), 3.57 (8, 3H, Tp*-C*H*$_3$), 5.11 (5, 1H, Tp*-C*H*), 5.67 (3, 1H, Tp*-C*H*), 10.86 (29, 3H, dipp-C*H*$_3$), 11.24 (38, 5H, Ph: *m*/*o*-C*H* + dipp-C*H*$_3$), 13.30 (9, 3H, Tp*-C*H*$_3$), 17.80 (7, 3H, Tp*-C*H*$_3$), 17.90 (t, 1H, dipp: *p*-C*H*, *J* = 8 Hz), 19.06 (3, 1H, Tp*-C*H*), 21.71 (4, 1H, dipp: *i*-PrC*H*), 30.26 (5, 1H, Tp*-C*H*), 73.20 (11, 3H, Tp*-C*H*$_3$). ^{11}B NMR (C_6D_6, 25 ºC): δ = -43.72. IR (KBr) ν_{B-H} = 2563, 2519 cm^{-1}; $\nu_{C=O}$ = 1695 cm^{-1}.

2.3.8 Synthesis of Tp*$_2$U[=N-C(=N(*p*RPh)(Ar)] (**11-12**):

In a 20 mL scintillation vial, Tp*$_2$U(N-*p*-RPh) (R = OMe: 0.120 g, 0.126 mmol; CH_3: 0.120 g, 0.128 mmol) was dissolved in 8 mL THF. To this deep red solution, one equivalent of nitrile (R = OMe: benzonitrile:13.0 μL; 4-cyanopyridine: 0.013 g, 0.126 mmol; R = CH_3: benzonitrile: 13.2 μL; 4-cyanopyridine: 0.013 g) was added. Within five minutes of stirring, the solutions became a red-orange color, at which point, volatiles were removed in vacuo. The resulting orange powders were washed with n-pentane (2 × 5 mL) and subsequently

dried affording in orange powders assigned as Tp*$_2$U[=NC(NpRPh)-Ar] (R = OMe, Ar = Ph (**11-Ph**) 0.105 g, 0.099 mmol, 79% yield; py (**11-py**), 0.111 g, 0.104 mmol, 83% yield; R = CH3, Ar = Ph (**12-Ph**), 0.100 g, 0.096 mmol, 75% yield; py (**12-py**), 0.104 g, 0.100 mmol, 78% yield). Single crystals were obtained at -35 °C by layering n-pentane into a concentrated diethyl ether solution (5:1 ratio) (**12-py**), vapor diffusion of diethyl ether into toluene (**12-Ph**), or concentrated solution of diethyl ether (**11-py**).

11-Ph: Elemental Analysis of $C_{44}H_{56}B_2N_{14}OU$: Calculated: C, 50.01; H, 5.34; N, 18.56. Experimental: C, 49.87; H, 5.77; N, 18.58. ^{1}H NMR (benzene-d$_6$, ambient temperature): δ = -81.54 (50, 3H, Tp*-C*H*$_3$), -77.93 (15, 3H, Tp*-C*H*$_3$), -28.85 (5, 1H, Tp* B-*H*), -24.96 (3, 1H, Tp* B-*H*), -20.71 (22, 1H, Tp*-C*H*), -19.92 (8, 1H, Tp*-C*H*), -18.81 (7, 3H, Tp*-C*H*$_3$), -18.85 (10, 3H, Tp*-C*H*$_3$), -14.66 (19, 3H, Tp*-C*H*$_3$), -12.43 (9, 3H, Tp*-C*H*$_3$), -6.91 (9, 1H, Tp*-C*H*), -6.83 (4, 1H, Tp*-C*H*), -5.32 (8, 1H, Tp*-C*H*), -3.25 (3, 3H, Tp*-C*H*$_3$), -2.57 (48, 2H, Ar-*H*), 5.36 (9, 3H, *p*OC*H*$_3$), 7.35 (6, 3H, Tp*-C*H*$_3$), 16.82 (25, 2H, Ar-*H*), 18.98 (53, 3H, Tp*-C*H*$_3$), 22.43 (70, 3H, Tp*-C*H*$_3$), 37.70 (23, 2H, Ar-*H*), 41.64 (7, 1H, Tp*-C*H*), 41.75 (7, 1H, Tp*-C*H*), 49.30 (25, 2H, Ar-*H*), 64.95 (75, 3H, Tp*-C*H*$_3$), 73.16 (19, 3H, Tp*-C*H*$_3$). ^{11}B NMR (benzene-d$_6$, ambient temperature): δ = -86, -76. IR (KBr pellet): $\nu_{B\text{-}H}$ = 2553, 2521 cm^{-1}.

11-py: Elemental Analysis of $C_{43}H_{55}B_2N_{15}OU$: Calculated: C, 48.83; H, 5.24; N, 19.86. Experimental: C, 49.91; H, 5.80; N, 20.18. ^{1}H NMR (benzene-d$_6$, ambient temperature): δ = -81.41 (17, 3H, Tp*-C*H*$_3$, -77.81 (18, 3H, Tp*-C*H*$_3$), -28.79 (4, 1H, Tp* B-*H*), -24.88 (3, 1H, Tp* B-*H*), -20.70 (12, 1H, Tp*-C*H*), -19.90 (8, 1H, Tp*-C*H*), -18.80 (10, 3H, Tp*-C*H*$_3$), -18.54 (13, 3H, Tp*-C*H*$_3$), -14.66 (13, 3H, Tp*-C*H*$_3$), -12.43 (9, 3H, Tp*-C*H*$_3$), -6.92 (10, 1H, Tp*-C*H*), -5.32 (12, 1H, Tp*-C*H*), -3.25 (6, 3H, Tp*-C*H*$_3$), -2.56 (17, 2H, Ar-C*H*), 5.32 (10, 3H, OC*H*$_3$), 7.31 (11, 3H, Tp*-C*H*$_3$), 16.81 (24, 2H, Ar-C*H*), 18.94 (21, 3H, Tp*-C*H*$_3$), 22.38 (23, 3H, Tp*-C*H*$_3$), 37.65 (29, 2H, Ar-C*H*), 41.54 (13, 1H, Tp*-C*H*), 41.65 (27, 1H, Tp*-C*H*), 49.31 (13, 2H, Ar-C*H*), 64.79 (42, 3H, Tp*-C*H*$_3$), 73.00 (22, 3H, Tp*-C*H*$_3$). ^{11}B NMR (benzene-d$_6$, ambient temperature): δ = -86, -75. IR (KBr pellet): $\nu_{B\text{-}H}$ = 2551, 2517 cm^{-1}.

12-Ph: Elemental Analysis of $C_{44}H_{56}B_2N_{14}U$: Calculated: C, 50.78; H, 5.42; N, 18.84. Experimental: C, 49.66; H, 5.53; N, 19.34. ^{1}H NMR (benzene-d$_6$, ambient temperature): δ = -81.31 (15, 3H, Tp*-C*H*$_3$), -77.72 (16, 3H, Tp*-C*H*$_3$), -28.68 (5, 1H, Tp*

B-*H*), -24.84 (4, 1H, Tp* B-*H*), -20.67 (12, 1H, Tp*-C*H*), -19.86 (12, 1H, Tp*-C*H*), -18.77 (9, 3H, Tp*-C*H*$_3$), -18.51 (12, 3H, Tp*-C*H*$_3$), -14.64 (11, 3H, Tp*-C*H*$_3$), -12.41 (9, 3H, Tp*-C*H*$_3$), -6.89 (24, 1H, Tp*-C*H*), -5.29 (11, 1H, Tp*-C*H*), -3.22 (6, 3H, Tp*-C*H*$_3$), -2.54 (14, 2H, Ar-C*H*), 5.32 (9, 3H, *para*-C*H*$_3$), 7.32 (9, 3H, Tp*-C*H*$_3$), 16.81 (22, 3H, Tp*-C*H*$_3$), 18.91 (16, 2H, Ari-C*H*), 37.62 (10, 1H, Tp*-C*H*), 41.51 (10, 1H, Tp*-C*H*), 41.63 (9, 1H, Tp*-C*H*), 49.17 (22, 2H, Ar-C*H*), 64.73 (51, 3H, Tp*-C*H*$_3$), 72.96 (19, 3H, Tp*-C*H*$_3$). ^{11}B NMR (benzene-d$_6$, ambient temperature): δ = -82, -76. IR (KBr pellet): ν_{B-H} = 2550, 2522 cm^{-1}.

12-py: Elemental Analysis of $C_{43}H_{55}B_2N_{15}U$: Calculated: C, 49.58; H, 5.32; N, 20.17. Experimental: C, 49.05; H, 5.52; N, 19.71. ^{1}H NMR (benzene-d$_6$, ambient temperature): δ = -82.66 (12, 3H, Tp*-C*H*$_3$), -77.25 (13, 3H, Tp*-C*H*$_3$), -27.82 (2, 1H, Tp* B-*H*), -25.63 (3, 1H, Tp* B-*H*), -20.44 (8, 4H, Tp*-C*H*$_3$ + Tp*-C*H*), -18.75 (7, 3H, Tp*-C*H*$_3$), -18.61 (37, 3H, Tp*-C*H*$_3$), -14.17 (9, 3H, Tp*-C*H*$_3$), -12.84 (19, 3H, Tp*-C*H*$_3$), -7.08 (73, 1H, Tp*-C*H*), -5.66 (8, 1H, Tp*-C*H*), -3.99 (47, 3H, Tp*-C*H*$_3$), -2.50 (89, 2H, Ar-C*H*), 5.89 (7, 3H, *p*Tol-C*H*$_3$), 6.36 (3, 1H, Tp*-C*H*), 8.11 (20, 1H, Tp*-C*H*), 17.20 (18, 2H, Ar-C*H*), 20.01 (98, 3H, Tp*-C*H*$_3$), 21.76 (16, 3H, Tp*-C*H*$_3$), 37.43 (21, 2H, Ar-C*H*), 41.74 (6, 1H, Tp*-C*H*), 41.89 (6, 1H, Tp*-C*H*), 49.97 (6, 2H, Ar-C*H*), 66.45 (73, 3H, Tp*-C*H*$_3$), 70.73 (16, 3H, Tp*-C*H*$_3$). ^{11}B NMR (benzene-d$_6$, ambient temperature): δ = -83, -76. IR (KBr pellet): ν_{B-H} = 2551, 2519 cm^{-1}.

2.3.9 Synthesis of Tp*$_2$U[NC(=N-4-R-*para*-cyanobenzene] (**13-R**).

A 20 mL scintillation vial was charged with Tp*$_2$U(N-*p*RPh) (R = CH$_3$: 0.225 g, 0.240 mmol; OCH$_3$: 0.225 g, 0.240 mmol) in 8 mL THF. To this red solution, an equivalent of terephthalonitrile (R = CH$_3$: 0.031 g, 0.210 mmol; R= OCH3: 0.027 g, 0.240 mmol) was added and a slight color change to red-orange was noted. After 30 minutes, volatiles were removed *in vacuo* which resulted in an orange powder. This powder was washed with *n*-pentane (2 5 mL) and dried, affording a pale orange powder (R = CH$_3$: 0.219 g, 0.203 mmol, 85% yield; R = OCH$_3$: 0.184 g, 0.168 mmol, 80% yield) assigned as Tp*$_2$U[NC(=N-*p*RPh)-*p*-cyanobenzene] (R = CH$_3$ = **13-Tol**; OCH$_3$ **= 13-OMe**). Single crystals suitable for X-ray crystallographic analysis were obtained from vapor diffusion of concentrated diethyl ether solution into toluene at -35 °C.

13-Tol: ^{1}H NMR (benzene-d_6, ambient temperature): δ = -82.78 (12, 3H, Tp*-C*H*$_3$), -77.41 (7, 3H, Tp*-C*H*$_3$), -27.28 (1, 1H, B-*H*), -25.06 (6, 1H, B-*H*), -20.38 (3, 1H, Tp*-C*H*), -20.31 (3, 1H, Tp*-C*H*), -18.71 (4, 3H, Tp*-C*H*$_3$), -18.57 (12, 3H, Tp*-C*H*$_3$), -13.88 (11, 3H, Tp*-C*H*$_3$), -12.67 (10, 3H, Tp*-C*H*$_3$), -7.10 (8, 1H, Tp*-C*H*), -5.87 (9, 1H, Tp*-C*H*), -4.32 (4, 3H, *p*-tolyl-C*H*$_3$), -2.99 (11, 1H, Tp*-C*H*), 6.05 (4, 3H, Tp*-C*H*$_3$), 7.35 (5, 3H, Tp*-C*H*$_3$), 15.57 (9, 2H, C*H*), 20.09 (43, 3H, Tp*-C*H*$_3$), 22.04 (10, 3H, Tp*-C*H*$_3$), 36.37 (11, 2H, C*H*), 41.86, (10, 1H, Tp*-C*H*), 41.96 (3, 1H, Tp*-C*H*), 53.61 (20, 2H, C*H*), 65.81 (51, 3H, Tp*-C*H*$_3$), 70.66 (222, 3H, Tp*-C*H*$_3$). ^{11}B NMR (benzene-d_6, ambient temperature): δ = -83, -76. IR (KBr pellet). Elemental analysis of $C_{46}H_{58}N_{15}B_2U_1$: Calculated, C, 51.12; H, 5.41; N, 19.44. Found, C, 50.79; H, 5.20; N, 19.17.

13-OMe: ^{1}H NMR (benzene-d_6, ambient temperature): δ = -81.73 (25, 3H, Tp*-CH_3), -78.07 (9, 3H, Tp*-CH_3), -28.48 (3, 1H, Tp*-BH), -24.70 (7, 1H, Tp*-BH), -20.64 (5, 1H, Tp*-CH), -19.91 (4, 1H, Tp*-CH), -18.80 (5, 3H, Tp*-CH_3), -14.41 (9, 3H, Tp*-CH3), -12.31 (4, 3H, Tp*-CH_3), -6.99 (5, 1H, Tp*-CH), -5.54 (5, 1H, Tp*-CH), -3.50 (3, Tp*-CH_3), 5.46 (5, 3H, -OCH_3), 6.46 (3, 2H, Ar-CH), 7.50 (5, 3H, Tp*-CH_3), 15.22 (13, 2H, Ar-CH), 19.05 (11, 3H, Tp*-CH_3), 22.70 (11, 3H, Tp*-CH_3), 36.61 (63, 2H, Ar-CH), 41.71 (6, 1H, Tp*-CH), 41.81 (4, 1H, Tp*-CH), 53.06 (81, 2H, Ar-CH), 64.32 (742, 3H, Tp*-CH_3), 73.01 (11, 3H, Tp*-CH_3). ^{11}B NMR (benzene-d_6, ambient temperature): δ = -85, -76. IR (KBr pellet): $\nu_{B\text{-}H}$ = 2561, 2520 cm^{-1}; ν_{CN} = 2230 cm^{-1}. Elemental analysis of $C_{46}H_{58}N_{15}B_2OU$: Calculated, C, 50.38; H, 5.33; N, 19.16. Found, C, 50.28; H, 5.14; N, 19.03.

2.4 Results and Discussion

2.4.1 Preparation of U(IV) Imido Compounds

Building on our previous family of U(IV) imido compounds, including Tp*$_2$U(N-Ph) (**7-Ph**), Tp*$_2$U(N-Mes), and Tp*$_2$(N-Ad) (**7-Ad**),[111] we prepared more imidos of this formula to study variation in their steric and electronic differences with respect to their reactivity. Therefore, **2-Bn** was treated with organoazides, N_3R (R = Bn, *p*Tol, *p*OMePh, detp, dipp), which caused immediate bubbling of the solution indicative of nitrogen gas evolution (Fig 2.1) As with formation of **7-Ph** and **7-Mes**, one-half equivalent of bibenzyl

was observed by ^{1}H NMR spectroscopy, supporting oxidation to the corresponding uranium(IV) imido compounds, Tp*$_2$UNR (R = Bn (**7-Bn)**, *p*-Tol (**7-*p*Tol**), *p*OMePh (**7-OMe**), detp (**7-detp**), dipp (**7-dipp**)) had occurred. This process gave products as purple (**7-Bn**, **7-detp**, **7-dipp**) or red-violet (**7-*p*Tol**, **7-OMe**) solids in good yields (65% - 82%). Alternatively, the series can be synthesized from Tp*$_2$UI and N_3R with subsequent addition of KC_8 (82-87%).

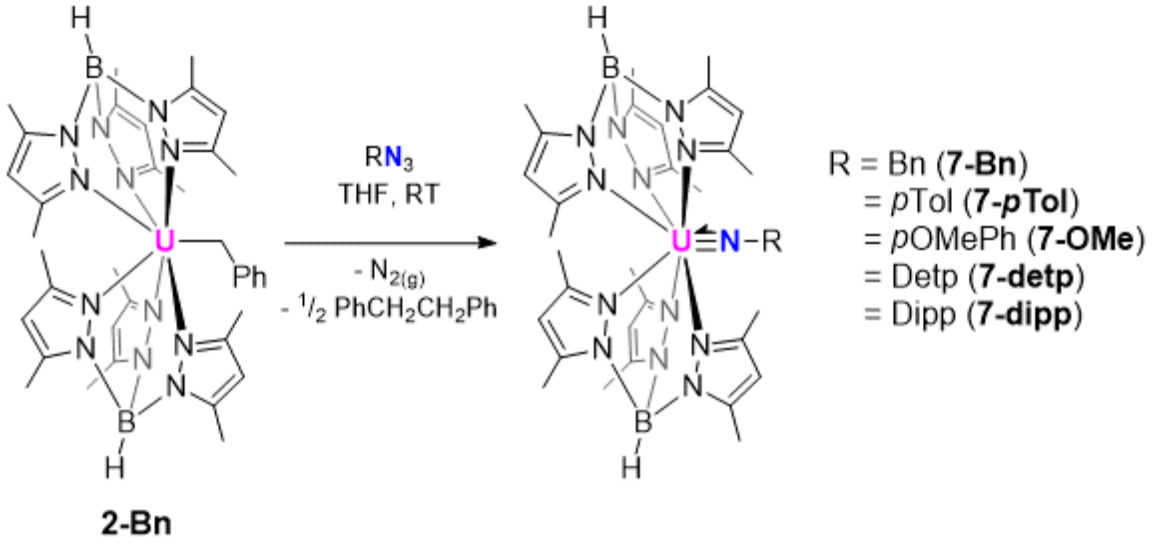

Figure 2.1. Synthesis of U(IV) imido compounds from **2-Bn**.

As previously reported for **7-Ph**, infrared spectroscopic data for **7-Bn**, **7-*p*Tol, 7-OMe, 7-detp**, and **7-dipp** show two $\nu_{B\text{-}H}$ stretches (2518-2560 cm^{-1}), confirming the presence of two Tp* ligands. Analysis of these species by ^{1}H NMR spectroscopy shows paramagnetically broadened and shifted spectra with the number of resonances and their integration values consistent for C_{2v} symmetry. ^{11}B NMR spectroscopy shows resonances for **7-Bn**, **7-*p*Tol**, **7-OMe**, **7-detp**, and **7-dipp** (-65, -67, -66, -77, -75 ppm, respectively) consistent with previously reported Tp* uranium(IV) compounds[41] and analogous to **7-Ph** (-67 ppm). These resonances are shifted significantly from the corresponding precursor uranium(III) complexes (**2-Bn** = -15 ppm; **1-I** = 4 ppm), which indicates that oxidation of the uranium(III) ion has taken place.

In an effort to evaluate the structural properties of these new entries in the uranium(IV) imido family, single crystals of each were obtained from either diffusion of

diethyl ether into a solution of toluene at -35 ºC (**7-Bn**, **7-*p*Tol**, **7-detp**) or from a concentrated solution of diethyl ether at -35 ºC (**7-dipp**) and analyzed by X-ray crystallography (Figure 2.2). Refinement of data collected for **7-Bn**, **7-*p*Tol**, **7-detp**, and **7-dipp** displayed a series of analogous distorted pentagonal bipyramidal uranium(IV) imido species that feature two κ^3-Tp* ligands per uranium center (**7-Bn** - U-$N_{pyrazole}$: 2.533(2)-2.737(2) Å; **7-*p*Tol** - U-$N_{pyrazole}$: 2.526(6)-2.786(6) Å; **7-detp** - 2.511(9)-2.727(10) Å; **7-dipp** (2.533(6)-2.681(6) Å). The U=N_{imido} distances (**7-Bn** - U=N_{imido}: 1.972(2) Å; **7-*p*Tol** - U=N_{imido}: 2.011(9) Å, **7-detp** - U=N_{imido}: 2.004(12) Å; **7-dipp** - U=N_{imido}: 2.003(7) Å) are consistent with other uranium(IV) imido complexes, including Cp*$_2$UNMes* (Cp* = [η^5-C_5Me_5], Mes* = 2,4,6-*t*$Bu_3C_6H_2$) (1.952(12) Å),[117] Tp*$_2$UNMes (1.976(3) Å),[111] Cp'$_2$UN*p*Tol (Cp' = η^5-1,2,4-$(Me_3C)_3C_5H_2$) (1.988(5) Å),[48] and $(OPPh_3)_3U(NMes*)Cl_2$ (2.009(3) Å).[118] The U1-N_{imido}-C_{imido} bond angles for **7-Bn** (165.7(2)º), **7-detp** (173.8(9)º), **7-dipp** (180.0º), and **7-*p*Tol** (163.6(9)º) are on the order of bond angles observed for other uranium(IV) imido complexes, including Cp*$_2$UNdipp (172.6(5)º),[119] Cp'$_2$UN*p*Tol (172.3(5)º),[48] Tp*U(NMes)(Bn)(THF) (177.7(5)º),[17] and U(Ndipp)$(I)_2(THF)_4$ (178.9(2)º).[120]

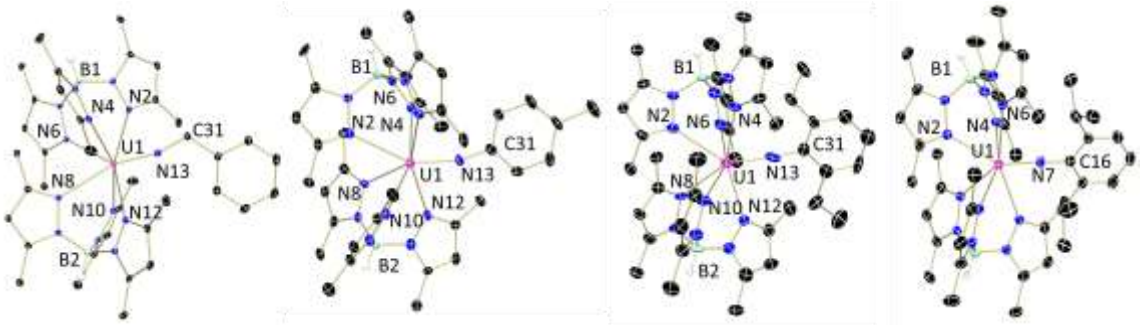

Figure 2.2. Molecular structures of **7-Bn**, **7-*p*Tol**, **7-detp**, and **7-dipp** (left to right) displayed at 30% probability ellipsoids. Selected hydrogen atoms and solvent molecules omitted for clarity.

The optical properties of complexes **7-Bn**, **7-*p*Tol**, **7-OMe**, **7-detp**, and **7-dipp** were examined by electronic absorption spectroscopy. Data for the series were recorded in THF over the range of 300-1800 nm at ambient temperature. The spectra exhibited analogous weak, but sharp f-f transitions in the near-infrared range (800-1800 nm),

consistent with previously reported Tp*$_2$-U(IV) compounds,[111] as well as bands in the visible region (**7-Bn**: 518 nm (884 $M^{-1}cm^{-1}$); **7-*p*Tol:** 514 nm (1103 $M^{-1}cm^{-1}$); **7-detp:** 544 nm (514 M^{-1} cm^{-1}); **7-dipp:** 549 nm (2500 $M^{-1}cm^{-1}$)) (Figure 2.3) that are responsible for their reddish purple appearance.

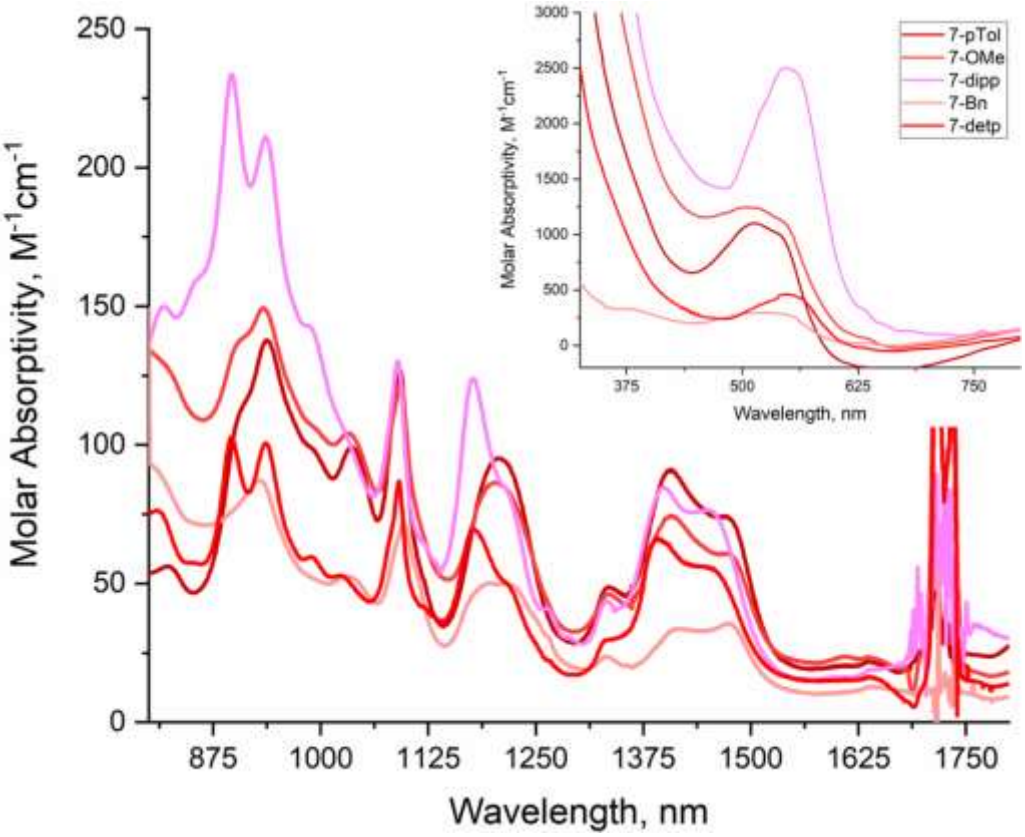

Figure 2.3. Electronic absorption spectrum of **7-*p*Tol**, **7-OMe**, **7-Bn**, **7-detp**, and **7-dipp** recorded from 325-1800 nm in THF at ambient temperatures.

A computational analysis of the extent of steric crowding of the uranium center for the new imido series was possible using Solid-G,[63] which calculates the percentage of a metal's coordination sphere that is blocked by its ligand(s) based on parameters obtained from experimental molecular structures. This analysis was performed to compare the relative size of the imido substituent for **7-*p*Tol**, **7-detp**, and **7-dipp** and the results obtained as the G(imido) value are presented in Table 2.1, along with the uranium-imido

multiple bond distances. The results show that for the aryl imido series, in moving from **7-*p*Tol**, **7-detp**, and **7-dipp**, the percentage of shielding increases steadily as expected for the respective *ortho*-H, -Et, and -*i*Pr groups. The G(complex) value represents the sum of all ligands, and takes absolute sphere shielding into account by shielding of any ligands.[63] Thus, this value also trends similarly to the G(imido), where there is a steady increase in the shielding percentage from **7-*p*Tol**, **7-detp**, **7-dipp** as expected.

Table 2.1. Solid angle parameters obtained from crystallographic data using Solid-G. Experimental uranium-nitrogen multiple bond distances are presented for comparison.

	7-*p*Tol	**7-detp**	**7-dipp**
U=N dist (Å)	2.011(9)	2.004(12)	2.003(7)
G(imido), %	17.44	19.93	22.20
G(Tp*), %	38.00	38.20	37.85
	38.23	37.94	37.86
G(complex), %	87.98	90.58	91.66

2.4.2 [2+2] Cycloaddition with Tp*$_2$UNR Family

With an understanding of the relative steric demands of these new entries in the uranium(IV) imido family, their reactivity for [2+2] cycloaddition chemistry was probed. The first study was performed by treating **7-Ph** with PhNCE (E = O, S, Se), as this should produce a series of symmetric phenyl urea cycloaddition products. Upon addition of PhNCO to **7-Ph**, rapid reaction was observed signified by a color change from red to orange in only fifteen minutes (Figure 2.4). Following work-up, analysis of the obtained product by ^{1}H NMR spectroscopy revealed thirteen broad resonances ranging from -32.97 to 32.05 ppm, consistent with C_2 symmetry. Six resonances assignable as Tp*-C*H*$_3$ protons and three resonances for Tp*-C*H* are observed, as well as one broad signal for the B-*H* protons (-11.32 ppm). Analysis by ^{11}B NMR spectroscopy gives a spectrum that displays a single resonance at -49.62 ppm for symmetric Tp* ligands in solution. Infrared spectroscopy in the solid state (KBr pellet) confirmed the presence of two Tp* ligands ($\nu_{B\text{-}H}$ = 2557 cm^{-1}; 2521 cm^{-1}), and provided evidence for a carbonyl moiety ($\nu_{C=O}$ = 1708 cm^{-1}), leading to the assignment of the orange powder as the κ^2-ureato complex Tp*$_2$U[κ^2-(*N*,*N*'-diphenylureato)] (**8-Ph**).

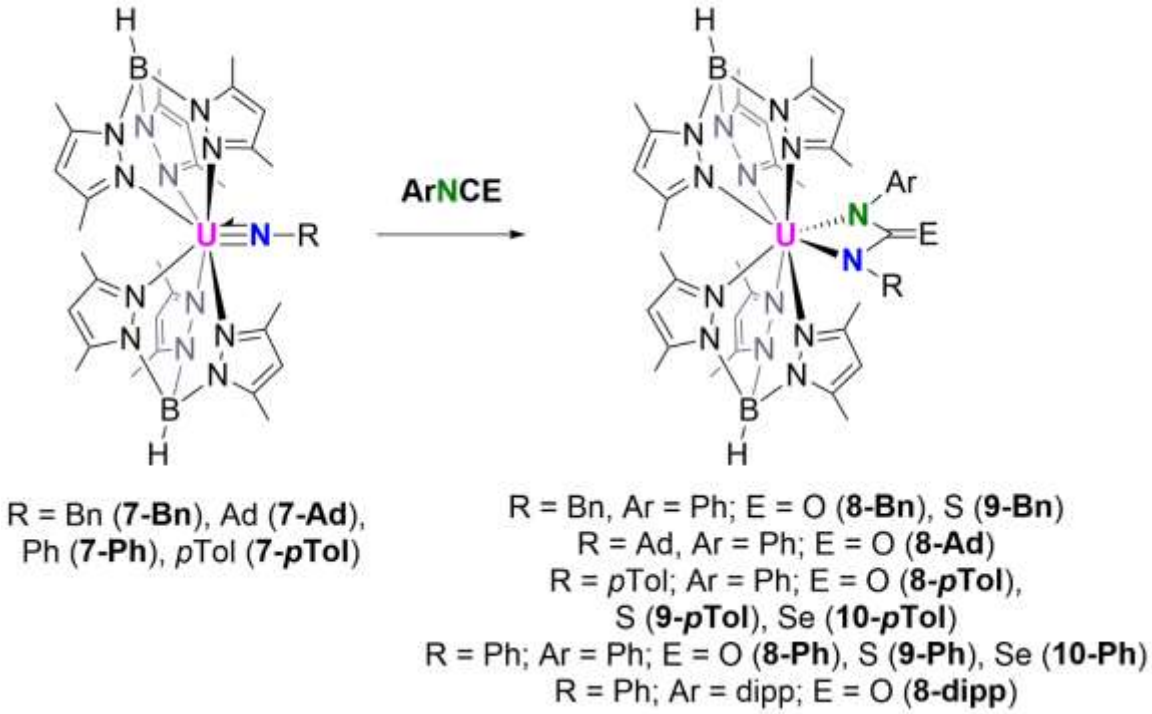

Figure 2.4. Products of [2+2] cycloaddition with isocyanates.

The next experiments were aimed at exploring analogous reactivity with phenylisothiocyanate, as the thione should be less nucleophilic and potentially less reactive. Thioureato complexes displaying various coordination modes[121, 122] have been synthesized previously by salt metathesis[123] and [2π+2π] cycloaddition.[98] Treating **7-Ph** with PhNCS afforded C_2 symmetric Tp*$_2$U[κ^2-(*N*,*N*'-diphenylthioureato)] (**9-Ph**) as an orange powder (82%). The ^{1}H and ^{11}B NMR spectra reveal peak distributions and symmetries that are analogous to the oxygen analogue, **8-Ph**. Infrared spectroscopy confirms retention of Tp* by similar $\nu_{B\text{-}H}$ stretches (2565, 2519 cm^{-1}) to **8-Ph**, while the $\nu_{C=S}$ stretch at 1542 cm^{-1} supports formation of the cycloaddition product.[124]

Due to the scarcity of κ^2-selenourato as ligands in organometallic chemistry, formation of the uranium(IV) κ^2-selenoureate was targeted by the same method. Treating **7-Ph** with phenylisoselenocyanate (PhNCSe) produced the desired κ^2-selenoureato complex, Tp*$_2$U[κ^2-(*N*,*N*'-diphenyselenoureato)] (**10-Ph**), albeit with a slightly longer reaction time (8 hours). Analyses by ^{1}H and ^{11}B NMR spectroscopy confirmed the formation of **10-Ph** by analogy to complexes **8-Ph** and **9-Ph** based on the peak distribution and their integration values. Retention of bound Tp* ligands was supported by IR

spectroscopy, which showed similar B-H stretches (**10-Ph** = 2566, 2508 cm^{-1}) to **8-Ph** and **9-Ph**. The stretch for C=Se ($\nu_{C=Se}$: **10-Ph** = 1542 cm^{-1}) is consistent with previous reports of carbon-selenium multiple bonds ($\nu_{C=Se}$: 1529-1570 cm^{-1}).[113, 124, 125] The longer reaction times required for PhNCSe as compared to PhNCO or PhNCS for **7-Ph** may be attributed to either the decreased nucleophilicity of the C=Se or the increased size of selenium as compared to oxygen and sulfur. Complex **10-Ph** represents the first reported crystal structure of a selenoureato ligand in the κ^2-coordination mode, although one example has been reported as an oil[126] and another in the gas phase.[127] Such ligands have been reported with binding through selenium in an end-on (κ^1) fashion with antimony,[128] cobalt,[129] gold,[130, 131] mercury,[132] palladium,[133] and platinum.[133]

A comparison of the ^{1}H NMR spectra across the series of compounds, **8-Ph - 10-Ph**, is presented in Figure 2.5. As discussed, *C*$_2$ symmetry is retained in solution across the series, with 6 resonances (6H each) for the *endo*- and *exo*-Tp* methyl groups and three resonances (2H each) for the CH protons of Tp*. For each compound, the phenyl protons are visible as three resonances between 6 and 12 ppm, including a doublet (4H), triplet (4H), and triplet (2H) for the *ortho*, *meta*, and *para* protons, respectively. While previous studies across chalcogenide series generally show a trend in chemical shift as the column is descended (i.e. Cp*$_2$U(EPh)$_2$, (E = S, Se, Te)),[134] a smooth progression is not noted in this case, as the data for **10-Ph** seems to lie in between that of **8-Ph** and **9-Ph**.

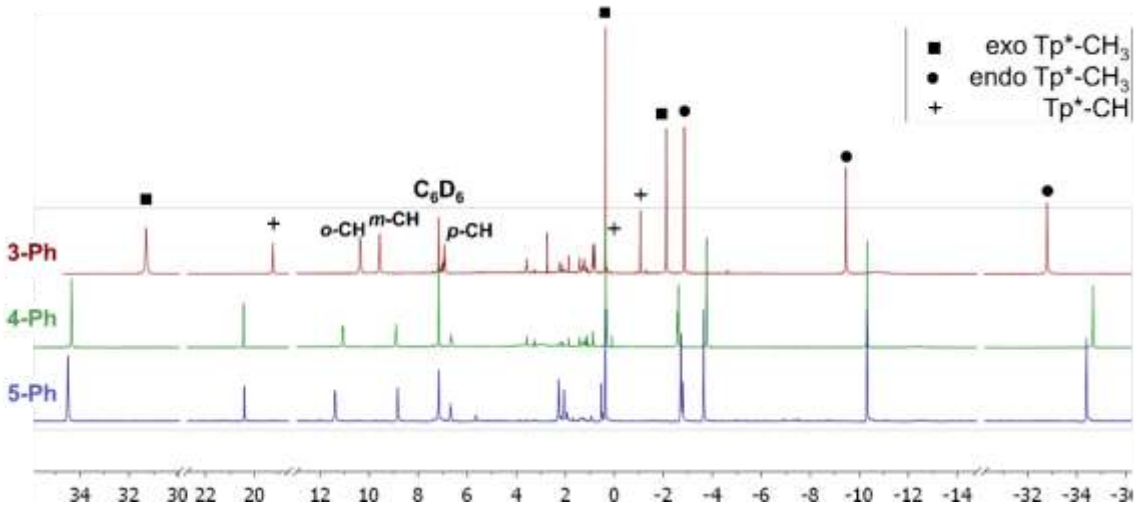

Figure 2.5. Comparison of ^{1}H NMR spectra for **8-Ph**, **9-Ph**, and **10-Ph** recorded in C_6D_6 at ambient temperature.

To compare structural parameters among the symmetric diphenylureato series, the molecular structures of **8-Ph**, **9-Ph**, and **10-Ph** were elucidated using single crystal X-ray crystallography (Figure 2.6). All three compounds show analogous structures, each exhibiting square antiprismatic geometries. As is commonly observed for bis(Tp*) uranium complexes, each ligand features two long U-$N_{pyrazole}$ distances (2.565-2.673 Å) and one short U-$N_{pyrazole}$ distance (2.460-2.485 Å).[18] The κ^2-ureato ligands have two U-N bond distances that are in the range of 2.301-2.394 Å, showing a significant bond elongation as compared to typical uranium(IV) imidos, which is expected based on the cleavage of the π-bonds. The C=E double bond distance increases (**8-Ph** = 1.231(13) Å; **9-Ph** = 1.699(7) Å; **10-Ph** = 1.840(6) Å) and the N-C-N bond angles decrease (**8-Ph** =59.4(5)º; **9-Ph** = 56.26(16)º; **10-Ph** = 56.6(2)º) as the chalcogenide group is descended, corresponding to the increase in the atomic radius.

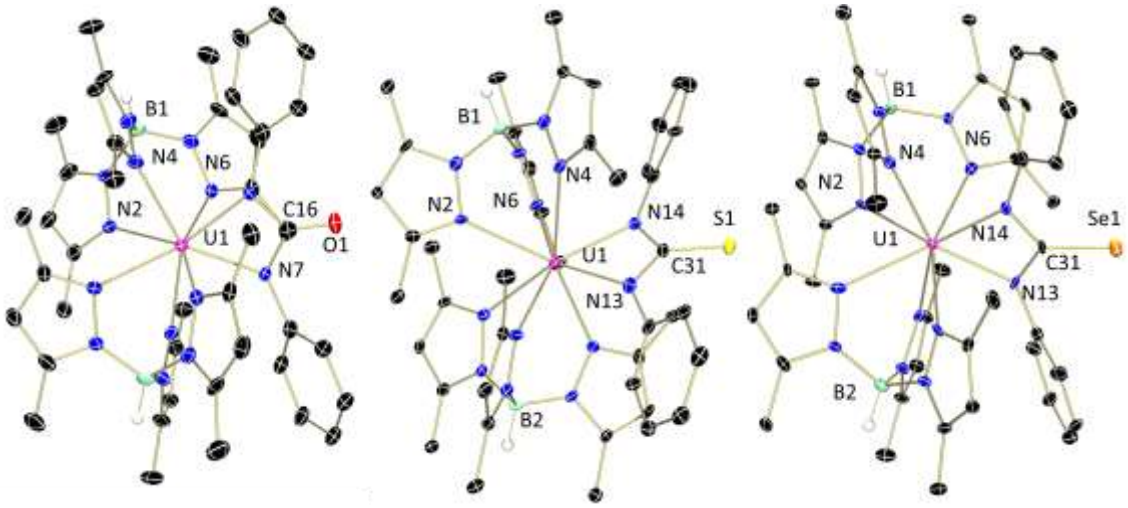

Figure 2.6. Molecular structures of **8-Ph**, **9-Ph**, and **10-Ph** (left to right) shown as 30% probability ellipsoids. Selected hydrogen atoms and co-crystallized solvent molecules omitted for clarity.

The structural parameters of **8-Ph** are best compared with (κ^2-1-Mes-3-dipp-NC(O)N)U(Cl)$_2$(OPPh$_3$)$_2$,[101] since both species have U(IV) ions. In the latter case, the U-N ureato distances of 2.259(4) and 2.263(4) Å are on the order of those in **8-Ph** (*cf* 2.340(17) Å). However, the symmetric uranium(V) ureato, (($^{t\text{Bu}}$ArO)$_3$tacn])U(κ^2-*N*,*N*-diphenylurea),[102] shows U-N$_{ureato}$ bond distances (2.310(4) and 2.329(4) Å) that are remarkably similar to **8-Ph**. When examining metrical parameters of both literature examples, it appears that a sterically encumbered uranium center produces longer bond distances and a smaller bond angle in order to accommodate the bulky κ^2-coordinated ligand. The longer ureato bond lengths observed for the sterically crowded tacn compound are similar to that for **8-Ph**, despite the smaller ionic radius of the uranium(V) ion, indicating that sterics play a significant role in urea ligand binding. The thiourea derivative, **9-Ph**, is the second entry of a κ^2-thioureato ligand that has been characterized in the solid state. The other example features a molybdenum complex with a κ^2-thioureato ligand (Mo[κ^2-(*N*,*N*'(1-phenyl-3-dipp)thioureato)](Ndipp)(OBu^t)$_2$), formed as a result of cycloaddition of an isothiocyanate with a molybdenum bis-imido compound.[98]

Similar reactivity with PhNCO was observed for the rest of the imido family, specifically **7-Ad**, **7-Bn**, and **7-*p*Tol**, resulting in asymmetric ureato ligands, generating Tp*$_2$U[κ^2-(*N*,*N*'(1-phenyl-3-adamantylureato))] (**8-Ad**), Tp*$_2$U[κ^2-(*N*,*N*'(1-phenyl-3-

benzylureato))] (**8-Bn**), and Tp*$_2$U[κ^2-(*N*,*N*'(1-phenyl-3-(*p*-tolyl)ureato))] (**8-*p*Tol**). As expected, based on the asymmetry of the ureato ligand, *Cs* symmetric ^{1}H NMR spectra are observed. Analysis by ^{11}B NMR spectroscopy shows resonances similar to **8-Ph** (-29 ppm (**8-Bn**); -48 ppm (**8-*p*Tol**)), supporting analogous cycloaddition chemistry occurred. Infrared spectroscopic data for **8-Ad** ($\nu_{C=O}$ = 1696 cm^{-1}, ν_{B-H} = 2559, 2515 cm^{-1}), **8-Bn** ($\nu_{C=O}$ = 1698 cm^{-1}, ν_{B-H} = 2556, 2512 cm^{-1}), and **8-*p*Tol** ($\nu_{C=O}$ = 1711 cm^{-1}, ν_{B-H} = 2561, 2507 cm^{-1}) are analogous to those recorded for **8-Ph**. The IR analysis also confirmed that both Tp* ligands revert to their typical κ^3-bonding modes upon cycloaddition with **7-Ad** to form **8-Ad**, consistent with our previous studies.[111]

To expand the family of known thiourea derivatives, **7-*p*Tol** and **7-Bn** were also treated with PhNCS, which afforded asymmetric Tp*$_2$U[κ^2-(*N*,*N*'-(1-phenyl-3-(*p*-tolyl)thioureato))] (**9-*p*Tol**) and Tp*$_2$U[κ^2-(*N*,*N*'(1-phenyl-3-benzyl)thioureato)] (**9-Bn**). As for **8-*p*Tol** and **8-Bn**, the ^{1}H NMR spectra are complicated by the asymmetry in the thiourea ligand, but the chemical shifts in the ^{11}B NMR spectra are as expected based on **9-Ph**. Infrared data confirms the presence of two Tp* ligands in each case, with similar ν_{B-H} stretches (**9-*p*Tol**: 2563, 2517 cm^{-1}; **9-Bn**: 2561, 2525 cm^{-1}) to **8**. Both compounds also display $\nu_{C=S}$ stretches at 1542 cm^{-1} that are consistent with previously reported values.[124]

Cycloaddition of PhNCSe to **7-*p*Tol** furnished the asymmetric κ^2-selenoureato complex Tp*$_2$U[κ^2-(*N*,*N*'-(1-phenyl-3-(*p*-tolyl)selenoureato))] (**10-*p*Tol**). As in the formation of **10-Ph**, cycloaddition with PhNCSe required longer reaction times (up to 8 hours) to reach conversion. Analysis by ^{1}H and ^{11}B NMR spectroscopy confirmed the formation of **10-*p*Tol** in analogy to complex **10-Ph**, while the retention of bound Tp* ligands was aided by IR spectroscopy (ν_{B-H} : **10-*p*Tol** = 2564, 2522 cm^{-1}). The absorption for the C=Se double bond in **10-*p*Tol** was found at 1542 cm^{-1} and is consistent with previous reports ($\nu_{C=Se}$: 1529-1570 cm^{-1}).[113, 124, 125]

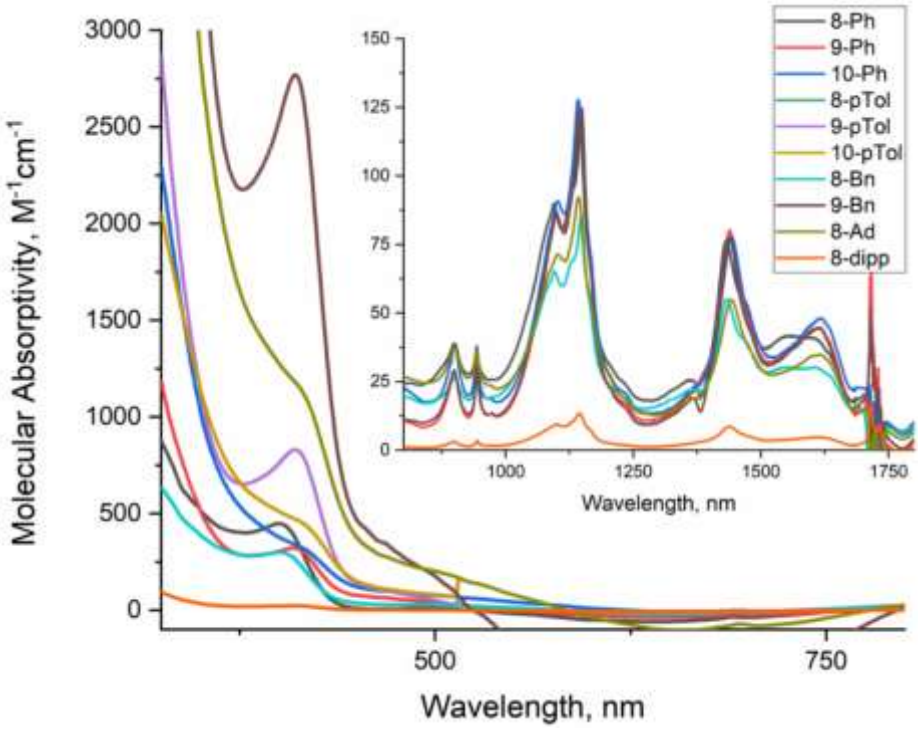

Figure 2.7. Electronic absorption spectroscopy of **8**, **9**, and **10** recorded in THF at ambient temperature from 325-1800 nm.

The orange THF solutions of all cycloaddition products were studied by electronic absorption spectroscopy at ambient temperature from 300-1800 nm, and the data for **8-Ph**, **8-Ad**, **8-Bn**, **8-*p*Tol**, **9-Ph, 9- *p*Tol**, **9-Bn**, **10-Ph**, and **10-*p*Tol** are presented in Figure 2.6. Overall, the entire family displays minimal variations regardless of the identity of the chalcogen, indicating analogous electronic structures. Examination of the near infrared region (800-1800 nm) revealed sharp, weakly intense f-f transitions for all eight compounds, consistent with a U(IV), f^2 configuration (Figure 2.7).[135] All complexes display weak visible absorbances or shoulders ranging from 410-415 nm, which are likely responsible for the orange appearance of all of the products.

The [2π+2π] cycloaddition reaction likely proceeds through one of two possible pathways (Figure 2.8). As shown in **Path A**, the isocyanate fragment could approach uranium in an end-on fashion leading with the chalcogen, which would be the sterically preferred configuration. Following cycloaddition, isomerization of the new κ^2-*N,E*-ureate ligand could occur, generating the observed κ^2-*N,N*-ureato species. In the sterically less preferred scenario, **Path B**, the isocyanate could line up with the hydrocarbon pointed

towards the uranium, with cycloaddition proceeding to directly generate the κ^2-*N,N*-ureato complexes without the need for isomerization. Based on the steric accessibility of the uranium center in the family of imido derivatives, as well as the literature precedent for ligand isomerization,[101, 102] we hypothesize that **Path A** is the more likely mechanism for the [2π+2π] cycloaddition reaction studied here.

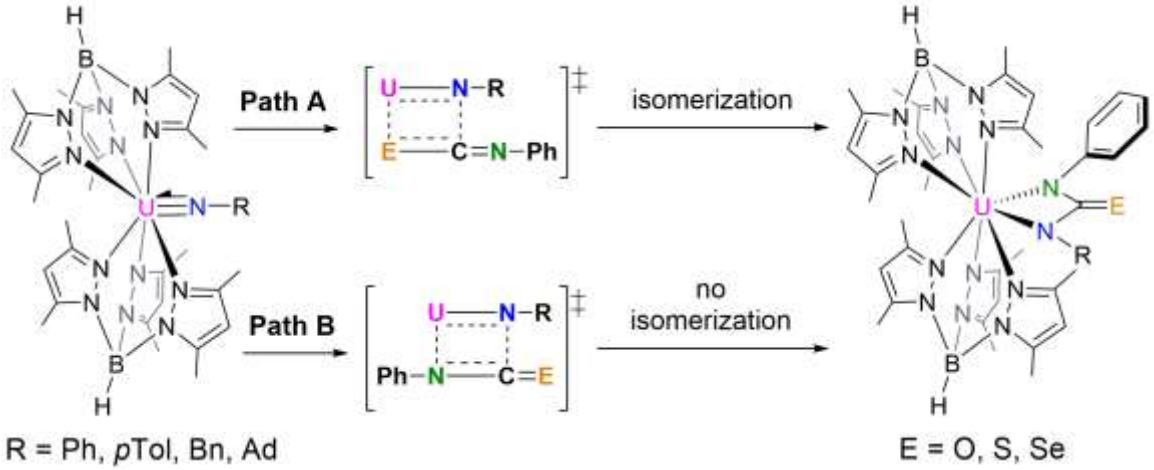

Figure 2.8. Depiction of mechanistic pathways possible for [2+2] cycloaddition.

To further our mechanistic inquiry, the reactivity of the last member, **7-dipp,** towards PhNCO was also examined. In this case, the anticipated κ^2-ureato derivative was not produced; instead, no reaction was observed even after prolonged heating at 110 ºC for 12 hours. Minimal (<5%) decomposition of **7-dipp** was noted. We hypothesized this lack of reactivity was likely due to the sterically encumbered 2,6-diisopropyl substituent on the imido nitrogen, which precludes approach of the isocyanate for the desired cycloaddition process. This is corroborated by examining the G(complex) values obtained from Solid G, which show respective values of 88.73% and 87.98% for **7-Bn** and **7-*p*Tol**, whereas the calculated value of 91.66% obtained for **7-dipp** is higher, indicating an inaccessible uranium center. As an illustration of this correlation, it was found that treating sterically accessible **7-Ph** with the bulky isocyanate, 2,6-diisopropylphenyl isocyanate, resulted in an immediate reaction, producing an orange powder after workup assigned as Tp*$_2$U[κ^2-(*N,N'*-1-phenyl,3-dippureato] (**8-dipp**). The spectroscopic features of **8-dipp** trend with other asymmetric κ^2-ureato compounds as expected and its formation highlights the ability

of the [Tp*$_2$U] system to support very large ligands such as 1-phenyl, 3-dippureato. Thus, the lack of reactivity observed for **7-dipp** is likely due to the inability of the isocyanate to approach the uranium-nitrogen multiple bond, supporting the mechanistic proposal depicted in **Path A**.

2.4.3 Reactions with nitriles

The addition of benzonitrile to **7-OMe** led to a color change from red-violet to red-orange within five minutes; work-up of the reaction mixture afforded an orange powder (Figure 2.9). Analysis of a benzene-d_6 solution of this powder by ^{1}H NMR spectroscopy revealed a C_s symmetric spectrum with chemical shifts in the range from −85 to 72 ppm. Twelve chemical shifts corresponding to the methyl group of the two Tp* ligands (3H each) and six shifts (1H each) for the C-H of the pyrazolyl rings were noted, as well. Two broad resonances for the B-H of the Tp* ligands are observed at −28.85 and −24.96 ppm. Four chemical shifts equating to two protons each are assigned as aryl protons. A chemical shift worth three protons is also observed at 5.36 ppm, which is attributed to the para methoxy group. Two chemical shifts were seen by ^{11}B NMR spectroscopy (−86, −76 ppm), neither of which corresponded to **7-OMe**, suggesting full conversion of the starting material.

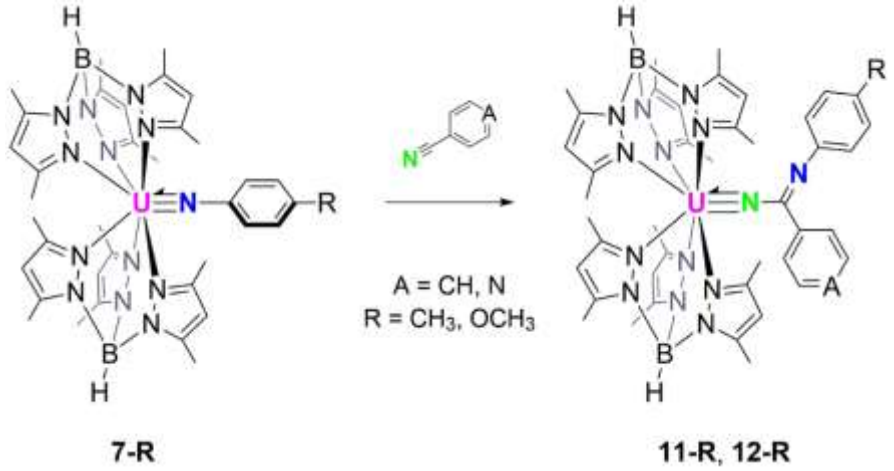

Figure 2.9. Synthetic scheme for the preparation of amidinate compounds **11-R**, and **12-R** from **7-R**.

To ascertain the identity and coordination mode of the isolated orange powder (79% yield), its molecular structure was elucidated using X-ray crystallography. Analysis of single crystals confirmed the retention of two κ3-Tp* ligands to a seven-coordinate uranium with U-$N_{pyrazolyl}$ bond distances (2.518(10)–2.701(3) Å) which are similar to other reported bis(Tp^*)U compounds (Fig. 2.10; Table 2.1) ($Tp^*_2U(CH_3)$ = 2.542(9)–2.700(8) Å;[34] Tp^*_2U(S-Ph) = 2.496(4)–2.674(5) Å;[16] Tp^*_2U(O-Mes) = 2.506(12)–2.697(14) Å).[64] In contrast to prior [2π + 2π] cycloaddition chemistry with actinide imido compounds, the reaction of **7-OMe** with benzonitrile does not result in a κ^2-bound ligand, rather a κ^1-bound amidinate with a new U=N bond is observed, and the previous N-*p*OMePh fragment has a newly formed C=N bond. The bond distance of the new U–N bond (2.004(3) Å) is consistent with reported U(IV) imido bond lengths, including (tBu_2bpy)UI_2(N-*t*Bu)$(THF)_2$ = 1.931(5) Å;[120] $Cp^PU(^{Mes}PDI^{Me})$(N-dipp) (Cp^P = 1-(7,7-dimethylbenzyl)cyclopentadienide; $^{Mes}PDI^{Me}$ = 2,6-((Mes)N = CMe)$_2C_5H_3N$) = 1.984(4) Å;[136] **7-*p*Tol** = 2.011(9) Å).[33] The U-N-C bond angle (178.1(2)°) is nearly linear, which is consistent with bisTp^*U(IV) imido compounds (**7-Bn** = 165.7(2)°; **7-detp** = 173.8(9)°).[33] The bond lengths corresponding to the remainder of the amidinate fragment show inequivalent N⎯C bond distances, where N13–C31 (1.357(4) Å) is slightly longer than N14–C31 (1.305(5) Å), which can be assigned to the η^1-amidinate ligand, N-C(=N-*p*OMePh)Ph. Overall, the product of **7-OMe** with benzonitrile is assigned as Tp^*_2U[=N-C(=N-*p*OMePh)Ph (**11-Ph**).

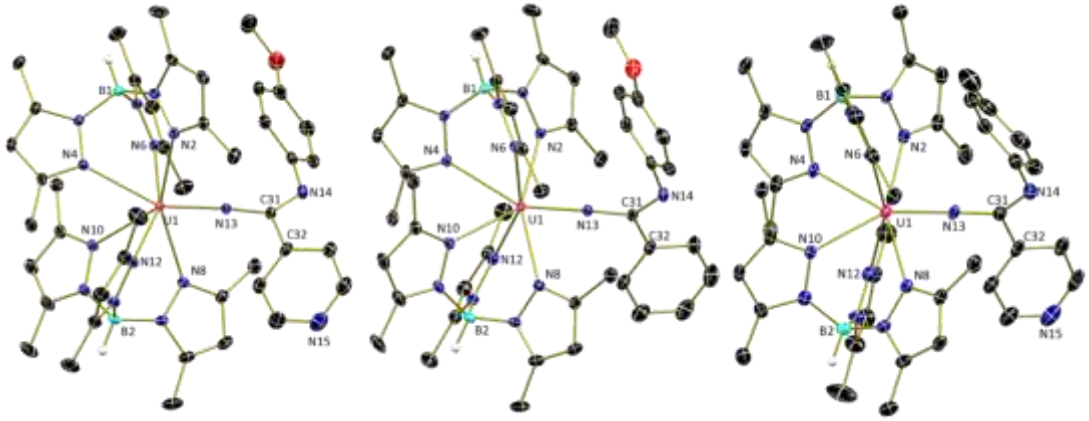

Figure 2.10. Molecular structures of **11-pyr**, **11-Ph**, and **12-pyr** (left to right) shown as 30% probability ellipsoids. Selected hydrogen atoms and co-crystallized solvent molecules omitted for clarity.

A previous example of benzonitrile reacting with an actinide imido was reported by Zi and co-workers. Treatment of $[\eta^5\text{-}1,2,4\text{-}(Me_3C)_3C_5H_2]_2Th(N\text{-}p\text{Tol})$ with benzonitrile resulted in a κ^2-binding mode to a Th(IV) center.[110] Amidinate ligands have been employed with actinide complexes before, but those reported have bound through both nitrogen atoms of the ligand.[137] At the time of submission, there were no other reported compounds with such a κ^1-binding motif as seen with **11-Ph**.

Table 2.2. Selected bond metrics for **11-Ph**, **11-pyr**, **12-pyr**, **13-Tol**, and **13-OMe**.

	11-Ph	**11-pyr**	**12-pyr**	**13-Tol**	**13-OMe**
U1-$N_{pyrazolyl}$	2.518(3)-2.701(3) Å	2.524(2)-2.690(2) Å	2.510(4)-2.687(4) Å	2.512(6)-2.776(5) Å	2.515(4)-2.674(4) Å
U1-N13	2.004(3) Å	2.012(2) Å	2.013(4) Å	2.019(6) Å	2.047(5) Å
N13-C31	1.357(4) Å	1.354(3) Å	1.362(6) Å	1.346(8) Å	1.300(7) Å
C31-C32	1.494(5) Å	1.507(4) Å	1.528(7) Å	1.503(9) Å	1.522(7) Å
C31-N14	1.305(5) Å	1.302(3) Å	1.296(7) Å	1.318(8) Å	1.314(7) Å
U1-N13-C31	178.1(2)°	175.92(17)°	177.6(4)°	174.8(4)°	175.9(4)°

To study any effect of any heteroatom incorporation, **7-OMe** was treated with 4-cyanopyridine, which also produced a color change to red-orange. The pale orange powder obtained from work-up (83% yield) was analyzed by ^{1}H NMR spectroscopy as a benzene-d_6 solution, and showing similar resonance distribution with chemical shifts in the range of −81–73 ppm and pattern to **11-Ph**. This similar compound is assigned as **11-py**, which also features two chemical shifts in its ^{11}B NMR spectrum (−86, −75 ppm) in the same region as **11-Ph**. Molecular structure of orange **11-py** was confirmed by X-ray diffraction, showing a seven-coordinate uranium ion with the same η^1-bonding of the amidinate as **11-Ph** (Fig. 2.10, left; Table 2.2). The molecular structure of **7-py** has U–$N_{pyrazolyl}$ distances (2.524(2)–2.690(2) Å) in a range similar to **11-Ph**. An imido fragment, identified as κ^1-amidinate N-C(=N-*p*OMePh)pyr, is κ^1-bound through a nitrogen atom with a short U-N

bond distance of 2.012(2) Å, which signifies a U(IV) imido. Additionally, **11-py** features a linear U-N-C bond angle (175.92(17)°) within its amidinate fragment.

To determine if electronic changes in uranium imido play any role in product formation, the methyl-substituted aryl imido, **7-*p*Tol**, was treated with benzonitrile and 4-cyanopyridine. Both reagents gave a color change from red-violet to red-orange. Upon work-up, orange powders were isolated and assigned as **12-Ph** (75% yield) and **12-py** (78% yield) (Figure 2.9). Both iterations have ^{1}H and ^{11}B NMR and IR spectra similar to their *p*-OMe substituted counterparts. For confirmation of the molecular structure, **12-py** was analyzed using X-ray diffraction (Fig. 2.10, right). Data refinement shows a seven-coordinate uranium center with two κ^3-Tp* ligands with U-N bond distances that are similar to **11-py** and **11-Ph** (Table 2.2), as well as formation of a κ^1-amidinate with the formula -NC(=N-*p*-Tol)pyr. This U-N bond length (2.013(4) Å) is similar to the other discussed U-N bond lengths in this report.

Compounds **11-Ph**, **11-py**, **12-Ph**, and **12-py** display similar features in their electronic absorption spectroscopic profiles (Fig. 2.11). The near-infrared (NIR) region has low molar absorptivity f-f transitions throughout, which are consistent with U(IV), f^2 configuration.[135] All four of these compounds also display a local λ_{max} (about 500 nm) that corresponds to their pale orange color.

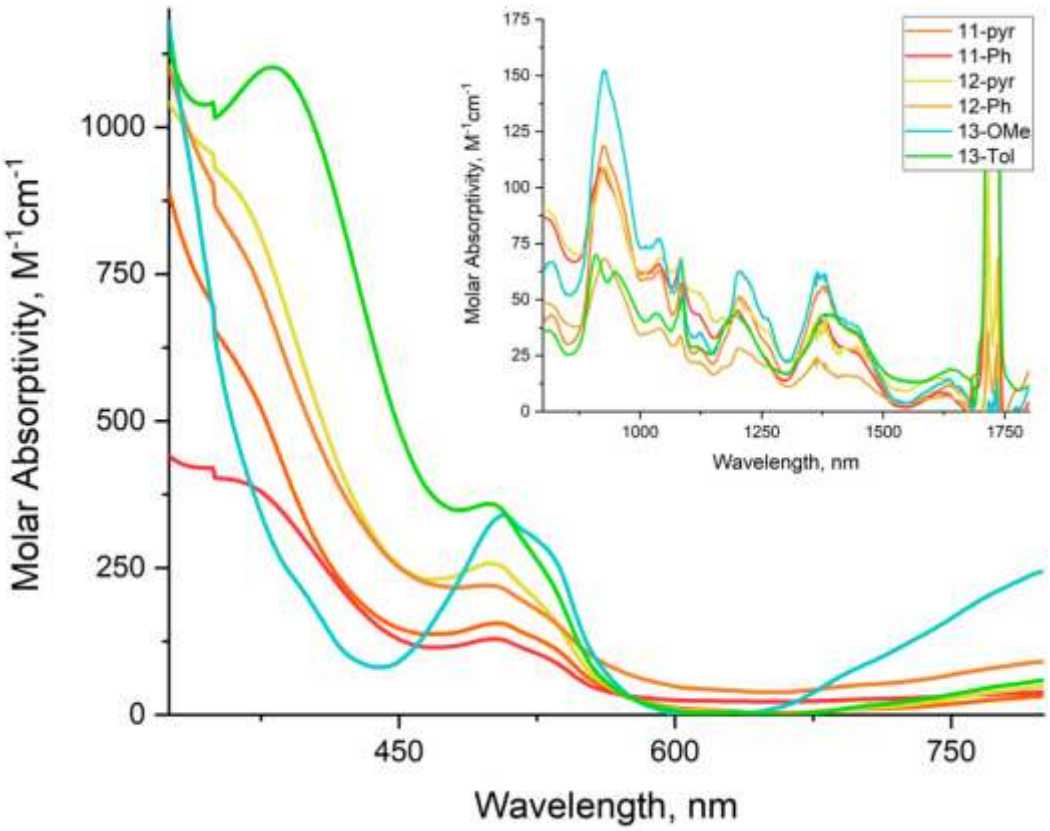

Figure 2.11. Electronic absorption spectrum of **11**, **12**, and **13** recorded from 325-1800 nm in a THF solution at ambient temperature.

The formation of dinuclear species was attempted by adding one-half an equivalent of 1,4-dicyanobenzene to a stirring solution of **7-*p*Tol** in THF, which caused a slight color change from red to red-orange (Figure 2.12). After work-up, an orange powder was isolated (85% yield) and analyzed as a C_6D_6 solution by ^{1}H NMR spectroscopy. As noted with the other nitrile reactions, a *C*s symmetric NMR spectrum with resonances in the range of −83–71 ppm was observed. Further analysis of the orange powder by infrared spectroscopy (KBr) showed two absorptions assignable to the B-H stretches (2517, 2557 cm^{-1}) of the Tp^* ligands. A strong absorption at 2227 cm^{-1} was also present, indicating a nitrile functional group was still intact, inconsistent with formation of a dinuclear species.

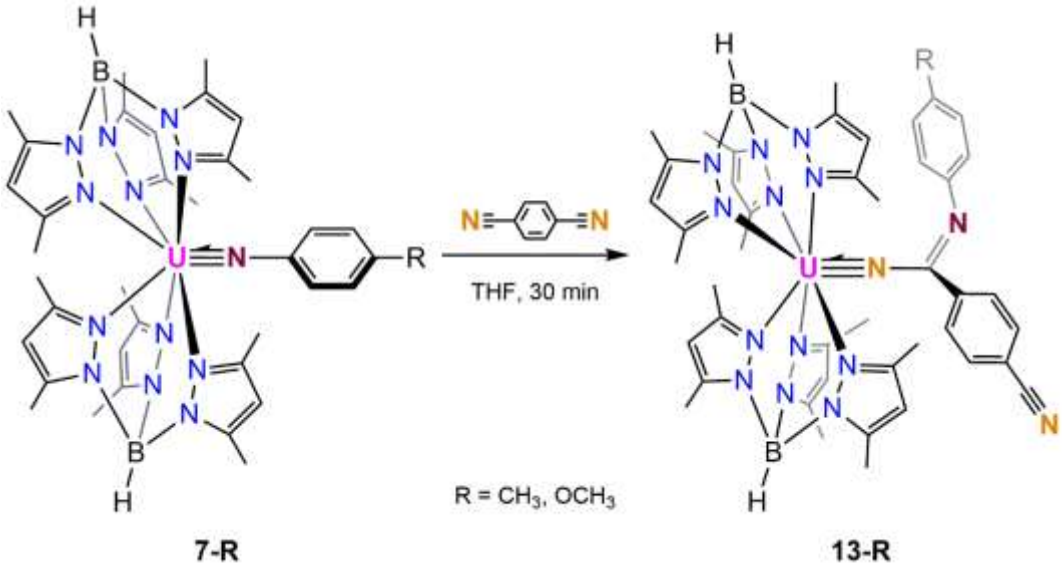

Figure 2.12. Synthetic scheme for reactions of **7** with 1,4-dicyanobenzene.

To further probe the molecular structure of this orange powder, crystals grown from vapor diffusion of a concentrated diethyl ether solution into toluene and analyzed by X-ray diffraction. This technique provided confirmation that two Tp* ligands were coordinated to a pentagonal bipyramid uranium center (Fig. 2.13, left). The U-$N_{pyrazole}$ bond lengths (2.512(6)–2.776(5) Å) are similar to the previously discussed compounds (Table 2.2). Crystallography also revealed formation of a κ^1-amidinate ligand, with a short U-N bond length of 2.019(6) Å, which is in the range of other U=N multiple bond lengths presented here. The U-$N_{amidinate}$-C bond angle is nearly linear at 174.8(4)°. When examining bond distances further, N13–C31 (1.346(8) Å) and N15–C31 (1.318(8) Å) are within range for the other compounds (Table 2.2). The C=N bond length (1.147(10) Å) indicates that there has not been any reduction or activation of the second nitrile group. This confirmation allows for the assignment as Tp^*_2U(=N-C(=N-*p*Tol)-*p*-cyanobenzene (**13-Tol**). Compound **13-Tol** was also probed by electronic absorption spectroscopy, which displayed characteristic weak absorbances in the NIR region (Fig. 2.11) similar to those present for compounds **11** and **12**. The UV–Vis region displays an absorbance at 515 nm, which likely gives **13-Tol** its red-orange color. This result contrasts work from Kiplinger and co-workers who used 1,4-dicyanobenzene to prepare bimetallic actinide complexes

through nitrile insertion chemistry, which gave a bridging diketimide product. $[(C_5H_4Et)_2(Cl)U]_2(\mu\text{-}[N{=}C\text{-}(CH_3)\text{-}C_6H_4\text{-}(CH_3)C{=}N])$.[138]

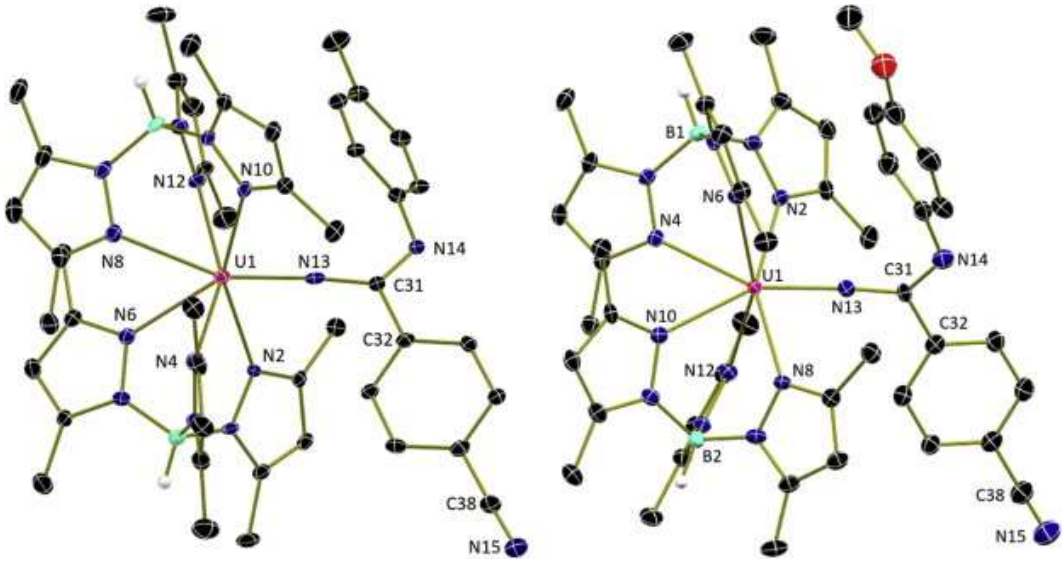

Figure 2.13. Molecular structures of **13-Tol** (left) and **13-OMe** (right) displayed at 30% probability ellipsoids. Selected hydrogen atoms and co-crystallized solvent molecules omitted for clarity.

Studying 1,4-dicyanobenzene with **7-OMe** provides another opportunity to track reactivity using different electronic groups. Similar to the reaction to yield **13-Tol**, an orange powder is isolated upon workup (80% yield), which has a C_S symmetric ^{1}H NMR spectrum (C_6D_6, ambient temperature) with 24 resonances ranging from −82 to 72 ppm. This orange powder also displays three notable stretches by IR spectroscopy; two absorbances correspond with the B–H of Tp* (2561, 2520 cm^{-1}) and a strong stretch (2230 cm^{-1}) is assigned to a nitrile functional group. The similar spectroscopic data gives the assignment of the orange powder as Tp^*_2U[NC(=N-*p*OMePh)-*p*-cyanobenzene] (**13-OMe**).

An examination of **13-OMe**'s molecular structure was studied using X-ray crystallography (grown from a concentrated diethyl ether solution at −35 °C) (Fig. 2.13, right). A pentagonal bipyramid uranium ion with two bound κ^2-Tp*ligands with U-$N_{pyrazolyl}$ bond lengths (2.515(4)–2.674(4) Å) that are similar to **13-Tol** (Table 2.2). Confirmation of the same κ^1-amidinate ligand was also observed by crystallography, with U-

$N_{amidinate}$ (2.047(5) Å) and U-N-C (175.9(4)°) within range of the four κ^1-amidinate complexes presented (Table 2.2). The C-$N_{nitrile}$ bond length (1.143(9) Å) shows no activation at the second nitrile, just like **13-Tol**.

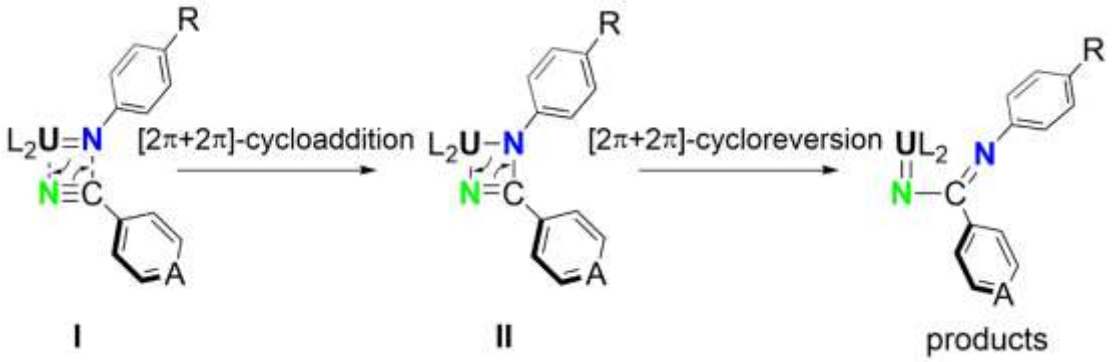

Figure 2.14. Proposed mechanistic pathway for product formation.

Formation of the new amidinate ligands for **11-Ph**, **11-py**, **12-Ph**, **12-py**, **13-OMe**, and **13-Tol** likely occurs from a [2π+2π] cycloaddition event between the imido fragment and the incoming nitrile (**I** in Figure 2.14), which leads to a metalacyclic product, **II**. From here, [2π+2π]-cycloreversion of the C=N bond of the added nitrile fragment and the U-N bond of the starting imido continues, generating the κ^1-amidinate products. Thus, the work in this article diverges from previous examples, such as Boncella's imido group switching[100] or Zi's Th example leading to a κ^2-bound ligand.[110]

2.5 Conclusions

New U(IV) imido compounds were synthesized and fully characterized through spectroscopic and structural methods. A computational analysis of this family demonstrated that the imido substituents have varying degrees of steric influence on the uranium center. To test this idea, [2π+2π]-cycloaddition chemistry with PhNCE (E = O, S, Se) was carried out to afford a full series of symmetric and asymmetric κ^2-ureato complexes bearing their respective functional groups. Reactions featuring **7-detp** or **7-dipp**, which contain large imido substituents, show no evidence of cycloaddition chemistry

taking place. Therefore, these studies correlate a quantitative measure of ligand sterics with cycloaddition reactivity.

To further explore multiple bond metathesis, we have demonstrated that bis-Tp*U(IV) amidinate compounds can be synthesized from multiple bond metathesis of uranium(IV) imido compounds with nitriles. This is successful regardless of electronic changes (methyl vs. methoxy) in the imido group or the type of nitrile employed. Full characterization of these compounds using multinuclear NMR, infrared, and electronic absorption spectroscopies, with the aid of X-ray crystallography, confirmed the unanticipated κ^1-coordination of the amidinate ligands as well as their tetravalent nature.

Interestingly, the imido reactivity observed here diverges from what has been reported. Using nitriles sees these imidos undergo consecutive multiple bond metathesis pathways, rather than just one, yielding new sterically hindered amidinates not typically observed in cycloaddition chemistry.

CHAPTER 3. ARYL-BRIDGED DINUCLEAR U(III) AND U(IV) COMPOUNDS

Reprinted (adapted) with permission from Tatebe, C.J., Kiernicki, J.J., Higgins, R.F., Ward, R.J., Natoli, S.N., Langford, J.C., Clark, C.L., Zeller, M., Wenthold, P., Shores, M.P., Walensky, J.R., Bart, S.C., *Organometallics*, **2019**, *38*, 1031-1040. Copyright 2019, American Chemical Society.

3.1 Abstract

A family of dinuclear bis(Tp*) (Tp* = hydrotris(3,5-dimethylpyrazolyl)borate) uranium compounds with conjugated organic linkers was synthesized to explore possible electronic communication between uranium ions. Trivalent diuranium phenyl alkynyl compounds, Tp*$_2$UCC(1,3-C$_6$H$_4$)CCUTp*$_2$ (**14-*meta***) or Tp*$_2$UCC(1,4-C$_6$H$_4$)CCUTp*$_2$ (**14-*para***), and tetravalent diuranium phenylimido compounds, Tp*$_2$U(N-1,3-C$_6$H$_4$-N)UTp*$_2$ (**15-*meta***) and Tp*$_2$U(N-1,4-C$_6$H$_4$-N)UTp*$_2$ (**15-*para***), were generated from trivalent Tp*$_2$UCH$_2$Ph. All compounds were fully characterized both spectroscopically and structurally. The electronic structures of all derivatives were interrogated using magnetic measurements, electrochemistry, and were the subject of computational analyses. All of this data combined established that little electronic communication exists between the uranium centers in these trivalent and tetravalent diuranium molecules.

3.2 Introduction

Transition metal (TM) species of the type [TM]-(Linker)-[TM] have been extensively studied[139, 140] for their fascinating electron transfer properties.[141] Such molecules have potential applicability to serve as molecular wires[142] and photovoltaic materials.[143] Diuranium complexes have not undergone such thorough study, but are gaining in popularity due to their interesting magnetic properties,[144, 145] ability to support surprising bonding motifs,[146-151] and unprecedented reactivity.[152-156]

Few examples of uranium complexes linked by conjugated carbon-based or multiply-bonded bridging organic frameworks currently exist.[11, 138, 145, 157-159] Andersen and co-workers reported diuranium(V) compounds, Cp′$_3$U=NC$_6$H$_4$N=UCp′$_3$ (Cp′ = η^5-C$_5$H$_4$Me),

as both the *meta* and *para* isomers. However, only the *para*-isomer displayed significant antiferromagnetic coupling of the $5f^1$ centers, as measured by SQUID magnetometry.[157] Another reported dinuclear U(V) complex from Walensky and co-workers exhibits some coupling between the two uranium centers.[160] Di- and tri-nuclear U(IV) alkynyl compounds have been reported by Shores to show weak magnetic communication between the uranium centers,[158] while benzoquinoid-bridged U(IV) centers did not exhibit any appreciable communication.[159] Electronic communication between 1,4-phenylenediketimide linked U(IV) centers was observed electrochemically by Kiplinger.[138] Notably rare in this research area is the study of U(III) ions for electronic delocalization and magnetic coupling, presumably because of limitations in the synthesis of U(III)-(linker)-U(III) platforms. Some exceptions to this include inverse sandwich complexes reported by Cummins and Diaconescu[149] as well as Liddle,[161] which all feature two uranium(III) centers with bridging dianionic arenes. Mazzanti has just recently described a unique nitrido bridged uranium(III) variant that is stabilized by the bulky siloxide ligand, -OSiOtBu[162].

Given that the hydrotris(3,5-dimethylpyrazolyl)borate (Tp*) ligand enables access to low-valent uranium alkyl complexes[24, 163] their reactivity,[16, 17, 36, 75, 111, 112] and is an ideal system to study electronic communication in dinuclear molecules of the form [Tp*$_2$U]-(Linker)-[UTp*$_2$]. Herein, we report the synthesis of a family of diuranium complexes bridged by either alkynyl (U(III) derivatives) or imido (U(IV) derivatives) linkers. Full structural and spectroscopic characterization of these species is reported. Analysis of electrochemical and magnetic properties as well as computational modelling are used to assess the electronic structures of these unique species.

3.3 Results and Discussion

3.3.1 General Considerations

All air- and moisture-sensitive manipulations were performed using standard Schlenk techniques or in an MBraun inert atmosphere drybox with an atmosphere of purified nitrogen. The MBraun drybox is equipped with a cold well designed for freezing samples in liquid nitrogen as well as two -35 °C freezers for cooling samples and crystallizations.

Solvents for sensitive manipulations were dried and deoxygenated using literature procedures with a Seca solvent purification system.[28] Deuterated solvents were purchased from Cambridge Isotope Laboratories. Benzene-d_6 was dried with molecular sieves and sodium, and degassed by three freeze–pump–thaw cycles. Acetonitrile-d_3 was distilled from CaH_2 prior to use. THF-d_8 was filtered over alumina and stored on Na^0. Tp*$_2$U(CH_2Ph) (**2-Bn**),[24] Tp*$_2$UCCPh,[16] 1,4-diethynylbenzene,[164] 1,4-diazidobenzene,[165, 166] and 1,3-diazidobenzene[166, 167] were prepared according to literature procedures. 1,3-diethynylbenzene (Sigma), and $KBPh_4$ (Alfa Aesar) were purchased from commercial sources. 1,3-Diethynylbenzene was degassed by three freeze-pump-thaw-cycles and filtered over dry alumina before use.

^{1}H NMR spectra were recorded on a Varian Inova 300 spectrometer operating at 299.992 MHz. ^{11}B NMR spectra were recorded on a Varian Inova 300 spectrometer operating at 96.24 MHz. All chemical shifts are reported relative to the peak for $SiMe_4$, using ^{1}H (residual) chemical shifts of the solvent (C_6D_6 = 7.16 ppm; CD_3CN = 1.94 ppm; C_4H_8O = 3.58, 1.73 ppm) as a secondary standard. The spectra for paramagnetic molecules were obtained by using an acquisition time of 0.5 s, thus the peak widths reported have an error of ±2 Hz. For paramagnetic molecules, the ^{1}H NMR data are reported with the chemical shift, followed by the peak width at half height in Hertz, the integration value, and, where possible, the peak assignment. ^{11}B chemical shifts are reported relative to the peak for $BF_3 \cdot Et_2O$ (0.0 ppm). All voltammetric data were obtained under inert atmosphere conditions using external electrical ports of the MBraun inert drybox. All data were obtained using a Gamry Instruments Interface 1000 model potentiostat using the Gamry Instruments Laboratory software. All samples were collected in THF with 1.0 mM [Bu_4N][OTf] in 4 mL of dry THF. Solutions were analyzed in 10 mL beakers, consisting of a 3 mm glassy carbon working electrode, a Pt wire counter electrode, and an Ag wire quasi-reference electrode. Potentials were corrected using a ferrocene standard at the end of runs. Elemental analyses were performed by the UIUC Microanalysis Laboratory or Midwest-Microlab, LLC. Electronic absorption spectroscopic measurements were recorded at ambient temperature in sealed 1 cm quartz cuvettes with a Cary 6000i UV-Vis-NIR spectrophotometer. Infrared spectra were recorded using a Thermo Nicolet iS5 FT-IR spectrometer. Samples were mixed with dry KBr and recorded.

Magnetic susceptibility data were collected using a Quantum Design MPMS XL SQUID magnetometer. All sample preparations were performed inside a dinitrogen-filled glovebox (MBRAUN Labmaster 130). Powdered microcrystalline samples were loaded into polyethylene bags and sealed in the glovebox. The bags that contained compounds **14-*meta*** and **14-*para***, and Tp*$_2$UCCPh were subsequently sealed in an additional polyethylene bag to ensure inert conditions as these complexes showed heightened air-sensitivity. After sealing in the bags, the samples were inserted into a straw and transported to the magnetometer under dinitrogen. Ferromagnetic impurities were checked through a variable field analysis (0 to 10 kOe) of the magnetization at 100 K (Figures S24-S29), which showed that for **14-*para***, **15-*meta*** and **15-*para*** major ferromagnetic impurities were likely not present. As a precaution, the variable temperature magnetic susceptibility data for **14-*meta***, Tp*$_2$UCCPh, and Tp*$_2$U(N-*p*Tolyl) were collected at 5000 Oe due to non-linearity in the low field magnetization data collected at 100 K. Magnetic susceptibility data were collected at temperatures ranging from 2 to 300 K (Figure 5). Reproducibility of magnetic susceptibility data was assessed through measurements on two different batches for all compounds (with the exception of Tp*$_2$UCCPh). Relative consistency at all temperatures was observed for all samples (Figures S30-S34). Magnetization measurements were collected at 1.8 K while varying the applied field up to 50 kOe (Figures S41-S42). Fits acquired with the program PHI[168] to determine a potential coupling constant for **14-*meta***, **14-*para***, **15-*meta***, and **15-*para*** used spin Hamiltonians with the general form: $\widehat{H} = -2J\widehat{S_1} \cdot \widehat{S_2}$ Data were corrected for the diamagnetic contributions of the sample holder and bag by subtracting empty containers; diamagnetic corrections for the sample were calculated using Pascal's constants.[169]

The electronic structures of complexes **14-15** were examined using the Gaussian16 suite of software[170] at the B3LYP[171] (Becke-3[172] exchange and Lee-Yang-Parr[173] correlation functional) level. All structures were truncated by replacing methyl substituents with hydrogen atoms, and stationary points were determined to be global minima using analytical frequency calculations with the Stuttgart/Dresden triple-ζ quality basis set[174] and the corresponding effective core potential (ECP) for uranium. The Pople double-ζ quality basis set, 6-31G, was used for all remaining atoms. Bader's Atoms in Molecules (AIM) analysis was performed using Multiwfn.

Single crystals of **14-*para*** and **15-*para*** suitable for X-ray diffraction were coated with poly(isobutylene) oil in a glovebox and quickly transferred to the goniometer head of a Rigaku Rapid II image plate diffractometer equipped with a MicroMax002+ high intensity copper X-ray source with confocal optics. Preliminary examination and data collection were performed with Cu Kα radiation (λ = 1.54184 Å). Crystals of **15-*meta*** were transferred to the goniometer head of a Bruker APEX II CCD diffractometer and analyzed at 100 K using monochromatic Mo Kα radiation (λ = 0.71073 Å) with the omega scan technique. Single crystals of **5-MeCN** and **14-*meta*** were transferred to the goniometer head of a Bruker Quest diffractometer equipped with a single crystal curved graphite incident beam monochromator and a Photon100 CMOS area detector. Examination and data collection were performed with Mo Kα radiation (λ = 0.71073 Å). Data were collected, unit cells determined, and the data integrated and corrected for absorption and other systematic errors using the Apex2 or Apex3 suites of programs. The space groups were assigned and the structures were solved by direct methods using XPREP within the SHELXTL suite of programs and refined by full matrix least squares against F^2 with all reflections using Shelxl 2014 or Shelxl 2017[32] and the graphical interface Shelxle. Complete crystallographic data, in CIF format, have been deposited with the Cambridge Crystallographic Data Centre.

3.3.2 Synthesis of Tp*$_2$UCCPhCCUTp*$_2$ (**14-*meta***, **14-*para***)

A 20 mL scintillation vial was charged with Tp*$_2$UCH$_2$Ph (**2-Bn**) (0.250 g, 0.271 mmol) and 5 mL of THF and cooled to -35 °C. A separate vial was charged with half an equivalent of 1,3-diethynylbenzene (0.017 g, 0.135 mmol) or 1,4-diethynylbenzene (0.017 g, 0.135 mmol) in 5 mL of THF and cooled to -35 °C. The solution of diethynylbenzene was added to the thawing solution of **2-Bn** and allowed to warm to room temperature. After 30 min, volatiles were removed in vacuo. The resulting solid was washed with cold *n*-pentane (2 × 10 mL), and dried to afford green powder assigned as Tp*$_2$UCC(1,3-C$_6$H$_4$)CCUTp*$_2$ (**14-*meta***) (0.206 g, 0.115 mmol, 85%) or Tp*$_2$UCC(1,4-C$_6$H$_4$)CCUTp*$_2$ (**14-*para***) (0.218 g, 0.122 mmol, 90%). Single, X-ray quality crystals were obtained from a concentrated THF solution stored at -35 °C (**14-*meta***) or from a concentrated 1,2-dimethoxyethane solution stored at -35 °C (**14-*para***).

14-*meta*: ^{1}H NMR (benzene-d_6, 25 °C): δ = -14.84 (4, 2H, B-*H*), -13.64 (6, 2H, B-*H*), -12.58 (19, 36H, Tp*-C*H*$_3$), 0.83 (4, 36H, Tp*-C*H*$_3$), 7.97 (11, 12H, Tp*-C*H*), 13.40 (t, 1H, aryl-C*H*, *J* = 6 Hz), 27.29 (d, 2H, aryl-C*H*, *J* = 7 Hz), 34.62 (9, 1H, aryl-C*H*). ^{11}B NMR (benzene-d_6, ambient temperature) δ = 5.47. IR (KBr pellet) ν (B-H) = 2547, 2523 cm^{-1}. Elemental analysis of $C_{70}H_{92}N_{24}B_4U_2$: Calculated, C, 47.00; H, 5.18; N, 18.79. Found, C, 46.62; H, 5.34; N, 18.01.

14-*para*: ^{1}H NMR (benzene-d_6, 25 °C): δ = -14.88 (3, 4H, B-*H*), -12.49 (25, 36H, Tp*-C*H*$_3$), 1.00 (11, 36H, Tp*-C*H*$_3$), 8.15 (11, 12H, Tp*-C*H*), 23.99 (11, 4H, aryl-C*H*). ^{11}B NMR (benzene-d_6, ambient temperature) δ = -3.67, -2.56. IR (KBr pellet) ν (B-H) = 2559, 2524, 2046 (C≡C) cm^{-1}. Elemental analysis of $C_{70}H_{92}N_{24}B_4U_2$: Calculated, C, 47.00; H, 5.18; N, 18.79. Found, C, 47.08; H, 5.36; N, 18.55.

3.3.3 Synthesis of Tp*$_2$UNPhNUTp*$_2$ (**15-*meta***, **15-*para***).

A 20 mL scintillation vial was charged with **2-Bn** (0.325 g, 0.352 mmol) and 5 mL of THF and frozen. A separate vial was charged with half an equivalent of 1,3-diazidobenzene (0.028 g, 0.175 mmol) or 1,4-diazidobenzene (0.028 g, 0.175 mmol) in 5 mL of THF and frozen. On thawing, the solution of azide was added to the thawing solution of **2-Bn** resulting in an immediate color change from green to deep red-purple. After 15 min, volatiles were removed in vacuo. The resulting solid was washed with *n*-pentane and dried to afford red-purple powder assigned as Tp*$_2$UN(1,3-C$_6$H$_4$)NUTp*$_2$ (**15-*meta***) (0.298 g, 0.168 mmol, 95%) or Tp*$_2$UN(1,4-C$_6$H$_4$)NUTp*$_2$ (**15-*para***) (0.289 g, 0.163 mmol, 93%). Single, X-ray quality crystals of either **15-*meta*** or **15-*para*** were obtained by slow diffusion of diethyl ether into a concentrated THF solution at -35 °C.

15-*meta*: ^{1}H NMR (benzene-d_6, ambient temperature): δ = -18.59 (120, 4H, B-*H*), -6.60 (19, 36H, Tp*-C*H*$_3$), 7.00 (57, 12H, Tp*-C*H*), 11.75 (163, 36H, Tp*-C*H*$_3$), 98.36 (22, 2H, 4,6-Ph-C*H*), 98.82 (11, 1H, 5-Ph-C*H*), 153.63 (51, 1H, 2-Ph-C*H*). ^{11}B NMR (benzene-d_6, ambient temperature) δ = -61.02. IR (KBr pellet) ν = 2554, 2528 cm^{-1} (B-H). Elemental analysis of $C_{66}H_{92}N_{26}B_4U_2$: Calculated, C, 44.81; H, 5.24; N, 20.59. Found, C, 45.33; H, 5.31; N, 19.78.

15-*para*: ^{1}H NMR (benzene-d_6, ambient temperature): δ = -15.64 (140, 4H, B-*H*), -3.48 (7, 36H, Tp*-C*H*$_3$), 10.04 (17, 12H, Tp*-C*H*), 12.31 (62, 36H, Tp*-C*H*$_3$), 121.23 (27,

4H, Ph-C*H*). ^{11}B NMR (benzene-d_6, ambient temperature) δ = -58.84. IR (KBr pellet) ν = 2554, 2527 cm^{-1} (B-H). Elemental analysis of $C_{66}H_{92}N_{26}B_4U_2$: Calculated, C, 44.81; H, 5.24; N, 20.59. Found, C, 44.88; H, 4.99; N, 19.61.

3.3.4 Synthesis of [Tp*$_2$U(THF)][BPh$_4$] (**5-THFb**).

A 20 mL scintillation vial was charged with Tp*$_2$UI (**1-I**) (0.500 g, 0.521 mmol) and 10 mL of THF. While stirring, potassium tetraphenylborate (0.186 g, 0.521 mmol) was added and stirred for 3 hr. The solution was filtered over Celite and dried in vacuo. The resulting solid was washed with toluene to afford a blue powder (0.470 g, 0.384 mmol, 74%) assigned as [Tp*$_2$U(THF)][BPh$_4$] (**5-THFb**). Single, X-ray quality crystals were obtained from a concentrated THF solution stored at -35 °C.

^{1}H NMR (benzene-d_6, ambient temperature): δ = -11.95 (36, 18H, Tp*-C*H*$_3$), 0.32 (10, 18H, Tp*-C*H*$_3$), 1.43 (16, 4H, THF), 3.58 (14, 4H, THF), 7.42 (8, 6H, Tp*-C*H*). ^{11}B NMR (benzene-d_6, ambient temperature) δ = 4.66. IR (KBr pellet) υ (B-H) = 2553, 2518 cm^{-1}. Elemental analysis of $C_{58}H_{72}N_{12}B_3OU$: Calculated, C, 56.93; H, 5.93; N, 13.74. Found, C, 56.59; H, 5.85; N, 13.69.

3.3.5 Synthesis of [Tp*$_2$U(MeCN)$_2$][BPh$_4$] (**5-MeCN**).

A 20 mL scintillation vial was charged with Tp*$_2$UI (**1-I**) (0.525 g, 0.547 mmol) in 12 mL acetonitrile. Addition of KBPh$_4$ (0.196 g, 0.547 mmol) rapidly produced a green solution. After 3 hr, the green suspension was filtered over Celite and concentrated under reduced pressure, affording a green solid. This solid was washed with diethyl ether (5 mL) and *n*-pentane (2 × 5 mL) and dried in vacuo. The resulting green powder (0.574 g, 460 mmol, 84% yield) was assigned as [Tp*$_2$U(MeCN)$_2$][BPh$_4$] (**5-MeCN**). Single, X-ray quality crystals were obtained from a concentrated acetonitrile solution stored at -35 °C. Continued attempts at elemental analysis were unsuccessful.

^{1}H NMR (CD$_3$CN, ambient temperature): δ = -11.04 (12, 18H, Tp*-C*H*$_3$), 2.07 (4, 18H, Tp*-C*H*$_3$), 6.86 (t, *J* = 9, 4H, *p*-BPh$_4$-C*H*), 7.01 (t, *J* = 9, 8H, *m*-BPh$_4$-C*H*), 7.29 (m, 8H, *o*-BPh$_4$-C*H*), 8.06 (4, 6H, Tp*-C*H*). ^{11}B NMR (CD$_3$CN, ambient temperature) δ = 6.0 (Tp*), -5.9 (BPh$_4$). IR (KBr pellet): υ (B-H) = 2561, 2518 (B-H); 2263 (C≡N) cm^{-1}.

Elemental analysis of $C_{58}H_{70}N_{14}B_3U$: Calculated, C, 56.45; H, 5.72; N, 15.89. Found, C, 53.40; H, 5.35; N, 14.37.

Alternate synthesis of **5-MeCN**. A 20 mL scintillation vial was charged with $[Tp^*_2U(THF)][BPh_4]$ (**5-THFb**) (0.550 g, 0.573 mmol). Addition of acetonitrile (12 mL) rapidly produced a green solution. Removal of volatiles in vacuo quantitatively produced a green solid that was taken up in 5 mL acetonitrile. After 4 hr, volatiles were removed in vacuo and the resulting green powder was washed with *n*-pentane (2 × 5 mL), affording (**5-MeCN**) (0.515 g, 0.412 mmol, 72% yield).

3.3.6 Synthesis of $[Tp^*_2UNCPhCN]_n[BPh_4]_n$ (**5-n**).

A 20 mL scintillation vial was charged with $[Tp^*_2U(THF)][BPh_4]$ (**5-THFb**) (0.214 g, 0.175 mmol) and 5 mL of THF. While stirring, terephthalonitrile (0.024 g, 0.187 mmol) was added and stirred for 1 hr. The solution was then layered with 10 mL of *n*-pentane and stored at -35 °C for 16 hr resulting in the precipitation of a blue solid (0.179 g, 0.073 mmol, 84%) assigned as $[Tp^*_2UNCPhCN]_n[BPh_4]_n$ (**5-n**). Single, X-ray quality crystals were obtained from a concentrated THF/*n*-pentane (5:1) solution stored at -35 °C. These crystals were green, and when redissolved in THF produced a bright blue solution. Reliable elemental analysis of this extended structure was not possible.

IR (KBr pellet) of green single crystals: υ = 2554 (B-H), 2528 (B-H), 2239 (C≡N) cm^{-1}

Elemental analysis of $C_{68}H_{74}N_{15}B_3U$: Calculated, C, 59.53; H, 5.44; N, 15.31. Found, C, 46.97; H, 5.07; N, 15.00.

3.4 Results and Discussion

3.4.1 Preparation of Diuranium Bridging Complexes

In order to synthesize low-valent diuranium complexes with an organic linker, we expanded on our modified preparation of Takats' Tp^*_2UCCPh.[16, 64] A cold solution (-35 °C) of $Tp^*_2U(CH_2Ph)$ (**2-Bn**)[24] was treated with one-half an equivalent of cold 1,3-diethynylbenzene (*meta*-DEB) or 1,4-diethynylbenzene (*para*-DEB). Although no color change is noted, a difference in solubility is apparent upon workup. The starting material is readily soluble in diethyl ether, aromatic solvents, and *n*-pentane, but the green powder isolated in this reaction is insoluble in diethyl ether and *n*-pentane (Figure 3.1, top).

Analyses of C_6D_6 solutions of Tp*$_2$UCC(1,3-C_6H_4)CCUTp*$_2$ (**14-*meta***) and Tp*$_2$UCC(1,4-C_6H_4)CCUTp*$_2$ (**14-*para***) by ^{1}H NMR spectroscopy (25 °C) revealed eight or five paramagnetically shifted resonances, respectively. Two singlets (36H each) are assigned to the *endo*-(**14-*meta***: -13.64 ppm; **14-*para*:** -12.49 ppm) and *exo*-Tp* methyl groups (**14-*meta***: 0.83 ppm; **14-*para***: 1.00 ppm). The pyrazolyl CH is assigned as a singlet (12H: **14-*meta***: 7.97 ppm; **14-*para***: 8.15 ppm) while a broad singlet appears for the B-H proton of the Tp* ligands at -14.84 or -14.88 ppm for **14-*meta*** and **14-*para***, respectively. In the ^{1}H NMR spectrum for **2-*meta***, three resonances are observed for the aryl bridge, including a triplet corresponding to one proton (13.40 ppm), a doublet (27.29 ppm) assigned to protons in positions 4 and 6, and a singlet (1H, 34.62 ppm) for the proton in the alpha position from the two alkynyl carbons (position 2). In the ^{1}H NMR spectrum for **14-*para***, a singlet at 23.99 ppm corresponds to the four *meta*- and *ortho*-protons on the aryl linker. Infrared spectroscopy (KBr pellet) revealed characteristic B-H stretches (**14-*meta***: 2554, 2523 cm^{-1}; **14-*para***: 2559, 2524 cm^{-1}) and a single C≡C absorption (**14-*para***: 2046 cm^{-1}), which are consistent with those reported for Tp*$_2$UCCPh.[64] Across repeated attempts, the analogous absorption was not observed for **14-*meta***.

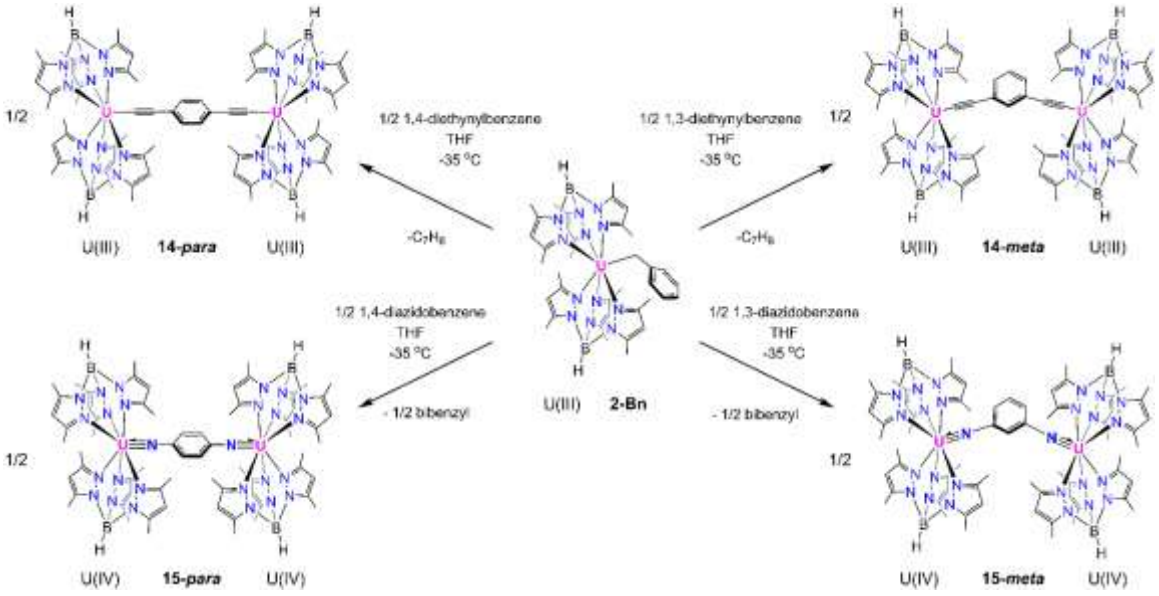

Figure 3.1. Preparation of **14-*para***, **14-*meta***, **15-*para***, and **15-*meta*** from **2-Bn**.

Single crystals of **14-*meta*** and **14-*para***, were grown from concentrated DME (**14-*para***) or diethyl ether (**14-*meta***) solutions and analyzed using X-ray diffraction to probe the coordination mode. Data refinement revealed that both compounds consisted of two Tp^*_2U units tethered by a DEB unit (Figure 3.2, Table 1). The range of $U\text{-}N_{pyrazolyl}$ bond distances (**14-*meta***: 2.546(8)-2.708(9) Å; **14-*para***: 2.422(18)-2.73(3) Å) falls within the range of previously reported trivalent bis(Tp*)U complexes (2.496-2.764 Å).[18, 24, 34] The U-C bonds (**14-*meta***: 2.486(10), 2.551(8) Å; **14-*para***: 2.48(2), 2.47(3) Å) for both compounds are similar to other trivalent uranium alkyls, including $U[CH(SiMe_3)_2]_3$ (2.48(2) Å)[21] and $TpTp^*UCH_2Ph$ (Tp = hydrotris(pyrazolyl)borate; 2.56(2) Å[18]). The $CC_{alkynyl}$ bonds for **14-*meta*** (1.208(10), 1.206(10) Å) and **14-*para*** (1.29(3), 1.34(4) Å) do not differ from each other. The bis(Tp*)U units in **14-*para*** are aligned in a perpendicular fashion (angle between planes defined by B1-U1-$B1^i$ and B2-U2-$B2^i$ = 89.23°) with the uranium centers separated by 9.064(4) Å. The molecular structure of **14-*para*** is highly disordered, making further discussion of the organic linker not feasible.

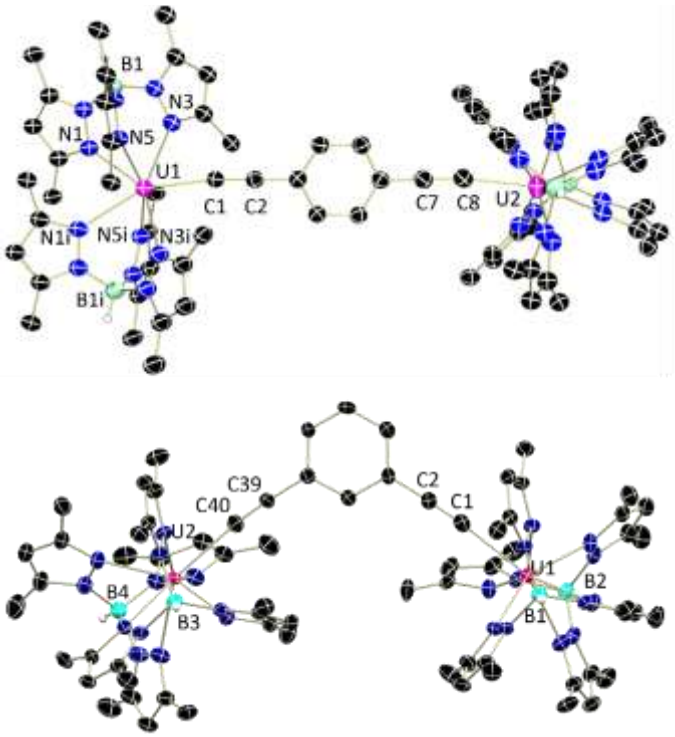

Figure 3.2. Molecular structures of **14-*para*** (top) and **14-*meta*** (bottom) displayed with 30% probability ellipsoids. Selected hydrogen atoms and co-crystallized solvent molecules have been omitted for clarity.

Both alkynyl compounds were studied by electronic absorption spectroscopy. Analysis of THF solutions of **14-*para*** and **14-*meta*** at ambient temperature revealed features that are consistent with trivalent U(III) complexes[75, 163] around 1250 nm (400 $M^{-1}cm^{-1}$), including broad features up to 1650 nm (Figure 3.3, green). The UV-visible regions (Figure 2, inset) for both alkynyl dimers display characteristic absorbances similar to Tp^*_2UBn and its derivatives, which are all dark green, U(III) alkyl compounds.[24, 163] This is highlighted by a broad absorption around ~680 nm, which is responsible for the observed green color. Absorbances around ~500-800 nm are established to be color-giving d-f transitions in U(III) systems.[135]

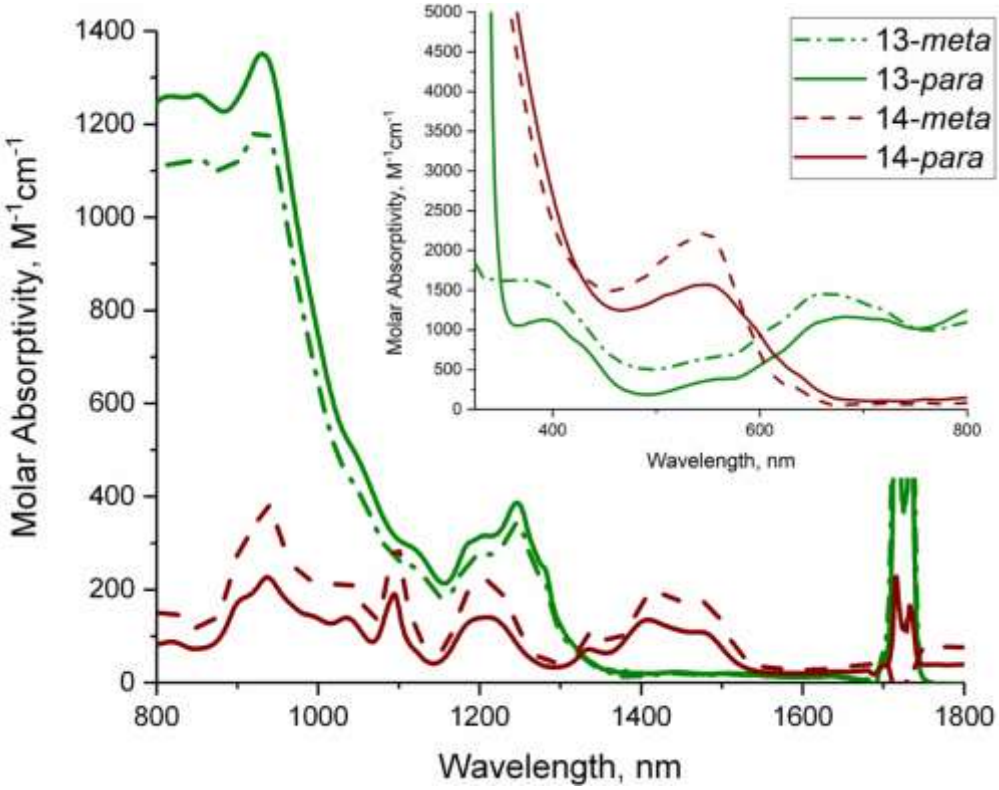

Figure 3.3. Electronic absorption spectra of **14-*meta*** (green, dashed), **14-*para*** (green, solid), **15-*meta*** (maroon, dashed), and **15-*para*** (maroon, solid) recorded from 300-1800 nm in THF at ambient temperature.

Generation of dinuclear imido U(IV) derivatives was accomplished using oxidizing azides. One-half of an equivalent of 1,4- or 1,3-diazidobenzene was added to a solution of

2-Bn, causing a rapid color change from dark green to red-purple. Effervescence of N_2 was also noted, as is typically observed for azide activation, concurrent with formation of uranium imido complexes (Scheme 1, bottom). The isolated bright red-pink powders were assigned as Tp*$_2$U(N-1,3-C_6H_4-N)UTp*$_2$ (**15-*meta***) and Tp*$_2$U(N-1,4-C_6H_4-N)UTp*$_2$ (**15-*para***), respectively. Product characterization by ^{1}H NMR spectroscopy (C_6D_6, 25° C) revealed seven and five paramagnetically shifted resonances, for **15-*meta*** and **15-*para***, respectively. The resonances assigned to the aryl bridge are significantly shifted downfield (**15-*para***: 121.63 ppm; **15-*meta***: 97.07, 97.54, 151.57 ppm). Both compounds have diagnostic B-H absorptions in their corresponding IR spectra (**15-*meta***: 2554, 2528 cm^{-1}; **15-*para***: 2554, 2527 cm^{-1}).

Structural confirmation of the dinuclear nature of **15-*meta*** and **15-*para*** was possible using X-ray crystallography (Figure 3.4). The U-$N_{pyrazolyl}$ ranges (**15-*meta***: 2.531(7)-2.759(7) Å; **15-*para***: 2.508(7)-2.753(8) Å) are similar to reported tetravalent U compounds with the bis(Tp*) framework (Table 3.1).[36, 42] The U-N_{imido} bond lengths (**15-*meta***: 1.971(7), 1.980(7) Å; **15-*para***: 1.973(9) Å) are within the range of previously reported U(IV) imido complexes, including **7-detp** = 2.004(12) Å,[33] Cp*$_2$U(NMes*) (Mes* = 2,4,6-tri-*tert*-butylphenyl) = 1.952(12) Å,[117] and ($OPPh_3$)$_2$U(NMes*)Cl_2 = 2.009(3) Å.[118] The U-N-C angle of **15-*para*** is closer to linearity at 168.5(8)°, as compared to **15-*meta*.** This is notable since the ligand environment of **15-*meta*** is more crowded, and the imido fragments are only slightly more bent (166.1(6), 163.9(7)°). The change in substitution can be quantified by the distance between the two uranium atoms; **15-*meta*** (8.165 Å) has a closer U-U distance than **15-*para*** (9.525 Å). Another quantifiable metric for the two imido compounds is that **15-*para*** features parallel bis(Tp*)U fragments, but those of **15-*meta*** have a twist angle of 38.47°.

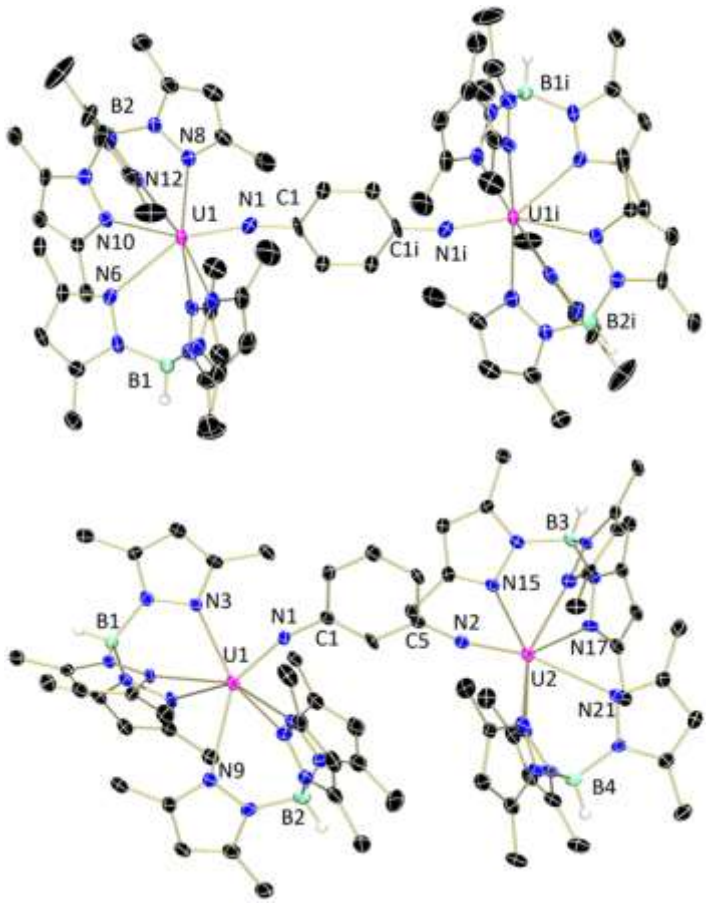

Figure 3.4. Molecular structures of **15-*para*** (top) and **15-*meta*** (bottom) shown as 30% probability ellipsoids. Selected hydrogen atoms and co-crystallized solvent molecules have been omitted for clarity.

Table 3.1. Selected Bond Lengths of **14-*meta***, **14-*para***, **15-*meta***, and **15-*para.***

Bond Metric	**14-*meta***	**14-*para***	**15-*meta***	**15-*para***
U=N_{linker}	--	--	1.971(7), 1.980(7) Å	1.973(9) Å
U-C_{linker}	2.486(10), 2.551(8) Å	2.48(2), 2.47(3) Å	--	--
$CC_{alkynyl}$	1.208(10), 1.206(10) Å	1.29(3), 1.34(4) Å	--	--

Examination of the electronic absorption spectra for complexes **15** show distinct features as compared to what was observed for **14**. Both **15-*meta*** and **15-*para*** display sharp, weak *f-f* transitions in the near-IR region from ca. 880-1550 nm, which are characteristic of uranium(IV) ions (Figure 3.3, maroon). This is in contrast to U(III) ions, where these

absorptions are much more broad. Complexes **3** display absorbances at ~549 nm that are of slightly lower energy than the monomeric species Tp*$_2$UNR (R = benzyl, *p*-tolyl, 2,6-diethylphenyl),[33] but are responsible for the red-violet color of these powders.

With the structural characterization of dinuclear U(III) and U(IV) compounds completed, we sought to expand the library to include a bridged U(III) species with a datively-bound linker for structural comparisons. Stirring 1,4-dicyanobenzene with a solution of [Tp*$_2$U(THF)][BPh$_4$] (**5-THFb**) produced a color change from purple to blue. Upon work-up, a blue solid was isolated (Figure 3.5), but was largely insoluble in aromatic solvents. Characterization of this blue compound by IR spectroscopy (KBr pellet) revealed B-H (2554, 2528 cm^{-1}) and nitrile (2239 cm^{-1}) absorptions. Interestingly, analysis by X-ray crystallography did not show a dinuclear uranium complex bridged through a single dicyanobenzene unit as expected, but instead, an extended structure where each uranium atom is bound to two dicyanobenzene ligands (Figure 3.6), [Tp*$_2$U(NCPhCN)]$_n$[BPh$_4$]$_n$ (**5-n**).

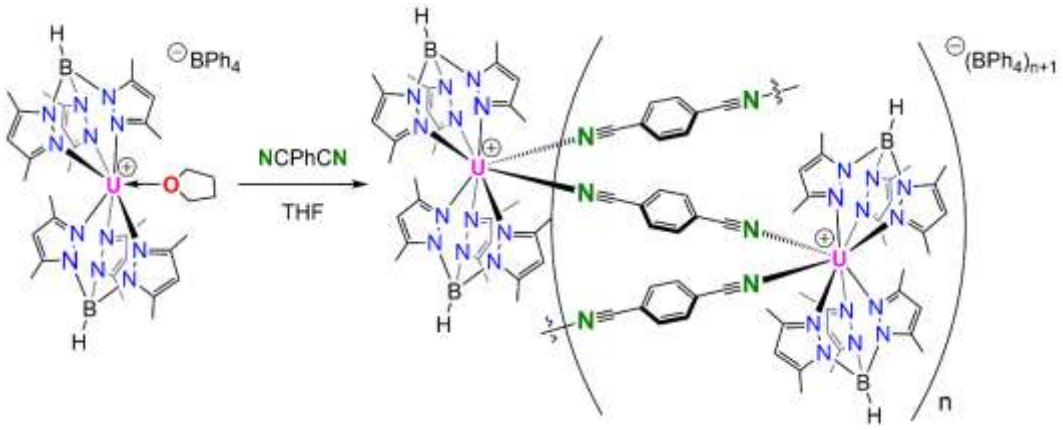

Figure 3.5. Equilibrium of **5-n**.

Upon dissolution of **5-n** in acetonitrile-*d*$_3$, a color change to green is noted, and ^{1}H NMR spectroscopy shows dissociated 1,4-dicyanobenzene and paramagnetically-shifted resonances assigned as [Tp*$_2$U(MeCN)$_2$][BPh$_4$] (**5-MeCN**). Independent preparation of **5-MeCN** was accomplished by treating an acetonitrile solution of Tp*$_2$UI with an equivalent of KBPh$_4$.

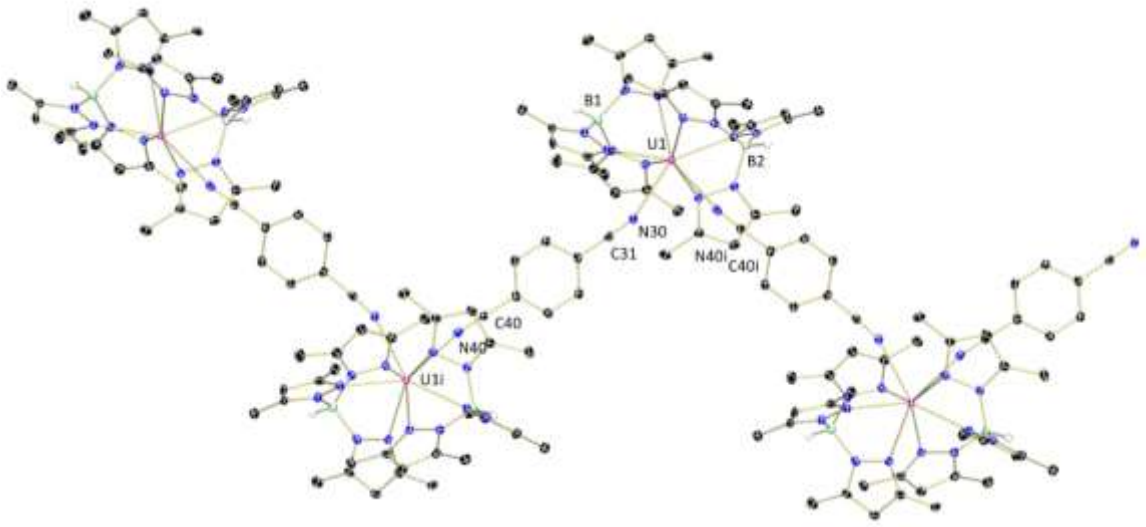

Figure 3.6. Molecular structure of **5-n** displayed with 30% probability ellipsoids. Selected hydrogen atoms, counter ions, and co-crystallized solvent molecules have been omitted for clarity.

Table 3.2. Selected bond lengths of **5-THFb**, **5-MeCN**, and **5-n**.

Selected Bond (dist in Å)	**5-THFb**	**5-MeCN**	**5-n**
U1-N2	2.523(4)	2.576(5)	2.529(4)
U1-N4	2.587(4)	2.675(6)	2.629(4)
U1-N6	2.598(4)	2.643(6)	2.599(4)
U1-N8	2.587(4)	2.662(5)	2.635(4)
U1-N10	2.563(4)	2.533(5)	2.532(4)
U1-N12	2.544(4)	2.679(6)	2.600(4)
U1-O1	2.600(4)	-	-
U1-N13	-	2.705(7)	2.696(4)
N1-N14	-	2.693(7)	2.677(4)

To compare the binding modes of **5-n** and **5-MeCN**, single crystals were obtained from a concentrated acetonitrile solution (**5-MeCN**) or by layering THF and *n*-pentane (5:1) (**5-n**) (-35 °C for both) (Figures 3.6, 3.7). Both molecular structures feature eight-coordinate uranium ions with two Tp* ligands with U-$N_{pyrazolyl}$ distances (**5-MeCN**: 2.533(5)-2.675(6) Å; **5-n**: 2.529(4)-2.635(4) Å) that fall into the range of the bond lengths for **13** and **14** (Table 3.2). Both compounds feature one tetraphenylborate anion per uranium ion and two neutrally bound acetonitrile molecules to uranium forming a square antiprismatic geometry. The U-$N_{nitrile}$ bond lengths (**5-MeCN**: 2.693(7), 2.705(7) Å; **5-n**:

2.677(4), 2.696(4) Å) are indicative of neutral interactions and consistent with reported distances for nitrile coordination ($Tp^*UI_3(NCMe)$ = 2.557(6) Å).[175] The molecular structure of **5-MeCN** proves to be unique as an extended structure is observed for **5-n**.

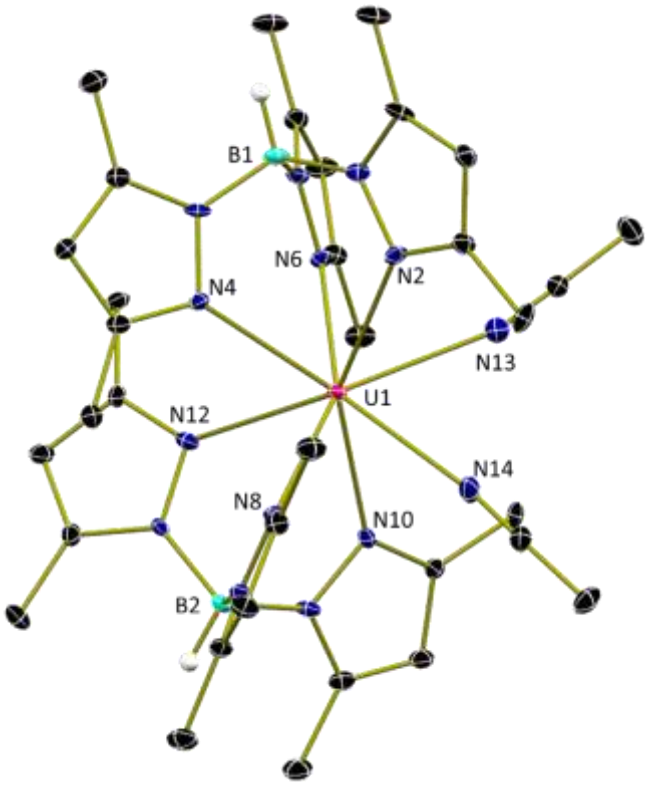

Figure 3.7. Molecular structure of **5-MeCN** shown as 30% probability ellipsoids. Selected hydrogen atoms, counter ions, and co-crystallized acetonitrile omitted for clarity.

3.4.2 Computation

Elucidation of the electronic structures of **14-*para***, **14-*meta***, **15-*meta,*** and **15-*para*** was aided using Density Functional Theory (DFT) at the B3LYP level, which has been used effectively for examining orbital interactions in actinide complexes.[119, 176] For ease in computing, the crystal structures were truncated by replacing the methyl groups on Tp* to hydrogen atoms. The agreement between experimental and computational bond distances is good with all distances within 0.05 Å. The calculated bond distances are slightly shorter due to the truncation which diminishes steric factors in these complexes. For uranium(III) alkynyl complexes, **14-*para*** and **14-*meta***, the septet state was found to be the lowest in

energy. Little covalent character is observed as evidenced by the spin density of 2.99 for both compounds. Uranium(III), f^3 complexes should display a spin density of 3.00 (having three unpaired electrons), but since no deviation was found, this supports negligible metal-ligand covalent interaction. We can also compare this spin density to that of **2-Bn**, for which no metal-ligand multiple bonding should be present. Indeed, the spin density for **2-Bn** is 3.00. Uranium(IV), f^2 imido complexes **15-*para*** and **15-*meta***, should exhibit spin densities of 2.00 (having two unpaired electrons); however, spin densities of 2.18 are observed for both compounds, indicating a higher degree, albeit very slight, of metal-ligand covalent interaction due to the uranium-nitrogen multiple bond. This result is expected, given that the corresponding U(IV) terminal oxo, $Tp^*_2U(O)$, has a calculated spin density of 2.13.[42]

The lowest energy conformation for **15-*para*** was found to be a quintet ground state with C_2-symmetry, therefore the molecular orbitals are degenerate. The HOMO-5, HOMO-6, and HOMO-34 are shown in Figure 3.8 which represent the two π bonds and σ bond, respectively, that comprise the uranium-imido bond (Appendix).

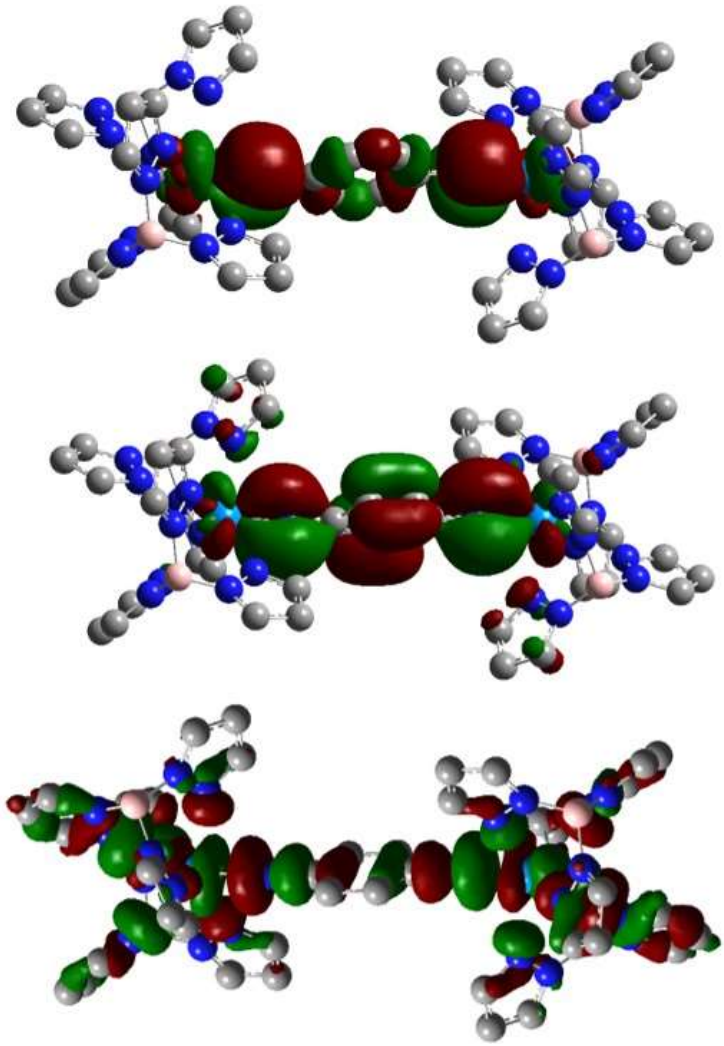

Figure 3.8. One σ (bottom, HOMO-34) and two π (top, HOMO-5, and middle, HOMO-6) orbitals that comprise the uranium-nitrogen triple bond in **15-*para*** are shown (isolevel = 0.02).

3.4.3 Magnetometry

In order to gain insight into the possibility of electronic communication between uranium ions in **14-*meta/para*** and **15-*meta/para,*** the magnetic properties of these species were probed by collecting variable temperature magnetic susceptibility data in the solid state (Figure 3.9). Previous examples have demonstrated that bridged actinide ions can show magnetic superexchange coupling through conjugated linkers, such as those from

Andersen,[157] Long,[177] and Shores.[158] However, this is not always the case,[159, 178] thus potential communication was evaluated for this system.

Compound **14-*para*** shows a room temperature $\chi_M T$ value of 2.93 cm^3Kmol^{-1} (μ_{eff} = 4.84), which decreases monotonically across all temperatures until 2 K, where the $\chi_M T$ value reaches 0.87 cm^3Kmol^{-1} (μ_{eff} = 2.64). These data are consistent with the presence of two U(III) ions, as the expected room temperature $\chi_M T$ value for two non-interacting $^4I_{9/2}$ ground states is 3.29 cm^3Kmol^{-1} (μ_{eff} = 5.13).[179] A magnetic saturation experiment (1.8 K) shows near-saturation at 1.61 μ_B with an applied field of 50 kOe (Table 3.3 and Appendix), further suggesting the presence of two U(III) ions in **14-*para***.[145] Meanwhile, **14-*meta*** shows analogous data over the applied temperature range; magnetization data collected at 1.8 K also support the presence of two U(III) ions.

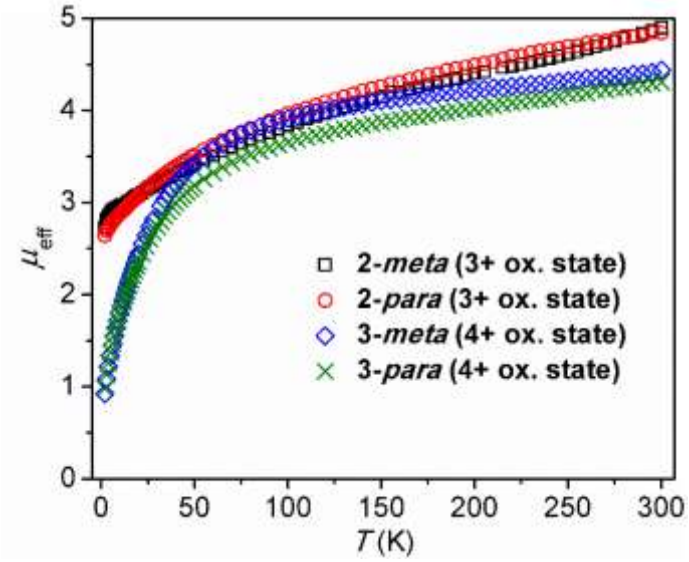

Figure 3.9. Temperature-dependent magnetic susceptibility data. Compound **14-*para*** (red circle) and **15-*meta*** (blue diamond) and **15-*para*** (green ×) collected at 1000 Oe: compound **14-*meta*** (black square) collected at 5000 Oe.

Table 3.3. Selected magnetic properties for the dinuclear complexes **14-*meta/para*** and **15-*meta/para*.**

Complex	$\chi_M T$ (cm^3Kmol^{-1}) 300 K, (μ_{eff})	per ion $\chi_M T$ (cm^3Kmol^{-1}) 300 K, (μ_{eff})	$\chi_M T$ (cm^3Kmol^{-1}) 2 K, (μ_{eff})	per ion $\chi_M T$ (cm^3Kmol^{-1}) 2 K, (μ_{eff})	M (μ_B) 50 kOe, 1.8 K
14-*para*	2.93 (4.84)	1.47 (3.43)	0.87 (2.64)	0.44 (1.88)	1.61
14-*meta*	3.00 (4.90)	1.50 (3.46)	0.93 (2.73)	0.47 (1.94)	1.73
15-*para*	2.32 (4.31)	1.66 (3.64)	0.12 (0.98)	0.06 (0.69)	0.33
15-*meta*	2.47 (4.44)	1.24 (3.15)	0.11 (0.93)	0.06 (0.69)	0.35

Given temperature dependent magnetic behaviors are similar to free ions, we would expect that the ions in **14-*para*** and **14-*meta*** are magnetically non-interacting. However, since the interactions can result in subtle effects on magnetic susceptibility values, a subtraction method reported by Rinehart *et al.* was applied to further investigate the potential for magnetic exchange coupling in the dinuclear species.[158] As part of this analysis, magnetic data were collected for the corresponding mononuclear species, Tp*$_2$UCCPh:[16] as expected, they show magnetic properties typical for mononuclear U(III) complexes (Appendix).[179] After subtraction of the mononuclear data from those obtained for **14-*para*** or **14-*meta***, the remaining susceptibility data do not indicate significant interactions between the U(III) ions for either **14-*para*** or **14-*meta*** (Appendix). In addition, no reasonable fits are obtained when using PHI[168] to fit the subtracted data to extract an intramolecular coupling constant (J) value. The closest intermolecular U···U distances are 9.064(4) and 9.9665(6) Å for **14-*para*** and **14-*meta***, respectively, which are likely far enough separated to preclude through-space magnetic interactions between ions. The molecular structure obtained in the solid state does not display obvious H-bonding or π-stacking interactions, eliminating other communication pathways between U(III) ions in these alkynyl-bridged species.

The magnetic data for **15-*para*** and **15-*meta*** show typical trends for dinuclear U(IV) complexes with redox-innocent ligands that have multiple bonding character.[158, 179] At room temperature, the susceptibility products give values of 2.32 and 2.46 cm^3Kmol^{-1} (μ_{eff} = 4.31 and 4.44), respectively (Figure 3.9, Table 3.3). Upon cooling, values for **15-*para*** and **15-*meta*** decrease gradually until around 100 K where the downturn becomes pronounced, reaching respective values of 0.12 and 0.11 cm^3Kmol^{-1} (μ_{eff} = 0.98 and 0.94)

at 2 K. To further confirm the ground states for **15-*para*** and **15-*meta***, magnetization data were collected (1.8 K) up to an applied field of 50 kOe. Consistent with U(IV) ions, these data are small in magnitude (0.35 and 0.33 μ_B for **15-*para*** and **15-*meta***, respectively) and do not saturate. Typically, magnetization values for a U(IV), $5f^2$ ion approach 0 μ_B at low temperature due to thermal depopulation, but generally show some occupation of magnetic excited states at higher temperatures.

To address the question of possible magnetic exchange for **15-*para*** and **15-*meta*,** the same subtraction method used for **15-*para*** and **15-*meta*** was applied using **7-Tol**[33] as the mononuclear surrogate (Appendix).[177] Attempts to fit these data with PHI[168] were unsuccessful using a *J* tensor in the applied Hamiltonian. Furthermore, no obvious inflection point is observed in a plot of the χ_M vs *T* data (Appendix), indicating no long range magnetic ordering. Thus, we conclude that the uranium ions in dinuclear **15-*meta/para*** are likely magnetically non-interacting.

3.4.4 Electrochemistry

The potential for electronic communication in dinuclear **14-*meta/para*** and **15-*meta/para*** was also probed using electrochemistry (Figure 3.10). For trivalent **14-*para*** and **14-*meta***, the cyclic voltammograms display a single, two-electron oxidation process **A** (U^{III} to U^{IV}) within the potential solvent window (potentials provided in Table 3.4). The two potentials are similar and are comparable to results reported by Shores and co-workers for *para*- and *meta*-diethynylbenzene bridged U(IV) ($N(CH_2CH_2NSi^tBuMe_2)_3$) complexes.[158] The oxidation potentials of **14-*para*** and **14-*meta*** compared to **2-Bn** are anodically shifted, which is indicative of decreased electron density around the U(III) ion, likely due to the replacement of the strong σ-donor benzyl ligand with the π-accepting alkynyl linker.

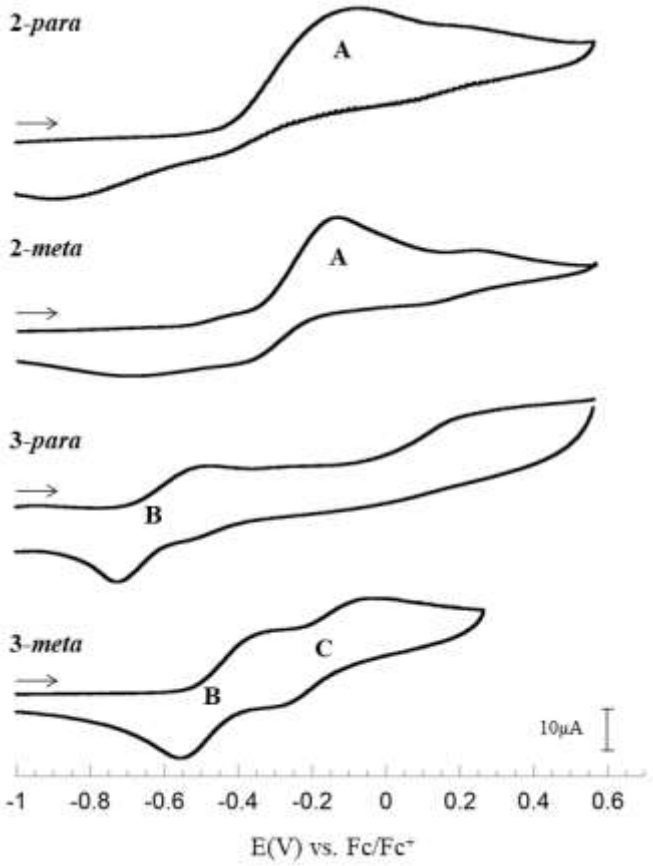

Figure 3.10. Cyclic voltammograms (CV's) recorded for compounds **14** - **15** in 0.1 M THF solution of Bu_4NOTf at a scan rate of 0.10 Vs^{-1}.

The tetravalent imido derivatives, **15-*para*** and **15-*meta***, were analyzed analogously. The CV for **15-*para*** possesses a single two-electron quasi-reversible oxidation **B** (U^{IV} to U^{V}), whereas that for **15-*meta*** shows two stepwise one electron events - a reversible couple at **B** and an irreversible couple at **C** (U^{IV} to U^{V}). Thus, the general trend in electron density at the uranium ion is: **14-*meta/para*** > **2-Bn** > **15-*meta/para***. Similar trends in electron density were reported by Kiplinger and co-workers for a series of mononuclear U^{V} complexes, $[(Cp^*)_2U(=N-Ar)(X)]$ (X = Cl, Me, C_2Ph, $N=CPh_2$; Ar = dipp, Mes*).[180, 181] Variation of electrolytes, solvents, and working electrodes lead only to ill-defined waves or had little effect on the voltammograms of **2-Bn (**Appendix), **5-THFb** (Appendix), **14-*meta/para***, and **15-*meta/para***.

Table 3.4. Redox potentials (V, vs Fc/Fc^+) for **2-Bn**, **14-*para***, **14-*meta***, **15-*para***, and **15-*meta*.**

Compound	(A) U(IV/III)	(B) U(V/IV) ($E_{p,a}$-$E_{p,c}$, i_c/i_a)	(C) U(V/IV) ($E_{p,a}$-$E_{p,c}$, i_c/i_a)
2-Bn	-0.31[a]	-	-
14-*para*	-0.07[a]	-	-
14-*meta*	-0.14[a]	-	-
15-*para*	-	-0.60[b] (0.20, 0.60)	-
15-*meta*	-	-0.46 (0.19,0.86)	-0.15[b] (0.19,0.68)

The higher valent metal centers of **15-*meta*** and **15-*para*** are more oxidized than **14-*meta*** and **14-*para***, and are stabilized by their metal-ligand multiple bonding environments,[180] therefore have access to a greater range of oxidation states under electrochemical conditions. Measurements using varying scan rates were taken for **15-*meta*** and **15-*para*** (Appendix). For **15-*meta***, the peak current (i_p) increases linearly with the square root of the scan rate ν (Vs^{-1}), while the peak-to-peak separation increases. This behavior is consistent with a non-surface bound, quasi-reversible electrochemical process. Furthermore, after rinsing and transferring the working electrode to a fresh electrolyte solution, no detectable electrochemical features appear in the CVs of any U(Tp*) compounds, suggesting that there are no strongly adsorbed surface species,[182, 183] and that the analyte solution remains homogeneous throughout voltammetry experiments. The second oxidation (**C**) of **15-*meta*** is likely the result of a reversible electron transfer followed by a slow chemical reaction involving the loss of a co-ligand, or a conformational change of the Tp* ligand on uranium. At scan rates approaching 0.5 V s^{-1}, the second reduction of **15-*meta*** becomes chemically reversible, indicating moderate stability of higher oxidation states under electrochemical conditions (Appendix). Varying scan rate measurements for **15-*para*** did not lead to improved reversibility, suggesting an accelerated rate of decomposition occurs upon oxidation.

Based on its voltammogram, the first oxidation of **14-*para*** is broader than expected for a single-electron process and as compared to that for **14-*meta***. This broadening of the $E_{p,a}$ potential in **14-*para*** may be attributed to a weak degree of charge transfer between both uranium centers. The stepwise potential observed for **15-*meta*** is a clear indication of a stronger electrostatic contribution than electronic resonance. The distance between

uranium ions (**15-*para*** U1–U2 9.524(3) Å and **15-*meta*** U1–U2 8.165(1) Å) overpowers any resonance advantage gained from structural connectivity (i.e. *para* vs. *meta*). Similar observations were reported for a series of bimolecular U(IV/IV) tris(amide) complexes, where enhanced coupling was observed across the *meta* diethynylbenzene bridge over the *para* isomer.[159] In a recent report by J. Arnold and co-workers involving bimolecular U(IV/IV) quinoid complexes, stepwise potentials were noted, and proposed to be the result of geometrical changes at the uranium rather than electronic resonance contributions.[184]

3.5 Conclusions

In summary, dinuclear U(III) and U(IV) compounds were successfully prepared using organic linkers and Tp^*_2U as a supporting scaffold. Two uranium(III) alkynyl-bridged compounds (**14-*meta*** and **14-*para***) were synthesized via protonation chemistry, and join other examples of low-valent bridging uranium species.[147, 150, 156] The dinuclear U(IV) imido compounds (**15-*meta*** and **15-*para***) were synthesized using aryldiazides, which furnished the desired bridging species in high yields. Magnetic studies and electronic absorption spectroscopy were integral to this study, as they were able to support the oxidation state assignments in all compounds. Overall, spectroscopic, structural, computational, magnetic, and electrochemical characterization established the non-interacting nature of the uranium ions in these systems and demonstrated that there is little electronic communication between uranium ions in all bridged species reported here.

The results of this study are in contrast to those for dinuclear U(V), f^1 compounds, such as those reported by Andersen,[157] Boncella,[185] and Mazzanti[156], which do show interaction between uranium ions. While no electronic communication was noted in the cases of the trivalent and tetravalent compounds reported here, these observations are consistent with other U(IV) examples.[186, 187] Future studies will be aimed at exploring the possibility of magnetic resonance in these systems.

CHAPTER 4. TAILORING THE ELECTRONIC STRUCTURE OF URANIUM MONO(IMIDO) SPECIES THROUGH LIGAND VARIATION

Reprinted (adapted) with permission from Kiernicki, J.J., Tatebe, C.J., Zeller, M., Bart, S.C., *Inorganic Chemistry*, **2018**, *57*, 1870-1879. Copyright 2018, American Chemical Society.

4.1 Abstract

Uranium mono(imido) species have been prepared via oxidation of Cp*U(^{Mes}PDI^{Me})(THF) (**16-Cp***) and [Cp^{P}U(^{Mes}PDI^{Me})]$_2$ (**16-Cp^{P}**) (Cp* = η^5-1,2,3,4,5-pentamethylcyclopentadienide; Cp^{P} = 1-(7,7-dimethylbenzyl)cyclopentadienide; ^{Mes}PDI^{Me} = 2,6-((Mes)N=CMe)$_2$C$_5$H$_3$N, Mes = 2,4,6-trimethylphenyl) with organoazides. Treating either with N_3DIPP formed uranium(IV) mono(imido) complexes, Cp^{P}U(NDIPP)(^{Mes}PDI^{Me}) (**17-Cp^{P}**) and Cp*U(NDIPP)(^{Mes}PDI^{Me}) (**17-Cp***), featuring reduced [^{Mes}PDI^{Me}]$^{1-}$. Addition of electron-donating 1-azidoadamantane (N_3Ad) to **16-Cp*** generated a dimeric product, [Cp*U(NAd)(^{Mes}HPDI^{Me})]$_2$ (**18**), from radical coupling at the *para*-pyridine position of the pyridine(diimine) ligand and H-atom abstraction, formed through a monomeric intermediate that was observed in solution but could not be isolated. To support this, Cp*U(^{t}Bu-^{Mes}PDI^{Me})(THF) (**16-^{t}Bu**), which has a *tert*-butyl group protecting the *para*-position, was also treated with N_3Ad, and the monomeric product, Cp*U(NAd)(^{t}Bu-^{Mes}PDI^{Me}) (**17-^{t}Bu**), was isolated. All isolated complexes were analyzed spectroscopically and structurally, and dynamic solution behavior was examined using electronic absorption spectroscopy.

4.2 Introduction

At the bottom of the periodic table, the actinide elements have long been explored to understand how their chemistry compares to their transition metal counterparts.[1] One such area of interest is uranium-element multiple bonds,[79, 80] with many elusive targets being discovered in recent years.[42, 49, 52, 188-192] The electronic structures,[193-195] bonding trends,[36, 42] and reaction mechanisms[48, 112] that occur for these multiply-bonded actinide species are

unique and can only be studied when paired with synthetic efforts to access such moieties. A focus for many groups,[103, 106, 108, 117, 119, 192, 196-199] including ours,[33, 111, 193, 200-202] has been the synthesis of uranium-nitrogen multiple bonds in the form of imido ligands, as these substituents are more versatile than oxo ligands due to their steric and electronic modularity, but are oxidizing enough to stabilize interesting electronic structures.

The synthesis of imido complexes from azide activation involves a two-electron oxidation process, which can be challenging since actinides generally undergo one-electron redox processes.[15, 46, 135, 191, 203, 204] As a result, alternate synthetic pathways have been developed.[117, 205] One such way that has become popular recently is the use of redox-active ligands, those that store electron density in their conjugated π-system, as these electrons are easily accessed in subsequent chemistry.[206-208] Recently, imido moieties have been installed on actinides using reduced forms of 2,2-bipyridine,[48, 209, 210] pyridine(diimine),[193] and N,N-dimethylbenzamide.[15]

In 2016, we reported the synthesis of a family of novel uranium *trans*-bis(imido) complexes, $Cp^{X}U(NAr)_2(^{Mes}PDI^{Me})$ (Cp^{X} = Cp* (Cp* = η^5-1,2,3,4,5-pentamethylcyclopentadienide), Cp^{P} (Cp^{P} = 1-(7,7-dimethylbenzyl)cyclopentadienide); Ar = phenyl, *p*-tolyl; $^{Mes}PDI^{Me}$ = 2,6-((Mes)N=CMe)$_2C_5H_3N$, Mes = 2,4,6-trimethylphenyl), formed from arylazide (N_3Ar) or diazene reduction by $Cp^*U(^{Mes}PDI^{Me})(THF)$ (**16-Cp***) and $[Cp^{P}U(^{Mes}PDI^{Me})]_2$ (**16-Cp^{P}**) (Figure 4.1).[195] Tetravalent **16-Cp*** and **16-Cp^{P}** both contain $[^{Mes}PDI^{Me}]^{3-}$ chelates,[211] thus these ligand-based electrons, in concert with those from uranium, are removed by oxidation to generate derivatives with differing electronic structures. Interestingly, mono(imido) intermediates were never observed, even when single equivalents of N_3Ar were added. Instead, rapid formation of half an equivalent of the uranium *trans*-bis(imido) species were always noted, consistent with the thermodynamic driving force of the inverse trans influence (ITI).[195]

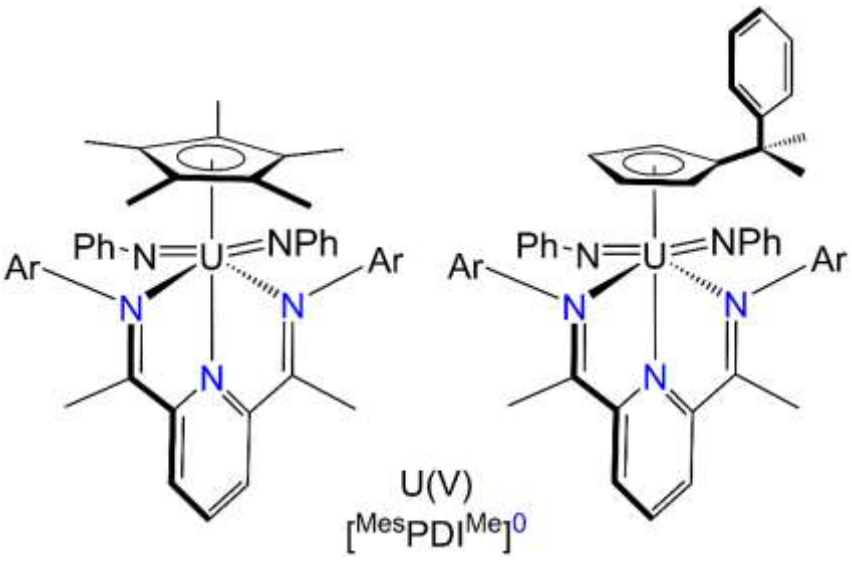

Figure 4.1. Previously reported uranium(V) bis(imido) species.[195]

We hypothesized that employing bulkier azides could facilitate isolation of these mono(imido) species by sterically saturating the uranium center, preventing addition of a second imido substituent. Herein, we present our efforts toward the formation of uranium mono(imido) complexes by variation of the Cp, ^{Mes}PDI^{Me}, and imido ligands, along with their full spectroscopic and structural characterization. These derivatives represent the first examples of uranium(IV) imido species featuring ligand radicals.

4.2.1 General considerations

All air- and moisture-sensitive manipulations were performed using standard Schlenk techniques or in an MBraun inert atmosphere drybox with an atmosphere of purified nitrogen. The MBraun drybox is equipped with a cold well designed for freezing samples in liquid nitrogen as well as two -35 °C freezers for cooling samples and crystallizations. Solvents for sensitive manipulations were dried and deoxygenated using literature procedures with a Seca solvent purification system.[28] Deuterated solvents were purchased from Cambridge Isotope Laboratories. Benzene-d_6 was dried with molecular sieves and sodium, and degassed by three freeze–pump–thaw cycles. 1-Azidoadamantane was purchased from commercial sources. Cp*U(^{Mes}PDI^{Me})(THF) (**16-Cp***),[211] [Cp^{P}U(^{Mes}PDI^{Me})]$_2$ (**16-Cp^{P}**),[14] Cp*U(^{t}Bu-^{Mes}PDI^{Me})(THF),[194] UI$_3$(THF)$_4$,[30] KC$_8$,[212]

potassium 1-(7,7-dimethylbenzyl)cyclopentadienide (KCp^P),[213] and 2,6-diisopropylphenylazide[116] were prepared according to literature procedures.

^1H NMR spectra were recorded on a Varian Inova 300 spectrometer operating at 299.992 MHz. All chemical shifts are reported relative to the peak for $SiMe_4$, using ^1H (residual) chemical shifts of the solvent (C_6D_6: 7.16 ppm; C_7H_8: 2.09 ppm) as a secondary standard. The spectra for paramagnetic molecules were obtained by using an acquisition time of 0.5 s, thus the peak widths reported have an error of ±2 Hz. For paramagnetic molecules, the ^1H NMR data are reported with the chemical shift, followed by the peak width at half height in Hertz, the integration value, and, where possible, the peak assignment. Elemental analyses were performed by Complete Analysis Laboratories, Inc or Midwest Microlab, LLC. Electronic absorption spectroscopic measurements were recorded at ambient temperature, unless stated otherwise, in sealed 1 cm quartz cuvettes with either a Cary 6000i UV-Vis-NIR spectrophotometer or Jasco V-6700 spectrophotometer.

Single crystals of **18**, and **17-^{t}Bu** suitable for X-ray diffraction were coated with poly(isobutylene) oil in a glovebox and quickly transferred to the goniometer head of a Rigaku Rapid II image plate diffractometer equipped with a MicroMax002+ high intensity copper X-ray source with confocal optics. Examination and data collection were performed with Cu Kα radiation (λ = 1.54184 Å). In a similar fashion, single crystals of **19-I_2** suitable for X-ray diffraction, were transferred to the goniometer head of a Nonius KappaCCD diffractometer equipped with a single crystal, incident beam monochromator. Single crystals of **17-Cp^P** and **17-Cp*** were transferred to the goniometer head of a Bruker Quest diffractometer equipped with a single crystal curved graphite incident beam monochromator and a Photon100 CMOS area detector. More information regarding data processing and refinement is available in the Supporting Information. Complete crystallographic data, in CIF format (CCDC 1554590, 1554591, 1554593, 1554594, 1582610) have been deposited with the Cambridge Crystallographic Data Centre.

4.2.2 Synthesis of $Cp^PU(NDIPP)(^{Mes}PDI^{Me})$ (**17-Cp^P**)

A 20 mL scintillation vial was charged with 0.269 g (0.165 mmol) of $[Cp^PU(^{Mes}PDI^{Me})]_2$ (**16-Cp^P**) and 5 mL of toluene and frozen in the cold well. Upon thawing, 0.067 g (0.330

mmol) of 2,6-diisopropylphenylazide was added resulting in $N_{2(g)}$ evolution as evidenced by effervescence of the solution. After 1 hr, volatiles were removed *in vacuo*. The resulting solid was washed with cold pentane (~10 mL, -35 °C) to afford dark brown solid (0.228 g, 0.229 mmol, 70%) assigned as $Cp^{P}U(NDIPP)(^{Mes}PDI^{Me})$ (**17-Cp^{P}**). Single, X-ray quality, crystals were obtained from a saturated toluene solution at -35 °C. Elemental analysis of $C_{54}H_{63}N_4U$: Calculated, C, 64.46; H, 6.31; N, 5.57. Found, C, 64.64; H, 6.56; N, 5.61. ^{1}H NMR (C_6D_6, 25 °C): δ = -251.50 (200, 1H, *para*-pyr-C*H*), -54.20 (139, 2H, *meta*-pyr-C*H*), -11.43 (13, 6H, CH_3), -6.84 (30, 6H, CH_3), -4.11 (4, 6H, Cp^{P}-CH_3), -2.19 (6, 2H, Ar-C*H*), 0.68 (d, *J* = 6, 3H, ^{i}Pr-CH_3), 1.37 (d, *J* = 6, 3H, ^{i}Pr-CH_3), 1.47 (d, *J* = 8, 3H, ^{i}Pr-CH_3), 1.71 (6, 1H, Ar-C*H*), 1.99 (6, 3H, ^{i}Pr-CH_3), 2.13 (6, 1H, Ar-C*H*), 3.81 (sept, *J* = 6, 1H, ^{i}Pr-C*H*), 4.19 (sept, *J* = 8, 1H, ^{i}Pr-C*H*), 4.62 (19, 2H, Ar-C*H*), 6.75 (6, 1H, Ar-C*H*), 7.31 (6, 2H, Ar-C*H*), 13.82 (17, 1H, Ar-C*H*), 19.88 (12, 2H, Ar-C*H*), 25.32 (70, 2H, Ar-C*H*), 31.56 (65, 6H, CH_3), 47.41 (60, 2H, Ar-C*H*), 164.93 (152, 6H, imine-CH_3).

4.2.3 Synthesis of Cp*U(NDIPP)(^{Mes}PDI^{Me}) (**17-Cp***)

A 20 mL scintillation vial was charged with 0.150 g (0.177 mmol) of Cp*U(^{Mes}PDI^{Me})(THF) (**16-Cp***) and 5 mL of toluene. While stirring, 0.036 g (0.177 mmol) of 2,6-diisopropylphenylazide was added resulting in an immediate color change to dark green with $N_{2(g)}$ evolution as evidenced by effervescence of the solution. After 15 min, volatiles were removed *in vacuo*. The resulting solid was washed with cold diethyl ether (10 mL, -35 °C) to afford dark green solid (0.103 g, 0.109 mmol, 62%) assigned as Cp*U(NDIPP)(^{Mes}PDI^{Me}) (**17-Cp***). Single, X-ray quality, crystals were obtained from a concentrated diethyl ether solution at -35 °C. Elemental analysis of $C_{49}H_{63}N_4U$: Calculated, C, 62.21; H, 6.71; N, 5.92. Found, C, 62.26; H, 6.59; N, 5.80. ^{1}H NMR (C_7D_8, -80 °C): δ = -60.73 (245, 1H, Ar-C*H*), -57.56 (240, 1H, Ar-C*H*), -47.37 (121, 6H, CH_3), -41.92 (121, 6H, CH_3), -29.64 (241, 2H, Ar-C*H*), -28.10 (236, 2H, Ar-C*H*), -24.26 (121, 6H, CH_3), -23.59 (238, 6H, CH_3), -12.73 (171, 6H x 2, *o*-Mes-CH_3), -9.21 (140, 2H, Ar-C*H*), 10.89 (94, 2H, Ar-C*H*), 21.07 (280, 15H, Cp*), 32.47 (61, 2H, Ar-C*H*). UV-Vis (THF; λ_{max}, molar abs.): 665 nm 11,372 $M^{-1}cm^{-1}$.

4.2.4 Synthesis of [Cp*U(NAd)(^{Mes}HPDI^{Me})]$_2$ (**18**)

A 20 mL scintillation vial was charged with 0.400 g (0.475 mmol) Cp*U(^{Mes}PDI^{Me})(THF) (**16-Cp***) and 8 mL toluene. While stirring, 1-azidoadamantane (0.085 g, 0.480 mmol) was added resulting in an immediate color change to dark green with $N_{2(g)}$ evolution as evidenced by effervescence of the solution. After stirring for 5 min, the color gradually darkened to dark brown, and over the next 16 hr became dark brown-purple. After 16 hr, volatiles were removed in vacuo. The resulting mixture was washed with 40 mL pentane and dried to afford dark brown-purple powder (0.092 g, 0.050 mmol, 21%) assigned as [Cp*U(NAd)(^{Mes}HPDI^{Me})]$_2$ (**18**). Single, X-ray quality, crystals were obtained from a benzene solution stored at room temperature. Elemental analysis of $C_{94}H_{124}N_8U_2$: Calc. C, 61.29; H, 6.78; N, 6.08. Found C, 61.74; H, 6.60; N, 5.84. ^{1}H NMR (C_6D_6, 23 °C): δ = -16.00 (76, 3H, C*H*$_3$), -7.05 (77, 3H, C*H*$_3$), -5.92 (58, 3H, C*H*$_3$), -5.54 (50, 3H, C*H*$_3$), 1.02 (109, 15H Cp*), 1.41 (27, 1H, C*H*), 1.78 (6, 3H, C*H*$_3$), 2.41 (6, 3H, C*H*$_3$), 3.57 (19, 1H, C*H*), 3.69 (13, 1H, C*H*), 4.64 (11, 1H, C*H*), 5.57 (13, 1H, C*H*), 6.85 (58, 3H, C*H*$_3$), 7.03 (21, 1H, C*H*), 8.36 (25, 3H, C*H*$_3$), 10.33 (39, 3H, C*H*$_3$), 13.55, (85, 1H, C*H*), 13.89 (33, 3H, C*H*$_3$), 20.47 (311, 3H x 2, C*H*$_3$), 23.77 (108, 1H, C*H*), 26.83 (137, 1H, C*H*), 44.84 (251, 3H, C*H*$_3$).

4.2.5 Synthesis of Cp*U(NAd)(^{t}Bu-^{Mes}PDI^{Me}) (**17-^{t}Bu**)

A 20 mL scintillation vial was charged with 0.282 g Cp*U(^{t}Bu-^{Mes}PDI^{Me})(THF) (**16-^{t}Bu**) (0.314 mmol) and 5 mL of toluene. While stirring, 1-azidoadamantane (0.055 g, 0.310 mmol) was added resulting in an immediate color change to dark green with $N_{2(g)}$ evolution as evidenced by effervescence of the solution. After stirring for 5 min, volatiles were removed in vacuo. The resulting mixture was washed with 10 mL of cold (-35 °C) pentane and dried to afford black powder (0.242 g, 0.250 mmol, 80%) assigned as Cp*U(NAd)(^{t}Bu-^{Mes}PDI^{Me}) (**17-^{t}Bu**). Single, X-ray quality, crystals were obtained from a concentrated diethyl ether/hexamethyldisiloxane solution (5:1) stored at -35 °C. Elemental analysis of $C_{51}H_{69}N_4U$: Calc. C, 63.33; H, 7.20; N, 5.79. Found C, 62.35; H, 7.14; N, 5.91. ^{1}H NMR (C_6D_6, 23 °C): δ = -17.53 (10, 12H, Ar-*o*-C*H*$_3$), -5.15 (11, 6H, Cp^p-C*H*$_3$), -3.07 (4, 6H, Ar-*p*-C*H*$_3$), -3.03 (6, 4H, Ar-*m*-C*H*), 5.65 (4, 9H, C(C*H*$_3$)$_3$), 9.06 (61, 6H, N=CC*H*$_3$), 10.97 (t, *J* = 7, 1H, *p*-Ph-C*H*), 11.71 (50, 2H, Cp-C*H*), 12.62 (t, *J* = 7, 2H, *m*-Ph-C*H*), 14.44 (7, 2H,

pyr-C*H*), 17.19 (51, 2H, Cp-C*H*), 21.05 (d, *J* = 6, 2H, *o*-Ph-C*H*).UV-Vis (THF; λ_{max}, molar abs.): 669 nm 4487 $M^{-1}cm^{-1}$.

4.2.6 Synthesis of $Cp^{P}UI_2(^{t}Bu\text{-}^{Mes}PDI^{Me})$ (**19-I$_2$**)

A 20 mL scintillation vial was charged with 0.300 g (0.331 mmol) of $UI_3(THF)_4$, 0.150 g (0.331 mmol) of ($^{t}Bu\text{-}^{Mes}PDI^{Me}$), and 10 mL of toluene and stirred for 15 min. Volatiles were removed affording a brown solid. The solid was redissolved in 15 mL of toluene. While stirring, 0.074 g (0.333 mmol) of KCp^{P} was added and allowed to stir for 30 min. The brown suspension was filtered over Celite and volatiles were removed *in vacuo* to yield brown solid that was washed with cold (-35 °C) *n*-pentane affording $Cp^{P}UI_2(^{t}Bu\text{-}^{Mes}PDI^{Me})$ (**19-I$_2$**) (0.344 g, 0.305 mmol, 92%). Single, X-ray quality, crystals were obtained from a concentrated toluene/pentane (1:1) solution at -35 ºC. Elemental analysis of $C_{45}H_{54}N_3I_2U$: Calculated, C, 47.88; H, 4.82; N, 3.72. Found, C, 47.79; H, 5.00; N, 3.80. ^{1}H NMR (C_6D_6, 23 °C): δ = -17.53 (10, 12H, Ar-*o*-C*H*$_3$), -5.15 (11, 6H, Cp^{P}-C*H*$_3$), -3.07 (4, 6H, Ar-*p*-C*H*$_3$), -3.03 (6, 4H, Ar-*m*-C*H*), 5.65 (4, 9H, C(C*H*$_3$)$_3$), 9.06 (61, 6H, N=CC*H*$_3$), 10.97 (t, *J* = 7, 1H, *p*-Ph-C*H*), 11.71 (50, 2H, Cp-C*H*), 12.62 (t, *J* = 7, 2H, *m*-Ph-C*H*), 14.44 (7, 2H, pyr-C*H*), 17.19 (51, 2H, Cp-C*H*), 21.05 (d, *J* = 6, 2H, *o*-Ph-C*H*).

4.2.7 Synthesis of $Cp^{P}UI(^{t}Bu\text{-}^{Mes}PDI^{Me})$ (**19-I**)

A 20 mL scintillation vial was charged with 0.141 g (0.125 mmol) of **19-I$_2$** and 5 mL of toluene. While stirring, one equivalent of sodium triethylborohydride (1.0 M in toluene) was added via volumetric pipet resulting in release of hydrogen as evidenced by effervescence of the solution. After 5 min, volatiles were removed *in vacuo*. The product was extracted with diethyl ether and filtered over Celite. Evaporation of solvent from the filtrate afforded brown powder (0.103 g, 0.103 g, 82%) assigned as $Cp^{P}UI(^{t}Bu\text{-}^{Mes}PDI^{Me})$ (**19-I**). Elemental analysis of $C_{45}H_{54}N_3IU$: Calculated, C, 53.95; H, 5.43; N, 4.19. Found, C, 53.95; H, 5.55; N, 4.20. ^{1}H NMR (C_6D_6, 23 °C): δ = -60.69 (28, 6H, C*H*$_3$), -46.75 (56, 6H, C*H*$_3$), -20.63 (280, 2H, Ar-C*H*), -8.16 (10, 2H, Ar-C*H*), -7.37 (10, 2H, Ar-C*H*), -3.45 (5, 6H, C*H*$_3$), 3.08 (15, 6H, C*H*$_3$), 8.19 (225, 4H, *o*,*m*-Ph-C*H*), 17.82 (24, 1H, *p*-Ph-C*H*), 21.48 (26, 2H, Ar-C*H*), 22.38 (10, 9H, *tert*-butyl C*H*$_3$), 45.98 (42, 2H, Ar-C*H*), 65.42 (25, 3H, Cp^{P}-C*H*$_3$), 71.56 (44, 3H, Cp^{P}-C*H*$_3$).

4.3 Results and Discussions

We postulated that using sterically demanding aryl azides could form mono(imido) species that would be large enough to prevent addition of a second imido ligand. This was tested by adding one equivalent of N_3DIPP (DIPP = 2,6-diisopropylphenyl) to toluene solutions of one-half equivalent of dimeric **16-Cp^P** and one equivalent of monomeric **16-Cp***, which resulted in immediate color changes to light brown and dark green, respectively. Upon addition, effervescence of the solution was noted, consistent with N_2 loss and suggesting formation of imido products (Figure 4.2). Analysis by ^{1}H NMR spectroscopy was consistent with complete conversion to the desired uranium mono(imido) complexes, Cp^{P}U(NDIPP)(^{Mes}PDI^{Me}) (**17-Cp^P**) and Cp*U(NDIPP)(^{Mes}PDI^{Me}) (**17-Cp***), respectively. If *trans*-bis(imido) species had been generated as observed for smaller azides,[195] one half equivalent of starting material, **16-Cp^P** or **16-Cp***, would remain; however, this was not observed by ^{1}H NMR spectroscopy in these cases.

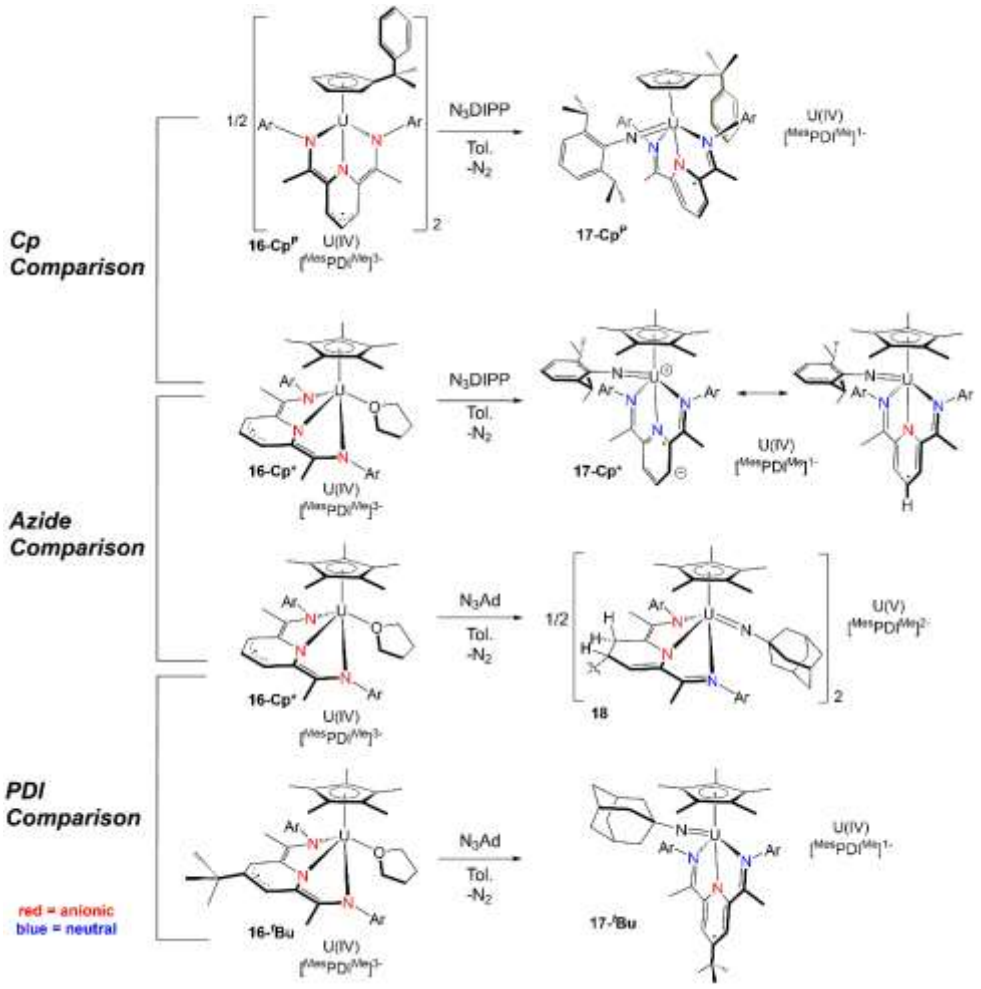

Figure 4.2. Synthesis of mono(imido) complexes **17-Cp^{P}**, **17-Cp***, **18**, and **17-^{t}Bu**. Dative (blue) and ionic (red) bonds are shown to indicate electronic structures. The electronic structures shown represent results from characterization by solution NMR spectra (25° C) and X-ray crystallography.

To confirm mono(imido) formation, single, X-ray quality crystals of **17-Cp^{P}** and **17-Cp*** were analyzed. Data refinement of each compound showed η^5-Cp ligands (U-Ct = 2.562 (**17-Cp^{P}**) and 2.510 Å (**17-Cp***); Ct = centroid) coordinated to ^{Mes}PDI^{Me} uranium mono(imido) complexes (Fig 4.3 and Fig 4.4). The U-N_{imido} distances are similar to one another (**17-Cp^{P}** = 1.984(4); **17-Cp*** = 1.9926(17) Å) as well as to those in tetravalent (^{Mes}PDI^{Me})UI_2(NMes)(THF)[193] (1.984 Å) and Cp^*_2U(NDIPP)(THF)[21] (2.006 Å). However, differences between **17-Cp^{P}** and **17-Cp*** are noted when comparing bond metrics involving the ^{Mes}PDI^{Me} chelate (Fig 4.4).[14] For **17-Cp^{P}**, the U-N_{PDI} linkages of 2.535(4), 2.480(4), and 2.477(4) Å suggest significant delocalization of the anionic charge of the

[^{Mes}PDI^{Me}]$^{1-}$ ligand. Additionally, ligand reduction is apparent by inspecting the C=N$_{imine}$ and C$_{imine}$-C$_{pyr}$ distances. Elongation of the imine bond (N3-C8 = 1.340(6) Å) and contraction of the C$_{imine}$-C$_{pyr}$ bond (1.473(7) Å) supports population of the ligand π* orbitals.[214] In contrast, **17-Cp*** displays three U-N$_{PDI}$ distances (U1-N1 = 2.5737(19); U1-N2 = 2.4979(17); U1-N3 = 2.5688(18) Å) that are significantly longer than in **17-Cp^{P}**, suggesting three dative interactions. However, inspection of the ^{Mes}PDI^{Me} intraligand bond distances shows loss of aromaticity in the pyridine ring, as evidenced by the elongated C3-C4 (1.469(3) Å) and C6-C7 (1.470(3) Å) bonds, both of which are on the order of single bonds and support ligand reduction (Figure 4.4). This dichotomy of electronic structure, as compared to **17-Cp^{P}**, is similar to the reported uranium pinacolate complexes, Cp^{P}U(O$_2$C$_2$Ph$_4$)(^{Mes}PDI^{Me}) and Cp*U(O$_2$C$_2$Ph$_2$H$_2$)(^{Mes}PDI^{Me}).[14] As established for Cp*U(O$_2$C$_2$Ph$_2$H$_2$)(^{Mes}PDI^{Me}), **17-Cp*** is best described as a zwitterionic uranium(IV) complex with a monoanionic [^{Mes}PDI^{Me}]$^{1-}$ ligand by X-ray crystallography.

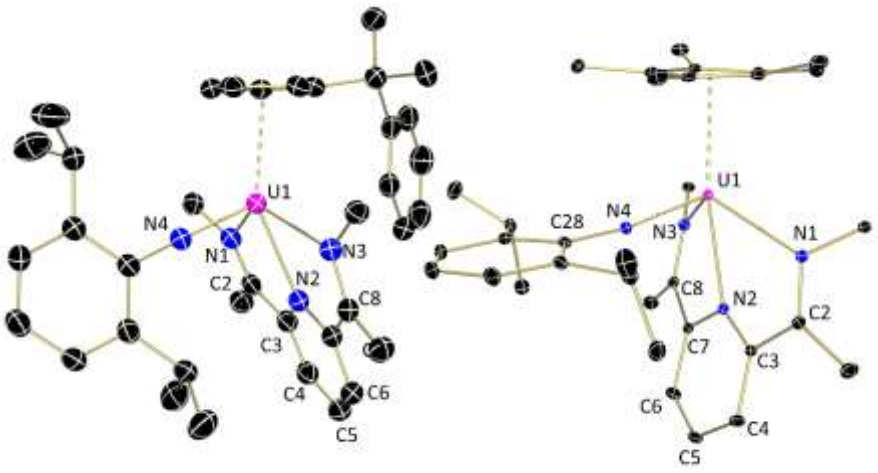

Figure 4.3. Molecular structures of **17-Cp^{P}** (left) and **17-Cp*** (right) displayed with 30% probability ellipsoids. Hydrogen atoms, mesityl moieties, and co-crystallized solvent molecules have been omitted for clarity.

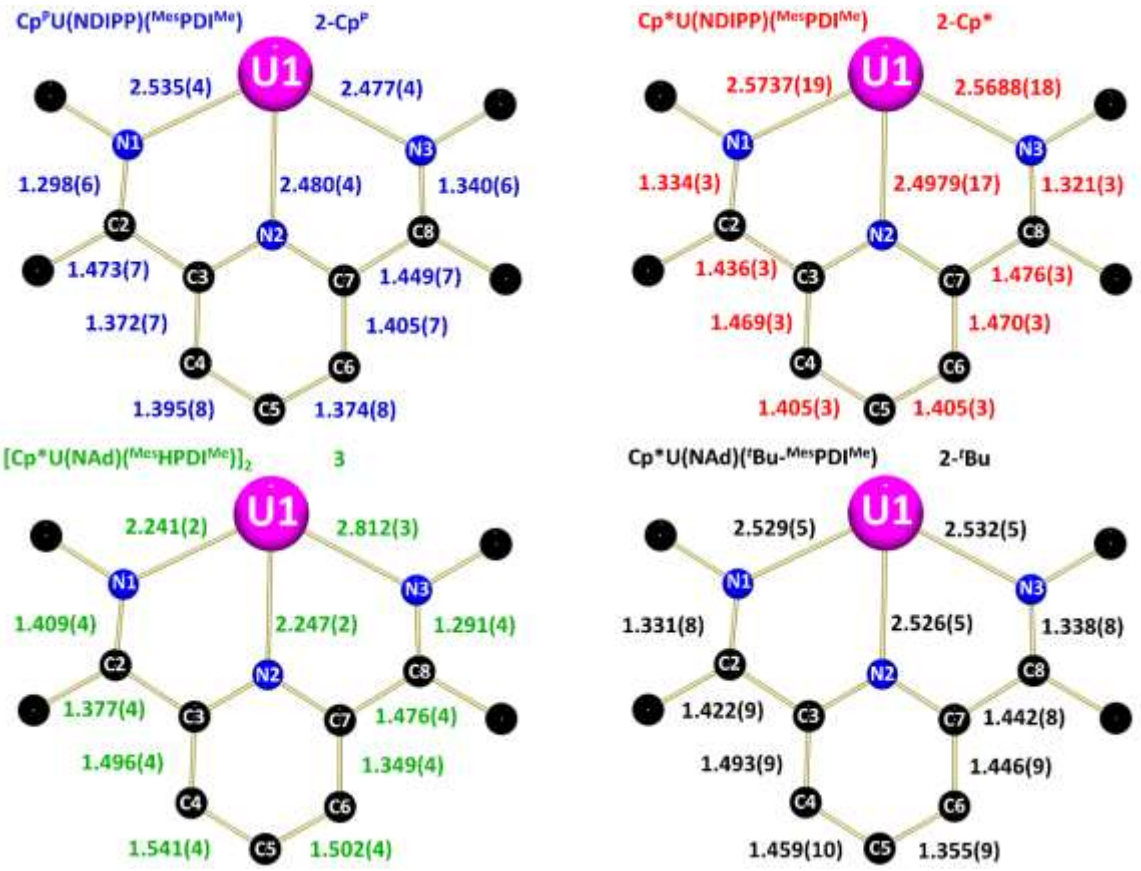

Figure 4.4. Comparison of pyridine(diimine) bond distances (Å).

This dichotomy in electronic structure is evident from electronic absorption spectroscopic analysis of THF solutions of **17-Cp^{P}** and **17-Cp*** (300-2100 nm, 25 °C) (Fig 4.5). The spectrum of green **17-Cp*** displays an intense absorption at 665 nm (11,300 $M^{-1}cm^{-1}$). In comparison, the absorption spectrum of **17-Cp^{P}** shows broadened features throughout the visible region. A striking difference between **17-Cp^{P}** and **17-Cp*** is clear in the near-infrared region; **17-Cp*** displays low intensity (30-65 $M^{-1}cm^{-1}$) *f-f* transitions, whereas **17-Cp^{P}** displays an ill-defined, more intense transition (λ_{max} = 1865 nm, 870 $M^{-1}cm^{-1}$) assigned as an intramolecular electron transfer band. This band has been noted in uranium(IV) complexes with the same electronic structure.[14] The lack of this band for **17-Cp*** along with the UV-Vis absorptions support localized charge on $^{Mes}PDI^{Me}$.[14]

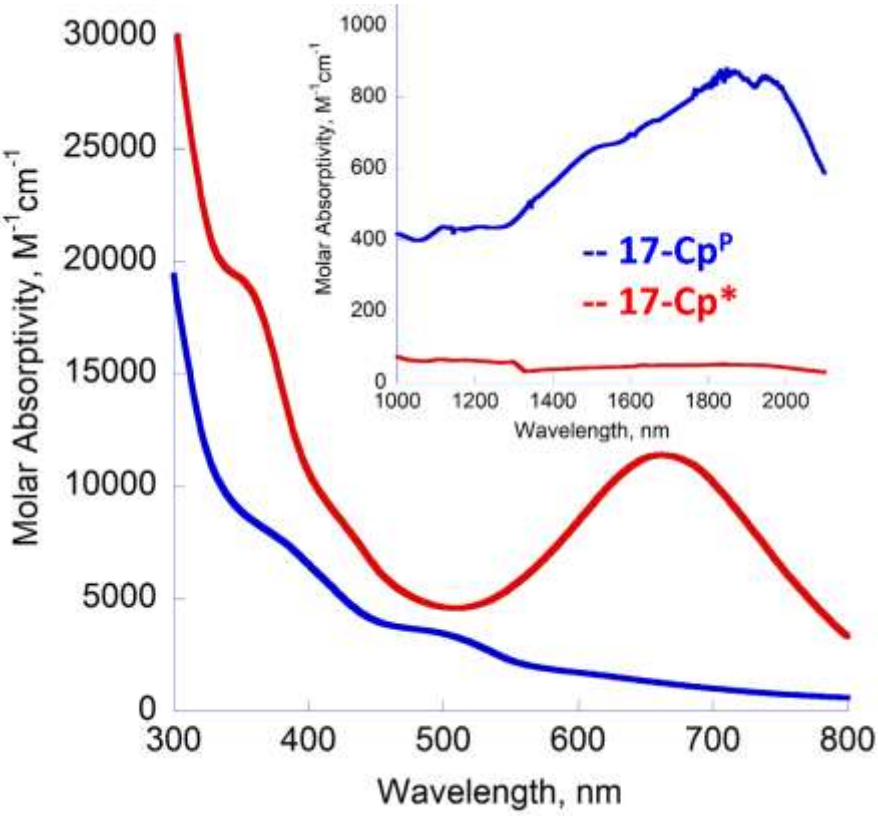

Figure 4.5. Electronic absorption spectra of complexes **17-Cp^{P}** (blue) and **17-Cp*** (red) collected in THF at ambient temperature (solvent overtones from 1670-1760 nm were removed for clarity).

To further characterize **17-Cp^{P}** and **17-Cp***in solution, ^{1}H NMR spectroscopy was used. Analysis of **17-Cp^{P}** (C_6D_6, 25 °C) revealed a paramagnetically broadened spectrum (-252 to 165 ppm) consistent with C_s symmetry in solution. Those signals furthest upfield (-251.50 ppm, 1H; -54.20 ppm, 2H) and downfield (164.93 ppm, 6H) are assigned to the ^{Mes}PDI^{Me} pyridine-C*H* and imine-CH_3 protons, respectively, consistent with unpaired electron density in the pyridine(diimine) plane. For uranium complexes bearing redox-active supporting ligands, wide-ranging chemical shifts have been observed due to radical character localized on the ligand as in Cp^{P}U(X)$_2$(^{Mes}PDI^{Me}) (X = I, Cl, SPh, SePh, TePh),[215] Cp^{P}U(O$_2$C$_2$Ph$_4$)(^{Mes}PDI^{Me})[14], Cp*$_2$U(2,2'-bipyridyl),[216] and (DOPO^{sq})UI$_2$(THF)$_2$[217] (DOPO = 2,4,6,8-tetra-*tert*-butyl-1-oxo-1*H*-phenoxazin-9-olate). In contrast, the ^{1}H NMR spectrum of **17-Cp*** (C_6D_6, 25 °C) displays a complicated paramagnetic spectrum with resonances consistent with a major and minor species (-40 to 47 ppm). While assignment

was not possible at this stage, no significant shift in product ratio was observed at room temperature when solvent polarity was varied (C_6D_6 vs. C_5D_5N).

The dynamic behavior of **17-Cp*** was probed by employing variable temperature ^{1}H NMR spectroscopy and electronic absorption spectroscopy. The ^{1}H NMR spectroscopic data (Appendix) acquired at -80 °C (toluene-d_8) shows a broad spectrum with resonances indicating symmetry in the molecule. Heating to 80 °C causes the resonances to increase in number, indicating an equilibrium process at high temperature. Due to the paramagnetism and peak resolution in the sample, reliable integration values that would allow extraction of meaningful Van't Hoff parameters was not possible. Data from variable temperature electronic absorption spectroscopy was collected over the same temperature range in toluene (Figure 4.6). At -80 °C, the λ_{max} of the visible region (683 nm) gradually hypsochromically shifts to 654 nm (Δ = 29 nm) upon warming to 80 °C, suggesting a conformation change consistent with the ^{1}H NMR spectroscopic data. Compound **17-Cp*** also displays negative solvatochromism at 20 °C from toluene to tetrahydrofuran (Δ = 11 nm) (Appendix). In THF, **17-Cp*** does not display as significant of changes in its absorption spectrum upon cooling to -80 °C (Appendix). Given the visible absorption is assigned to the ligand radical character of **17-Cp***, we hypothesize the dynamic process is a temperature dependent equilibrium involving the conjugated portion of the ^{Mes}PDI^{Me} (*vide infra*), although attempts to isolate either equilibrium species for characterization have thus far been unsuccessful.

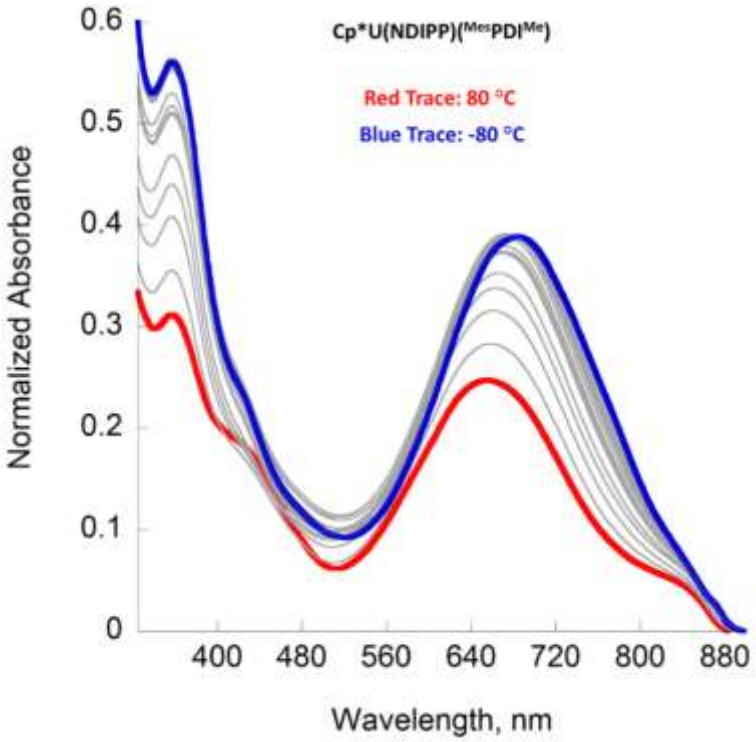

Figure 4.6. Variable temperature electronic absorption spectrum of **17-Cp*** recorded in toluene from 320-900 nm in the temperature range of -80 °C to 80 °C. The red trace represents 80 °C and the blue trace represents -80 °C. The intermittent grey lines represent 10 °C increments. Each scan was normalized to an absorbance of zero at 900 nm.

Variable temperature EPR studies were also used to provide insight into the identity of the two equilibrium species, to potentially confirm ligand radical involvement. Examination of a toluene solution of **17-Cp*** at room temperature displayed a broadened isotropic signal (g_{iso} = 1.974) consistent with the presence of a radical containing species at room temperature (Figure 4.7, Appendix). The observed hyperfine coupling, although poorly resolved, as well as the resonating field are both consistent with pyridyl-based radicals[195, 218] and radicals associated with uranium,[194, 219] respectively. Data collection at 10 K under analogous conditions did not reveal a signal, suggesting quenching of the ligand radical. These data support that at low temperature **17-Cp*** exists as a dimeric species derived from radical coupling at the *para*-pyridine, while at elevated temperature the monomeric ligand radical complex is present.

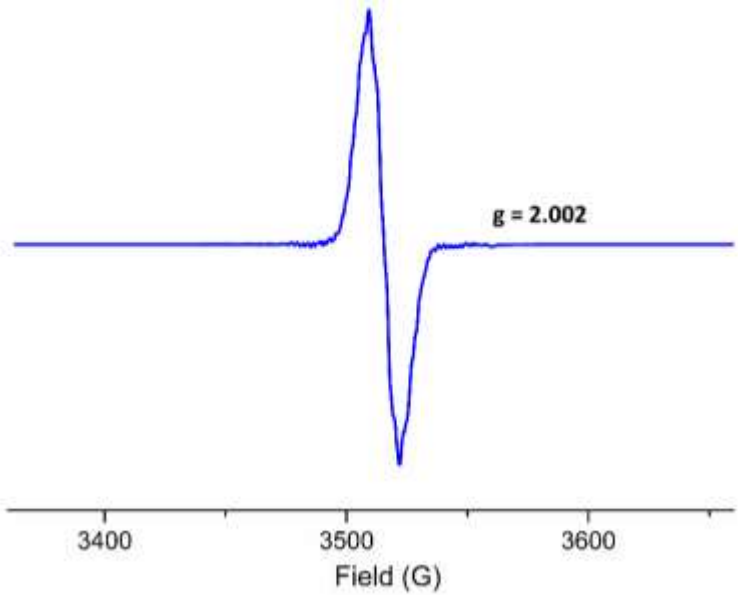

Figure 4.7. EPR spectrum of **17-Cp^{P}** recorded in toluene (2.10 mM) at ambient temperature. Conditions: power = 1.00 mW; modulation = 0.10 mT/100 kHz.

Considering all of the structural and variable temperature spectroscopic data together, formation of **17-Cp^{P}** and **17-Cp*** proceeds by reduction of N_3DIPP with electrons derived solely from [^{Mes}PDI^{Me}]$^{3-}$. Thus, the uranium(IV) oxidation state is maintained while double oxidation of the ligand to [^{Mes}PDI^{Me}]$^{1-}$ occurs. Significantly, **17-Cp^{P}** and **17-Cp*** represent the first examples of uranium(IV) imido complexes with stored radical electron density on the supporting ligand. Typically, uranium mono(imido) formation by redox-active ligand oxidation has resulted in complete bankrupting of the electron cache,[193] sometimes accompanied by ligand loss.[48] Overall, distinct electronic structures for **17-Cp^{P}** and **17-Cp*** are observed, which is supported by characterization data acquired both in solution and in the solid state. While in these cases, the solution and solid state data for electronic structure assignment is consistent, it should be noted that several recent examples highlight that electronic structures observed in both solution and solid states may not necessarily correlate when redox-active ligands are used.[220, 221] The dichotomy likely stems from the electron-donating Cp* ligand, which produces an electron-rich uranium center that stabilizes the zwitterionic resonance form *via* a formal backbonding interaction to the pyridine(diimine) ligand. Such an interaction has been noted previously for this ligand on uranium.[222] This contrasts the dimethylbenzyl substituted Cp^{P}, which is a poorer

electron donor, generating an electron deficient uranium, reducing backbonding and preventing formation of the zwitterion.[14, 194]

With the unique electronic structure afforded **17-Cp*** by the electron-donating Cp* (vs. Cp^P) established, we sought to investigate if a more strongly electron-donating imido substituent would have the same effect. Analogous reactivity with **16-Cp*** was therefore attempted with 1-azidoadamantane (N_3Ad). Addition of one equiv of N_3Ad to a toluene solution of **16-Cp*** results in a rapid color change from brown to dark green—similar to **17-Cp*** (Scheme 1). However, the green color gradually dissipates to afford a dark brown-purple product, isolated as $[Cp^*U(NAd)(^{Mes}HPDI^{Me})]_2$ (**18**) in low yield. ^1H NMR spectroscopic analysis of **18** revealed a paramagnetically shifted spectrum (-16 to 45 ppm) that is significantly broader and absent of signs of the equilibrium observed for **17-Cp***.

To unambiguously determine the structure of **18**, single crystals were analyzed by X-ray crystallography. Surprisingly, **18** is a dimeric Cp*-uranium mono(imido) complex in which coupling occurred at the *para*-position of the pyridine concomitant with H-atom abstraction by the adjacent carbon (Fig 4.8, left). This coupling is reminiscent of that observed for the uranium(IV) η^2-hydrazido, $[Cp^*U(BCC)(^{Mes}HPDI^{Me})]_2$ (BCC = benzo[*c*]cinnoline).[219] In that instance, the $^{Mes}PDI^{Me}$ adopts a closed-shell dianionic configuration where a pyridine C-C double bond is disrupted by *para*-coupling and concomitant H-atom abstraction by the adjacent carbon. Similarly in **18**, closed shell $[^{Mes}PDI^{Me}]^{2-}$ is evident by two short U-N distances (2.241(2), 2.247(2) Å) and one dative interaction (U1-N3 = 2.812(3) Å) as well as alternating single and double bonds (save the C4-C5 positions) also observed in arene-bound iron(II) pyridine(diimine) complexes (Figure 4.4).[57] The $U\text{-}N_{imido}$ bond of 1.950(3) Å is significantly shorter than in **17-Cp^P** and **17-Cp***—consistent with increased donicity of the 1-adamantyl versus 2,6-diispropylphenyl substituent, but is comparable to uranium(V) mono(imido) species of the series $Cp^*_2U(NDIPP)(EPh)$ (E = O, S, Se, Te).[223] Thus, by charge balance considerations, **18** is best described as a uranium(V) mono(imido) with a pyridine(diimine) dianion.

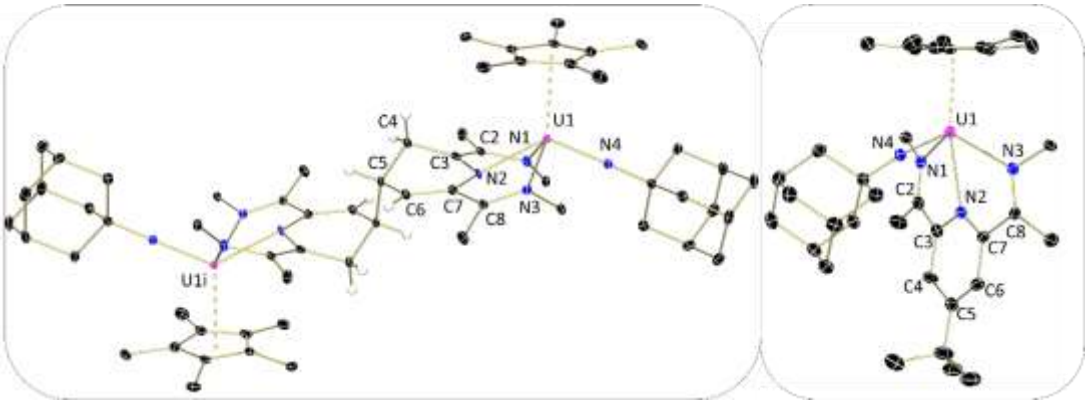

Figure 4.8. Molecular structures of **18** (left) and **17-^{t}Bu** (right) displayed with 30% probability ellipsoids. Selected hydrogen atoms, mesityl substituents, and co-crystallized solvents have been omitted for clarity.

In the synthesis of **18**, a rapid color change to green was noted before gradually changing to dark brown-purple. To probe the similarity of the green intermediate species to **17-Cp***, the reaction progress was monitored by electronic absorption spectroscopy (Figure 4.9). Upon addition of N_3Ad, a green, color producing band at 663 nm rapidly forms, comparable to that of **17-Cp*** ($\Delta\lambda_{max}$ = 8 nm). Unlike **17-Cp***, the band gradually dissipates as complex **18** is formed.

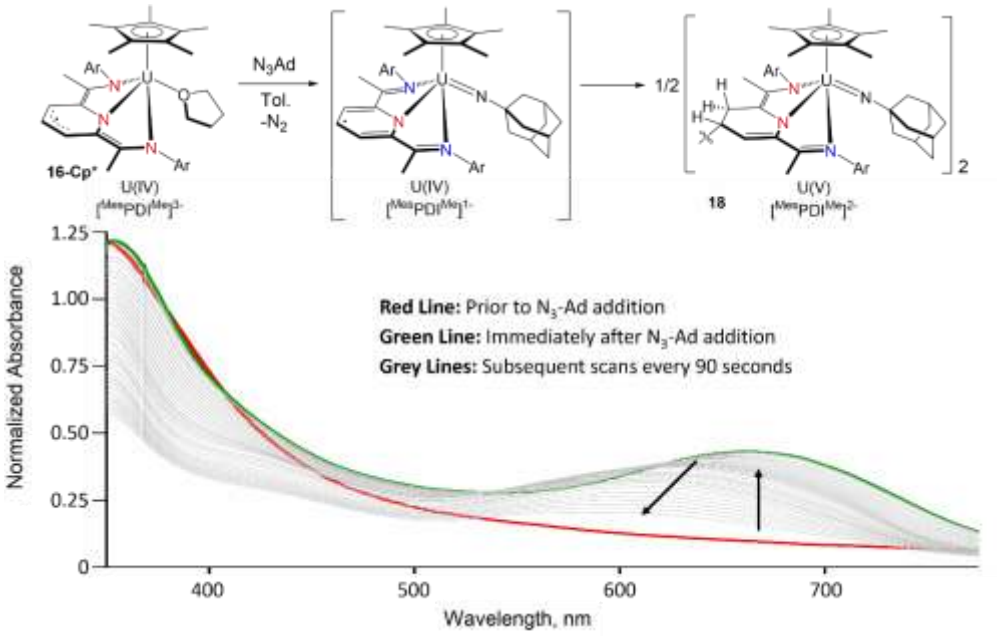

Figure 4.9. Electronic absorption spectra monitoring the reaction between **16-Cp*** and N_3Ad (toluene, ambient temperature). Displayed at top is the reaction scheme. The red line denotes **16-Cp*** (prior to addition). The green line denotes the second data point (immediately after N_3Ad addition). Subsequent data points (grey lines) were recorded every 90 seconds.

Preparation of **18** was performed in toluene-d_8 in order to determine if the abstracted H atom was derived from solvent or from cannibalization of the compound. Analysis of the reaction product using ^{2}H NMR spectroscopy showed no deuterium incorporation into the ligand of **18** (Figure 4.10), suggesting that H atom abstraction from the reaction medium does not occur. Instead, the source of the H-atom must be derived from either **16-Cp*** or **18**, ultimately contributing to the overall low yield of the reaction (21%).

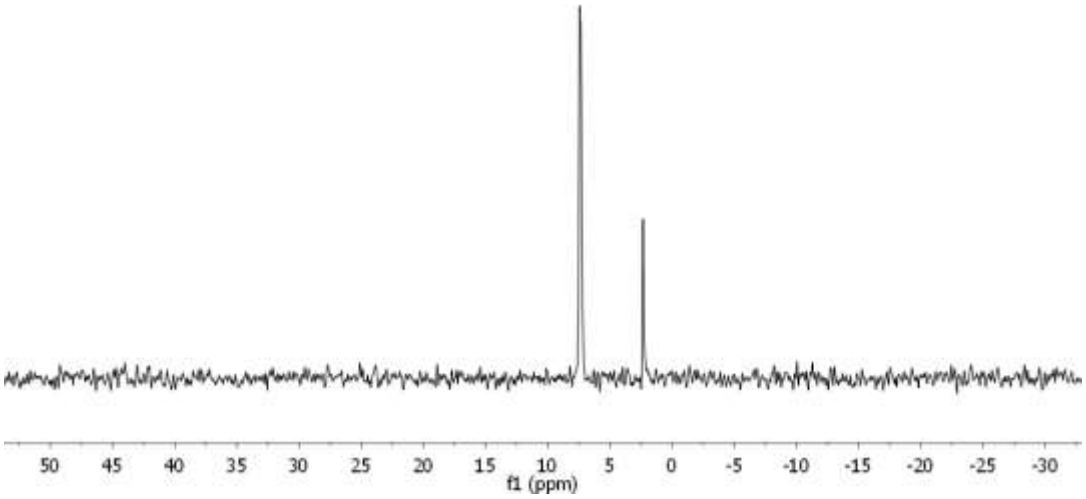

Figure 4.10. ^{2}H NMR spectrum (C_6H_6, 23 °C) of **18** from a sample that was synthesized in toluene-d_8.

The intermediate green color noted in the synthesis of **8** was probed further using Cp*U(^{t}Bu-^{Mes}PDI^{Me})(THF) (**16-^{t}Bu**), which features a *tert*-butyl moiety at the *para*-pyridine position that should preclude *para*-pyridine coupling.[195] Treating a toluene solution of **16-^{t}Bu** with one equiv of N_3Ad resulted in effervescence, presumably of N_2, along with a rapid color change from brown to dark green that persisted, suggesting a stable product, Cp*U(NAd)(^{t}Bu-^{Mes}PDI^{Me}) (**17-^{t}Bu**). Attempts to prepare the analogous Cp^{P} species, Cp^{P}U(NAd)(*t*Bu-^{Mes}PDI^{Me}), were unsuccessful. ^{1}H NMR analysis of **17-^{t}Bu** revealed thirteen paramagnetically shifted resonances (-46 to 51 ppm), consistent with C_s symmetry lacking signs of an equilibrium process.

To determine if **17-^{t}Bu** is a monomer, X-ray diffraction of single crystals was performed. Analysis revealed a monomeric uranium mono(imido) akin to **17-Cp^{P}** (Fig 4.8, right) with a U-N_{imido} distance of 1.941(6) Å that is within error of **8**, and similar to other uranium(IV) mono(alkylimido) complexes including (^{t}Bu$_2$bpy)U(N^{t}Bu)I$_2$(THF)$_2$.[120] The uranium-chelate and intraligand distances for ^{Mes}PDI^{Me} are nearly identical to those of **17-Cp***, suggesting a monoanionic [^{Mes}PDI^{Me}]$^{1-}$ ligand (Fig 4.4).[195]

Although **17-^{t}Bu** was confirmed to be the monomeric relative of **18**, the ^{Mes}PDI^{Me} oxidation state renders the complexes inherently different: uranium(IV) vs. uranium(V).

To confirm differences in electronic structure, both **17-^{t}Bu** and **18** were investigated by electronic absorption spectroscopy (THF, 25 °C) (Fig 4.11). For **17-^{t}Bu**, the near-infrared region is comprised of weak transitions, whereas the visible region is dominated by an intense (4487 $M^{-1}cm^{-1}$) color-producing band at 669 nm—red shifted 4 nm from that of **17-Cp*** at this temperature. Conversely, the near-infrared region of **18** displays a typical uranium(V) spectrum[180] with a sharp absorbance at 1634 nm (221 $M^{-1}cm^{-1}$) similar to the uranium(V) bis(imido) complexes, $Cp^{X}U(NPh)_2(^{Mes}PDI^{Me})$ (Cp^{X} = Cp^{P}, Cp*).[195] Despite the closed shell $[^{Mes}PDI^{Me}]^{2-}$, **18** does not contain a notable far-visible/near-infrared absorbance like in tetravalent Cp*U(BCC)(^{t}Bu-^{Mes}PDI^{Me}),[53] Cp*UI(^{Mes}PDI^{Me}),[46] and $Cp^{P}UI(^{t}Bu\text{-}^{Mes}PDI^{Me})$ (Appendix)

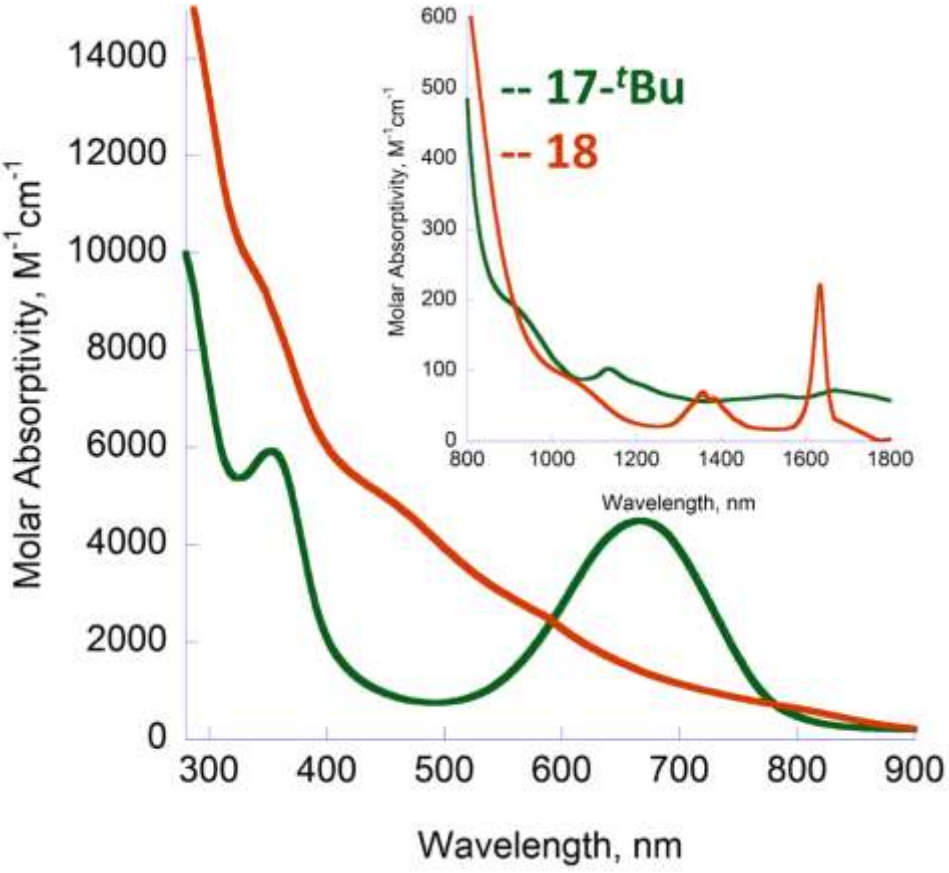

Figure 4.11. Electronic absorption spectra of complexes **18** (orange) and **17-^{t}Bu** (green) collected in THF at ambient temperature (solvent overtones from 1670-1760 nm are omitted for clarity).

Spectroscopic and structural characterization of **18** and **17-^{t}Bu** gives insight into the equilibrium process noted in the NMR spectroscopic data for **17-Cp***that was previously discussed. The dimeric structure of **18**, formed from coupling of pyridine ligand radicals, supports the equilibrium noted in the spectrum of **2-Cp*** is likely due to an analogous ligand radical. The ligand radical would likely be stabilized by the polar THF solvent, facilitating further reactivity of this moiety via a) *para*-pyridine coupling, b) radical H-atom abstraction, or c) both (by analogy to **18**).

To determine which process was operative, the reaction to generate **17-Cp*** was performed neat in the H-atom donor 1,4-cyclohexadiene. No change in the reaction or the ^{1}H NMR spectrum was noted, thus it is hypothesized that the equilibrium process is reversible *para*-pyridine C-C coupling with *no* H-atom abstraction. Thus, at elevated temperature, both the monomer and dimer are present, which is consistent with the complicated ^{1}H NMR spectrum recorded at 25 °C discussed earlier. In the case of **18,** the electron-donating adamantyl substituent serves to increase electron density on ^{Mes}PDI^{Me}, favoring *para*-pyridine C-C coupling with subsequent H-atom abstraction. As the dimeric uranium(V) structure is not observed for **17-Cp***, it is proposed that subsequent H-atom abstraction must be slow in comparison to the C-C coupling equilibrium, facilitating the reverse process. Isolation of **17-^{t}Bu**, which is established to contain a *para*-pyridine radical, also corroborates that H-atom abstraction/oxidation to U(V) for **18** must occur after dimerization since this is not noted for **17-^{t}Bu**. H-atom abstraction has been noted in related uranium systems.[219] Thus, while the zwitterion is the prevalent resonance structure for **17-Cp*** as observed from spectroscopic and structural characterization, another resonance structure, one that has a stabilized radical, must also contribute to the overall electronic structure (Figure 4.2). This alternate structure can be formed from resonating the radical around the pyridine ring, generating a radical at the *para*-carbon which would directly precede dimerization to form the coupled product.

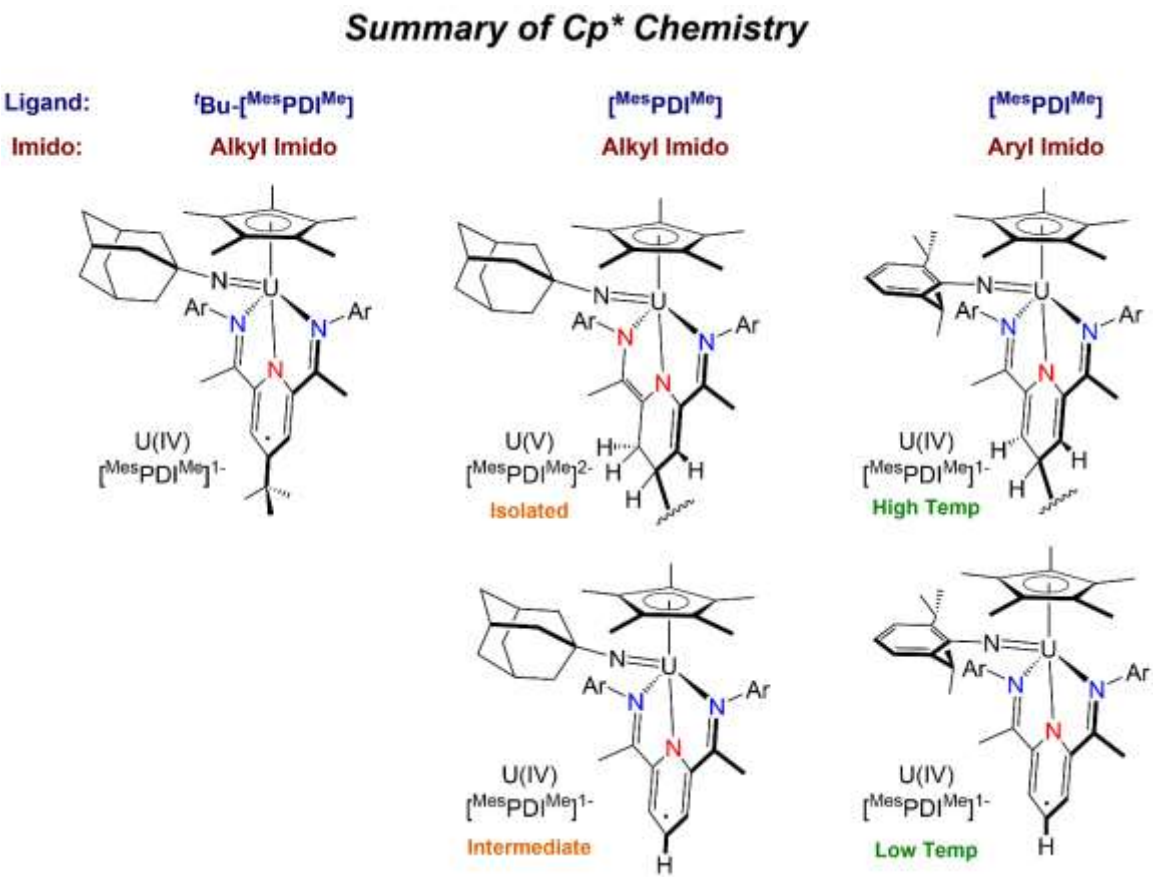

Figure 4.12. Summary of complexes in the Cp*-mono(imido) series.

For all of the monoimido species reported here, their U-N_{imido} distances range from 1.941(6) to 1.9926(17) Å. As compared to the related uranium bis(imido) compounds reported previously,[195] these distances are slightly elongated, due to the fact that the uranium(IV) ion has a larger ionic radius than uranium(V) or (VI) ions in those molecules. The more interesting comparison here is with ancillary ligand free uranium species with multiple imido groups. Neutral, hexavalent $U(NDIPP)_3(THF)_3$ displays U-N distances of 1.986(14), 2.000(16), and 2.010(15) Å,[201] which are in the range of those of **17-Cp***, **17-Cp^P**, **18**, and **17-^{t}Bu**, despite the fact that the ionic radius of U(VI) is approximately 0.2 Å smaller. Even more interesting is the fact that the distances for **17-Cp***, **17-Cp^P**, **18**, and **17-^{t}Bu** are *shorter* than those for the tetrahedral tetrakis(imido) uranate dianion, $[U(NDIPP)_4]^{2-}$, which has U–N bonds of 2.064(3) and 2.060(3) Å,[200] despite the small U(VI) ion. Elongation and activation of the U-N bonds in the latter species is established to result from competition of imido substituents for f-electron density due to the presence

of four substituents. Thus, characterization of the monoimido species, **17-Cp***, **17-Cp^{P}**, **18**, and **17-^{t}Bu**, supports that when only one imido substituent is present, shorter U-N_{imido} distances are observed compared to the tris- and tetrakis(imido) species.

4.4 Conclusions

Overall, this work highlights that bulky organoazides facilitate the isolation of elusive mono(imido) intermediates in the Cp/^{Mes}PDI^{Me} system. It is clear that slight variation in these compounds, derived through 1) choice of ancillary ligand, 2) electron donicity of the imido substituent, and 3) steric factors of the redox active ligand all create drastic changes in the resulting uranium mono(imido) complexes. Changing the Cp ligand, Cp^{P} vs. Cp*, has a profound effect on the electronics of the molecule, in particular whether the redox-active ^{Mes}PDI^{Me} participates in *para*-pyridine C-C coupling. The steric and electronic-donating considerations of the imido substituent help to build up charge on the ^{Mes}PDI^{Me} ligand. Further, use of the *tert*-butyl substituent in the *para*-pyridine position blocks undesirable side-reactivity (H-atom abstraction and dimerization). With the insights gained from this family of mono(imido) species, further studies are underway to evaluate the effects of ancillary ligands and imido electron donicity on bis- and tris(imido) systems.

APPENDIX

ADDITIONAL DATA

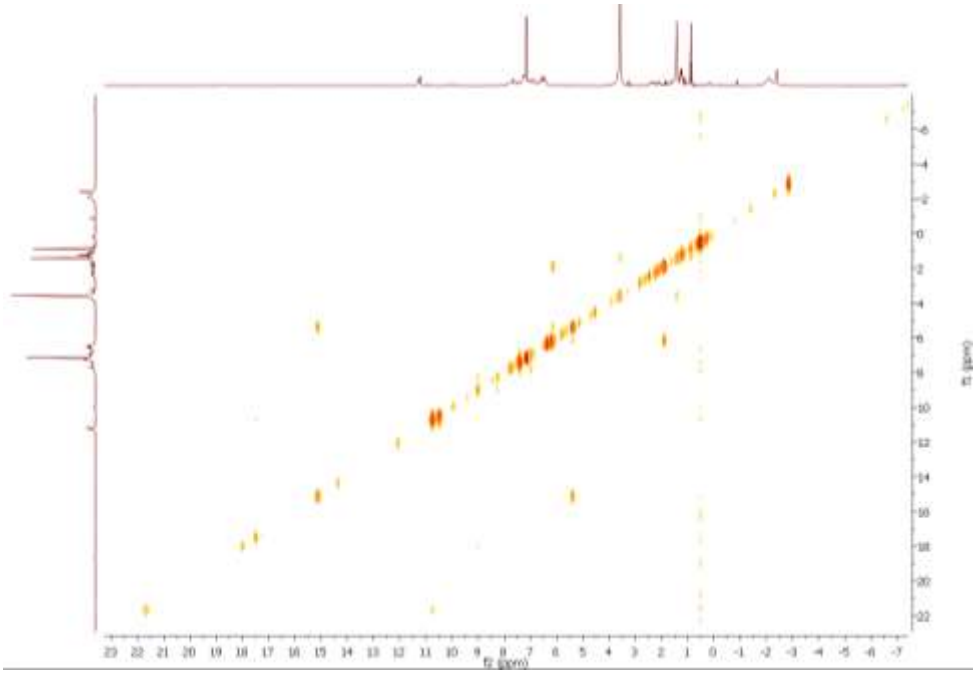

^{1}H correlation spectroscopy (COSY) spectrum (C_6D_6, 25 °C) of **4-Ph**.

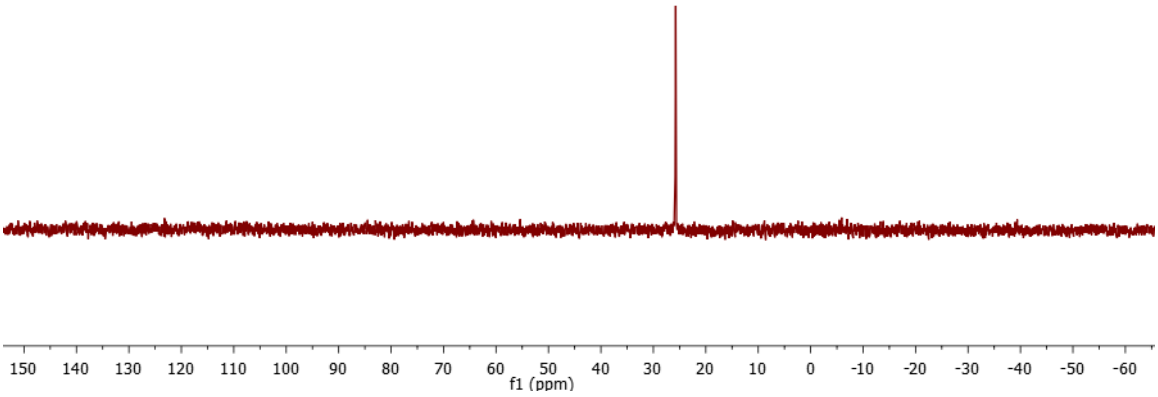

^{31}P NMR spectrum (C_6D_6, 25 °C) of $OPPh_3$.

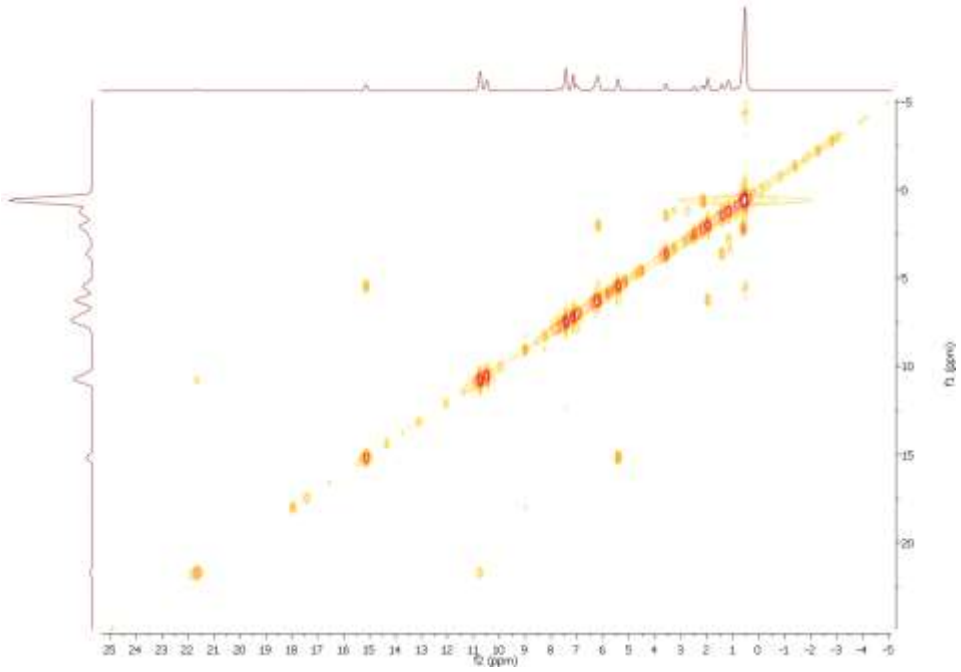

^{1}H correlation spectroscopy (COSY) spectrum (C_6D_6, 25 °C) of **4-^{i}Pr**.

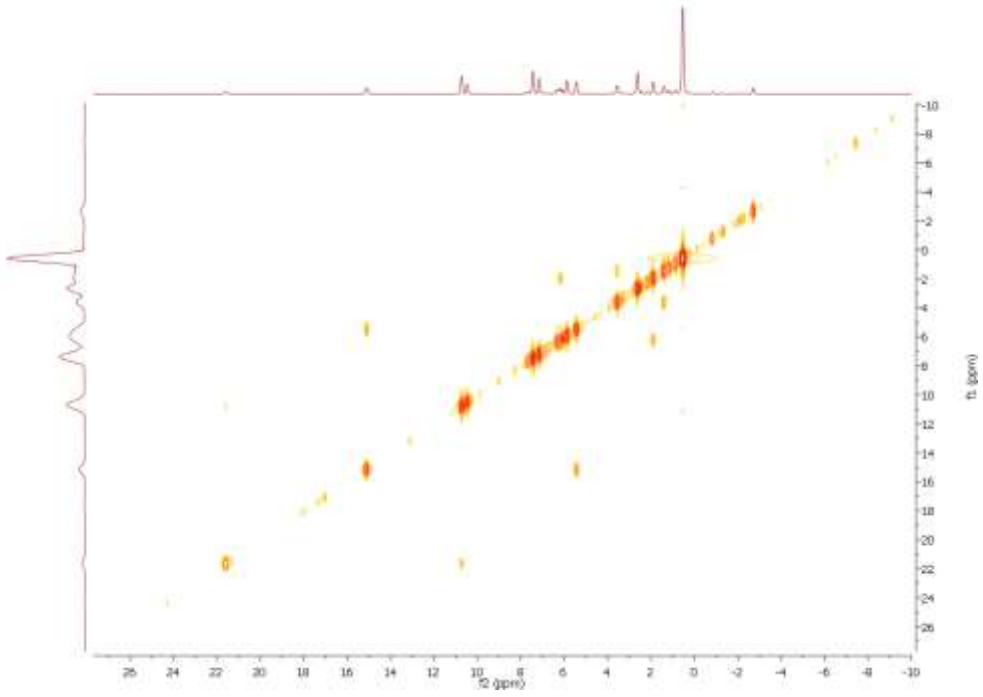

^{1}H correlation spectroscopy (COSY) spectrum (C_6D_6, 25 °C) of **4-OMe**.

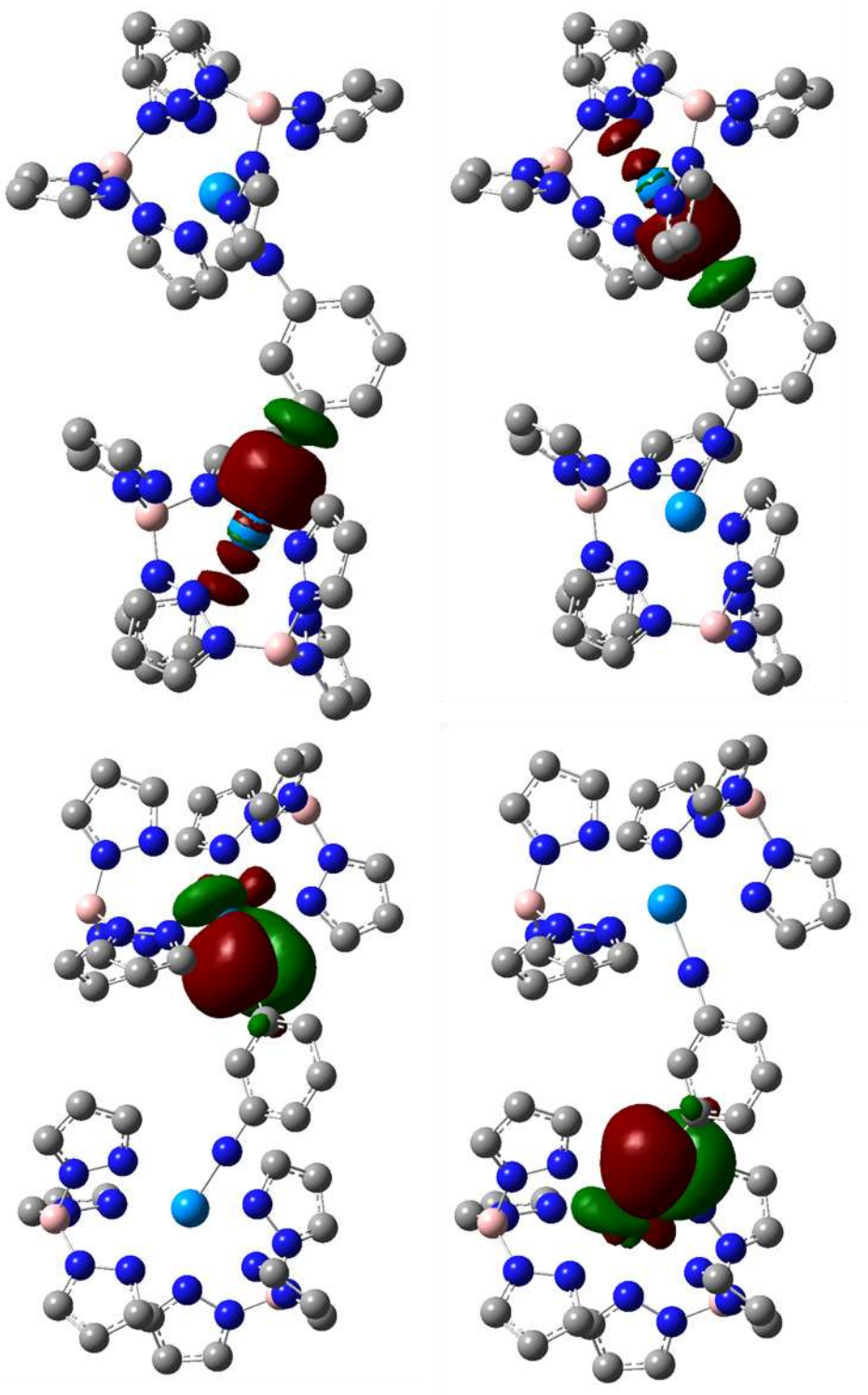

Sigma bonds (top left, HOMO-62 and top right, HOMO-63) and π-bonds (bottom left, HOMO-16 and bottom right, HOMO-17) that comprise the uranium-nitrogen triple bond in **15-*meta*** are shown.

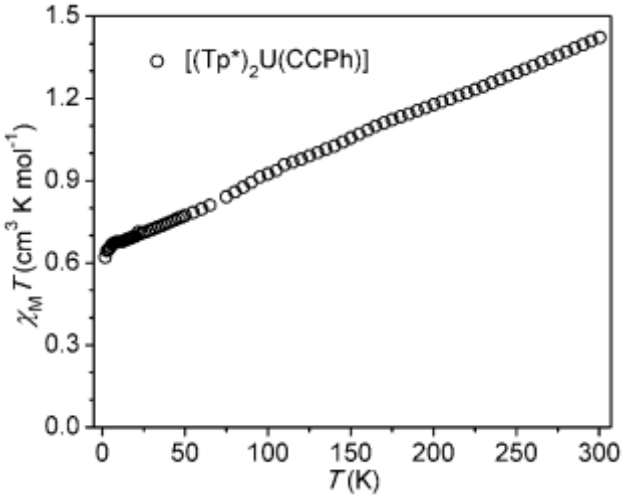

Temperature dependence of the magnetic susceptibility for Tp*$_2$UCCPh collected at 5000 Oe.

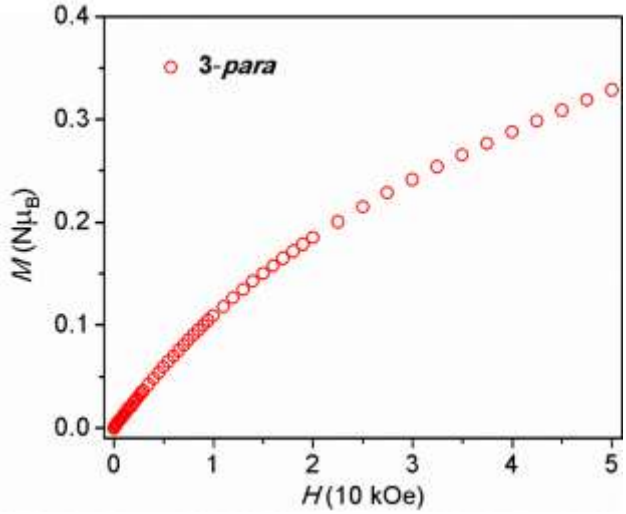

Field dependence of magnetization for **15**-***para*** collected at 1.8 K.

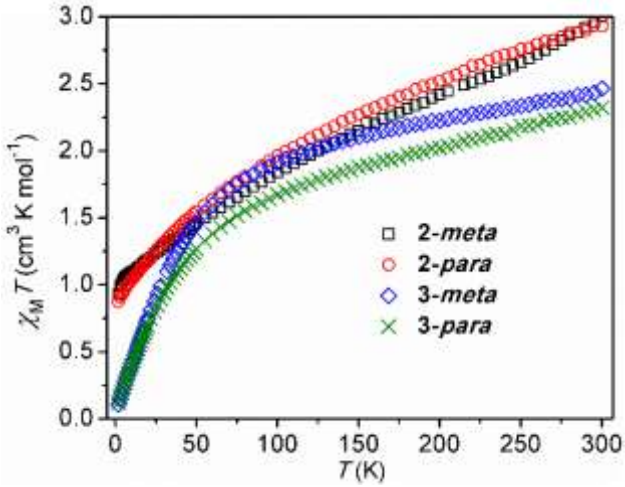

Temperature magnetic susceptibility data for the dinuclear complexes **14-*meta*** (black square)**/*para*** (red circle) and **15-*meta*** (blue diamond)**/*para*** (green x) collected at 1000 Oe except for **14-*meta***, where the data were collected at 5000 Oe.

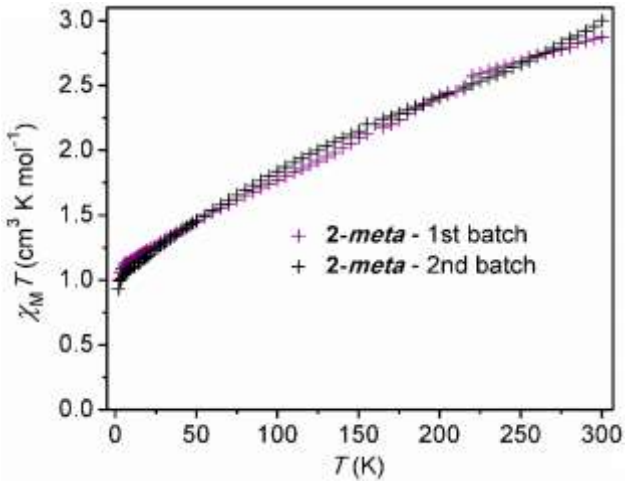

Temperature dependence of the magnetic susceptibility for two different batches of **14-*meta***, both collected at 5000 Oe.

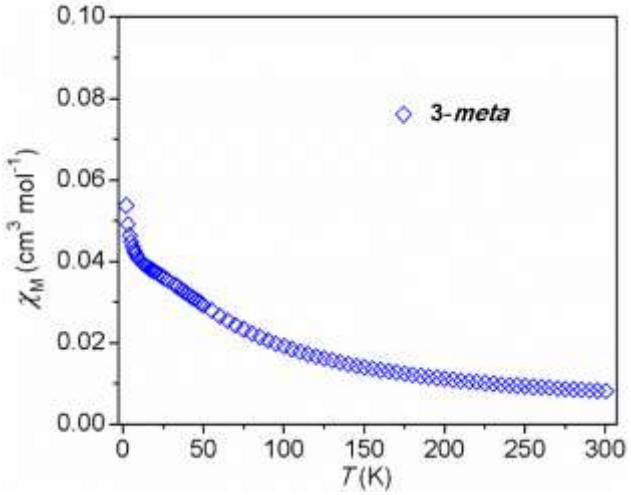

Temperature dependence of the magnetic susceptibility for **15-*meta***, both collected at 1000 Oe.

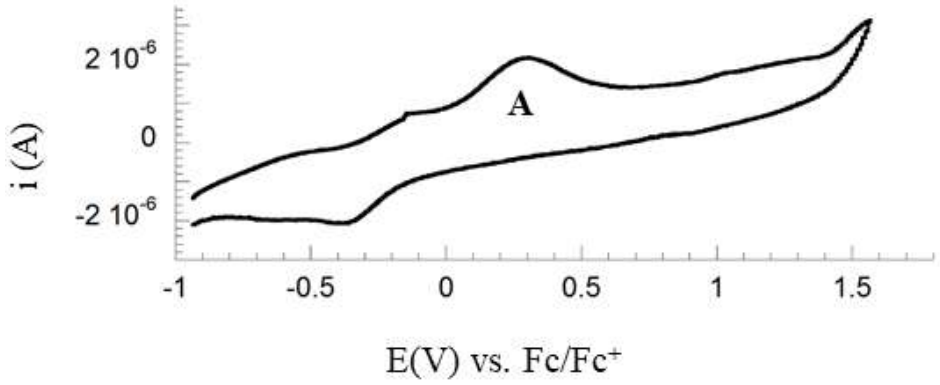

Cyclic voltammogram (CV) recorded for compound **2-Bn** in a 0.1 M THF solution of Bu_4NOTf at a scan rate of 0.10 Vs^{-1} referenced against Ag/Ag^+.

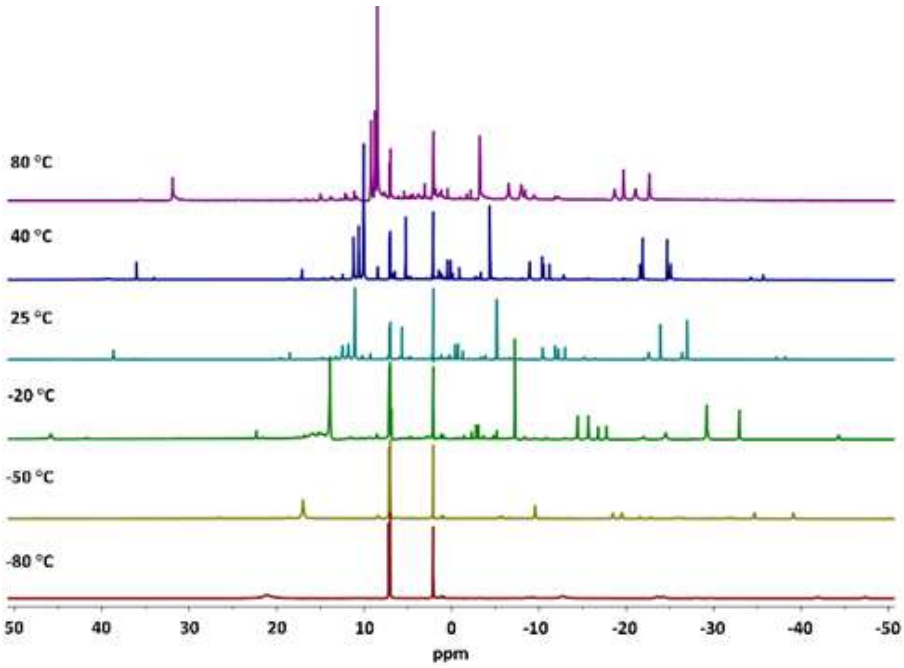

Variable temperature ^{1}H NMR spectrum (C_7D_8) of Cp*U(NDIPP)(^{Mes}PDI^{Me}) (**17-Cp***).

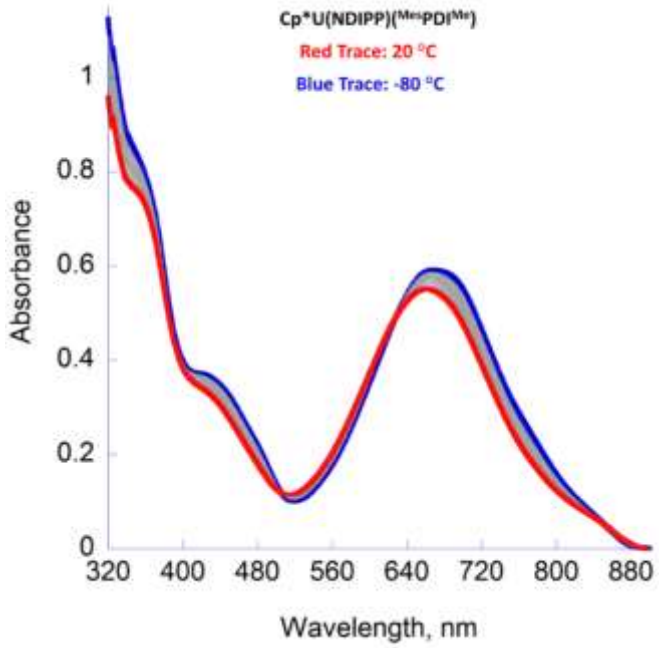

Variable temperature electronic absorption spectrum of **17-Cp*** recorded in tetrahydrofuran from 320-900 nm in the temperature range of -80 °C to 20 °C. The red trace represents 20 °C while the blue trace represents -80 °C. The intermittent grey lines represent 10 °C increments. Each scan was normalized to an absorbance of zero at 900 nm.

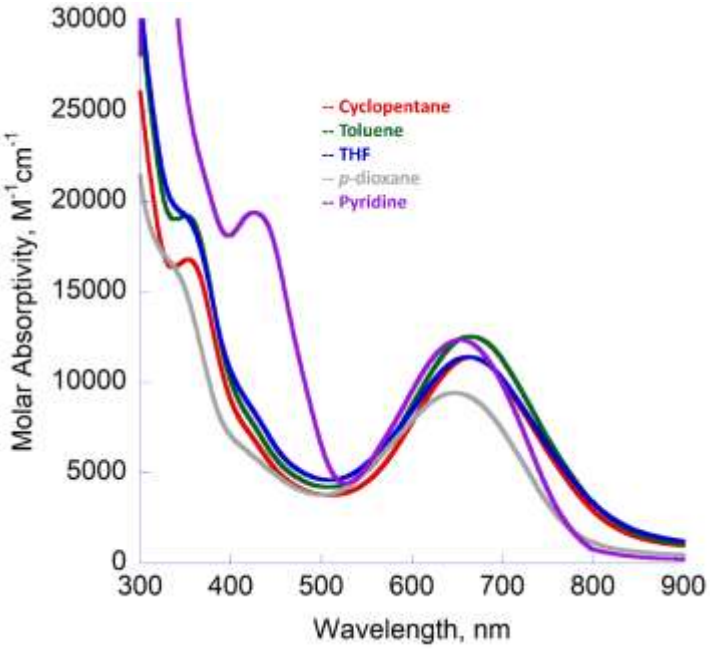

Electronic absorption spectra of **17-Cp*** in various solvents at ambient temperature.

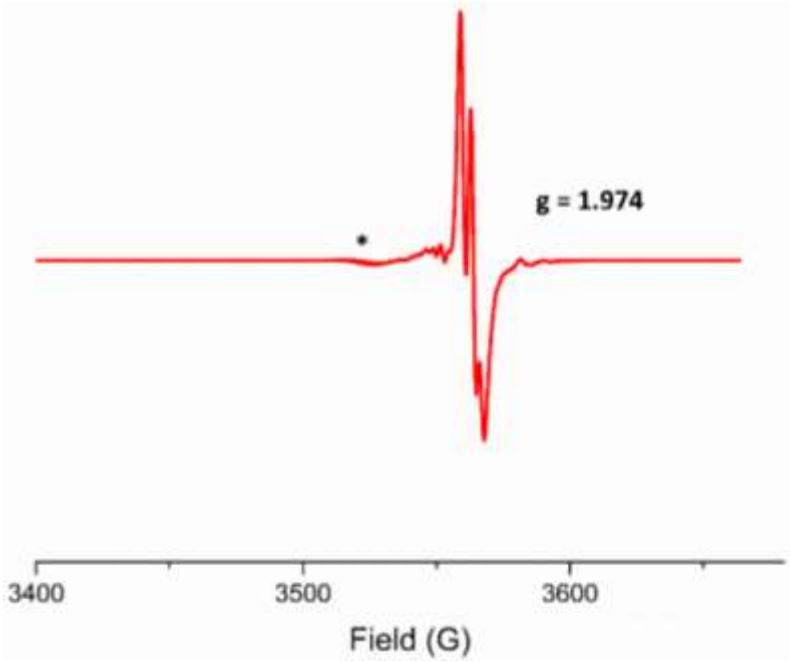

EPR spectrum of **17-Cp*** recorded in toluene (2.15 mM) at ambient temperature. Conditions: power = 1.00 mW; modulation = 0.15 mT/100 kHz. Asterisk (*) denotes a radical impurity not associated with the complex.

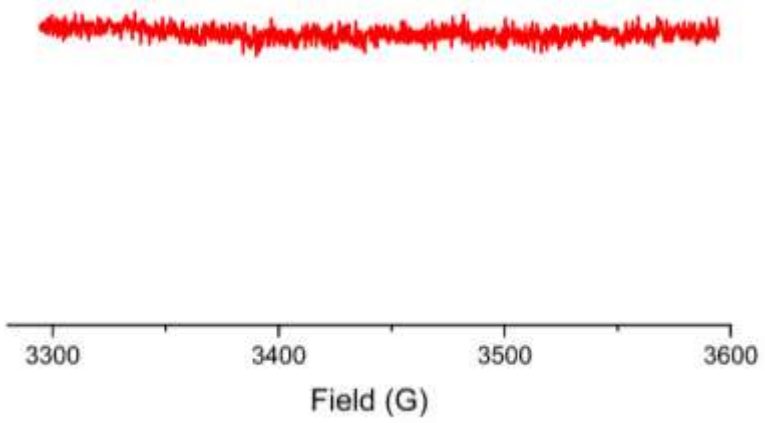

EPR spectrum of **17-Cp*** recorded in toluene (2.15 mM) at 10 K. Conditions: power = 1.00 mW; modulation = 0.15 mT/100 kHz.

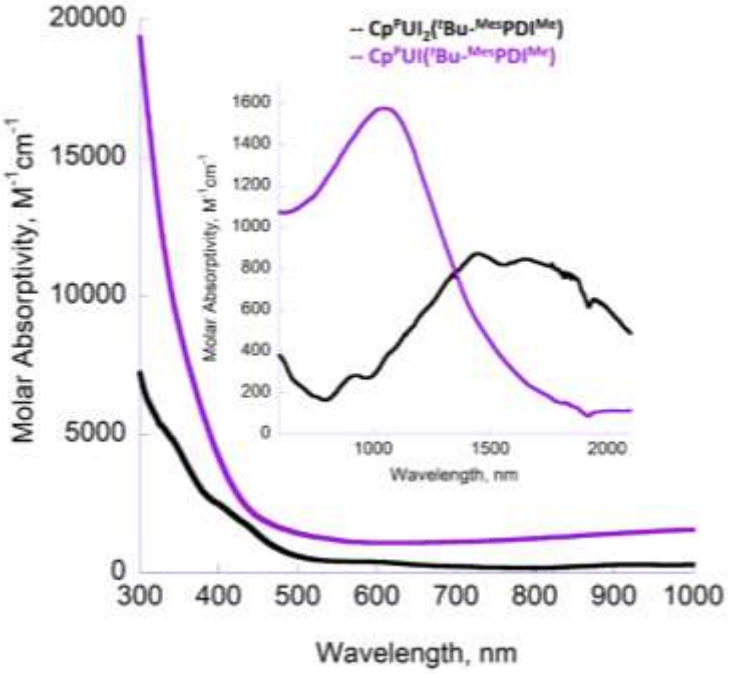

Electronic absorption spectra of $Cp^{P}UI_2(^{t}Bu\text{-}^{Mes}PDI^{Me})$ (**19-I$_2$**) (black) and $Cp^{P}UI(^{t}Bu\text{-}^{Mes}PDI^{Me})$ (**19-I**) (purple) recorded in THF at ambient temperature from 300-2100 nm. Solvent overtones from 1670-1760 nm have been omitted for improved clarity.

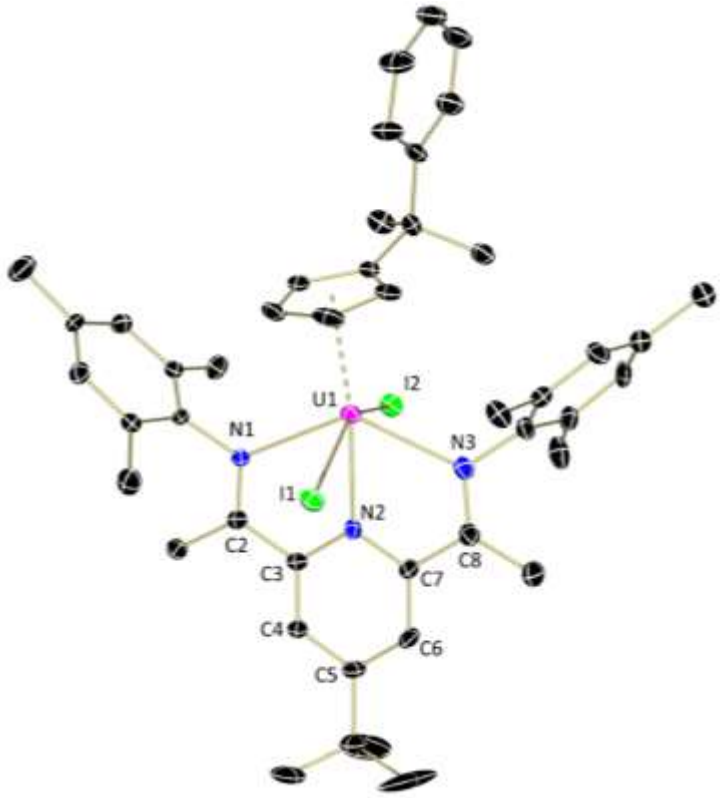

Molecular structure of $Cp^{P}UI_2(^{t}Bu\text{-}^{Mes}PDI^{Me})$ (**19-I_2**) displayed with 30% probability ellipsoids. Co-crystallized solvent molecules and hydrogen atoms have been omitted for clarity.

REFERENCES

1. Gilman, H., Some Personal Notes on More Than One-Half Century of Organometallic Chemistry. In *Adv in Organomet Chem*, Stone, F. G. A.; West, R., Eds. Academic Press1969; Vol. 7, pp 1-52.

2. Gilman, H.; Jones, R. G.; Bindschadler, E.; Blume, D.; Karmas, G.; Martin, G. A.; Nobis, J. F.; Thirtle, J. R.; Yale, H. L.; Yoeman, F. A., Organic Compounds of Uranium. I. 1,3-Dicarbonyl Chelates. *J Am Chem Soc* **1956,** *78*, 2790-2792.

3. Kiplinger, J. L.; Morris, D. E.; Scott, B. L.; Burns, C. J., Convenient Synthesis, Structure, and Reactivity of $(C_5Me_5)U(CH_2C_6H_5)_3$: A Simple Strategy for the Preparation of Monopentamethylcyclopentadienyl Uranium(IV) Complexes. *Organometallics* **2002,** *21*, 5978-5982.

4. Marks, T. J.; Seyam, A. M., Stable uranium(IV) alkyl and aryl complexes. *J Am Chem Soc* **1972,** *94*, 6545-6546.

5. Fortier, S.; Melot, B. C.; Wu, G.; Hayton, T. W., Homoleptic Uranium(IV) Alkyl Complexes: Synthesis and Characterization. *J Am Chem Soc* **2009,** *131*, 15512-15521.

6. Andreychuk, N. R.; Ilango, S.; Vidjayacoumar, B.; Emslie, D. J. H.; Jenkins, H. A., Uranium(IV) Alkyl Complexes of a Rigid Dianionic NON-Donor Ligand: Synthesis and Quantitative Alkyl Exchange Reactions with Alkyllithium Reagents. *Organometallics* **2013,** *32*, 1466-1474.

7. Duhović, S.; Monreal, M. J.; Diaconescu, P. L., Reactions of Aromatic Heterocycles with Uranium Alkyl Complexes. *Inorg Chem* **2010,** *49*, 7165-7169.

8. Johnson, S. A.; Bart, S. C., Achievements in uranium alkyl chemistry: celebrating sixty years of synthetic pursuits. *Dalton Trans* **2015,** *44*, 7710-7726.

9. Jones, M. B.; Gaunt, A. J., Recent Developments in Synthesis and Structural Chemistry of Nonaqueous Actinide Complexes. *Chemical Reviews* **2013,** *113*, 1137-1198.

10. Liddle, S. T., The Renaissance of Non-Aqueous Uranium Chemistry. *Angew Chem Int Ed Engl* **2015,** *54*, 8604-41.

11. Schelter, E. J.; Wu, R.; Scott, B. L.; Thompson, J. D.; Morris, D. E.; Kiplinger, J. L., Mixed valency in a uranium multimetallic complex. *Angew Chem* **2008,** *47*, 2993-6.

12. Lam, O. P.; Anthon, C.; Heinemann, F. W.; O'Connor, J. M.; Meyer, K., Structural and Spectroscopic Characterization of a Charge-Separated Uranium Benzophenone Ketyl Radical Complex. *Journal of the American Chemical Society* **2008,** *130*, 6567-6576.

13. Kraft, S. J.; Fanwick, P. E.; Bart, S. C., Synthesis and characterization of a uranium(III) complex containing a redox-active 2,2'-bipyridine ligand. *Inorg Chem* **2010,** *49*, 1103-1110.

14. Kiernicki, J. J.; Newell, B. S.; Matson, E. M.; Anderson, N. H.; Fanwick, P. E.; Shores, M. P.; Bart, S. C., Multielectron C-O bond activation mediated by a family of reduced uranium complexes. *Inorg Chem* **2014,** *53*, 3730-3741.

15. Mullane, K. C.; Cheisson, T.; Nakamaru-Ogiso, E.; Manor, B. C.; Carroll, P. J.; Schelter, E. J., Reduction of Carbonyl Groups by Uranium(III) and Formation of a Stable Amide Radical Anion. *Chem Eur J* **2018,** *24*, 826-837.

16. Matson, E. M.; Fanwick, P. E.; Bart, S. C., Formation of Trivalent U–C, U–N, and U–S Bonds and Their Reactivity toward Carbon Dioxide and Acetone. *Organometallics* **2011,** *30*, 5753-5762.

17. Matson, E. M.; Forrest, W. P.; Fanwick, P. E.; Bart, S. C., Synthesis and Reactivity of Trivalent Tp*U($CH_2Ph)_2$(THF): Insertion vs Oxidation at Low-Valent Uranium–Carbon Bonds. *Organometallics* **2013,** *32*, 1484-1492.

18. Matson, E. M.; Kiernicki, J. J.; Fanwick, P. E.; Bart, S. C., Expanding the Family of Uranium(III) Alkyls: Synthesis and Characterization of Mixed-Ligand Derivatives. *Eur J Inorg Chem* **2016,** *2016*, 2527-2533.

19. Johnson, S. A.; Kiernicki, J. J.; Fanwick, P. E.; Bart, S. C., New Benzylpotassium Reagents and Their Utility for the Synthesis of Homoleptic Uranium(IV) Benzyl Derivatives. *Organometallics* **2015,** *34*, 2889-2895.

20. Kraft, S. J.; Fanwick, P. E.; Bart, S. C., Carbon-carbon reductive elimination from homoleptic uranium(IV) alkyls induced by redox-active ligands. *J Am Chem Soc* **2012,** *134*, 6160-6168.

21. Van der Sluys, W. G.; Burns, C. J.; Sattelberger, A. P., First example of a neutral homoleptic uranium alkyl. Synthesis, properties, and structure of U[$CH(SiMe_3)_2]_3$. *Organometallics* **1989,** *8*, 855-857.

22. Fagan, P. J.; Manriquez, J. M.; Maatta, E. A.; Seyam, A. M.; Marks, T. J., Synthesis and properties of bis(pentamethylcyclopentadienyl) actinide hydrocarbyls and hydrides. A new class of highly reactive f-element organometallic compounds. *J Am Chem Soc* **1981,** *103*, 6650-6667.

23. Marks, T. J.; Seyam, A. M.; Kolb, J. R., Synthesis, chemistry, and spectroscopy of some tris(pentahapto-cyclopentadienyl)uranium(IV) alkyl and aryl compounds. *J Am Chem Soc* **1973,** *95*, 5529-5539.

24. Matson, E. M.; Forrest, W. P.; Fanwick, P. E.; Bart, S. C., Functionalization of carbon dioxide and carbon disulfide using a stable uranium(III) alkyl complex. *J Am Chem Soc* **2011,** *133*, 4948-4954.

25. Kraft, S. J.; Fanwick, P. E.; Bart, S. C., Exploring the Insertion Chemistry of Tetrabenzyluranium Using Carbonyls and Organoazides. *Organometallics* **2013,** *32*, 3279-3285.

26. Li Manni, G.; Walensky, J. R.; Kraft, S. J.; Forrest, W. P.; Perez, L. M.; Hall, M. B.; Gagliardi, L.; Bart, S. C., Computational insights into uranium complexes supported by redox-active alpha-diimine ligands. *Inorg Chem* **2012,** *51*, 2058-2064.

27. Matson, E. M.; Kiernicki, J. J.; Anderson, N. H.; Fanwick, P. E.; Bart, S. C., Isolation of a uranium(III) benzophenone ketyl radical that displays redox-active ligand behaviour. *Dalton Trans* **2014,** *43*, 17885-17888.

28. Pangborn, A. B.; Giardello, M. A.; Grubbs, R. H.; Rosen, R. K.; Timmers, F. J., Safe and Convenient Procedure for Solvent Purification. *Organometallics* **1996,** *15*, 1518-1520.

29. Busacca, C. A.; Raju, R.; Grinberg, N.; Haddad, N.; James-Jones, P.; Lee, H.; Lorenz, J. C.; Saha, A.; Senanayake, C. H., Reduction of Tertiary Phosphine Oxides with DIBAL-H. *J Org Chem* **2008,** *73*, 1524-1531.

30. Monreal, M. J.; Thomson, R. K.; Cantat, T.; Travia, N. E.; Scott, B. L.; Kiplinger, J. L., $UI_4(1,4\text{-dioxane})_2$, $[UCl_4(1,4\text{-dioxane})]_2$, and $UI_3(1,4\text{-dioxane})_{1.5}$: Stable and Versatile Starting Materials for Low- and High-Valent Uranium Chemistry. *Organometallics* **2011,** *30*, 2031-2038.

31. Sun, Y.; McDonald, R.; Takats, J.; Day, V. W.; Eberspacher, T. A., Synthesis and Structure of Bis[hydrotris(3,5-dimethylpyrazolyl)borato]iodouranium(III), $U[HB(3,5\text{-}Me_2pz)_3]_2I$: Unprecedented Side-On Interaction Involving a Hydrotris(pyrazolyl)borate Ligand. *Inorg Chem* **1994,** *33*, 4433-4434.

32. Sheldrick, G. M., Crystal structure refinement with SHELXL. *Acta Crystallogr C Struct Chem* **2015,** *71*, 3-8.

33. Tatebe, C. J.; Zeller, M.; Bart, S. C., [2pi+2pi] Cycloaddition of Isocyanates to Uranium(IV) Imido Complexes for the Synthesis of U(IV) kappa^2-Ureato Compounds. *Inorg Chem* **2017,** *56*, 1956-1965.

34. Matson, E. M.; Forrest, W. P.; Fanwick, P. E.; Bart, S. C., Use of Alkylsodium Reagents for the Synthesis of Trivalent Uranium Alkyl Complexes. *Organometallics* **2012,** *31*, 4467-4473.

35. Johnson, S. A.; Tatebe, C. J.; Gonzalez, S.; Zeller, M.; Bart, S. C., Synthesis and characterization of hydrotris(3-phenylpyrazolyl)borate ligands on low-valent uranium. *Polyhedron* **2017,** *125*, 107-112.

36. Matson, E. M.; Goshert, M. D.; Kiernicki, J. J.; Newell, B. S.; Fanwick, P. E.; Shores, M. P.; Walensky, J. R.; Bart, S. C., Synthesis of terminal uranium(IV) disulfido and diselenido compounds by activation of elemental sulfur and selenium. *Chem Eur J* **2013,** *19*, 16176-16180.

37. Berthet, J.-C.; Lance, M.; Nierlich, M.; Vigner, J.; Ephritikhine, M., Tricyclopentadienyluranium azide complexes. *Journal of Organomet Chem* **1991,** *420*, C9-C11.

38. Li, W.; Gao, G.; Gao, Y.; Yang, C.; Xia, W., Direct oxidation of the $C(sp^2)$–$C(sp^3)$ bond from benzyltrimethylsilanes to phenols. *Chem Commun* **2017,** *53*, 5291-5293.

39. Raviola, C.; Ravelli, D.; Protti, S.; Fagnoni, M., Methoxy-Substituted α,n-Didehydrotoluenes. Photochemical Generation and Polar vs Diradical Reactivity. *J Am Chem Soc* **2014,** *136*, 13874-13881.

40. Scholl, R. L.; Maciel, G. E.; Musker, W. K., Silicon-29 chemical shifts of organosilicon compounds. *J Am Chem Soc* **1972,** *94*, 6376-6385.

41. Clark, C. L.; Lockhart, J. J.; Fanwick, P. E.; Bart, S. C., Synthesis of low-valent uranium fluorides by C-F bond activation. *Chem Commun* **2015,** *51*, 14084-14087.

42. Kraft, S. J.; Walensky, J.; Fanwick, P. E.; Hall, M. B.; Bart, S. C., Crystallographic evidence of a base-free uranium(IV) terminal oxo species. *Inorg Chem* **2010,** *49*, 7620-7622.

43. Wildman, E. P.; Ostrowski, J. P. A.; King, D. M.; Lewis, W.; Liddle, S. T., Uranium–halide and –azide derivatives of the sterically demanding triamidoamine ligand TrenTPS [TrenTPS={N(CH2CH2NSiPh3)3}3−]. *Polyhedron* **2017,** *125*, 2-8.

44. Evans, W. J.; Montalvo, E.; Ziller, J. W.; DiPasquale, A. G.; Rheingold, A. L., Uranium Metallocene Complexes of the 1,3,4,6,7,8-Hexahydro-2*H*-pyrimido[1,2-*a*]pyrimidinato Ligand, $(hpp)^-$. *Inorg Chem* **2010,** *49*, 222-228.

45. Castro-Rodriguez, I.; Nakai, H.; Zakharov, L. N.; Rheingold, A. L.; Meyer, K., A Linear, O-Coordinated η^1CO_2 Bound to Uranium. *Science* **2004,** *305*, 1757.

46. Castro-Rodriguez, I.; Olsen, K.; Gantzel, P.; Meyer, K., Uranium Tris-aryloxide Derivatives Supported by Triazacyclononane: Engendering a Reactive Uranium(III) Center with a Single Pocket for Reactivity. *J Am Chem Soc* **2003,** *125*, 4565-4571.

47. Lam, O. P.; Franke, S. M.; Nakai, H.; Heinemann, F. W.; Hieringer, W.; Meyer, K., Observation of the Inverse Trans Influence (ITI) in a Uranium(V) Imide Coordination Complex: An Experimental Study and Theoretical Evaluation. *Inorg Chem* **2012,** *51*, 6190-6199.

48. Zi, G.; Jia, L.; Werkema, E. L.; Walter, M. D.; Gottfriedsen, J. P.; Andersen, R. A., Preparation and Reactions of Base-Free Bis(1,2,4-tri-tert-butylcyclopentadienyl)uranium Oxide, Cp'_2UO. *Organometallics* **2005,** *24*, 4251-4264.

49. Thomson, R. K.; Cantat, T.; Scott, B. L.; Morris, D. E.; Batista, E. R.; Kiplinger, J. L., Uranium azide photolysis results in C–H bond activation and provides evidence for a terminal uranium nitride. *Nature Chemistry* **2010,** *2*, 723.

50. Thomson, R. K.; Graves, C. R.; Scott, B. L.; Kiplinger, J. L., Noble Reactions for the Actinides: Safe Gold-Based Access to Organouranium and Azido Complexes. *European Journal of Inorganic Chemistry* **2009,** *2009*, 1451-1455.

51. Thomson, R. K.; Scott, B. L.; Morris, D. E.; Kiplinger, J. L., Synthesis, structure, spectroscopy and redox energetics of a series of uranium(IV) mixed-ligand metallocene complexes. *Comptes Rendus Chimie* **2010,** *13*, 790-802.

52. King, D. M.; Tuna, F.; McInnes, E. J. L.; McMaster, J.; Lewis, W.; Blake, A. J.; Liddle, S. T., Isolation and characterization of a uranium(VI)–nitride triple bond. *Nat Chem* **2013,** *5*, 482.

53. Dame, A. N.; Bharara, M. S.; Barnes, C. L.; Walensky, J. R., Synthesis of Thorium(IV) and Uranium(IV) Salicylaldiminate Pseudo-Halide Complexes. *Eur J Inorg Chem* **2015,** *2015*, 2996-3005.

54. Maria, L.; Santos, I. C.; Sousa, V. R.; Marçalo, J., Uranium(III) Redox Chemistry Assisted by a Hemilabile Bis(phenolate) Cyclam Ligand: Uranium–Nitrogen Multiple Bond Formation Comprising a trans-$\{RN{=}U(VI){=}NR\}^{2+}$ Complex. *Inorganic Chemistry* **2015,** *54*, 9115-9126.

55. Crawford, M.-J.; Ellern, A.; Mayer, P., UN_{21}^{3-}: A Structurally Characterized Binary Actinide Heptaazide Anion. *Angew Chem* **2005,** *44*, 7874-7878.

56. Nocton, G.; Pécaut, J.; Mazzanti, M., A Nitrido-Centered Uranium Azido Cluster Obtained from a Uranium Azide. *Angew Chem* **2008,** *47*, 3040-3042.

57. Fortier, S.; Wu, G.; Hayton, T. W., U(IV) and U(V) azide complexes supported by amide or aryloxide ligands. *Dalton Trans* **2010,** *39*, 352-354.

58. Stobbe, B. C.; Powell, D. R.; Thomson, R. K., Schiff base thorium(IV) and uranium(IV) chloro complexes: synthesis, substitution and oxidation chemistry. *Dalton Transactions* **2017,** *46*, 4888-4892.

59. Haiges, R.; Vasiliu, M.; Dixon, D. A.; Christe, K. O., The Uranium(VI) Oxoazides $[UO_2(N_3)_2{\cdot}CH_3CN]$, $[(bipy)_2(UO_2)_2(N_3)_4]$, $[(bipy)UO_2(N_3)_3]^-$, $[UO_2(N_3)_4]^{2-}$, and $[(UO_2)_2(N_3)_8]^{4-}$. *Chem Eur J* **2017,** *23*, 652-664.

60. Sherif, F. G.; Awad, A. M., The structure of uranyl azide—its instability constant in aqueous solutions. *Journal of Inorganic and Nuclear Chemistry* **1961,** *19*, 94-100.

61. Tamasi, A. L.; Rungthanapathsophon, P.; Dame, A. N.; Moody, M. A.; Barnes, C. L.; Wilkerson, M. P.; Walensky, J. R., Pseudo-halide uranyl salicylaldiminate complexes including the isolation of a rare uranyl azide. *Journal of Coordination Chemistry* **2016,** *69*, 1904-1913.

62. Castro-Rodriguez, I.; Meyer, K., Carbon Dioxide Reduction and Carbon Monoxide Activation Employing a Reactive Uranium(III) Complex. *J Am Chem Soc* **2005,** *127*, 11242-11243.

63. Guzei, I. A.; Wendt, M., An improved method for the computation of ligand steric effects based on solid angles. *Dalton Trans* **2006**, 3991-9.

64. Antunes, M. A.; Domingos, Â.; Santos, I. C. d.; Marques, N.; Takats, J., Synthesis and characterization of uranium(III) compounds supported by the hydrotris(3,5-dimethyl-pyrazolyl)borate ligand: Crystal structures of [U(TpMe$_2$)$_2$(X)] complexes (X=OC$_6$H$_2$-2,4,6-Me$_3$, dmpz, Cl). *Polyhedron* **2005,** *24*, 3038-3045.

65. Antunes, M. A.; Santos, I. C.; Bolvin, H.; Pereira, L. C. J.; Mazzanti, M.; Marçalo, J.; Almeida, M., Crystal structure diversity in the bis[hydrotris(3,5-dimethylpyrazolyl)borate]iodouranium(III) complex: from neutral to cationic forms. *Dalton Transactions* **2013,** *42*, 8861-8867.

66. Antunes, M. A.; Ferrence, G. M.; Domingos, Â.; McDonald, R.; Burns, C. J.; Takats, J.; Marques, N., Uranium (III) Scorpionates: Synthesis and Structure of [(TpMe$_2$)$_2$U{N(C$_6$H$_5$)$_2$}] and [(TpMe$_2$)$_2$U{N(SiMe$_3$)$_2$}]. *Inorg Chem* **2004,** *43*, 6640-6643.

67. Maier, R.; Müller, J.; Kanellakopulos, B.; Apostolidis, C.; Domingos, A.; Marques, N.; De Matos, A. P., Molecular structure and charge distribution in compounds of the 5f-elements—VI. 1:1 adducts of uranium(IV)-hydrotris(3,5-dimethylpyrazol-1-yl)borate-trichloride with Lewis bases. *Polyhedron* **1993,** *12*, 2801-2808.

68. Brennan, J. G.; Andersen, R. A.; Zalkin, A., Chemistry of trivalent uranium metallocenes: electron-transfer reactions. Synthesis and characterization of [(MeC$_5$H$_4$)3U]$_2$E (E = S, Se, Te) and the crystal structures of hexakis(methylcyclopentadienyl)sulfidodiuranium and tris(methylcyclopentadienyl)(triphenylphosphine oxide)uranium. *Inorg Chem* **1986,** *25*, 1761-1765.

69. Mansell, S. M.; Kaltsoyannis, N.; Arnold, P. L., Small Molecule Activation by Uranium Tris(aryloxides): Experimental and Computational Studies of Binding of N$_2$, Coupling of CO, and Deoxygenation Insertion of CO$_2$ under Ambient Conditions. *J Am Chem Soc* **2011,** *133*, 9036-9051.

70. Hoerger, C. J.; La Pierre, H. S.; Maron, L.; Scheurer, A.; Heinemann, F. W.; Meyer, K., Reductive disproportionation of nitric oxide mediated by low-valent uranium. *Chemical Communications* **2016,** *52*, 10854-10857.

71. Evans, W. J.; Traina, C. A.; Ziller, J. W., Synthesis of Heteroleptic Uranium (μ–η^6:η^6-$C_6H_6)^{2-}$ Sandwich Complexes via Facile Displacement of (η^5-$C_5Me_5)^{1-}$ by Ligands of Lower Hapticity and Their Conversion to Heteroleptic Bis(imido) Compounds. *J Am Chem Soc* **2009,** *131*, 17473-17481.

72. Maria, L.; Domingos, Â.; Galvão, A.; Ascenso, J.; Santos, I., The Role of Neutral Coligands on the Stabilization of Mono-TpiPr2 U(III) Complexes. *Inorg Chem* **2004,** *43*, 6426-6434.

73. Maria, L.; Paula Campello, M.; Domingos, A.; Santos, I.; Andersen, R., Synthesis and structure of uranium(III) complexes with dihydrobis(pyrazolyl)borates. *Dalton Transactions* **1999**, 2015-2020.

74. Gorobets, E.; Parvez, M.; Keay, B. A., Unprecedented Intramolecular Nucleophilic Aromatic Additions of Allyloxy Anions to Diphenylphosphinoyl-Substituted Benzene Rings: A Facile Method for Preparing Multisubstituted Benzopyrans. *Synlett* **2008,** *2008*, 129-133.

75. Matson, E. M.; Breshears, A. T.; Kiernicki, J. J.; Newell, B. S.; Fanwick, P. E.; Shores, M. P.; Walensky, J. R.; Bart, S. C., Trivalent uranium phenylchalcogenide complexes: exploring the bonding and reactivity with CS2 in the Tp*2UEPh series (E = O, S, Se, Te). *Inorg Chem* **2014,** *53*, 12977-85.

76. Kepp, K. P., A Quantitative Scale of Oxophilicity and Thiophilicity. *Inorg Chem* **2016,** *55*, 9461-9470.

77. Fox, A. R.; Bart, S. C.; Meyer, K.; Cummins, C. C., Towards uranium catalysts. *Nature* **2008,** *455*, 341-9.

78. La Pierre, H. S.; Meyer, K., Activation of Small Molecules by Molecular Uranium Complexes. In *Progress in Inorganic Chemistry*, Karlin, K. D., Ed. John Wiley & Sons2014; Vol. 58, pp 303-415.

79. Hayton, T. W., Metal-ligand multiple bonding in uranium: structure and reactivity. *Dalton Trans* **2010,** *39*, 1145-58.

80. Hayton, T. W., Recent developments in actinide-ligand multiple bonding. *Chem Commun* **2013,** *49*, 2956-73.

81. Duncan, A. P.; Bergman, R. G., Selective transformations of organic compounds by imidozirconocene complexes. *The Chemical Record* **2002,** *2*, 431-445.

82. Chirik, P. J., Dinitrogen functionalization with bis(cyclopentadienyl) complexes of zirconium and hafnium. *Dalton Trans* **2007**, 16-25.

83. Bazan, G. C.; Oskam, J. H.; Cho, H. N.; Park, L. Y.; Schrock, R. R., Living ring-opening metathesis polymerization of 2,3-difunctionalized 7-oxanorbornenes and 7-oxanorbornadienes by $Mo(CHCMe_2R)(NC_6H_3\text{-iso-}Pr_2\text{-}2,6)(O\text{-tert-}Bu)_2$ and $Mo(CHCMe_2R)(NC_6H_3\text{-iso-}Pr_2\text{-}2,6)(OCMe_2CF_3)_2$. *J Am Chem Soc* **1991,** *113*, 6899-6907.

84. Jin, J.; Mariott, W. R.; Chen, E. Y.-X., Polymerization of methyl methacrylate by metallocene imido complexes and tris(pentafluorophenyl)alane. *Journal of Polymer Science Part A: Polymer Chemistry* **2003,** *41*, 3132-3142.

85. Leung, W.-H., Synthesis and Reactivity of Organoimido Complexes of Chromium. *Eur J Inorg Chem* **2003,** *2003*, 583-593.

86. Akagi, F.; Suzuki, S.; Ishida, Y.; Hatanaka, T.; Matsuo, T.; Kawaguchi, H., Reactions of a Niobium Nitride Complex Prepared from Dinitrogen: Synthesis of Imide and Ureate Complexes and Ammonia Formation. *Eur J Inorg Chem* **2013,** *2013*, 3930-3936.

87. Bryan, J. C.; Burrell, A. K.; Miller, M. M.; Smith, W. H.; Burns, C. J.; Sattelberger, A. P., Synthesis and reactivity of technetium(VII) imido complexes. *Polyhedron* **1993,** *12*, 1769-1777.

88. Singh, A. K.; Levine, B. G.; Staples, R. J.; Odom, A. L., A 4-coordinate Ru(II) imido: unusual geometry, synthesis, and reactivity. *Chem Commun* **2013,** *49*, 10799-10801.

89. Dubberley, S. R.; Friedrich, A.; Willman, D. A.; Mountford, P.; Radius, U., Synthesis and Reactivity of Calix[4]arene-Supported Group 4 Imido Complexes. *Chem Eur J* **2003,** *9*, 3634-3654.

90. Darwish, W.; Seikel, E.; Käsmarker, R.; Harms, K.; Sundermeyer, J., Synthesis and X-ray crystal structures of imido and ureato derivatives of titanium(IV) phthalocyanine and their application in the catalytic formation of carbodiimides by metathesis from isocyanates. *Dalton Trans* **2011,** *40*, 1787-1794.

91. Edwards, A.; Hogarth, G.; Hollingsworth, N.; Oller, J. J., Illusive tungsten-imido-dithiocarbamate complexes: Facile carbon–nitrogen bond formation. *Inorg Chem Comm* **2011,** *14*, 1932-1936.

92. Blake, A. J.; Mountford, P.; Nikonov, G. I.; Swallow, D., Cycloaddition reactions of tetraaza macrocycle supported group 4 imido complexes and reversible addition of aryl isocyanate to a coordinated ureate ligand. *Chem Commun* **1996**, 1835-1836.

93. Casey, C. P.; Widenhoefer, R. A.; Hayashi, R. K., Reactions of $Cp^*_3Co_3(\mu_3\text{-}H)(\mu_2\text{-}H)_3$ with Carbon Dioxide, Carbon Disulfide, and Phenyl Isocyanate. *Inorg Chem* **1995,** *34*, 1138-1144.

94. Forster, G. D.; Hogarth, G., Reversible insertion of an isocyanate into an imido moiety at a dimolybdenum centre. Synthesis and X-ray crystal structure of $[Mo_2(NPh)_2(S_2CNEt_2)_2(\mu\text{-}NPh)\{\mu\text{-}PhNC(O)NPh\}]$. *Dalton Trans* **1993**, 2539-2540.

95. Hogarth, G.; Richards, I., Regioselective and reversible carbon–nitrogen bond formation: Synthesis, structure and reactivity of ureato-bridged complexes $[Mo_2(NAr)_2(\mu\text{-}X)\{\mu\text{-}ArNC(O)NAr\}(S_2CNR_2)_2]$ (Ar = Ph, *p*-tol; X = S, NAr; R = Me, Et, Pr). *Dalton Transactions* **2005**, 760-773.

96. Holland, A. W.; Bergman, R. G., Heterocumulene Metathesis by Iridium Guanidinate and Ureylene Complexes: Catalysis Involving Reversible Insertion To Form Six-Membered Metallacycles. *J Am Chem Soc* **2002,** *124*, 9010-9011.

97. Paul, F.; Osborn, J. A.; Fischer, J.; Ochsenbein, P., Metallacyclic Interconversions in the Chemistry of Palladium with Phenyl Isocyanate. *Angew Chem* **1993,** *32*, 1638-1640.

98. Gibson, V. C.; Redshaw, C.; Clegg, W.; Elsegood, M. R. J., Isocyanate versus isothiocyanate insertion into alkoxo and imido ligands. *Chem Commun* **1994**, 2635-2636.

99. Danopoulos, A. A.; Wilkinson, G.; Sweet, T. K. N.; Hursthouse, M. B., Reactions of imido complexes of iridium, rhodium and ruthenium. *Dalton Trans* **1996**, 3771-3778.

100. Spencer, L. P.; Yang, P.; Scott, B. L.; Batista, E. R.; Boncella, J. M., Imido Exchange in Bis(imido) Uranium(VI) Complexes with Aryl Isocyanates. *J Am Chem Soc* **2008,** *130*, 2930-2931.

101. Bart, S. C.; Anthon, C.; Heinemann, F. W.; Bill, E.; Edelstein, N. M.; Meyer, K., Carbon dioxide activation with sterically pressured mid- and high-valent uranium complexes. *Journal of the American Chemical Society* **2008,** *130*, 12536-12546.

102. Jilek, R. E.; Tomson, N. C.; Scott, B. L.; Boncella, J. M., [2 + 2] cycloaddition reactions at terminal imido uranium(IV) complexes to yield isolable cycloadducts. *Inorganica Chimica Acta* **2014,** *422*, 78-85.

103. Haskel, A.; Straub, T.; Eisen, M. S., Organoactinide-Catalyzed Intermolecular Hydroamination of Terminal Alkynes. *Organometallics* **1996,** *15*, 3773-3775.

104. Straub, T.; Haskel, A.; Neyround, T. G.; Kapon, M.; Botoshansky, M.; Eisen, M. S., Intermolecular Hydroamination of Terminal Alkynes Catalyzed by Organoactinide Complexes. Scope and Mechanistic Studies. *Organometallics* **2001,** *2001*, 5017-5035.

105. Zi, G.; Blosch, L. L.; Jia, L.; Andersen, R., Preparation and Reactions of Base-Free Bis(1,2,4-tri-*tert*-butylcyclopentadienyl)uranium Methylimide, $Cp'_2U{=}NMe$, and Related Compounds. *Organometallics* **2005,** *24*, 4602-4612.

106. Ren, W.; Zi, G.; Fang, D. C.; Walter, M. D., Thorium oxo and sulfido metallocenes: synthesis, structure, reactivity, and computational studies. *J Am Chem Soc* **2011,** *133*, 13183-96.

107. Zhang, C.; Yang, P.; Zhou, E.; Deng, X.; Zi, G.; Walter, M. D., Reactivity of a Lewis Base Supported Thorium Terminal Imido Metallocene toward Small Organic Molecules. *Organometallics* **2017,** *36*, 4525-4538.

108. Ren, W.; Zhou, E.; Fang, B.; Hou, G.; Zi, G.; Fang, D. C.; Walter, M. D., Experimental and computational studies on the reactivity of a terminal thorium imidometallocene towards organic azides and diazoalkanes. *Angew Chem Int Ed Engl* **2014,** *53*, 11310-4.

109. Ren, W.; Zhou, E.; Fang, B.; Zi, G.; Fang, D.-C.; Walter, M. D., Si–H addition followed by C–H bond activation induced by a terminal thorium imido metallocene: a combined experimental and computational study. *Chemical Science* **2014,** *5*.

110. Ren, W.; Zi, G.; Fang, D. C.; Walter, M. D., A base-free thorium-terminal-imido metallocene: synthesis, structure, and reactivity. *Chemistry - A European Journal* **2011,** *17*, 12669-82.

111. Matson, E. M.; Crestani, M. P.; Fanwick, P. E.; Bart, S. C., Synthesis of U(IV) imidos from $Tp^*_2U(CH_2Ph)$ (Tp* = hydrotris(3,5-dimethylpyrazolyl)borate) by extrusion of bibenzyl. *Dalton Trans* **2012,** *41*, 7952-7958.

112. Matson, E. M.; Fanwick, P. E.; Bart, S. C., Diazoalkane Reduction for the Synthesis of Uranium Hydrazonido Complexes. *Eur J Inorg Chem* **2012,** *2012*, 5471-5478.

113. Zakrzewski, J.; Krawczyk, M., Synthesis and Pesticidal Properties of Thio and Seleno Analogs of Some Common Urea Herbicides. *Phosphorus, Sulfur, and Silicon and the Related Elements* **2009,** *184*, 1880-1903.

114. Sharma, P.; Moorhouse, A. D.; Moses, J. E., Microwave-Enhanced Reaction of Thioacids with Azides in Aqueous Medium. *Synlett* **2011,** *2011*, 2384-2386.

115. Taskin, O. S.; Dadashi-Silab, S.; Kiskan, B.; Weber, J.; Yagci, Y., Highly Efficient and Reusable Microporous Schiff Base Network Polymer as a Heterogeneous Catalyst for CuAAC Click Reaction. *Macromolecular Chemistry and Physics* **2015,** *216*, 1746-1753.

116. Barral, K.; Moorhouse, A. D.; Moses, J. E., Efficient Conversion of Aromatic Amines into Azides: A One-Pot Synthesis of Triazole Linkages. *Org Lett* **2007,** *9*, 1809-1811.

117. Arney, D. S. J.; Burns, C. J., Synthesis and Properties of High-Valent Organouranium Complexes Containing Terminal Organoimido and Oxo Functional Groups. A New Class of Organo-f-Element Complexes. *J Am Chem Soc* **1995,** *117*, 9448-9460.

118. Jilek, R. E.; Tomson, N. C.; Shook, R. L.; Scott, B. L.; Boncella, J. M., Preparation and reactivity of the versatile uranium(IV) imido complexes $U(NAr)Cl_2(R_2bpy)_2$ (R = Me, *t*Bu) and $U(NAr)Cl_2(tppo)_3$. *Inorg Chem* **2014,** *53*, 9818-26.

119. Graves, C. R.; Yang, P.; Kozimor, S. A.; Vaughn, A. E.; Clark, D. L.; Conradson, S. D.; Schelter, E. J.; Scott, B. L.; Thompson, J. D.; Hay, P. J.; Morris, D. E.; Kiplinger, J. L., Organometallic Uranium(V)−Imido Halide Complexes: From Synthesis to Electronic Structure and Bonding. *J Am Chem Soc* **2008,** *130*, 5272-5285.

120. Jilek, R. E.; Spencer, L. P.; Kuiper, D. L.; Scott, B. L.; Williams, U. J.; Kikkawa, J. M.; Schelter, E. J.; Boncella, J. M., A general and modular synthesis of monoimidouranium(IV) dihalides. *Inorg Chem* **2011,** *50*, 4235-7.

121. Al-Daher, A. G. M.; Bagnall, K. W.; Benetollo, F.; Polo, A.; Bombieri, G., Uranium(IV) and thorium(IV) halide and pseudohalide complexes with substituted amide and urea ligands. *Journal of the Less Common Metals* **1986,** *122*, 167-173.

122. Al-Kazzaz, Z. M. S.; Bagnall, K. W.; Brown, D.; Whittaker, B., Octathiocyanato- and octaselenocyanato-complexes of the tetravalent actinide elements. *Dalton Transactions* **1972**, 2273-2277.

123. Koksharova, T. K.; Prisyazhnyuk, A. I., Formation of a Complex of Nickel(II) with *N*,*N*`-Diphenylthiourea. *Zh. Neorg. Khim.* **1984,** *20*, 597-629.

124. Jensen, K. A.; Nielsen, P. H., Infrared Spectra of Thioamides and Selenoamides. *Acta Chemica Scandinavica* **1966,** *20*, 597-629.

125. Koketsu, M.; Takakura, N.; Ishihara, H., Efficient Synthesis of Selenoureas from the Corresponding Carbodiimides. *Synthetic Communications* **2002,** *32*, 3075-3079.

126. Célariès, B.; Rima, G.; Court, L.; Lion, C.; Laval, J.-D., Radioprotective Activity and Synthesis of Siladithioacetals and Germadithioacetals Derived from N-substituted Naphthylethylimidazoline. *Metal-Based Drugs* **2001,** *8*, 199-210.

127. Trujillo, C.; Mó, O.; Yáñez, M.; Tortajada, J.; Salpin, J.-Y., Selenourea−Ca^{2+} Reactions in Gas Phase. Similarities and Dissimilarities with Urea and Thiourea. *The Journal of Physical Chemistry B* **2008,** *112*, 5479-5486.

128. Maiti, N.; Im, S. H.; Lee, Y. H.; Kim, C.-H.; Seok, S. I., Solvent-assisted growth of Sb_2Se_3 nanocompounds from a single-source precursor under mild reaction conditions. *CrystEngComm* **2011,** *13*, 3767-3772.

129. Rija, A. P.; Nicolescu, A.; Soran, A.; Coropceanu, E. B.; Bulhac, I. I.; Bologa, O. A.; Deleanu, C.; Bourosh, P. N., Cobalt(III) dimethylglyoximates containing selenourea and an unusual diselenourea ligand: Synthesis and structures. *Russian Journal of Coordination Chemistry* **2011,** *37*, 757.

130. Fettouhi, M.; Wazeer, M. I. M.; Ahmad, S.; Isab, A. A., X-ray structure and ^{77}Se, ^{31}P and ^{13}C MAS NMR of the dinuclear complex 1,2-bis(selenourea)-1\κSe,2\κSe-1,2-bis(trimethylphosphine)digold(I) chloride. *Polyhedron* **2004,** *23*, 1-4.

131. Bredenkamp, A.; Zeng, X.; Mohr, F., Metal complexes of an N-selenocarbamoyl benzamidine. *Polyhedron* **2012,** *33*, 107-113.

132. Carty, A. J.; Malone, S. F.; Taylor, N. J., The selenium-mercury interaction: synthesis, spectroscopic and x-ray structural studies of methylmercury-selenourea complexes. *Journal of Organomet Chem* **1979,** *172*, 201-211.

133. Fregona, D.; Graziani, R.; Faraglia, G.; Caselato, U.; Sitran, S., Palladium and platinum complexes with N,N-dimethylselenourea. *Polyhedron* **1996,** *15*, 2523-2533.

134. Evans, W. J.; Miller, K. A.; Ziller, J. W.; DiPasquale, A. G.; Heroux, K. J.; Rheingold, A. L., Formation of $Cp^*_2U(EPh)Me$, $Cp^*_2U(EPh)_2$, and $Cp^*_2U(\eta^2\text{-}TeC_6H_4)$ from $Cp^*_2UMe_2$ and PhEEPh (E = S, Se, Te). *Organometallics* **2008,** *26*, 4287-4293.

135. Castro-Rodriguez, I.; Meyer, K., Small molecule activation at uranium coordination complexes: control of reactivity via molecular architecture. *Chem Commun* **2006**, 1353-68.

136. Kiernicki, J. J.; Tatebe, C. J.; Zeller, M.; Bart, S. C., Tailoring the Electronic Structure of Uranium Mono(imido) Species through Ligand Variation. *Inorg Chem* **2018,** *57*, 1870-1879.

137. Hayes, C. E.; Leznoff, D. B., Actinide coordination and organometallic complexes with multidentate polyamido ligands. *Coord Chem Rev* **2014,** *266-267*, 155-170.

138. Schelter, E. J.; Veauthier, J. M.; Graves, C. R.; John, K. D.; Scott, B. L.; Thompson, J. D.; Pool-Davis-Tournear, J. A.; Morris, D. E.; Kiplinger, J. L., 1,4-dicyanobenzene as a scaffold for the preparation of bimetallic actinide complexes exhibiting metal-metal communication. *Chem Eur J* **2008,** *14*, 7782-90.

139. Ren, T., Diruthenium σ-Alkynyl Compounds: A New Class of Conjugated Organometallics. *Organometallics* **2005,** *24*, 4854-4870.

140. Ren, T., Sustainable metal alkynyl chemistry: 3d metals and polyaza macrocyclic ligands. *Chem Commun* **2016,** *52*, 3271-3279.

141. Launay, J.-P., Long-distance intervalence electron transfer. *Chemical Society Reviews* **2001,** *30*, 386-397.

142. Szafert, S.; Gladysz, J. A., Update 1 of: Carbon in One Dimension: Structural Analysis of the Higher Conjugated Polyynes. *Chem Rev* **2006,** *106*, PR1-PR33.

143. Zhou, G.-J.; Wong, W.-Y., Organometallic acetylides of Pt^{II}, Au^{I} and Hg^{II} as new generation optical power limiting materials. *Chem Soc Rev* **2011,** *40*, 2541-2566.

144. Liddle, S. T.; van Slageren, J., Actinide Single-Molecule Magnets. In *Lanthanides and Actinides in Molecular Magnetism*,2015; pp 315-340.

145. Mills, D. P.; Moro, F.; McMaster, J.; van Slageren, J.; Lewis, W.; Blake, A. J.; Liddle, S. T., A delocalized arene-bridged diuranium single-molecule magnet. *Nat Chem* **2011,** *3*, 454-460.

146. J. Miller, M.; Streitwieser, A., Bis(bicyclooctatetraenyl)diuranium, "biuranocenylene". *Journal of Organomet Chem* **1981,** *209*, C52-C54.

147. Diaconescu, P. L.; Arnold, P. L.; Baker, T. A.; Mindiola, D. J.; Cummins, C. C., Arene-Bridged Diuranium Complexes: Inverted Sandwiches Supported by δ Backbonding. *J Am Chem Soc* **2000,** *122*, 6108-6109.

148. Fox, A. R.; Arnold, P. L.; Cummins, C. C., Uranium−Nitrogen Multiple Bonding: Isostructural Anionic, Neutral, and Cationic Uranium Nitride Complexes Featuring a Linear U═N═U Core. *J Am Chem Soc* **2010,** *132*, 3250-3251.

149. Diaconescu, P. L.; Cummins, C. C., μ-η^6,η^6-Arene-Bridged Diuranium Hexakisketimide Complexes Isolable in Two States of Charge. *Inorg Chem* **2012,** *51*, 2902-2916.

150. Vlaisavljevich, B.; Diaconescu, P. L.; Lukens, W. L.; Gagliardi, L.; Cummins, C. C., Investigations of the Electronic Structure of Arene-Bridged Diuranium Complexes. *Organometallics* **2013,** *32*, 1341-1352.

151. Rookes, T. M.; Gardner, B. M.; Balázs, G.; Gregson, M.; Tuna, F.; Wooles, A. J.; Scheer, M.; Liddle, S. T., Crystalline Diuranium Phosphinidiide and μ-Phosphido Complexes with Symmetric and Asymmetric UPU Cores. *Angew Chem* **2017,** *56*, 10495-10500.

152. Camp, C.; Antunes, M. A.; García, G.; Ciofini, I.; Santos, I. C.; Pécaut, J.; Almeida, M.; Marçalo, J.; Mazzanti, M., Two-electron versus one-electron reduction of chalcogens by uranium(III): synthesis of a terminal U(V) persulfide complex. *Chem Sci* **2014,** *5*, 841-846.

153. Camp, C.; Pécaut, J.; Mazzanti, M., Tuning Uranium–Nitrogen Multiple Bond Formation with Ancillary Siloxide Ligands. *J Am Chem Soc* **2013,** *135*, 12101-12111.

154. Chatelain, L.; Scopelliti, R.; Mazzanti, M., Synthesis and Structure of Nitride-Bridged Uranium(III) Complexes. *J Am Chem Soc* **2016,** *138*, 1784-1787.

155. Falcone, M.; Chatelain, L.; Mazzanti, M., Nucleophilic Reactivity of a Nitride-Bridged Diuranium(IV) Complex: CO_2 and CS_2 Functionalization. *Angew Chem* **2016,** *55*, 4074-8.

156. Falcone, M.; Poon, L. N.; Fadaei Tirani, F.; Mazzanti, M., Reversible Dihydrogen Activation and Hydride Transfer by a Uranium Nitride Complex. *Angew Chem* **2018,** *57*, 3697-3700.

157. Rosen, R. K.; Andersen, R. A.; Edelstein, N. M., $[(MeC_5H_4)_3U]_2[\mu\text{-}1,4\text{-}N_2C_6H_4]$: a bimetallic molecule with antiferromagnetic coupling between the uranium centers. *J Am Chem Soc* **1990,** *112*, 4588-4590.

158. Newell, B. S.; Rappé, A. K. S.; Shores, M. P., Experimental evidence for magnetic exchange in di- and trinuclear uranium(IV) ethynylbenzene complexes. *Inorg Chem* **2010,** *49*, 1595-606.

159. Hohloch, S.; Pankhurst, J. R.; Jaekel, E. E.; Parker, B. F.; Lussier, D. J.; Garner, M. E.; Booth, C. H.; Love, J. B.; Arnold, J., Benzoquinonoid-bridged dinuclear actinide complexes. *Dalton Transactions* **2017,** *46*, 11615-11625.

160. Myers, A. J.; Rungthanaphatsophon, P.; Behrle, A. C.; Vilanova, S. P.; Kelley, S. P.; Lukens, W. W.; Walensky, J. R., Structure and properties of $[(4,6\text{-}tBu_2C_6H_2O)_2Se]_2An(THF)_2$, An = U, Np, and their reaction with *p*-benzoquinone. *Chemical Communications* **2018,** *54*, 10435-10438.

161. Wooles, A. J.; Mills, D. P.; Tuna, F.; McInnes, E. J. L.; Law, G. T. W.; Fuller, A. J.; Kremer, F.; Ridgway, M.; Lewis, W.; Gagliardi, L.; Vlaisavljevich, B.; Liddle, S. T., Uranium(III)-carbon multiple bonding supported by arene δ-bonding in mixed-valence hexauranium nanometre-scale rings. *Nature Communications* **2018,** *9*, 2097.

162. Falcone, M.; Barluzzi, L.; Andrez, J.; Fadaei Tirani, F.; Zivkovic, I.; Fabrizio, A.; Corminboeuf, C.; Severin, K.; Mazzanti, M., The role of bridging ligands in dinitrogen reduction and functionalization by uranium multimetallic complexes. *Nat Chem* **2019,** *11*, 154-160.

163. Tatebe, C. J.; Johnson, S. A.; Zeller, M.; Bart, S. C., Generation of $Tp^*_2U(N_3)$ from a family of new uranium(III) alkyl complexes. *Journal of Organomet Chem* **2018,** *857*, 152-158.

164. Takahashi, S.; Kuroyama, Y.; Sonogashira, K.; Hagihara, N., A Convenient Synthesis of Ethynylarenes and Diethynylarenes. *Synthesis* **1980,** *1980*, 627-630.

165. Minato, M.; Lahti, P. M., Characterizing Triplet States of Quinonoidal Dinitrenes as a Function of Conjugation Length. *Journal of the American Chemical Society* **1997,** *119*, 2187-2195.

166. Ryu, B.-Y.; Emrick, T., Bisphenol-1,2,3-triazole (BPT) Epoxies and Cyanate Esters: Synthesis and Self-Catalyzed Curing. *Macromolecules* **2011,** *44*, 5693-5700.

167. Victorovich, C. S.; Hideo, T., Photochemical Transformations of Quintet m-Phenylenedinitrenes. *Bulletin of the Chemical Society of Japan* **2003,** *76*, 2075-2089.

168. Chilton, N. F.; Anderson, R. P.; Turner, L. D.; Soncini, A.; Murray, K. S., PHI: a powerful new program for the analysis of anisotropic monomeric and exchange-coupled polynuclear d- and f-block complexes. *J Comput Chem* **2013,** *34*, 1164-1175.

169. Bain, G. A.; Berry, J. F., Diamagnetic Corrections and Pascal's Constants. *J Chem Ed* **2008,** *85*, 532.

170. Frisch, M. J.; Trucks, G. W.; Schlegel, H. B.; Scuseria, G. E.; Robb, M. A.; Cheeseman, J. R.; Scalmani, G.; Barone, V.; Petersson, G. A.; Nakatsuji, H.; Li, X.; Caricato, M.; Marenich, A. V.; Bloino, J.; Janesko, B. G.; Gomperts, R.; Mennucci, B.; Hratchian, H. P.; Ortiz, J. V.; Izmaylov, A. F.; Sonnenberg, J. L.; Williams; Ding, F.; Lipparini, F.; Egidi, F.; Goings, J.; Peng, B.; Petrone, A.; Henderson, T.; Ranasinghe, D.; Zakrzewski, V. G.; Gao, J.; Rega, N.; Zheng, G.; Liang, W.; Hada, M.; Ehara, M.; Toyota, K.; Fukuda, R.; Hasegawa, J.; Ishida, M.; Nakajima, T.; Honda, Y.; Kitao, O.; Nakai, H.; Vreven, T.; Throssell, K.; Montgomery Jr., J. A.; Peralta, J. E.; Ogliaro, F.; Bearpark, M. J.; Heyd, J. J.; Brothers, E. N.; Kudin, K. N.; Staroverov, V. N.; Keith, T. A.; Kobayashi, R.; Normand, J.; Raghavachari, K.; Rendell, A. P.; Burant, J. C.; Iyengar, S. S.; Tomasi, J.; Cossi, M.; Millam, J. M.; Klene, M.; Adamo, C.; Cammi, R.; Ochterski, J. W.; Martin, R. L.; Morokuma, K.; Farkas, O.; Foresman, J. B.; Fox, D. J. *Gaussian 16 Rev. B.01*: Wallingford, CT, 2016.

171. Stephens, P. J.; Devlin, F. J.; Chabalowski, C. F.; Frisch, M. J., Ab Initio Calculation of Vibrational Absorption and Circular Dichroism Spectra Using Density Functional Force Fields. *The Journal of Physical Chemistry* **1994,** *98*, 11623-11627.

172. Becke, A. D., Density- functional thermochemistry. III. The role of exact exchange. *Journal of Chemical Physics* **1993,** *98*, 5648-5652.

173. Lee, C.; Yang, W.; Parr, R. G., Development of the Colle-Salvetti correlation-energy formula into a functional of the electron density. *Physical Review B* **1988,** *37*, 785-789.

174. Küchle, W.; Dolg, M.; Stoll, H.; Preuss, H., Energy- adjusted pseudopotentials for the actinides. Parameter sets and test calculations for thorium and thorium monoxide. *Journal of Chemical Physics* **1994,** *100*, 7535-7542.

175. Enriquez, A. E.; Scott, B. L.; Neu, M. P., Uranium(III)/(IV) Nitrile Adducts Including $UI_4(N{\equiv}CPh)_4$, a Synthetically Useful Uranium(IV) Complex. *Inorg Chem* **2005,** *44*, 7403-7413.

176. Seaman, L. A.; Walensky, J. R.; Wu, G.; Hayton, T. W., In Pursuit of Homoleptic Actinide Alkyl Complexes. *Inorg Chem* **2013,** *52*, 3556-3564.

177. Rinehart, J. D.; Harris, T. D.; Kozimor, S. A.; Bartlett, B. M.; Long, J. R., Magnetic Exchange Coupling in Actinide-Containing Molecules. *Inorg Chem* **2009,** *48*, 3382-3395.

178. Gardner, B. M.; King, D. M.; Tuna, F.; Wooles, A. J.; Chilton, N. F.; Liddle, S. T., Assessing crystal field and magnetic interactions in diuranium-μ-chalcogenide triamidoamine complexes with U^{IV}-E-U^{IV} cores (E = S, Se, Te): implications for determining the presence or absence of actinide-actinide magnetic exchange. *Chem Sci* **2017,** *8*, 6207-6217.

179. Kindra, D. R.; Evans, W. J., Magnetic Susceptibility of Uranium Complexes. *Chem Rev* **2014,** *114*, 8865-8882.

180. Graves, C. R.; Vaughn, A. E.; Schelter, E. J.; Scott, B. L.; Thompson, J. D.; Morris, D. E.; Kiplinger, J. L., Probing the Chemistry, Electronic Structure and Redox Energetics in Organometallic Pentavalent Uranium Complexes. *Inorg Chem* **2008,** *47*, 11879-11891.

181. Morris, D. E.; Da Re, R. E.; Jantunen, K. C.; Castro-Rodriguez, I.; Kiplinger, J. L., Trends in Electronic Structure and Redox Energetics for Early-Actinide Pentamethylcyclopentadienyl Complexes. *Organometallics* **2004,** *23*, 5142-5153.

182. Natoli, S. N.; Hight, L. M.; Zeller, M.; McMillin, D. R., Photophysical Properties of Pt(II) Polypyridines with Five- versus Six-Membered Chelate Rings: Trade-Offs in Angle Strain. *Inorg. Chem.* **2018,** *57*, 6521-6529.

183. Bard, A. J. F., L. R. Electrochemical Methods: Fundamental and Applications, 2nd ed.; John Wiley & Sons: Hoboken, NJ, 2001.

184. Hohloch, S.; Pankhurst, J. R.; Jaekel, E. E.; Parker, B. F.; Lussier, D. J.; Garner, M. E.; Booth, C. H.; Love, J. B.; Arnold, J., Benzoquinonoid-bridged dinuclear actinide complexes. *Dalton Trans.* **2017,** *46*, 11615-11625.

185. Spencer, L. P.; Schelter, E. J.; Yang, P.; Gdula, R. L.; Scott, B. L.; Thompson, J. D.; Kiplinger, J. L.; Batista, E. R.; Boncella, J. M., Cation-cation interactions, magnetic communication, and reactivity of the pentavalent uranium ion [U(NtBu)2]+. *Angew Chem Int Ed Engl* **2009,** *48*, 3795-8.

186. Lam, O. P.; Heinemann, F. W.; Meyer, K., Activation of elemental S, Se and Te with uranium(III): bridging U–E–U (E = S, Se) and diamond-core complexes U–$(E)_2$–U (E = O, S, Se, Te). *Chemical Science* **2011,** *2*, 1538-1547.

187. Gardner, B. M.; Stewart, J. C.; Davis, A. L.; McMaster, J.; Lewis, W.; Blake, A. J.; Liddle, S. T., Homologation and functionalization of carbon monoxide by a recyclable uranium complex. *Proceedings of the National Academy of Sciences* **2012,** *109*, 9265-9270.

188. Gardner, B. M.; Balázs, G.; Scheer, M.; Tuna, F.; McInnes, E. J. L.; McMaster, J.; Lewis, W.; Blake, A. J.; Liddle, S. T., Triamidoamine–Uranium(IV)-Stabilized Terminal Parent Phosphide and Phosphinidene Complexes. *Angew Chem* **2014,** *53*, 4484-4488.

189. Brown, J. L.; Fortier, S.; Wu, G.; Kaltsoyannis, N.; Hayton, T. W., Synthesis and Spectroscopic and Computational Characterization of the Chalcogenido-Substituted Analogues of the Uranyl Ion, $[OUE]^{2+}$ (E = S, Se). *J Am Chem Soc* **2013,** *135*, 5352-5355.

190. Brown, J. L.; Fortier, S.; Lewis, R. A.; Wu, G.; Hayton, T. W., A Complete Family of Terminal Uranium Chalcogenides, $[U(E)(N\{SiMe_3\}_2)_3]^-$ (E = O, S, Se, Te). *J Am Chem Soc* **2012,** *134*, 15468-15475.

191. Bart, S. C.; Anthon, C.; Heinemann, F. W.; Bill, E.; Edelstein, N. M.; Meyer, K., Carbon Dioxide Activation with Sterically Pressued Mid- and High-Valent Uranium Complexes. *J Am Chem Soc* **2008,** *130*, 12536-12546.

192. Hayton, T. W.; Boncella, J. M.; Scott, B. L.; Palmer, P. D.; Batista, E. R.; Hay, P. J., Synthesis of Imido Analogs of the Uranyl Ion. *Science* **2005,** *310*, 1941-1943.

193. Anderson, N. H.; Odoh, S. O.; Yao, Y.; Williams, U. J.; Schaefer, B. A.; Kiernicki, J. J.; Lewis, A. J.; Goshert, M. D.; Fanwick, P. E.; Schelter, E. J.; Walensky, J. R.; Gagliardi, L.; Bart, S. C., Harnessing redox activity for the formation of uranium tris(imido) compounds. *Nat Chem* **2014,** *6*, 919-926.

194. Kiernicki, J. J.; Cladis, D. P.; Fanwick, P. E.; Zeller, M.; Bart, S. C., Synthesis, Characterization, and Stoichiometric U-O Bond Scission in Uranyl Species Supported by Pyridine(diimine) Ligand Radicals. *J Am Chem Soc* **2015,** *137*, 11115-11125.

195. Kiernicki, J. J.; Ferrier, M. G.; Lezama Pacheco, J. S.; La Pierre, H. S.; Stein, B. W.; Zeller, M.; Kozimor, S. A.; Bart, S. C., Examining the Effects of Ligand Variation on the Electronic Structure of Uranium Bis(imido) Species. *J Am Chem Soc* **2016,** *138*, 13941-13951.

196. Burns, C. J.; Smith, W. H.; Huffman, J. C.; Sattelberger, A. P., Uranium(VI) organoimido complexes. *J Am Chem Soc* **1990,** *112*, 3237-3239.

197. Hayton, T. W.; Boncella, J. M.; Scott, B. L.; Batista, E. R., Exchange of an Imido Ligand in Bis(imido) Complexes of Uranium. *J Am Chem Soc* **2006,** *128*, 12622-12623.

198. Graves, C. R.; Scott, B. L.; Morris, D. E.; Kiplinger, J. L., Facile Access to Pentavalent Uranium Organometallics: One-Electron Oxidation of Uranium(IV) Imido Complexes with Copper(I) Salts. *J Am Chem Soc* **2007,** *129*, 11914-11915.

199. Straub, T.; Frank, W.; Reiss, G. J.; Eisen, M. S., Uranium(IV) bis(amido), imido and bis(acetylide) complexes: synthesis, molecular structure, solution dynamics and interconversion reactions. *Dalton Tran* **1996**, 2541-2546.

200. Anderson, N. H.; Xie, J.; Ray, D.; Zeller, M.; Gagliardi, L.; Bart, S. C., Elucidating bonding preferences in tetrakis(imido)uranate(VI) dianions. *Nat Chem* **2017,** *9*, 850-855.

201. Anderson, N. H.; Yin, H.; Kiernicki, J. J.; Fanwick, P. E.; Schelter, E. J.; Bart, S. C., Investigation of Uranium Tris(imido) Complexes: Synthesis, Characterization, and Reduction Chemistry of [U(NDIPP)$_3$(thf)$_3$]. *Angew Chem Int Ed* **2015,** *54*, 9386-9389.

202. Tatebe, C. J.; Collins, T. S.; Barnett, G. R.; Zeller, M.; Bart, S. C., Preparation of U(IV) κ^1-amidinate complexes by nitrile metathesis. *Polyhedron* **2019,** *158*, 1-7.

203. Warner, B. P.; Scott, B. L.; Burns, C. J., A Simple Preparative Route to Bis(imido)uranium(VI) Complexes by the Direct Reductions of Diazenes and Azides. *Angew Chem* **1998,** *37*, 959-960.

204. Mullane, K. C.; Lewis, A. J.; Yin, H.; Carroll, P. J.; Schelter, E. J., Anomalous One-Electron Processes in the Chemistry of Uranium Nitrogen Multiple Bonds. *Inorg Chem* **2014,** *53*, 9129-9139.

205. Hayton, T. W.; Boncella, J. M.; Scott, B. L.; Batista, E. R.; Hay, P. J., Synthesis and Reactivity of the Imido Analogues of the Uranyl Ion. *J Am Chem Soc* **2006,** *128*, 10549-10559.

206. De Bruin, B.; Gualco, P.; Paul, N. D., Redox Non-innocent Ligands. In *Ligand Design in Metal Chemistry*, John Wiley & Sons, Ltd: Chichester, UK, 2016; pp 176-204.

207. Chirik, P. J.; Wieghardt, K., Radical Ligands Confer Nobility on Base-Metal Catalysts. *Science* **2010,** *327*, 794-795.

208. Luca, O. R.; Crabtree, R. H., Redox-active ligands in catalysis. *Chem Soc Rev* **2013,** *42*, 1440-1459.

209. Ren, W.; Zi, G.; Walter, M. D., Synthesis, Structure, and Reactivity of a Thorium Metallocene Containing a 2,2′-Bipyridyl Ligand. *Organometallics* **2012,** *31*, 672-679.

210. Garner, M. E.; Hohloch, S.; Maron, L.; Arnold, J., A New Supporting Ligand in Actinide Chemistry Leads to Reactive Bis(NHC)borate-Supported Thorium Complexes. *Organometallics* **2016,** *35*, 2915-2922.

211. Cladis, D. P.; Kiernicki, J. J.; Fanwick, P. E.; Bart, S. C., Multi-electron reduction facilitated by a trianionic pyridine(diimine) ligand. *Chem Commun* **2013,** *49*, 4169-4171.

212. Soma, C.; Jayanta, C.; Wenhua, G.; Edward, B. W., Functionalization of Potassium Graphite. *Angew Chem* **2007,** *46*, 4486-4488.

213. Alt, H. G.; Reb, A.; Kundu, K., ω-Phenylalkyl substituted amido functionalized ansa half-sandwich complexes of titanium and zirconium and metallacycles thereof as catalyst precursors for homogeneous ethylene polymerization. *Journal of Organomet Chem* **2001,** *628*, 211-221.

214. Knijnenburg, Q.; Gambarotta, S.; Budzelaar, P. H. M., Ligand-centred reactivity in diiminepyridine complexes. *Dalton Trans* **2006**, 5442-5448.

215. Kiernicki, J. J.; Fanwick, P. E.; Bart, S. C., Utility of a redox-active pyridine(diimine) chelate in facilitating two electron oxidative addition chemistry at uranium. *Chem Commun* **2014,** *50*, 8189-92.

216. Mohammad, A.; Cladis, D. P.; Forrest, W. P.; Fanwick, P. E.; Bart, S. C., Reductive heterocoupling mediated by $Cp^*_2U(2,2'\text{-bpy})$. *Chem Commun* **2012,** *48*, 1671-1673.

217. Pattenaude, S. A.; Kuehner, C. S.; Dorfner, W. L.; Schelter, E. J.; Fanwick, P. E.; Bart, S. C., Spectroscopic and Structural Elucidation of Uranium Dioxophenoxazine Complexes. *Inorg Chem* **2015,** *54*, 6520-6527.

218. Herasymchuk, K.; Chiang, L.; Hayes, C. E.; Brown, M. L.; Ovens, J. S.; Patrick, B. O.; Leznoff, D. B.; Storr, T., Synthesis and electronic structure determination of uranium(VI) ligand radical complexes. *Dalton Tran* **2016,** *45*, 12576-12586.

219. Kiernicki, J. J.; Higgins, R. F.; Kraft, S. J.; Zeller, M.; Shores, M. P.; Bart, S. C., Elucidating the Mechanism of Uranium Mediated Diazene N=N Bond Cleavage. *Inorg Chem* **2016,** *55*, 11854-11866.

220. Fortier, S.; Veleta, J.; Pialat, A.; Le Roy, J.; Ghiassi, K. B.; Olmstead, M. M.; Metta-Magaña, A.; Murugesu, M.; Villagrán, D., $[U(bipy)_4]$: A Mistaken Case of U^0? *Chem Eur J* **2016,** *22*, 1931-1936.

221. Schelter, E. J.; Wu, R.; Scott, B. L.; Thompson, J. D.; Cantat, T.; John, K. D.; Batista, E. R.; Morris, D. E.; Kiplinger, J. L., Actinide Redox-Active Ligand Complexes: Reversible Intramolecular Electron-Transfer in $U(dpp\text{-}BIAN)_2$/$U(dpp\text{-}BIAN)_2(THF)$. *Inorg Chem* **2010,** *49*, 924-933.

222. Anderson, N. H.; Odoh, S. O.; Williams, U. J.; Lewis, A. J.; Wagner, G. L.; Lezama Pacheco, J.; Kozimor, S. A.; Gagliardi, L.; Schelter, E. J.; Bart, S. C., Investigation of the electronic ground states for a reduced pyridine(diimine) uranium series: evidence for a ligand tetraanion stabilized by a uranium dimer. *J Am Chem Soc* **2015,** *137*, 4690-4700.

223. Graves, C. R.; Scott, B. L.; Morris, D. E.; Kiplinger, J. L., Selenate and tellurate complexes of pentavalent uranium. *Chem Commun* **2009**, 776-778.

VITA

Caleb J. Tatebe was born and raised in the Mahoning Valley (NE Ohio) and obtained his B. Sc. in chemistry from Youngstown State University in Youngstown, Ohio in May of 2012. He had multiple undergraduate research experiences, including perovskites (under the direction of Prof. Tim Wagner) and carbohydrate chemistry (with Prof. Peter Norris). Continuing research in synthetic organic chemistry, he remained at YSU for a M.Sc. in chemistry (August 2014) under the supervision of Prof. Norris.

He then moved to West Lafayette, Indiana and continued graduate studies at Purdue University. In the fall of 2014, he was accepted into the research group of Professor Suzanne Bart, where he studied organouranium chemistry. Use of uranium(III) alkyl compounds led to a number of research reports while learning air- and moisture-sensitive handling techniques. Through the years, his work has been published in various peer-reviewed journals, as well as a book chapter reviewing actinide imido reactivity.

Compound	CCDC number or local name
$Tp^{Ph}UI_2$	1488924
$Tp^{Ph}UI_2$(Phpz)	1488925
$Tp^{Ph}UI$(OPh)	1488926
Tp^*_2U(N-dipp) (**7-dipp**)	1495230
Tp^*_2U(N-*p*Tol) (**7-Tol**)	1495232
Tp^*_2U(N-detp) (**7-detp**)	1507653
Tp^*_2U(N-Bn) (**7-Bn**)	1495231
Tp^*_2U[κ^2-(*N*,*N*'-diphenylureato)] (**8-Ph**)	1495078
Tp^*_2U[κ^2-(*N*,*N*'-diphenylthioureato)] (**9-Ph**)	1495080
Tp^*_2U[κ^2-(*N*,*N*'-diphenylselenoureato)] (**10-Ph**)	1495079
Cp^PU(NDIPP)(^{Mes}PDI^{Me}) (**17-Cp^P**)	1582610
Cp*U(NDIPP)(^{Mes}PDI^{Me}) (**17-Cp***)	1554591
[Cp*U(NAd)(^{Mes}HPDI^{Me})]$_2$ (**18**)	1554594
Cp*U(NAd)(^{t}Bu-^{Mes}PDI^{Me}) (**17-^{t}Bu**)	1554593
Cp^PUI_2(^{t}Bu-^{Mes}PDI^{Me}) (**19-I$_2$**)	1554590
Tp^*_2U(CH_2-*p*-*i*PrPh) (**2-*p*-^{i}Pr**)	1567339
Tp^*_2U(CH_2-*p*-^{t}Bu) (**2-*p*-^{t}Bu**)	1567341
Tp^*_2U(CH_2-*m*OMePh) (**2-OMe**)	1567338
Tp^*_2U(CH_2pyr) (**2-*o*-picolyl**)	1567340
Tp^*_2U(N_3) (**3-N$_3$**)	1567337
Tp^*_2U[OP(C_6H_5)$_2$($C_6H_5CH_2C_6H_5$)] (**4-Ph**)	1587812
Tp^*_2U[OP(C_6H_5)$_2$($C_6H_5CH_2$-*p*-^{i}PrC_6H_4)] (**4-^{i}Pr**)	1587813
Tp^*_2U[OP(C_6H_5)$_2$($C_6H_5CH_2$-*m*-$OCH_3C_6H_4$)] (**4-OMe**)	1587807
Tp^*_2U(THF)($BnBPh_3$) (**5-THF**)	1587804
Tp^*_2U[=NC(N*p*OMePh)-Ph] (**11-Ph**)	1854085
Tp^*_2U[=NC(N*p*OMePh)-pyr] (**11-pyr**)	1854086
Tp^*_2U[=NC(N*p*CH_3Ph)-pyr] (**12-pyr**)	1854084
Tp^*_2U[NC(=N-*p*OMePh)-*p*-cyanobenzene] (**13-OMe**)	1873124
Tp^*_2U[NC(=N-*p*CH_3Ph)-*p*-cyanobenzene] (**13-Tol**)	1852446
Tp^*_2UCC(1,3-C_6H_4)CCUTp^*_2 (**14-*meta***)	1852448
Tp^*_2UCC(1,4-C_6H_4)CCUTp^*_2 (**14-*para***)	1852445
Tp^*_2UN(1,3-C_6H_4)NUTp^*_2 (**15-*meta***)	1852450
Tp^*_2UN(1,4-C_6H_4)NUTp^*_2 (**15-*para***)	1852444
[Tp^*_2U(THF)][BPh_4] (**5-THFb**)	1852443
[Tp^*_2U(MeCN)$_2$][BPh_4] (**5-MeCN**)	1852447
[Tp^*_2UNCPhCN]$_n$[BPh_4]$_n$ (**5-n**)	1852449
Tp^*_2U(O(CH_2)$_4$P(Ph)) (**6**)	CT956
Tp^*_2U($OBPh_2$)	CT962g
Tp*U(NHdipp)$_3$	CT986
Tp*U(NHMes)$_3$	CT953

PUBLICATIONS

Inorganic Chemistry

Article

pubs.acs.org/IC

[2π+2π] Cycloaddition of Isocyanates to Uranium(IV) Imido Complexes for the Synthesis of U(IV) κ²-Ureato Compounds

Caleb J. Tatebe, Matthias Zeller, and Suzanne C. Bart*

H.C. Brown Laboratory, Department of Chemistry, Purdue University, West Lafayette, Indiana 47906, United States

Supporting Information

ABSTRACT: A new family of uranium(IV) imido complexes of the form $Tp^*_2U(NR)$ (Tp^* = hydrotris(3,5-dimethylpyrazolyl)borate; R = benzyl (Bn), *para*-tolyl (*p*-Tol), 2,6-diethylphenyl (detp), and 2,6-diisopropylphenyl (dipp)) have been generated by bibenzyl extrusion from Tp^*_2UBn. $Tp^*_2U(NBn)$, $Tp^*_2U(Np\text{-}Tol)$, and $Tp^*_2U(Ndetp)$, along with previously reported $Tp^*_2U(NPh)$ and $Tp^*_2U(NAd)$ (Ad = 1-adamantyl), readily undergo [2π+2π] cycloaddition with isocyanates and isothiocyanates to generate κ²-ureato and κ²-thioureato derivatives, respectively. These new uranium(IV) complexes were characterized via multinuclear NMR, vibrational and electronic absorption spectroscopies, and, where possible, X-ray crystallography. The steric demands of the ligands were quantitatively assessed using computational modeling, and it was shown that cycloaddition only occurs for imido species where ligands occupy 90% or less of the coordination sphere.

INTRODUCTION

Cycloaddition to transition metal−nitrogen multiple bonds is a key transformation that has broad applications across organic synthesis,[1] dinitrogen activation,[2] polymerization,[3,4] and small molecule formation.[5] This process can be more specifically applied to the synthesis of urea derivatives, which are fairly common based on the variety of κ²-ureato complexes of niobium,[6] rhenium,[7] ruthenium,[8,9] titanium,[10,11] tungsten,[12] and zirconium[13] synthesized via [2 + 2] cycloadditions of isocyanates.[7,11,12,14−20]

Urea derivatives of uranium complexes fashioned from cycloaddition are much less common. In 2008, Boncella invoked formation of a uranium(VI) κ²-ureato derivative from cycloaddition as an intermediate in imido exchange chemistry.[21] Computational comparison of the *N,N*- and *N,O*-bound isomers indicated that the former is actually lower in energy, a surprising result given the oxophilicity of uranium. This finding was corroborated by Meyer later that year with the report of the first solid state characterization of a κ²-ureato ligand on uranium(V) in $((^{tBu}ArO)_3tacn)U(\kappa^2\text{-}N,N'\text{-diphenylureato})$ ($(^{tBu}ArOH)_3tacn$ = 1,4,7-tris(3,5-*tert*-butyl-2-hydroxybenzylate)-1,4,7-diazacyclononane), which is symmetrically coordinated through both nitrogen atoms after proposed isomerization from the *N,O*-bound isomer.[22] In subsequent studies in 2014, Boncella and co-workers reported the tetravalent κ²-ureato complex, $(\kappa^2\text{-}N,N'\text{-}1\text{-Mes-}3\text{-dipp-ureato})U(Cl)_2(OPPh_3)_2$ (Mes = 2,4,6-trimethylphenyl), which was formed from cycloaddition of dipp isocyanate (dipp = 2,6-diisopropylphenyl) to $U(Ndipp)Cl_2(OPPh_3)_2$.[23]

In recent studies, we have demonstrated [2π+2π] cycloaddition chemistry by a family of uranium(IV) imido species supported by the bulky bis-Tp* (Tp* = hydrotris(3,5-dimethylpyrazolyl)borate) ligand framework, including tetravalent imido derivatives, $Tp^*_2U(NR)$ (R = Ph, Mes, Ad) (Ad = 1-adamantyl),[24] as well as the fleeting uranium(IV) hydrazido intermediate, $Tp^*_2U(\eta^1\text{-}N_2CHSiMe_3)$.[25] These compounds all feature reactive uranium−nitrogen multiple bonds that are sterically accessible to react with a variety of substrates.[25] For instance, $Tp^*_2U(\eta^1\text{-}N_2CHSiMe_3)$ is trapped as the uranium(IV) metallacycle, $Tp^*_2UN(N{=}CHSiMe_3)CH{=}CPh_2$ by cycloaddition with the alkyne in phenylacetylene, rather than protonation chemistry from the terminal C−H bond in this substrate. This exciting result led us to hypothesize that [2π+2π] cycloaddition chemistry could be expanded to a variety of substrates, including isocyanate derivatives, as a general route to build actinide ureate derivatives. Herein we present our study examining the [2π+2π] cycloaddition chemistry of PhNCO, PhNCS, and PhNCSe with new members of the uranium(IV) imido family, including $Tp^*_2U(NR)$ (R = benzyl (Bn), *para*-tolyl (*p*Tol), 2,6-diethylphenyl (detp), (dipp)), along with their spectroscopic and structural characterization.

EXPERIMENTAL SECTION

General Considerations. All air- and moisture-sensitive manipulations were performed using standard Schlenk techniques or using an MBraun inert atmosphere drybox with an atmosphere of purified nitrogen. The MBraun drybox was equipped with a cold well designed for freezing samples in liquid nitrogen, as well as two −35 °C freezers for cooling samples and crystallizing compounds. Solvents for sensitive

Received: October 19, 2016
Published: February 6, 2017

DOI: 10.1021/acs.inorgchem.6b02567
Inorg. Chem. 2017, 56, 1956−1960

manipulations were dried and deoxygenated using literature procedures with a Seca solvent purification system.[20] Benzene-d_6 was purchased from Cambridge Isotope Laboratories, dried with molecular sieves and sodium, and degassed by three freeze−pump−thaw cycles. Phenylisocyanate and phenylisothiocyanate were purchased from Sigma-Aldrich and distilled from CaH_2. 2,6-Diisopropylphenylisocyanate was purchased from Alfa Aesar and distilled from CaH_2. 1-Azidoadamantane was purchased from Sigma-Aldrich and used as received. KTp*,[17] Tp*$_2$UBn (**1-Bn**),[19] Tp*$_2$UI,[19] Tp*$_2$U(N-Ph) (**2-Ph**),[24] Tp*$_2$UNAd (**2-Ad**),[24] phenylisoselenocyanate,[21] *para*-tolylazide,[21] and benzyl azide[22] were made using previously reported methods. Other azides (azidobenzene, 2,6-diethylphenylazide, 2,6-diisopropylphenylazide) were prepared using a modified literature procedure.[23]

^{1}H NMR spectra were recorded on a Varian Inova 300 spectrometer operating at 300 MHz. ^{11}B NMR spectra were recorded on a Varian Inova 300 spectrometer operating at a frequency of 96.24 MHz. All chemical shifts are reported relative to the peak for $SiMe_4$ using ^{1}H residual chemical shifts of the solvent as a secondary standard. ^{11}B chemical shifts are reported relative to the peak for BF_3·Et_2O. The spectra for paramagnetic molecules were obtained using an acquisition time of 0.5 s; thus, the peak widths reported have an error of ±2 Hz. For paramagnetic molecules, the ^{1}H NMR data are reported with the chemical shift, followed by the peak width at half height in Hertz, the integration value, and, where possible, the peak assignment. Elemental analyses were performed by Complete Analysis Laboratories, Inc., Parsippany, NJ, or by the Microanalysis Laboratory at the University of Illinois at Urbana−Champaign, Urbana, IL. Solid state infrared spectra were recorded using a Thermo Nicolet 6700 spectrophotometer; samples were made by crushing the solids, mixing with dry KBr, and pressing into a pellet. Electronic absorption spectroscopic measurements were recorded at 294 K in sealed 1 cm quartz cuvettes with a Cary 6000i UV−vis-NIR spectrophotometer.

Single crystals suitable for X-ray diffraction were coated with poly(isobutylene) oil in a glovebox and quickly transferred to the goniometer head of the specified instrument. Crystals of **2-Bn** and **2-dipp** were transferred to the goniometer head of a Nonius KappaCCD diffractometer equipped with a graphite crystal and incident beam monochromator and examined with Mo Kα radiation (λ = 0.71073 Å). Crystals of **2-detp**, **2-*p*Tol**, **3-Ph**, **4-Ph**, and **5-Ph** were transferred to the goniometer head of a Rigaku R-axis curved image plate diffractometer equipped with a MicroMax002+ high-intensity copper X-ray source with confocal optics and examined with Cu Kα radiation (λ = 1.54184 Å). Data were collected at low temperature (see cif data).

General Synthesis for Tp*$_2$U(IV) Imido Compounds. A 20 mL scintillation vial was charged with Tp*$_2$UBn (**1-Bn**) (0.100 g, 0.108 mmol) and 5 mL of toluene. To this green solution, 1 equiv of N_3R (R = Bn, detp, dipp, *p*Tol) (0.108 mmol; Bn = 0.014 g; detp = 0.019 g; dipp = 0.022 g; *p*Tol = 0.017 g) was added, followed by an immediate evolution of nitrogen gas and color change from deep green to red-violet. Volatiles were removed *in vacuo*. The product mixtures were washed with pentane (2 × 5 mL) and dried to afford powders assigned as imido products Tp*$_2$U(N-Bn) (**2-Bn**), Tp*$_2$U(N-detp) (**2-detp**), Tp*$_2$U(N-dipp) (**2-dipp**), and Tp*$_2$U(N-*p*Tol) (**2-*p*Tol**) (**2-Bn** = purple, 0.077 g, 0.082 mmol, 76% yield; **2-detp** = purple, 0.079 g, 0.080 mmol, 74% yield; **2-dipp** = deep purple, 0.088 g, 0.088 mmol, 81% yield; **2-*p*Tol** = red-purple, 0.066 g, 0.070 mmol, 65% yield). Single crystals of **2-Bn**, **2-*p*Tol**, and **2-detp** were obtained by outward diffusion of a concentrated diethyl ether solution into a toluene solution at −35 °C, and crystals of **2-dipp** were obtained from a concentrated solution of diethyl ether at −35 °C. **2-Bn**: Elemental analysis of $C_{37}H_{51}B_2N_{13}U$. Calculated: C, 47.40; H, 5.48; N, 19.42. Found: C, 46.87; H, 5.33; N, 18.95. ^{1}H NMR (C_6D_6, 25 °C): δ (ppm) = −20.58 (11, B-*H*), −6.79 (11, 18H, Tp*−CH_3), 1.50 (72, 18H, Tp*−CH_3), 5.28 (4, 6H, Tp*−*CH*), 16.91 (t, 1H, *p*−*CH*, J = 6.71 Hz), 19.87 (14, 2H, *m*/*o*−*CH*), 59.95 (84, 2H, *m*/*o*−*CH*).^{11}B NMR (C_6D_6, 25 °C): δ (ppm) = −64.75. IR (KBr): ν_{B-H} = 2560, 2515 cm^{-1}. **2-detp**: Reliable elemental analysis could not be obtained due to incomplete combustion: Elemental analysis of $C_{40}H_{57}B_2N_{13}U$. Calculated: C, 49.04; H, 5.87; N, 18.59. Found: C, 46.43; H, 5.63; N, 17.44. ^{1}H NMR (C_6D_6, 25 °C): δ (ppm) = −81.03 (11, 6H, Tp*−CH_3), −25.44 (7, B-*H*), −20.03 (2, 2H, Tp*−*CH*), −18.24 (5, 6H, Tp*−CH_3), −13.40 (4, 6H, Tp*−CH_3), −7.42 (5, 2H, Tp*−*CH*), 7.03 (4, 6H, -PhCH$_2$*CH*$_3$), 11.12 (21, 6H, Tp*−CH_3) 20.84 (24, 6H, Tp*−CH_3), 27.95 (13, 1H, *p*−*CH*), 41.88 (3, 2H, Tp*−*CH*), 53.87 (248, 2H, -PhCH$_2$CH$_3$) 54.83 (176, 2H, -PhCH$_2$CH$_3$), 55.90 (3, 2H, *m*/*o*−*CH*), 68.76 (15, 6H, Tp*−CH_3). ^{11}B NMR (C_6D_6, 25 °C): δ (ppm) = −76.92. IR (KBr): ν_{B-H} = 2550, 2521 cm^{-1}. **2-dipp**: Elemental analysis of $C_{52}H_{81}B_2N_{13}U$. Calculated: C, 49.76; H, 6.66; N, 17.69. Found: C, 49.98; H, 6.02; N, 17.89. ^{1}H NMR (C_6D_6, 25 °C): δ (ppm) = −82.00 (10, 6H, Tp*−CH_3), −25.24 (4.75, B-*H*), −21.19 (10, 2H, Tp*−*CH*), −18.03 (7, 6H, Tp*−CH_3), −14.53 (4, 6H, Tp*−CH_3), −9.12, (4, 2H, Tp*−*CH*), 8.08 (90, 6H, Tp*−CH_3), 11.61 (7, 6H, CH_3), 12.42 (7, 6H, CH_3), 21.39 (583, 6H, Tp*−CH_3), 28.02 (3, 1H, *p*−*CH*), 43.25 (3, 2H, Tp*−*CH*), 55.69 (4, 2H, *m*/*o*−*CH*), 65.87 (61, 1H, iPr−*CH*), 67.64 (41, 6H, Tp*−CH_3). ^{11}B NMR (C_6D_6, 25 °C): δ (ppm) = −75.35. IR (KBr): ν_{B-H} = 2553, 2521 cm^{-1}. **2-*p*Tol**: Elemental analysis of $C_{37}H_{51}B_2N_{13}U$. Calculated: C, 47.40; H, 5.48; N, 19.42. Found: C, 47.02; H, 5.25; N, 18.68. ^{1}H NMR (C_6D_6, 25 °C): δ −21.21, (0.25, B-*H*), −6.89 (4, 18H, Tp*−CH_3), 2.81 (22, 18H, Tp*−CH_3), 5.48 (7, 6H, Tp*−*CH*), 38.50 (5, 3H, CH_3), 53.82 (8, 2H, *m*−*CH*), 78.69 (16, 2H, *o*−*CH*). ^{11}B NMR (C_6D_6, 25 °C): δ (ppm) = −66.60. IR (KBr): ν_{B-H} = 2553, 2528 cm^{-1}.

Alternate Preparation of Tp*$_2$U(IV) Imido Compounds. A 20 mL scintillation vial was charged with Tp*$_2$UI (0.060 g, 0.063 mmol) and 5 mL of THF. To this deep blue solution, 1 equiv (0.063 mmol) of corresponding azide (Bn = 0.008 g; detp =0.011 g; dipp = 0.013 g; *p*Tol = 0.009 g) was added. An excess of potassium graphite (0.011 g, 0.079 mmol) was introduced, and the reaction was allowed to stir for 1.5 h. After stirring, the resulting graphite and KI were removed via filtration. The filtrate was concentrated under reduced pressure. Crude products were washed with pentane (2 × 10 mL) to give **2-Bn** (0.049 g, 0.052 mmol, 82% yield), **2-detp** (0.051g, 0.053 mmol, 84% yield), **2-dipp** (0.054 g, 0.053 mmol, 85% yield), or **2-*p*Tol** (0.051 g, 0.054 mmol, 87% yield).

Synthesis of Tp*$_2$U(IV) κ^2-Ureato Compounds. In a 20 mL scintillation vial, Tp*$_2$UNR (R = Ad: 0.060 g, 0.061 mmol; Bn: 0.060 g, 0.064 mmol; Ph: 0.052 g, 0.056 mmol; *p*Tol: 0.057 g, 0.061 mmol) was dissolved in 10 mL of THF. To the deep red solution, 1 equiv of phenyl isocyanate (R = Ad: 0.007 mL, 0.061 mmol; Bn: 0.008 mL, 0.064 mmol; Ph: 0.006 mL, 0.056 mmol; pTol: 0.007 mL, 0.061 mmol) was injected via microsyringe, and the reaction mixture was allowed to stir for 15 min, creating a red-orange solution. Volatiles were removed *in vacuo*. The crude products were washed with pentane (2 × 10 mL) to afford orange powders, assigned as Tp*$_2$U[κ^2-*N*,*N*′-1-phenyl-3-adamantylurea] (**3-Ad**), Tp*$_2$U[κ^2-(*N*,*N*′-1-phenyl-3-benzylureato)] (**3-Bn**), Tp*$_2$U[κ^2-(*N*,*N*′-diphenylureato)] (**3-Ph**), or Tp*$_2$U[κ^2-(*N*,*N*′-1-phenyl-3-*p*-tolylureato)] (**3-*p*Tol**) (**3-Ad**: 0.049 g, 0.045 mmol 73% yield; **3-Bn**: 0.061 g, 0.058 mmol, 90% yield; **3-Ph**: 0.048 g, 0.046 mmol, 82% yield; **3-*p*Tol**: 0.102 g, 0.097 mmol, 89% yield). **3-Ad**: Reliable elemental analysis could not be obtained due to incomplete combustion: Elemental analysis of $C_{47}H_{64}B_2N_{14}OU$. Calculated, C, 51.28; H, 5.86; N, 17.81. Found, C 47.39; H, 4.90; N, 16.16 ^{1}H NMR (C_6D_6, 25 °C): δ = −37.26 (33, 3H, Tp*−CH_3), −30.25 (25, 3H, Tp*−CH_3), −16.81 (9, 3H, Tp*−CH_3), −12.96 (137, H, B-*H*), −8.90 (3, 3H, Tp*−CH_3), −7.78 (2, 3H, Tp*−CH_3), −5.29 (5, 1H, Tp*−*CH*), −3.45 (12, 3H, Tp*−CH_3), −2.17 (3, 1H, Tp*−*CH*), −1.93 (4, 3H, Tp*−CH_3), −0.55 (5, 1H, Tp*−*CH*), −0.02 (22, 3H, Ad−*CH*), 0.30 (5, 3H, Ad−*CH*), 1.04 (d, 3H, Ad−*CH*, J = 10.64 Hz), 1.60 (d, 3H, Ad−*CH*, J = 11.41 Hz), 2.01 (9, 3H, Tp*−CH_3), 2.88 (12, 3H, Tp*−CH_3), 3.67 (11, 3H, Ad−*CH*), 4.18 (3, 3H, Tp*−CH_3), 7.95 (3, 1H, Tp*−*CH*), 9.98 (t, 1H, Ph: *p*−*CH*, J = 7.48 Hz), 14.01 (13, 5H, Tp*−CH_3/Ph: *o*/*m*−*CH*), 17.68 (2, 1H, Tp*−*CH*), 18.47 (2, 1H, Tp*−*CH*), 21.21 (17, 2H, Ph: *o*/*m*−*CH*), 42.89 (17, 3H, Tp*−CH_3). ^{11}B NMR (C_6D_6, 25 °C): δ (ppm) = −51.48, −19.31. IR (KBr): ν_{B-H} = 2559, 2515 cm^{-1}; $\nu_{C=O}$ = 1696 cm^{-1} **3-Bn**: Reliable elemental analysis could not be obtained due to incomplete combustion: Elemental analysis of $C_{48}H_{58}B_2N_{14}OU$. Calculated, C, 50.01; H, 5.34; N, 18.56. Found, C 48.69; H, 5.34; N, 17.82 ^{1}H NMR (C_6D_6, 25 °C): δ = −38.94 (6, 3H, Tp*−CH_3),

DOI: 10.1021/acs.inorgchem.6b02547
Inorg. Chem. 2017, 56, 1956−1965

−24.69 (9, 3H, Tp*−CH_3), −18.84 (182, B-*H*), −17.18 (131, 3H, Tp*−CH_3), −11.02 (10, 3H, Tp*−CH_3), −8.92 (4, 3H, Tp*−CH_3), −8.83 (2, 3H, Tp*−CH_3), −6.30 (3 3H, Tp*−CH_3), −3.81 (4, 3H, Tp*−CH_3), −3.76 (4, 1H, Tp*−*CH*), −3.58 (5, 1H, Tp*−*CH*), −1.41 (12, 1H, Tp*−*CH*), 2.23 (5, 2H, Bn: *m*/*o*−*CH*), 2.51 (7, 3H, Tp*−CH_3), 4.19 (26, 2H, −CH_2Ph), 4.59 (6, 3H, Tp*−CH_3), 8.77 (32, 1H, Bn: *p*−*CH*), 10.23 (t, 1H, Ph: *p*−*CH*, J = 7.32 Hz), 12.22 (t, 2H, Ph: *m*−*CH*, J = 7.70 Hz), 12.24 (21, 2H, Ph: *o*−*CH*), 17.11 (8, 1H, Tp*−*CH*), 20.55 (8, 1H, Tp*−*CH*), 27.32 (32, 2H, Bn: *m*/*o*−*CH*), 55.96 (13, 3H, Tp*−CH_3), 75.66 (4, 1H, Tp*−*CH*). ^{11}B NMR (C_6D_6, 25 °C): δ (ppm) = −28.68. IR (KBr): ν_{B-H} = 2556, 2512 cm^{-1}; $\nu_{C=O}$ = 1698 cm^{-1}. **3-Ph**: Elemental analysis of $C_{53}H_{58}B_2N_{14}OU$, Calculated, C, 49.53; H, 5.22; N, 18.81. Found, C 48.67; H, 5.13; N, 17.37. ^{1}H NMR (C_6D_6, 25 °C): δ = −32.97 (49, 6H, Tp*−CH_3), −11.32 (153, B-*H*), −9.67 (17, 6H, Tp*−CH_3), −3.12 (5, 6H, Tp*−CH_3), −2.25 (8, 6H, Tp*−CH_3), −1.10 (13, 2H, Tp*−*CH*), 0.27 (3, 6H, Tp*−CH_3), 0.54 (7, 2H, Tp*−*CH*), 6.94 (t, 2H, *p*−*CH*, J = 6.88 Hz), 9.51 (17, 4H, *m*−*CH*), 10.53 (173, 4H, *o*−*CH*), 19.51 (16, 2H, Tp*−*CH*), 32.05 (20, 6H, Tp*−CH_3). ^{11}B NMR (C_6D_6, 25 °C): δ (ppm) = −49.62. IR (KBr): ν_{B-H} = 2557, 2521 cm^{-1}; $\nu_{C=O}$ = 1707 cm^{-1}. **3-pTol**: Elemental analysis of $C_{44}H_{56}B_2N_{14}OU$, Calculated, C, 50.01; H, 5.34; N, 18.56. Found, C 49.23; H, 5.00; N, 18.86 ^{1}H NMR (C_6D_6, 25 °C): δ = −33.88 (8, 3H, Tp*−CH_3), −32.52 (46, 3H, Tp*−CH_3), −11.13 (23, B-*H*), −10.73 (21, B-*H*), −9.57 (75, 3H, Tp*−CH_3), −9.35 (28, 3H, Tp*−CH_3), −3.05 (53, 3H, Tp*−CH_3), −2.88 (7, 3H, Tp*−CH_3), −2.45 (9, 3H, Tp*−CH_3), −1.34 (5, 1H, Tp*−*CH*), −1.12 (152, 3H, Tp*−CH_3), 0.09 (4, 3H, Tp*−CH_3), 0.41 (6, 1H, Tp*−*CH*), 0.78 (6, 3H, Tp*−CH_3), 1.87 (3, 1H, Tp*−*CH*), 2.74 (3, 1H, Tp*−*CH*), 4.78 (6, 3H, −CH_3), 6.57 (t, 1H, Ph: *p*−*CH*, J = 7.07 Hz), 8.83 (d, 2H, Ph: *m*−*CH*, J = 6.23 Hz), 9.03 (d, 2H, Ph: *o*−*CH*, J = 7.29 Hz), 10.13 (d, 2H, *p*Tol: *m*−*CH*, J = 6.30 Hz), 11.90 (d, 2H, *p*Tol: *o*−*CH*, J = 7.20 Hz), 19.26 (15, 1H, Tp*−*CH*), 19.44 (38, 1H, Tp*−*CH*), 29.34 (72, 3H, Tp*−CH_3), 33.34 (1552, 3H, Tp*−CH_3). ^{11}B NMR (C_6D_6 25 °C): δ (ppm) = −48.41. IR (KBr): ν_{B-H} = 2561, 2507 cm^{-1}; $\nu_{C=O}$ = 1711 cm^{-1}.

Synthesis of Tp*$_2$U(IV) κ^2-Thioureato Compounds. A 20 mL scintillation vial was charged with Tp*$_2$UNR (R = Bn: 0.060 g, 0.064 mmol; Ph: 0.067 g, 0.073 mmol; *p*Tol: 0.100 g, 0.107 mmol) and 10 mL of THF. To the deep red solution, 1 equiv of phenylisothiocyanate (R = Bn: 0.011 mL, 0.064 mmol; Ph: 0.010 mL, 0.073 mmol; *p*Tol: 0.013 mL, 0.11 mmol) was added via microsyringe, and the reaction mixture was stirred for 15 min, creating a red-orange solution. Volatiles were removed *in vacuo*. The crude mixtures were washed with pentane (2 × 10 mL) to afford orange powders assigned as Tp*$_2$U[κ^2-(*N*,*N*′-1-phenyl-3-benzylthioureato)] (**4-Bn**), Tp*$_2$U[κ^2-(*N*,*N*′-diphenylthioureato)] (**4-Ph**), or Tp*$_2$U[κ^2-(*N*,*N*′-1-phenyl-3-*para*-tolylthioureato)] (**4-pTol**) (**4-Bn**: 0.062 g, 0.058 mmol, 90% yield; **4-Ph**: 0.073 g, 0.069 mmol, 96% yield; **4-pTol**: 0.102 g, 0.095 mmol, 89% yield). Red single crystals of **4-Ph**, which were suitable for X-ray diffraction, were grown from a concentrated benzene solution at room temperature. **4-Bn**: Reliable elemental analysis could not be obtained due to incomplete combustion: Elemental analysis of $C_{44}H_{56}N_{14}B_2SU$, Calculated C, 49.26; H, 5.26; N, 18. 28, Found, C, 45.41; H, 5.18; N, 16.96. ^{1}H NMR (C_6D_6, 25 °C): δ = −37.47 (19, 3H, Tp*−CH_3), −29.04 (19, 3H, Tp*−CH_3), −16.47 (204, B-*H*), −10.71 (16, 3H, Tp*−CH_3), −10.26 (15, 3H, Tp*−CH_3), −9.46 (77, 3H, Tp*−CH_3), −5.25 (15, 3H, Tp*−CH_3), −3.77 (26, 3H, Tp*−CH_3), −3.51 (17, 1H, Tp*−*CH*), −3.42 (77, 1H, Tp*−*CH*), −2.08 (15, 1H, Tp*−*CH*), −1.65 (16, 3H, Tp*−CH_3), −1.25 (15, 3H, Tp*−CH_3), 3.86 (29, 2H, −CH_2Ph), 4.69 (18, 2H, Bn: *m*/*o*−*CH*), 6.70 (28, 1H, Ph: *p*−*CH*), 7.42 (19, 3H, Tp*−CH_3), 7.78 (27, 2H, Ph: *m*/*o*−*CH*), 9.21 (25, 2H, Ph: *m*/*o*−*CH*), 15.27 (18, 3H, Tp*−CH_3), 18.71 (14, 1H, Tp*−*CH*), 22.05 (66, 1H, Bn: *p*−*CH*), 22.21 (24, 2H, Bn: *m*/*o*−*CH*), 49.66 (20, 3H, Tp*−CH_3),) 61.95 (35, 1H, Tp*−*CH*), 77.78 (36, 1H, Tp*−*CH*). ^{11}B NMR (C_6D_6, 25 °C): δ = −49.47. IR (KBr): ν_{B-H} = 2561, 2525 cm^{-1}; $\nu_{C=S}$ = 1542 cm^{-1}. **4-Ph**: Elemental analysis of $C_{51}H_{64}N_{14}B_2SU$, Calculated C, 48.78; H, 5.14; N, 18.52, Found, C, 47.48; H, 4.97; N, 17.42. ^{1}H NMR (C_6D_6, 25 °C): δ = −34.67 (6, 6H, Tp*−CH_3), −12.30 (133, B-*H*), −10.32 (9, 6H, Tp*−CH_3), −3.76 (3, 6H, Tp*−CH_3), −2.61 (6, 6H, Tp*−CH_3), −2.57 (4, 2H, Tp*−*CH*), 0.10 (1, 2H, Tp*−*CH*), 0.31 (3, 6H, Tp*−CH_3), 6.66 (t, 2H, *p*−*CH*, J = 7.27 Hz), 8.90 (t, 4H, *m*−*CH*, J = 7.07 Hz), 11.09 (d, 4H, *o*−*CH*, J = 7.12 Hz), 20.45 (3, 2H, Tp*−*CH*), 34.34 (17, 6H, Tp*−CH_3). ^{13}B NMR (C_6D_6, 25 °C): δ = −48.31. IR (KBr): ν_{B-H} 2565, 2519 cm^{-1}; $\nu_{C=S}$ 1542 cm^{-1}. **4-pTol**: Elemental analysis of $C_{51}H_{64}N_{14}B_2SU$, Calculated C, 49.26; H, 5.26; N, 18. 28, Found, C, 48.45; H, 5.39; N, 17.64. ^{1}H NMR (C_6D_6, 25 °C): δ = −35.25 (6, 3H, Tp*−CH_3), −34.05 (14, 3H, Tp*−CH_3), −12.73 (152, B-*H*), −11.87 (138, B-*H*), −10.37 (5, 3H, Tp*−CH_3), −10.25 (9, 3H, Tp*−CH_3), −3.95 (4, 3H, Tp*−CH_3), −3.48 (3, 3H, Tp*−CH_3), −3.44 (10, 3H, Tp*−CH_3), −2.62 (8, 2H, Tp*−*CH*), −1.83 (5, 3H, Tp*−CH_3), 0.07 (2, 1H, Tp*−*CH*), 0.13 (3, 3H, Tp*−CH_3), 0.60 (3, 3H, Tp*−CH_3), 0.77 (2, 1H, Tp*−*CH*), 4.16 (3, 3H, −CH_3), 6.40 (t, 1H, Ph: *p*−*CH*, J = 7.45 Hz), 8.60 (t, 2H, Ph: *m*−*CH*, J = 7.48 Hz), 9.13 (d, 2H, Ph: *o*−*CH*, J = 7.44 Hz), 10.05 (d, 2H, *p*Tol: *m*−*CH*, J = 7.58 Hz), 11.83 (2H, *p*Tol: *o*−*CH*, J = 7.76 Hz), 20.34 (3, 1H, Tp*−*CH*), 20.49 (3, 1H, Tp*−*CH*), 32.84 (11, 3H, Tp*−CH_3), 35.73 (14, 3H, Tp*−CH_3). ^{11}B NMR (C_6D_6, 25 °C): δ = −51.34. IR (KBr): ν_{B-H} = 2563, 2517 cm^{-1}; $\nu_{C=S}$ 1542 cm^{-1}.

Synthesis of Tp*$_2$U(IV) κ^2-Selenoureato Compounds. A 20 mL scintillation vial was charged with Tp*$_2$UNR (R = Ph: 0.080 g, 0.087 mmol; *p*Tol: 0.07 g, 0.075 mmol) and 10 mL of THF. To the deep red solution, 1 equiv of phenyl isoselenocyanate (R = Ph: 0.016 g, 0.087 mmol; 0.014 g *p*Tol, 0.075 mmol) was added via microsyringe, and the reaction mixture was allowed to stir for 8 h, creating a red-orange solution. Volatiles were removed *in vacuo*, and crude products were washed with pentane (4 × 10 mL) to yield orange powders, assigned as Tp*$_2$U[κ^2-(*N*,*N*′-diphenylselenoureato)] (**5-Ph**) or Tp*$_2$U[κ^2-(*N*,*N*′-1-phenyl-3-*para*-tolylselenoureato)] (**5-pTol**) (**5-Ph**: 0.077 g, 0.070 mmol, 80% yield; **5-pTol**: 0.062 g, 0.055 mmol, 74% yield). Single crystals of **5-Ph**, suitable for X-ray diffraction, were obtained from a concentrated benzene solution at room temperature. **5-Ph**: Reliable elemental analysis could not be obtained due to the instability of compound **5-Ph**. ^{1}H NMR (C_6D_6, 25 °C): δ −34.93 (5, 6H, Tp*−CH_3), −12.70 (137, B-*H*), −10.52 (2, 6H, Tp*−CH_3), −3.75 (4, 6H, Tp*−CH_3), −2.91 (2, 2H, Tp*−*CH*), −2.83 (47, 6H, Tp*−CH_3), 0.31 (2, 6H, Tp*−CH_3), 0.46 (2, 2H, Tp*−*CH*), 6.68 (t, 2H, *p*−*CH*, J = 7.49 Hz), 8.87 (t, 4H, *m*−*CH*, J = 7.54 Hz), 11.46 (d, 4H, *o*−*CH*, J = 7.63 Hz), 20.63 (52, 2H, Tp*−*CH*), 34.94 (19, 6H, Tp*−CH_3). ^{11}B NMR (C_6D_6, 25 °C): δ = −51.62. IR (KBr): ν_{B-H} = 2566, 2508 cm^{-1}; $\nu_{C=Se}$ = 1542 cm^{-1}. **5-pTol**: Reliable elemental analysis could not be obtained due to the instability of compound **5-pTol**. ^{1}H NMR (C_6D_6, 25 °C): δ −35.44 (17, 3H, Tp*−CH_3), −34.42 (8, 3H, Tp*−CH_3), −14.10 (19, B-*H*), −10.58 (2, 3H, Tp*−CH_3), −10.48 (18, 3H, Tp*−CH_3), −4.00 (2, 3H, Tp*−CH_3), −3.58 (2, 3H, Tp*−CH_3), −3.48 (3, 3H, Tp*−CH_3), −2.97 (2, 1H, Tp*−*CH*), −2.96 (3, 1H, Tp*−*CH*), −2.15 (3, 3H, Tp*−CH_3), 0.10 (2, 3H, Tp*−CH_3), 0.17 (2, 1H, Tp*−*CH*), 0.50 (2, 3H, Tp*−CH_3), 0.76 (2, 1H, Tp*−*CH*), 4.07 (2, 3H, −CH_3), 6.46 (t, 1H, Ph: *p*−*CH*, J = 7.47 Hz), 8.59 (t, 2H, Ph: *m*−*CH*, J = 7.59 Hz), 9.00 (d, 2H, Ph: *o*−*CH*, J = 7.55 Hz), 10.58 (d, 2H, *p*Tol: *m*−*CH*, J = 7.84 Hz), 12.07 (d, 2H, *p*Tol: *o*−*CH*, J = 7.56 Hz), 20.53 (2, 1H, Tp*−*CH*), 20.66 (28, 1H, Tp*−*CH*), 33.66 (7, 3H, Tp*−CH_3), 36.17 (9, 3H, Tp*−CH_3). ^{13}B NMR (C_6D_6, 25 °C): δ = −52.78. IR (KBr): ν_{B-H} = 2564, 2522 cm^{-1}; $\nu_{C=Se}$ = 1542 cm^{-1}.

Synthesis of Tp*$_2$U[κ^2-(*N*,*N*′-1-phenyl-3-dippureato)] (6). A 20 mL scintillation vial was charged with Tp*$_2$U(NPh) (0.085 g, 0.092 mmol) and 10 mL of THF. To the deep red solution, 1 equiv of dipp isocyanate (0.020 mL, 0.092 mmol) was added via microsyringe, and the reaction mixture was allowed to stir for 10 min, creating a red-orange solution. Volatiles were removed *in vacuo*, and the crude products were washed with pentane (4 × 10 mL) to yield an orange powder, assigned as Tp*$_2$U[κ^2-(*N*,*N*′-1-phenyl-3-dippureato)] (**6**) (0.084 g, 0.075 mmol, 81% yield). Reliable elemental analysis could not be obtained due to the instability of compound **6**. ^{1}H NMR (C_6D_6, 25 °C): δ = −43.81 (6, 3H, Tp*−CH_3), −28.72 (9, 3H, Tp*−CH_3), −24.80 (160, B-*H*), −17.21 (4, 3H, Tp*−CH_3), −15.71 (6, 3H, Tp*−CH_3), −14.60 (3, 1H, dipp: *i*-PrC*H*), −13.63 (4, 3H, Tp*−CH_3), −10.82 (3, 3H, Tp*−CH_3), −9.89 (d, 2H, dipp: *m*−*CH*, J = 8 Hz),

DOI: 10.1021/acs.inorgchem.6b02947
Inorg. Chem. 2017, 56, 1956−1965

−7.84 (3, 1H, Tp*−*CH*), −7.59 (3, 3H, Tp*−*CH*$_3$), −7.52 (3, 1H, Tp*−*CH*), −2.33 (4, 1H, Tp*−*CH*), −1.56 (4, 3H, dipp−*CH*$_3$), −1.11 (3, 3H, dipp−*CH*$_3$), 1.98 (3, 3H, Tp*−*CH*$_3$), 3.57 (8, 3H, Tp*−*CH*$_3$), 5.11 (5, 1H, Tp*−*CH*), 5.67 (5, 1H, Tp*−*CH*), 10.86 (29, 3H, dipp−*CH*$_3$), 11.24 (38, 5H, Ph: *m*/*o*−*CH* + dipp−*CH*$_3$), 13.30 (9, 3H, Tp*−*CH*$_3$), 17.80 (7, 3H, Tp*−*CH*$_3$), 17.90 (t, 1H, dipp: *p*−*CH*, J = 8 Hz), 19.06 (3, 1H, Tp*−*CH*), 21.71 (4, 1H, dipp: *i*-Pr*CH*), 30.26 (5, 1H, Tp*−*CH*), 73.20 (11, 3H, Tp*−*CH*$_3$). ^{11}B NMR (C_6D_6, 25 °C): δ = −43.72. IR (KBr): ν_{B-H} = 2563, 2519 cm^{-1}; $\nu_{C=O}$ = 1695 cm^{-1}.

RESULTS AND DISCUSSION

Synthesis of Terminal Uranium(IV) Imido Derivatives. Building on our previous work describing the synthesis of Tp*$_2$UNPh (**2-Ph**), Tp*$_2$UNMes (**2-Mes**), and Tp*$_2$UNAd (**2-Ad**), initial experiments were aimed at extending this family of uranium(IV) imido species to include greater variation in their steric and electronic properties. Thus, Tp*$_2$UBn (**1-Bn**) was treated with organoazides, N_3R (R = Bn, *p*Tol, detp, dipp), which caused immediate bubbling of the solution indicative of nitrogen gas evolution (eq 1). As with formation of **2-Ph** and **2-Mes**, one-half equivalent of bibenzyl was observed by ^{1}H NMR spectroscopy, supporting that oxidation to the corresponding uranium(IV) imido compounds, Tp*$_2$UNR (R = Bn (**2-Bn**), *p*-Tol (**2-*p*Tol**), detp (**2-detp**), dipp (**2-dipp**)) had occurred. This process gave products as purple (**2-Bn**, **2-detp**, **2-dipp**) or red-violet (**2-*p*Tol**) solids in good yields (65%−82%). Alternatively, the series can be synthesized from Tp*$_2$UI and N_3R with subsequent addition of KC_8 (82−87%).[24]

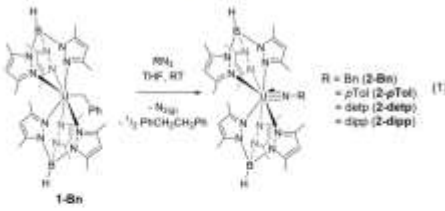

(1)

As previously reported for **2-Ph**, infrared spectroscopic data for **2-Bn**, **2-*p*Tol**, **2-detp**, and **2-dipp** show two ν_{B-H} stretches (2518−2560 cm^{-1}), confirming the presence of two Tp* ligands. Analysis of these species by ^{1}H NMR spectroscopy shows paramagnetically broadened and shifted spectra with the number of resonances and their integration values consistent for C_3 symmetry. ^{11}B NMR spectroscopy shows resonances for **2-Bn**, **2-*p*Tol**, **2-detp**, and **2-dipp** (−64.75, −66.60, −76.92, and −75.35 ppm, respectively), consistent with previously reported Tp* uranium(IV) compounds[14,33] and analogous to **2-Ph** (−66.81 ppm). These resonances are shifted significantly from the corresponding precursor uranium(III) complexes (**1-Bn** = −15.39 ppm; Tp*$_2$UI = 3.86 ppm), which indicates that oxidation of the uranium(III) ion has taken place.

In an effort to evaluate the structural properties of these new entries in the uranium(IV) imido family, single crystals of each were obtained either from diffusion of diethyl ether into a solution of toluene at −35 °C (**2-Bn**, **2-*p*Tol**, **2-detp**) or from a concentrated solution of diethyl ether at −35 °C (**2-dipp**) and analyzed by X-ray crystallography (Figure 1). Refinement of data collected for **2-Bn**, **2-*p*Tol**, **2-detp**, and **2-dipp** displayed a series of analogous distorted pentagonal bipyramidal uranium(IV) imido species that feature two κ^2-Tp* ligands per uranium center (**2-Bn** - U−$N_{pyrazole}$: 2.533(2)−2.737(2) Å; **2-*p*Tol** - U−$N_{pyrazole}$: 2.526(6)−2.786(6) Å; **2-detp** - 2.511(9)−2.727(10) Å; **2-dipp** (2.533(6)−2.681(6) Å). The U=N_{imido} distances (**2-Bn** - U=N_{imido}: 1.972(2) Å; **2-*p*Tol** - U=N_{imido}: 2.011(9) Å, **2-detp** - U=N_{imido}: 2.004(12) Å; **2-dipp** - U=N_{imido}: 2.003(7) Å) are consistent with other uranium(IV) imido complexes, including Cp*$_3$U(NMes*) (Cp* = [η^5-C_5Me_5], Mes* = 2,4,6-$tBu_3C_6H_2$) (1.952(12) Å),[36] Tp*$_2$U(NMes) (1.976(3) Å),[24] Cp′$_2$U(N*p*Tol) (Cp′ = η^5-1,2,4-$(Me_3C)_3C_5H_2$) (1.988(5) Å),[37] and $(OPPh_3)_3U(NMes^*)Cl_2$ (2.009(3) Å).[38] The U1−N_{imido}−C_{imido} bond angles for **2-Bn** (165.7(2)°), **2-detp** (173.8(9)°), **2-dipp** (180.0°), and **2-*p*Tol** (163.6(9)°) are on the order of bond angles observed for other uranium(IV) imido complexes, including Cp*$_2$U(Ndipp) (172.6(5)°),[39] Cp′$_2$U(N*p*Tol) (172.3(5)°),[37] Tp*U(NMes)(Bn)(THF) (177.7(5)°),[40] and U(Ndipp)(I)$_2$(THF)$_4$ (178.9(2)°).[41]

The optical properties of complexes **2-Bn**, **2-*p*Tol**, **2-detp**, and **2-dipp** were examined by electronic absorption spectroscopy. Data for the series were recorded in THF over the range 300−1800 nm at ambient temperature. The spectra exhibited analogous weak, but sharp f−f transitions in the near-infrared range (800−1800 nm), consistent with previously reported Tp*$_2$-U(IV) compounds,[24] as well as bands in the visible region (**2-Bn**: 518 nm (884 M^{-1} cm^{-1}); **2-*p*Tol**: 514 nm (1103 M^{-1} cm^{-1}); **2-detp**: 544 nm (514 M^{-1} cm^{-1}); **2-dipp**: 549 nm (2500 M^{-1} cm^{-1})) (Figure S1) that are responsible for their red-purple appearance.

A computational analysis of the extent of steric crowding of the uranium center for the new imido series was possible using Solid-G,[42,43] which calculates the percentage of a metal's coordination sphere blocked by its ligand(s) based on

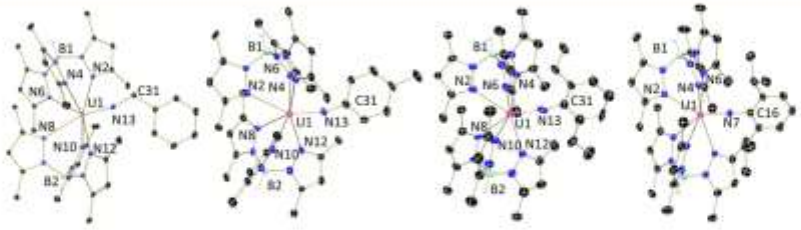

Figure 1. Molecular structures of **2-Bn**, **2-*p*Tol**, **2-detp**, and **2-dipp** (left to right), displayed with 30% probability ellipsoids. Selected hydrogen atoms and cocrystallized solvent molecules have been omitted for clarity.

DOI: 10.1021/acs.inorgchem.6b02947
Inorg. Chem. 2017, 56, 1956−1965

parameters obtained from experimental molecular structures. This analysis was performed to compare the relative size of the imido substituent for **2-*p*Tol**, **2-detp**, and **2-dipp**, and the results obtained as the G(imido) value are presented in Table 1,

Table 1. Solid Angle Parameters Obtained from Crystallographic Data Using Solid G[a]

	2-*p*Tol	2-detp	2-dipp
U=N dist (Å)	2.011(9)	2.004(12)	2.003(7)
G(imido), %	17.44	19.93	22.20
G(Tp*), %	38.00	38.20	37.85
	38.23	37.94	37.86
G(complex), %	87.98	90.58	91.66

[a]Experimental uranium−nitrogen multiple bond distances are presented for comparison.

along with the uranium-imido multiple bond distances. The results show that, for the aryl imido series, in moving from **2-*p*Tol**, **2-detp**, and **2-dipp**, the percentage of shielding increases steadily, as expected for the respective *ortho*-H, -Et, and -*i*Pr groups. The G(complex) value represents the sum of all ligands and takes absolute sphere shielding into account by shielding of any ligands.[42,43] Thus, this value also trends similarly to the G(imido), where there is a steady increase in the shielding percentage from **2-*p*Tol**, **2-detp**, and **2-dipp**, as expected.

[2π+2π] Cycloaddition with the Tp*$_2$UNR Family. With an understanding of the relative steric demands of these new entries in the uranium(IV) imido family, their reactivity for [2π+2π] cycloaddition chemistry was probed (Scheme 1). The first study was performed by treating **2-Ph** with PhNCE (E = O, S, Se), as this should produce a series of symmetric phenyl urea cycloaddition products. Upon addition of PhNCO to **2-Ph**, rapid reaction was observed, signified by a color change from red to orange in only 15 min. Following workup, analysis of the obtained product by ^{1}H NMR spectroscopy revealed 13 broad resonances ranging from −32.97 to 32.05 ppm, consistent with C_2 symmetry. Six resonances assignable as Tp*−C*H*$_3$ protons and three resonances for Tp*−C*H* are observed, as well as one broad signal for the B-*H* protons (−11.32 ppm). Analysis by ^{11}B NMR spectroscopy gives a spectrum that displays a single resonance at −49.62 ppm for symmetric Tp* ligands in solution. Infrared spectroscopy in the solid state (KBr pellet) confirmed the presence of two Tp* ligands (ν_{B-H} = 2557 cm^{-1}; 2521 cm^{-1}) and provided evidence for a carbonyl moiety ($\nu_{C=O}$ = 1708 cm^{-1}), leading to the assignment of the orange powder as the κ^2-ureato complex Tp*$_2$U[κ^2-(*N*,*N*′-diphenylureato)] (**3-Ph**) (Scheme 1).

The next experiments were aimed at exploring analogous reactivity with phenylisothiocyanate, as the thione should be less nucleophilic and potentially less reactive. Thioureato complexes displaying various coordination modes[44,45] have been synthesized previously by salt metathesis[46] and [2π+2π] cycloaddition.[19] Treating **2-Ph** with PhNCS afforded C_2 symmetric Tp*$_2$U[κ^2-(*N*,*N*′-diphenylthioureato)] (**4-Ph**) as an orange powder (82%). The ^{1}H and ^{11}B NMR spectra reveal peak distributions and symmetries that are analogous to the oxygen analogue, **3-Ph**. Infrared spectroscopy confirms retention of Tp* by similar ν_{B-H} stretches (2565 cm^{-1}; 2519 cm^{-1}) to **3-Ph**, while the $\nu_{C=S}$ stretch at 1542 cm^{-1} supports formation of the cycloaddition product.[47]

Due to the scarcity of κ^2-selenourato as ligands in organometallic chemistry, formation of the uranium(IV) κ^2-selenoureate was targeted by the same method. Treating **2-Ph** with phenylisoselenocyanate (PhNCSe) produced the desired κ^2-selenoureato complex, Tp*$_2$U[κ^2-(*N*,*N*′-diphenylselenourea-to)] (**5-Ph**), albeit with a slightly longer reaction time (8 h). Analyses by ^{1}H and ^{11}B NMR spectroscopy confirmed the formation of **5-Ph** by analogy to complexes **3-Ph** and **4-Ph** based on the peak distribution and their integration values. Retention of bound Tp* ligands was supported by IR spectroscopy, which showed similar B−H stretches (**5-Ph** = 2566, 2508 cm^{-1}) to **3-Ph** and **4-Ph**. The stretch for C=Se ($\nu_{C=Se}$; **5-Ph** = 1542 cm^{-1}) is consistent with previous reports of carbon−selenium multiple bonds ($\nu_{C=Se}$; 1529−1570 cm^{-1}).[30,47,48] The longer reaction times required for PhNCSe as compared to PhNCO or PhNCS for **2-Ph** may be attributed to either the decreased nucleophilicity of the C=Se or the increased size of selenium as compared to oxygen and sulfur. Complex **5-Ph** represents the first reported crystal structure of a selenoureato ligand in the κ^2-coordination mode, although examples have been reported in the liquid[49] and gas phases.[50] Such ligands have been reported with binding through selenium in an end-on (κ^1) fashion with antimony,[51] cobalt,[52] gold,[53,54] mercury,[55] palladium,[56] and platinum.[56]

A comparison of the ^{1}H NMR spectra across the series of compounds **3-Ph** to **5-Ph** is presented in Figure 2. As discussed, C_2 symmetry is retained in solution across the series, with six resonances (6H each) for the *endo*- and *exo*-Tp* methyl groups and three resonances (2H each) for the CH protons of Tp*. For each compound, the phenyl protons are visible as three resonances between 6 and 12 ppm, including a

Scheme 1. [2π+2π] Cycloaddition Chemistry of the Tp*$_2$UNR Family

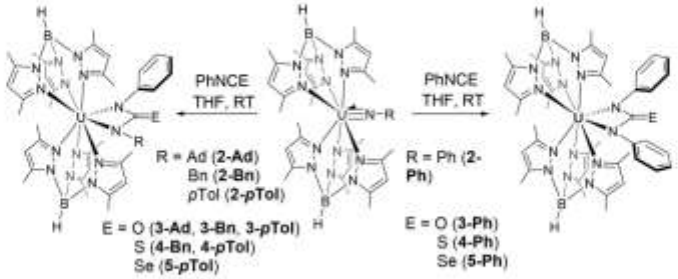

DOI: 10.1021/acs.inorgchem.6b02947
Inorg. Chem. 2017, 56, 1956−1965

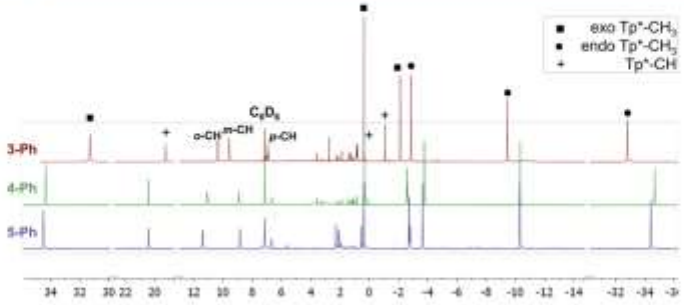

Figure 2. Stacked ^{1}H NMR spectra (in ppm) of **3-Ph**, **4-Ph**, and **5-Ph** taken in C_6D_6 at ambient temperature.

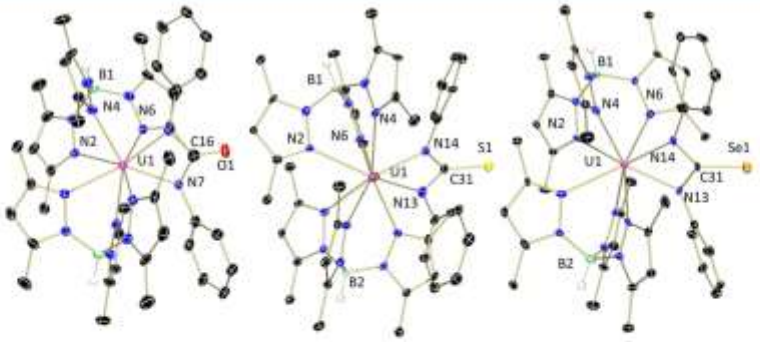

Figure 3. Molecular structures of **3-Ph** (left), **4-Ph** (middle), and **5-Ph** (right), displayed with 30% probability ellipsoids. Selected hydrogen atoms and cocrystallized solvent molecules have been omitted for clarity.

doublet (4H), triplet (4H), and triplet (2H) for the *ortho*, *meta*, and *para* protons, respectively. While previous studies across the chalcogenide series generally show a trend in chemical shift as the column is descended (i.e., $Cp^*_3U(EPh)_2$, (E = S, Se, Te)),[17] a smooth progression is not noted in this case, as the data for **5-Ph** seems to lie in between that of **3-Ph** and **4-Ph**.

To compare structural parameters among the symmetric diphenylureato series, the molecular structures of **3-Ph**, **4-Ph**, and **5-Ph** were elucidated using single crystal X-ray crystallography (Figure 3). All three compounds show analogous structures, each exhibiting square antiprismatic geometries. As is commonly observed for bis(Tp*) uranium complexes, each ligand features two long $U-N_{pyrazole}$ distances (2.565−2.673 Å) and one short $U-N_{pyrazole}$ distance (2.460−2.485 Å).[20] The κ^2-ureato ligands have two U−N bond distances that are in the range 2.301−2.394 Å, showing a significant bond elongation as compared to typical uranium(IV) imidos, which is expected based on the cleavage of the π-bonds. The C═E double bond distance increases (**3-Ph** = 1.231(13) Å; **4-Ph** = 1.699(7) Å; **5-Ph** = 1.840(6) Å), and the N−C−N bond angles decrease (**3-Ph** = 59.4(5)°; **4-Ph** = 56.26(16)°; **5-Ph** = 56.6(2)°) as the chalcogenide group is descended, corresponding to the increase in the ionic radius.

The structural parameters of **3-Ph** are best compared with (κ^2-1-Mes-3-dipp-NC(O)N)U(Cl)$_2$(OPPh$_3$)$_2$, since both species have U(IV) ions. In the latter case, the U−N ureato distances of 2.259(4) and 2.263(4) Å are on the order of those in **3-Ph** (*cf.* 2.340(17) Å). However, the symmetric uranium(V) ureato, ((^{tBu}ArO)$_3$tacn)U(κ^2-*N*,*N*-diphenylurea), shows $U-N_{ureato}$ bond distances (2.310(4) and 2.329(4) Å) that are remarkably similar to **3-Ph**. When examining metrical parameters of both literature examples, it appears that a sterically encumbered uranium center produces longer bond distances and a smaller bond angle in order to accommodate the bulky κ^2-coordinated ligand. The longer ureato bond lengths observed for the sterically crowded tacn compound are similar to that for **3-Ph**, despite the smaller ionic radius of the uranium(V) ion, indicating that sterics play a significant role in urea ligand binding. The thiourea derivative, **4-Ph**, is the second entry of a κ^2-thioureato ligand that has been characterized in the solid state. The other example features a molybdenum complex with a κ^2-thioureato ligand (Mo[κ^2-(*N*,*N*′(1-phenyl-3-dipp)thioureato)](Ndipp)(OBu^t)$_2$), formed as a result of cycloaddition of an isothiocyanate with a molybdenum bis-imido compound.[18]

Similar reactivity with PhNCO was observed for the rest of the imido family, specifically **2-Ad**, **2-Bn**, and **2-*p*Tol**, resulting in asymmetric ureato ligands, generating Tp*$_2$U[κ^2-(*N*,*N*′(1-phenyl-3-adamantylureato)] (**3-Ad**), Tp*$_2$U[κ^2-(*N*,*N*′(1-phenyl-3-benzylureato)] (**3-Bn**), and Tp*$_2$U[κ^2-(*N*,*N*′(1-phenyl-

DOI: 10.1021/acs.inorgchem.6b02947
Inorg. Chem. 2017, 56, 1956−1965

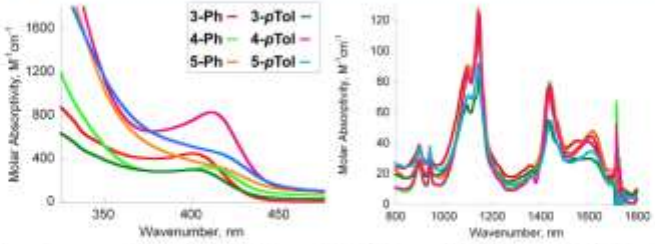

Figure 4. Electronic absorption spectra of **3-Ph** (red), **3-*p*Tol** (dark green), **4-Ph** (light green), **4-*p*Tol** (magenta), **5-Ph** (orange), and **5-*p*Tol** (blue) recorded from 300 to 1800 nm in THF at 25 °C.

Scheme 2. Depiction of Mechanistic Pathways Possible for [2π+2π] Cycloaddition

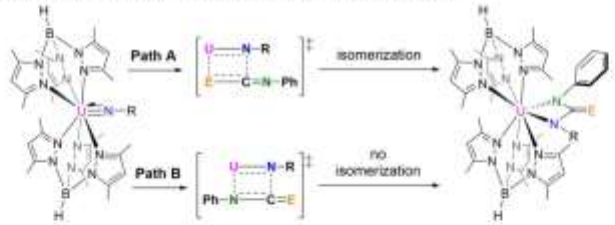

3-(*p*-tolyl)ureato))] (**3-*p*Tol**). As expected, based on the asymmetry of the ureato ligand, C_s symmetric ^{1}H NMR spectra are observed. Analysis by ^{11}B NMR spectroscopy shows resonances similar to **3-Ph** (−29 ppm (**3-Bn**); −48 ppm (**3-*p*Tol**)), supporting analogous cycloaddition chemistry occurred. Infrared spectroscopic data for **3-Ad** ($\nu_{C=O}$ = 1696 cm^{-1}, ν_{B-H} = 2559, 2515 cm^{-1}), **3-Bn** ($\nu_{C=O}$ = 1698 cm^{-1}, ν_{B-H} = 2556, 2512 cm^{-1}), and **3-*p*Tol** ($\nu_{C=O}$ = 1711 cm^{-1}, ν_{B-H} = 2561, 2507 cm^{-1}) are analogous to those recorded for **3-Ph**. IR spectroscopic analysis also confirmed that both Tp* ligands revert to their typical κ^3-bonding modes upon cycloaddition with **2-Ad** to form **3-Ad**, consistent with our previous studies.[39]

To expand the family of known thiourea derivatives, **2-*p*Tol** and **2-Bn** were also treated with PhNCS, which afforded asymmetric Tp*$_2$U[κ^3-(*N*,*N*′-(1-phenyl-3-(*p*-tolyl)-thioureato))] (**4-*p*Tol**) and Tp*$_2$U[κ^2-(*N*,*N*′(1-phenyl-3-benzyl)thioureato)] (**4-Bn**). As for **3-*p*Tol** and **3-Bn**, the ^{1}H NMR spectra are complicated by the asymmetry in the thiourea ligand, but the chemical shifts in the ^{11}B NMR spectra are as expected based on **4-Ph**. Infrared data confirms the presence of two Tp* ligands in each case, with similar ν_{B-H} stretches (**4-*p*Tol**: 2563, 2517 cm^{-1}; **4-Bn**: 2561, 2525 cm^{-1}) to **3**. Both compounds also display $\nu_{C=S}$ stretches at 1542 cm^{-1} that are consistent with previously reported values.[47]

Cycloaddition of PhNCSe to **2-*p*Tol** furnished the asymmetric κ^2-selenoureato complex Tp*$_2$U[κ^2-(*N*,*N*′-(1-phenyl-3-(*p*-tolyl)selenoureato))] (**5-*p*Tol**). As in the formation of **5-Ph**, cycloaddition with PhNCSe required longer reaction times (up to 8 h) to reach conversion. Analysis by ^{1}H and ^{11}B NMR spectroscopy confirmed the formation of **5-*p*Tol** in analogy to complex **5-Ph**, while the retention of bound Tp* ligands was aided by IR spectroscopy (ν_{B-H}: **5-*p*Tol** = 2564, 2522 cm^{-1}). The absorption for the C = Se double bond in **5-*p*Tol** was found at 1542 cm^{-1} and is consistent with previous reports ($\nu_{C=Se}$: 1529−1570 cm^{-1}).[30,47,48]

The orange THF solutions of all cycloaddition products were studied by electronic absorption spectroscopy at ambient temperature from 300 to 1800 nm, and the data for **3-Ph**, **3-*p*Tol**, **4-Ph**, **4-*p*Tol**, **5-Ph**, and **5-*p*Tol** are presented in Figure 4 (data for **3-Ad**, **3-Bn**, and **4-Bn** are displayed in Figure S2). Overall, the entire family displays minimal variations regardless of the identity of the chalcogen, indicating analogous electronic structures. Examination of the near-infrared region (800−1800 nm) revealed sharp, sharp f−f transitions for all eight compounds, consistent with a U(IV), f^2 configuration (Figure 4).[39] All complexes display weak visible absorbances or shoulders ranging from 410 to 415 nm, which are likely responsible for the orange appearance of all of the products.

The [2π+2π] cycloaddition reaction likely proceeds through one of two possible pathways (Scheme 2). As shown in **Path A**, the isocyanate fragment could approach uranium in an end-on fashion leading with the chalcogen, which would be the sterically preferred configuration. Following cycloaddition, isomerization of the new κ^2-*N*,*E*-ureate ligand could occur, generating the observed κ^2-*N*,*N*-ureato species. In the sterically less preferred scenario, **Path B**, the isocyanate could line up with the hydrocarbon pointed toward the uranium, with cycloaddition proceeding to directly generate the κ^2-*N*,*N*-ureato complexes without the need for isomerization. Based on the steric accessibility of the uranium center in the family of imido derivatives, as well as the literature precedent for ligand isomerization,[22,23] we hypothesize that **Path A** is the more likely mechanism for the [2π+2π] cycloaddition reaction studied here.

DOI: 10.1021/acs.inorgchem.6b02947
Inorg. Chem. 2017, 56, 1956−1965

To further our mechanistic inquiry, the reactivity of the last member, **2-dipp**, toward PhNCO was also examined. In this case, the anticipated κ^2-ureato derivative was not produced; instead, no reaction was observed even after prolonged heating at 110 °C for 12 h. Minimal (<5%) decomposition of **2-dipp** was noted. We hypothesized this lack of reactivity was likely due to the sterically encumbered 2,6-diisopropyl substituent on the imido nitrogen, which precludes approach of the isocyanate for the desired cycloaddition process. This is corroborated by examining the G(complex) values obtained from Solid G, which show respective values of 88.73% and 87.98% for **2-Bn** and **2-*p*Tol**, whereas the calculated value of 91.66% obtained for **2-dipp** is higher, indicating an inaccessible uranium center (Table 1). As an illustration of this correlation, it was found that treating sterically accessible **2-Ph** with the bulky isocyanate, 2,6-diisopropylphenyl isocyanate, resulted in an immediate reaction, producing an orange powder after workup assigned as $Tp^*_2U[\kappa^2$-(*N*,*N*′-1-phenyl,3-dippureato)] (**6**) (eq 2). The spectroscopic features of **6** trend with other asymmetric

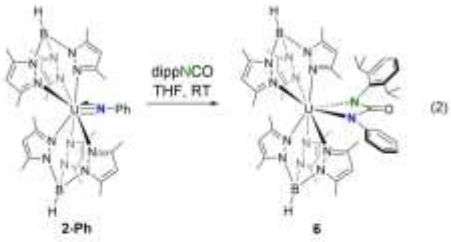

(2)

κ^2-ureato compounds as expected (Figure S2), and its formation highlights the ability of the $[Tp^*_2U]$ system to support very large ligands such as 1-phenyl, 3-dippureato. Thus, the lack of reactivity observed for **2-dipp** is likely due to the inability of the isocyanate to approach the uranium−nitrogen multiple bond, supporting the mechanistic proposal depicted in **Path A**.

CONCLUSIONS

Four new $Tp^*_2U(IV)$ imido complexes (**2-Bn**, **2-*p*Tol**, **2-detp**, **2-dipp**) were synthesized and fully characterized through spectroscopic and structural methods. A computational analysis of this family demonstrated that the imido substituents have varying degrees of steric influence on the uranium center. To test this idea, the [2π+2π] cycloaddition chemistry of these imido compounds with PhNCE (E = O, S, Se) was attempted and afforded a full series of symmetric (**3-Ph**, **4-Ph**, **5-Ph**) and asymmetric (**3-Ad**, **3-Bn**, **3-*p*Tol**, **4-Bn**, **4-*p*Tol**, **5-*p*Tol**) κ^2-ureato complexes bearing C═O, C═S, or C═Se functional groups. In the cases of **2-detp** and **2-dipp**, which have large imido substituents, no cycloaddition chemistry was noted, even at elevated temperatures. Thus, these studies correlate a quantitative measure of ligand sterics with cycloaddition reactivity. The first solid-state report of a κ^2-selenoureato ligand has also emerged from this work. Future work will focus on expanding the scope of reactivity for the compounds that contain sterically accessible imido substituents.

ASSOCIATED CONTENT

Supporting Information

The Supporting Information is available free of charge on the ACS Publications website at DOI: 10.1021/acs.inorgchem.6b02547.

CIF data of **2-Bn** (CIF)
CIF data of **2-dipp** (CIF)
CIF data of **2-*p*Tol** (CIF)
CIF data of **2-detp** (CIF)
CIF data of **3-Ph** (CIF)
CIF data of **4-Ph** (CIF)
CIF data of **5-Ph** (CIF)
^{1}H NMR spectra, ^{11}B NMR spectra, IR spectra, electronic absorption spectroscopy, and crystallographic details (PDF)

AUTHOR INFORMATION

Corresponding Author

*E-mail: sbart@purdue.edu.

ORCID

Suzanne C. Bart: 0000-0002-8918-9051

Notes

The authors declare no competing financial interest.

ACKNOWLEDGMENTS

The authors gratefully acknowledge a grant from the National Science Foundation (CHE-1149875, CAREER grant to SCB).

REFERENCES

(1) Duncan, A. P.; Bergman, R. G. Selective Transformations of Organic Compounds by Imidozirconocene Complexes. *Chem. Rec.* **2002**, *2*, 431−445.

(2) Chirik, P. J. Dinitrogen Functionalization with Bis(cyclopentadienyl) Complexes of Zirconium and Hafnium. *Dalton Trans.* **2007**, 16−25.

(3) Bazan, G. C.; Oskam, J. H.; Cho, H. N.; Park, L. Y.; Schrock, R. R. Living Ring-Opening Metathesis Polymerization of 2,3-Difunctionalized 7-Oxanorbornenes and 7-Oxanorbornadienes by Mo(CHCMe$_2$R) (NC$_6$H$_3$-*i*-Pr$_2$-2,6)(O-*tert*-Bu)$_2$ and Mo(CHCMe$_2$R)(NC$_6$H$_3$-*i*-Pr$_2$-2,6)(OCMe$_2$CF$_3$)$_2$. *J. Am. Chem. Soc.* **1991**, *113*, 6899−6907.

(4) Jin, J.; Mariott, W. R.; Chen, E. Y.-X. Polymerization of Methyl Methacrylate by Metallocene Imido Complexes and Tris(pentafluorophenyl)alane. *J. Polym. Sci., Part A: Polym. Chem.* **2003**, *41*, 3132−3142.

(5) Leung, W.-H. Synthesis and Reactivity of Organoimido Complexes of Chromium. *Eur. J. Inorg. Chem.* **2003**, 2003, 583−593.

(6) Akagi, F.; Suzuki, S.; Ishida, Y.; Hatanaka, T.; Matsuo, T.; Kawaguchi, H. Reactions of a Niobium Nitride Complex Prepared from Dinitrogen: Synthesis of Imide and Ureate Complexes and Ammonia Formation. *Eur. J. Inorg. Chem.* **2013**, *2013*, 3930−3936.

(7) Bryan, J. C.; Burrell, A. K.; Miller, M. M.; Smith, W. H.; Burns, C. J.; Sattelberger, A. P. Synthesis and Reactivity of technetium(VII) Imido Complexes. *Polyhedron* **1993**, *12*, 1769−1777.

(8) Leung, W.-H.; Wilkinson, G.; Hussain-Bates, B.; Hursthouse, M. B. Synthesis and Crystal Structures of [PPh$_4$][(MN{Bu^{t}NC(O)NBu^t}-Cl$_3$](M = Ru or Os); a New Reaction of *Tert*-Butyl Isocyanate. Synthesis of W[Bu^{t}NC(O)NBu^t]$_2$(NHBu^t)$_2$. *J. Chem. Soc., Dalton Trans.* **1991**, 2791−2794.

(9) Singh, A. K.; Levine, B. G.; Staples, R. J.; Odom, A. L. A 4-Coordinate Ru(II) Imido: Unusual Geometry, Synthesis, and Reactivity. *Chem. Commun.* **2013**, *49*, 10799−10801.

DOI: 10.1021/acs.inorgchem.6b02547
Inorg. Chem. 2017, 56, 1956−1965

(10) Dubberley, S. R.; Friedrich, A.; Willman, D. A.; Mountford, P. Radius, U. Synthesis and Reactivity of Calix[4]arene-Supported Group 4 Imido Complexes. *Chem. - Eur. J.* **2003**, *9*, 3634−3654.
(11) Darwish, W.; Seikel, E.; Käsmarker, R.; Harms, K.; Sundermeyer, J. Synthesis and X-Ray Crystal Structures of Imido and Ureato Derivatives of titanium(IV) Phthalocyanine and Their Application in the Catalytic Formation of Carbodiimides by Metathesis from Isocyanates. *Dalton Trans.* **2011**, *40*, 1787−1794.
(12) Edwards, A.; Hogarth, G.; Hollingsworth, N.; Oller, J. J. Illusive Tungsten-Imido-Dithiocarbamate Complexes: Facile Carbon−nitrogen Bond Formation. *Inorg. Chem. Commun.* **2011**, *14*, 1932−1936.
(13) Blake, A. J.; Mountford, P.; Nikonov, G. I. Swallow, D. Cycloaddition Reactions of Tetraaza Macrocycle Supported Group 4 Imido Complexes and Reversible Addition of Aryl Isocyanate to a Coordinated Ureate Ligand. *Chem. Commun.* **1996**, 1835−1836.
(14) Casey, C. P.; Widenhoefer, R. A.; Hayashi, R. K. Reactions of $Cp^*_3Co_3(\mu_3\text{-H})(\mu_2\text{-H})_3$ with Carbon Dioxide, Carbon Disulfide, and Phenyl Isocyanate. *Inorg. Chem.* **1995**, *34*, 1138−1144.
(15) Foerster, G. D.; Hogarth, G. Reversible Insertion of an Isocyanate into an Imido Moiety at a Dimolybdenum Centre. Synthesis and X-Ray Crystal Structure of $[Mo_2(NPh)_2(S_2CNEt_2)_2\ (\mu\text{-NPh})(\mu\text{-PhNC(O)NPh})]$. *J. Chem. Soc., Dalton Trans.* **1993**, 2539−2540.
(16) Hogarth, G.; Richards, I. Regioselective and Reversible Carbon−nitrogen Bond Formation: Synthesis, Structure and Reactivity of Ureato-Bridged Complexes $[Mo_2(NAr)_2(\mu\text{-X})\{\mu\text{-ArNC(O)NAr}\}(S_2CNR_2)_2]$ (Ar = Ph, *p*-Tol; X = S, NAr; R = Me, Et, Pr). *Dalton Trans.* **2005**, 760−773.
(17) Holland, A. W.; Bergman, R. G. Heterocumulene Metathesis by Iridium Guanidinate and Ureylene Complexes: Catalysis Involving Reversible Insertion To Form Six-Membered Metallacycles. *J. Am. Chem. Soc.* **2002**, *124*, 9010−9011.
(18) Paul, F.; Osborn, J. A.; Fischer, J.; Ochsenbein, P. Metallacyclic Interconversions in the Chemistry of Palladium with Phenyl Isocyanate. *Angew. Chem., Int. Ed. Engl.* **1993**, *32*, 1638−1640.
(19) Gibson, V. C.; Redshaw, C.; Clegg, W.; Elsegood, M. R. J. Isocyanate versus Isothiocyanate Insertion into Alkoxo and Imido Ligands. *J. Chem. Soc., Chem. Commun.* **1994**, 2635−2636.
(20) Danopoulos, A. A.; Wilkinson, G.; Sweet, T. K. N.; Hursthouse, M. B. Reactions of Imido Complexes of Iridium, Rhodium and Ruthenium. *J. Chem. Soc., Dalton Trans.* **1996**, *6133*, 3771−3778.
(21) Spencer, L. P.; Yang, P.; Scott, B. L.; Batista, E. R.; Boncella, J. M. Imido Exchange in Bis(imido) Uranium(VI) Complexes with Aryl Isocyanates. *J. Am. Chem. Soc.* **2008**, *130*, 2930−2931.
(22) Bart, S. C.; Anthon, C.; Heinemann, F. W.; Bill, E.; Edelstein, N. M.; Meyer, K. Carbon Dioxide Activation with Sterically Pressured Mid- and High-Valent Uranium Complexes. *J. Am. Chem. Soc.* **2008**, *130*, 12536−12546.
(23) Jilek, R. E.; Tomson, N. C.; Scott, B. L.; Boncella, J. M. [2 + 2] Cycloaddition Reactions at Terminal Imido Uranium(IV) Complexes to Yield Isolable Cycloadducts. *Inorg. Chim. Acta* **2014**, *422*, 78−85.
(24) Matson, E. M.; Crestani, M. G.; Fanwick, P. E.; Bart, S. C. Synthesis of U(IV) Imidos from $Tp^*_2U(CH_2Ph)$ (Tp* = hydrotris(3,5-Dimethylpyrazolyl)borate) by Extrusion of Bibenzyl. *Dalton Trans.* **2012**, *41*, 7952−7958.
(25) Matson, E. M.; Fanwick, P. E.; Bart, S. C. Diazoalkane Reduction for the Synthesis of Uranium Hydrazonido Complexes. *Eur. J. Inorg. Chem.* **2012**, *2012*, 5471−5478.
(26) Pangborn, A. B.; Giardello, M. A.; Grubbs, R. H.; Rosen, R. K.; Timmers, F. J. Safe and Convenient Procedure for Solvent Purification. *Organometallics* **1996**, *15*, 1518−1520.
(27) Preparation and Complexation of Tris(3,5-Dimethylpyrazolyl)-hydroborate. In *Inorganic Experiments*, 3rd ed.; Woollins, D. J., Ed.; Wiley: 2010; pp 70−72.
(28) Matson, E. M.; Forrest, W. P.; Fanwick, P. E.; Bart, S. C. Functionalization of Carbon Dioxide and Carbon Disulfide Using a Stable Uranium(III) Alkyl Complex. *J. Am. Chem. Soc.* **2011**, *133*, 4948−4954.
(29) Sun, Y.; McDonald, R.; Takats, J.; Day, V. W.; Eberspacher, T. A. Synthesis and Structure of Bis[hydrotris(3,5-dimethylpyrazolyl)-borato]iodouranium(III), $U[HB(3,5\text{-}Me_2pz)_3]_2I$: Unprecedented Side-On Interaction Involving a Hydrotris(pyrazolyl)borate Ligand. *Inorg. Chem.* **1994**, *33*, 4433−4434.
(30) Zakrzewski, J.; Krawczyk, M. Synthesis and Pesticidal Properties of Thio and Seleno Analogs of Some Common Urea Herbicides. *Phosphorus, Sulfur Silicon Relat. Elem.* **2009**, *184*, 1880−1903.
(31) Sharma, P.; Moorhouse, A.; Moses, J. Microwave-Enhanced Reaction of Thioacids with Azides in Aqueous Medium. *Synlett* **2011**, *2011*, 2384−2386.
(32) Taskin, O. S.; Dadashi-Silab, S.; Kiskan, B.; Weber, J.; Yagci, Y. Highly Efficient and Reusable Microporous Schiff Base Network Polymer as a Heterogeneous Catalyst for CuAAC Click Reaction. *Macromol. Chem. Phys.* **2015**, *216*, 1746−1753.
(33) Barral, K.; Moorhouse, A. D.; Moses, J. E. Efficient Conversion of Aromatic Amines into Azides: A One-Pot Synthesis of Triazole Linkages. *Org. Lett.* **2007**, *9*, 1809−1811.
(34) Clark, C. L.; Lockhart, J. J.; Fanwick, P. E.; Bart, S. C. Synthesis of Low-Valent Uranium Fluorides by C−F Bond Activation. *Chem. Commun.* **2015**, *51*, 14084−14087.
(35) Antunes, M. A.; Ferrence, G. M.; Domingos, Â.; McDonald, R.; Burns, C. J.; Takats, J.; Marques, N. Uranium (III) Scorpionates: Synthesis and Structure of $[(Tp^{Me2})_2U(N(C_6H_5)_2)]$ and $[(Tp^{Me2})_2U(N(SiMe_3)_2)]$. *Inorg. Chem.* **2004**, *43*, 6640−6643.
(36) Arney, D. S. J.; Burns, C. J. Synthesis and Properties of High-Valent Organouranium Complexes Containing Terminal Organoimido and Oxo Functional Groups. A New Class of Organo-F-Element Complexes. *J. Am. Chem. Soc.* **1995**, *117*, 9448−9460.
(37) Zi, G.; Jia, L.; Werkema, E. L.; Walter, M. D.; Gottfriedsen, J. P.; Andersen, R. A. Preparation and Reactions of Base-Free Bis(1,2,4-Tri-*Tert* -Butylcyclopentadienyl)uranium Oxide, Cp'_2UO. *Organometallics* **2005**, *24*, 4251−4264.
(38) Jilek, R. E.; Tomson, N. C.; Shook, R. L.; Scott, B. L.; Boncella, J. M. Preparation and Reactivity of the Versatile Uranium(IV) Imido Complexes $U(NAr)Cl_2(R_2Bpy)_2$ (R = Me, ^tBu) and $U(NAr)Cl_2(tppo)_x$. *Inorg. Chem.* **2014**, *53*, 9818−9826.
(39) Graves, C. R.; Yang, P.; Kozimor, S. A.; Vaughn, A. E.; Clark, D. L.; Conradson, S. D.; Schelter, E. J.; Scott, B. L.; Thompson, J. D.; Hay, P. J.; Morris, D. E.; Kiplinger, J. L. Organometallic Uranium(V)−Imido Halide Complexes: From Synthesis to Electronic Structure and Bonding. *J. Am. Chem. Soc.* **2008**, *130*, 5272−5285.
(40) Matson, E. M.; Forrest, W. P.; Fanwick, P. E.; Bart, S. C. Synthesis and Reactivity of Trivalent $Tp^*U(CH_2Ph)_2(THF)$: Insertion vs Oxidation at Low-Valent Uranium−Carbon Bonds. *Organometallics* **2013**, *32*, 1484−1492.
(41) Jilek, R. E.; Spencer, L. P.; Kuiper, D. L.; Scott, B. L.; Williams, U. J.; Kikkawa, J. M.; Schelter, E. J.; Boncella, J. M. A General and Modular Synthesis of Monoimidouranium(IV) Dihalides. *Inorg. Chem.* **2011**, *50*, 4235−4237.
(42) Guzei, I. A.; Wendt, M. An Improved Method for the Computation of Ligand Steric Effects Based on Solid Angles. *Dalton Trans.* **2006**, 3991−3999.
(43) Guzei, I. A.; Wendt, M. *Program Solid-G*; University of Wisconsin: Madison, WI, 2004.
(44) Al-Karaz, Z. M. S.; Bagnall, K. W.; Brown, D.; Whittaker, B. Octathiocyanato- and Octaselenocyanato-Complexes of the Tetravalent Actinide Elements. *J. Chem. Soc., Dalton Trans.* **1972**, *64*, 2273−2277.
(45) Al-Daher, A. G. M.; Bagnall, K. W.; Benetollo, F.; Polo, A.; Bombieri, G. Uranium(IV) and Thorium(IV) Halide and Pseudohalide Complexes with Substituted Amide and Urea Ligands. *J. Less-Common Met.* **1986**, *122*, 167−173.
(46) Koksharova, T. K.; Prisyazhnyuk, A. I. Formation of a Complex of Nickel(II) with *N,N'*-Diphenylthiourea. *Zh. Neorg. Khim.* **1984**, 1764−1766.
(47) Jensen, K. A.; Nielsen, P. H. Infrared Spectra of Thioamides and Selenoamides. *Acta Chem. Scand.* **1966**, *20*, 597−629.
(48) Koketsu, M.; Takakura, N.; Ishihara, H. Efficient Synthesis of Selenoureas from the Corresponding Carbodiimides. *Synth. Commun.* **2002**, *32*, 3075−3079.

DOI: 10.1021/acs.inorgchem.6b02947
Inorg. Chem. 2017, 56, 1956−1965

(49) Célariès, B.; Rima, G.; Court, L.; Lion, C.; Laval, J.-D. Radioprotective Activity and Synthesis of Siladithioacetals and Germadithioacetals Derived from *N*-Substituted Naphthylethylimidazoline. *Met. Based. Drugs* **2001**, *8*, 199−210.
(50) Trujillo, C.; Mó, O.; Yáñez, M.; Tortajada, J.; Salpin, J.-Y. Selenourea−Ca^{2+} Reactions in Gas Phase. Similarities and Dissimilarities with Urea and Thiourea. *J. Phys. Chem. B* **2008**, *112*, 5479−5486.
(51) Maiti, N.; Im, S. H.; Lee, Y. H.; Kim, C.-H.; Seok, S. Il. Solvent-Assisted Growth of Sb_2Se_3 Nanocompounds from a Single-Source Precursor under Mild Reaction Conditions. *CrystEngComm* **2011**, *13*, 3767−3772.
(52) Rija, A. P.; Niccolescu, A.; Soran, A.; Coropceanu, E. B.; Bulhac, I. I.; Bologa, O. A.; Deleanu, C.; Bourosh, P. N. Cobalt(III) Dimethylglyoximates Containing Selenourea and an Unusual Diselenourea Ligand: Synthesis and Structures. *Russ. J. Coord. Chem.* **2011**, *37*, 757−765.
(53) Fettouhi, M.; Waseer, M. I. M.; Ahmad, S.; Isab, A. A. X-Ray Structure and ^{77}Se, ^{31}P and ^{13}C MAS NMR of the Dinuclear Complex 1,2-bis(selenourea)-1\κSe,2\κSe-1,2-bis(trimethylphosphine)digold-(I)chloride. *Polyhedron* **2004**, *23*, 1−4.
(54) Bredenkamp, A.; Zeng, X.; Mohr, F. Metal Complexes of an *N*-Selenocarbamoyl Benzamidine. *Polyhedron* **2012**, *33*, 107−113.
(55) Carty, A. J.; Malone, S. F.; Taylor, N. J. The Selenium-Mercury Interaction: Synthesis, Spectroscopic and X-Ray Structural Studies of Methylmercury-Selenourea Complexes. *J. Organomet. Chem.* **1979**, *172*, 201−211.
(56) Fregona, D.; Graziani, R.; Faraglia, G.; Caselato, U.; Sitran, S. Palladium and Platinum Complexes with N,N-Dimethylselenourea. *Polyhedron* **1996**, *15*, 2523−2533.
(57) Evans, W. J.; Miller, K. A.; Ziller, J. W.; DiPasquale, A. G.; Heroux, K. J.; Rheingold, A. L. Formation of $Cp^*_2U(EPh)Me$, $Cp^*_2U(EPh)_2$, and $Cp^*_2U(\eta_2\text{-TeC}_6H_4)$ from $Cp^*_2UMe_2$ and PhEEPh (E = S, Se, Te). *Organometallics* **2007**, *26*, 4287−4293.
(58) Matson, E. M.; Kiernicki, J. J.; Fanwick, P. E.; Bart, S. C. Expanding the Family of Uranium(III) Alkyls: Synthesis and Characterization of Mixed-Ligand Derivatives. *Eur. J. Inorg. Chem.* **2016**, *2016*, 2527−2533.
(59) Castro-Rodriguez, I.; Meyer, K. Small Molecule Activation at Uranium Coordination Complexes: Control of Reactivity via Molecular Architecture. *Chem. Commun.* **2006**, 1353−1368.

DOI: 10.1021/acs.inorgchem.6b02947
Inorg. Chem. 2017, 56, 1956−1965